Correlation harvesting in the presence of Unruh and Hawking effects

by

Kensuke Gallock-Yoshimura

A thesis
presented to the University of Waterloo
in fulfillment of the
thesis requirement for the degree of
Doctor of Philosophy
in
Physics

Waterloo, Ontario, Canada, 2023

Examining Committee Membership

The following served on the Examining Committee for this thesis. The decision of the Examining Committee is by majority vote.

External Examiner:	Claudio Dappiaggi Associate Professor, Dept. of Physics, University of Pavia
Supervisor(s):	Robert B. Mann Professor, Dept. of Physics and Astronomy, University of Waterloo
Internal Member:	Adrian Lupascu Associate Professor, Dept. of Physics and Astronomy, University of Waterloo
Internal-External Member:	Eduardo Martín-Martínez Associate Professor, Dept. of Applied Mathematics, University of Waterloo
Internal-External Member:	Achim Kempf Professor, Dept. of Applied Mathematics, University of Waterloo

Author's Declaration

This thesis consists of material all of which I authored or co-authored: see Statement of Contributions included in the thesis. This is a true copy of the thesis, including any required final revisions, as accepted by my examiners.

I understand that my thesis may be made electronically available to the public.

Statement of Contributions

This thesis is based on the following published and forthcoming articles.

- Chapter 3 is based on

  Manar Naeem, **Kensuke Gallock-Yoshimura**, and Robert B. Mann, Mutual information harvested by uniformly accelerated particle detectors, Phys. Rev. D **107**, 065016 (2023)
  The first and the second authors contributed equally under the supervision of the Ph.D. supervisor.

- Chapter 4 is based on

  Kendra Bueley, Luosi Huang, **Kensuke Gallock-Yoshimura**, and Robert B. Mann, Harvesting mutual information from BTZ black hole spacetime, Phys. Rev. D **106**, 025010 (2022)
  The first two authors generated plots and the author of this thesis designed the study under the supervision of the Ph.D. supervisor.

- Chapter 5 is based on

  Ireneo James Membrere, **Kensuke Gallock-Yoshimura**, Laura J. Henderson, and Robert B. Mann, Tripartite entanglement extraction from the black hole vacuum, arXiv:2304.07847 (2023)
  The first author generated plots and the rest of the authors designed the study.

- Chapter 6 is based on

  Kensuke Gallock-Yoshimura, Erickson Tjoa, and Robert B. Mann, Harvesting entanglement with detectors freely falling into a black hole, Phys. Rev. D **104**, 025001 (2021)
  The first and the second authors contributed equally under the supervision of the Ph.D. supervisor.

Contributions not included in this thesis:

- **Kensuke Gallock-Yoshimura** and Robert B. Mann, Entangled detectors nonperturbatively harvest mutual information, Phys. Rev. D **104**, 125017 (2021)
- Erickson Tjoa and **Kensuke Gallock-Yoshimura**, Channel capacity of relativistic quantum communication with rapid interaction, Phys. Rev. D **105**, 085011 (2022)
- Diana Mendez-Avalos, Laura J. Henderson, **Kensuke Gallock-Yoshimura**, and Robert B. Mann, Entanglement harvesting of three Unruh-DeWitt detectors, Gen. Relativ. Gravit. **54**, 87 (2022)
- Diana Méndez Avalos, **Kensuke Gallock-Yoshimura**, Laura J. Henderson, and Robert B. Mann, Instant Extraction of Non-Perturbative Tripartite Entanglement, arXiv:2204.02983 [quant-ph] (2022)
- Dyuman Bhattacharya, **Kensuke Gallock-Yoshimura**, Laura J. Henderson, and Robert B. Mann, Extraction of entanglement from quantum fields with entangled particle detectors, Phys. Rev. D **107**, 105008 (2023)

Abstract

Quantum field theory (QFT) in curved spacetime is a study of quantum fields under the influence of the relativistic motion of particles or spacetime curvature. The famous outcomes of this subject are the Unruh and Hawking effects. The *Unruh effect* claims that a uniformly accelerating atom (people in the community tend to use a model called the *Unruh-DeWitt (UDW) particle detector*, which is a two-level quantum system coupled to a quantum field) thermalizes even though an inertial observer sees no particles. That is, an acceleration motion excites the internal degree of freedom of the atom in such a way that the atom experiences as if it is immersed in a thermal bath. *The Hawking effect* is a phenomenon where a black hole radiates thermal quanta. If one puts a UDW detector outside an event horizon, then it also perceives thermality. Both the Unruh and Hawking effects show thermality, which is the core theme of this thesis.

In recent years, a protocol called *entanglement harvesting* has attracted great interest. Entanglement harvesting utilizes multiple UDW detectors to extract (or 'harvest') entanglement pre-existed in a quantum field. The extracted entanglement is influenced by the geometry of spacetime and the trajectories of UDW detectors. One can also extract other types of correlations, and so we collectively call this the correlation harvesting protocol.

In this thesis, we examine how thermal effects influence the ability of correlation harvesting. In a previous study [1], the case of two inertial UDW detectors coupled to a thermal quantum field was investigated. It was shown that as the temperature of the field increases, the extracted entanglement between the detectors decreases while the quantum mutual information (the total correlations including classical and quantum correlations) increases. Since a single detector in uniform acceleration motion or hovering near a black hole experiences thermality as if it is immersed in a thermal quantum field, it is natural to ask if harvested correlations also behave in the same manner.

In contrast, we show that (i) the Unruh temperature of uniformly accelerating detectors prevents the detectors from extracting any correlations at the high temperatures, i.e., even the quantum mutual information vanishes at the extreme Unruh temperatures; (ii) high black hole temperatures also prevent the detectors from harvesting correlations, and this is no exception even for tripartite entanglement; and (iii) freely falling detectors in a black hole spacetime are less affected by this, and they have no trouble extracting correlations from the field even when detectors are causally disconnected by an event horizon.

Acknowledgements

First of all, I would like to thank my supervisor, Robert B. Mann, who has been really supportive. Without your support, the path $\gamma : \mathbb{R} \to \mathcal{M}$ in my life would have been very different.

I am grateful to the Keio University Global Fellowship for their full financial support during the first two years of my study.

Next, I thank my collaborators and friends in the group, especially, Erickson Tjoa, Laura J. Henderson, Diana Méndez-Avalos, Kendra Bueley, Luosi Huang, Ireneo James Membrere, Dyuman Bhattacharya, Manar Naeem, Lana Bozanic, and Sayan Gangopadhyay.

I also thank my parents, Jon David Gallock and Michiru Gallock-Yoshimura, who have always been supportive.

Finally, I thank my housemate, Oluwabamise Afolabi, a.k.a. Mr. Bam Bam. Without you, I would not have survived the depressing Covid era.

Table of Contents

List of Figures

Chapter 1

Introduction

The groundbreaking theories in theoretical physics in the twentieth century are undoubtedly quantum theory and the general theory of relativity (GR). Quantum theory describes the nature of microscopic particles such as electrons and photons, whereas GR is a theory of gravitational fields. Although these two pillars of modern theoretical physics are compatible with experimental observations, physicists do not know how to unify these two theories in a consistent manner to this date.

One attempt to describe gravitation within the quantum theory uses quantum field theory (QFT) in curved spacetime, which defines quantum fields (such as vector fields representing photons) on a classical curved spacetime [2]. Among the seminal works in this framework is a paper by Hawking, who showed that a classical black hole can emit particles (known as Hawking radiation) as a result of the presence of a quantum field [3]. Moreover, this phenomenon turns out to reduce the mass of the black hole, leading to the shrinkage (or "evaporation") of the hole. While it remains uncertain whether black holes vanish at the end of this evaporation process, if they do, it would lead to the so-called black hole information problem, which states that the principle of unitarity in quantum theory is incompatible with gravitational theory.

In recent years, people have realized that the tools developed in quantum information theory are valuable assets to deal with quantum information in black hole spacetimes. Examples include the Hayden-Preskill protocol [4] and von Neumann entropy in gauge/gravity duality [5, 6]. The importance of quantum information theory is recognized not only for the study of black holes but also in condensed matter physics [7], quantum gravity [8], and thermodynamics [9].

Similarly, the field of *relativistic quantum information* (RQI) has gained significant at-

tention in recent years. RQI has two main focuses. The first is to describe physical systems in which relativistic effects are important using the tools developed in quantum information theory. The second is to generalize quantum information protocols to a relativistic setting. One example of a branch of RQI is relativistic quantum communication (RQC). In everyday life, we use electromagnetic fields to send and receive information, and these fields are fundamentally relativistic quantum fields. RQC aims to understand how information can be transmitted from one point to another through a quantum field, and this can be analyzed by computing the channel capacity [10, 11, 12, 13, 14].

Another branch of RQI is the so-called *entanglement harvesting protocol*, which is a procedure that extracts entanglement from a quantum field by using multiple atoms. In the literature, people typically employ two Unruh-DeWitt (UDW) particle detectors [15, 16, 17] interacting with a quantum scalar field. Here, a UDW detector is a particular model for a qubit (i.e., a two-level quantum system), which travels in spacetime. The protocol is described as follows.

(i) Prepare two or multiple UDW detectors. Typically, we assume that the detectors are initially uncorrelated and that the quantum field is in a specific state, such as the vacuum state. Additionally, we assume that the detectors and the field are uncorrelated as well.
(ii) We let the detectors travel through spacetime and at some point they start to interact with the quantum field until the interaction is turned off. Thus, the detector-field coupling is time-dependent.
(iii) After the interaction, we collect the detectors and observe that they are entangled with each other. Entanglement is "harvested" from the field if the detectors are entangled at the end of the process.

One might ask where this entanglement comes from. The answer is from the quantum field since it is known that a quantum field is already in an entangled state even if it is a vacuum state [18, 19]. Hence, the entanglement pre-existent in the field is transferred to the detectors through interaction, and in this sense entanglement is "harvested" (or extracted) from the field. Moreover, the detectors can be entangled even when they are causally disconnected.

Such a harvesting process was first examined by Valentini in 1991 [20] and subsequently Reznik *et al.* in the early 2000s [21, 22]. Valentini considered two atoms coupled to an electric field (i.e., the light-matter interaction), which is perhaps a more realistic scenario. However, it was pointed out that the essential features in the light-matter interaction are captured in the UDW model so long as the detectors do not exchange angular momenta with

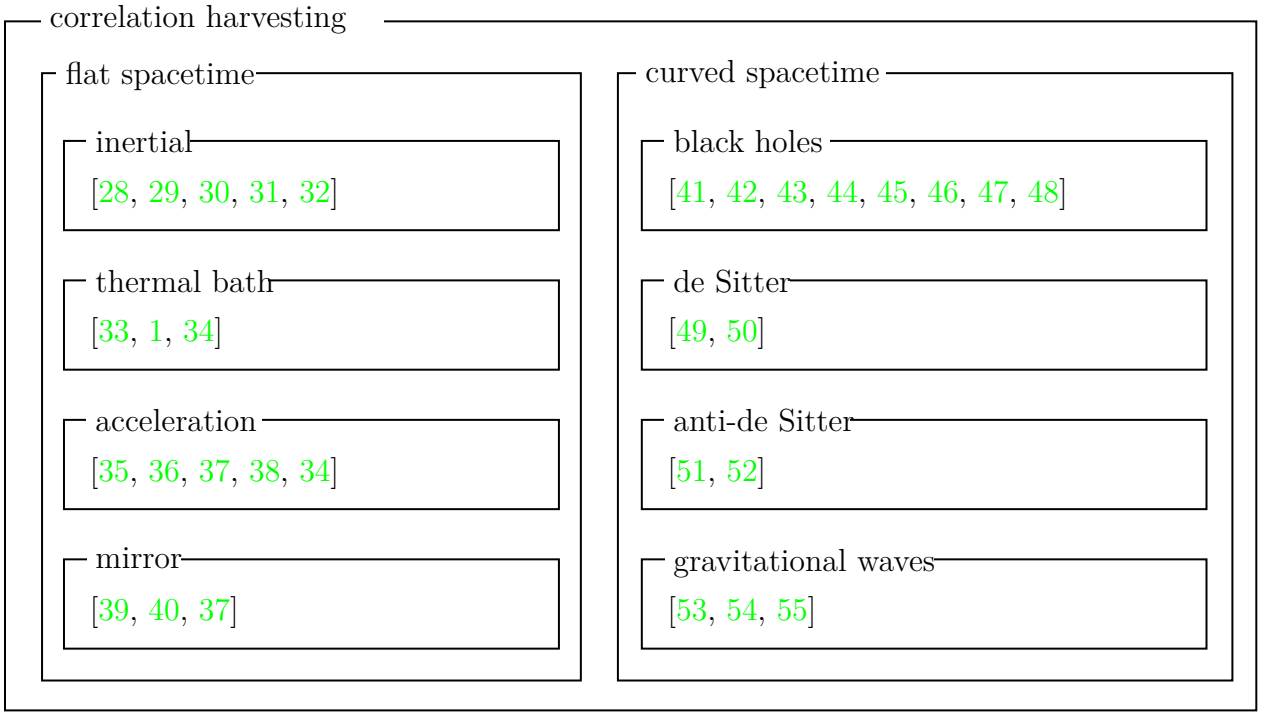

Figure 1.1: A list of articles on the correlation harvesting protocol.

the field [23, 24]. This fact reinforces the decision to use the UDW detector model, which is much easier to handle than the full light-matter interaction. For entanglement harvesting in the light-matter interaction, see [25] (also [26, 27] for the light-matter interaction and UDW detectors).

After these pioneering papers, people investigated the entanglement harvesting protocol extensively. The simplest case for this protocol is when two UDW detectors are at rest in Minkowski spacetime [28]. Additionally, the harvested entanglement shows a distinct property depending on the trajectories of the detectors and the geometry of spacetime. For example, uniformly accelerating detectors in the Minkowski vacuum will be influenced by the Unruh effect. Thus, the harvested entanglement tells us about the trajectories and the background geometry of spacetime. Furthermore, one can think of not only harvesting entanglement but also other types of correlations such as classical correlations or quantum discord, and so we can refer to the protocol as the *correlation harvesting protocol* in general. Figure 1.1 lists some papers on correlation harvesting.

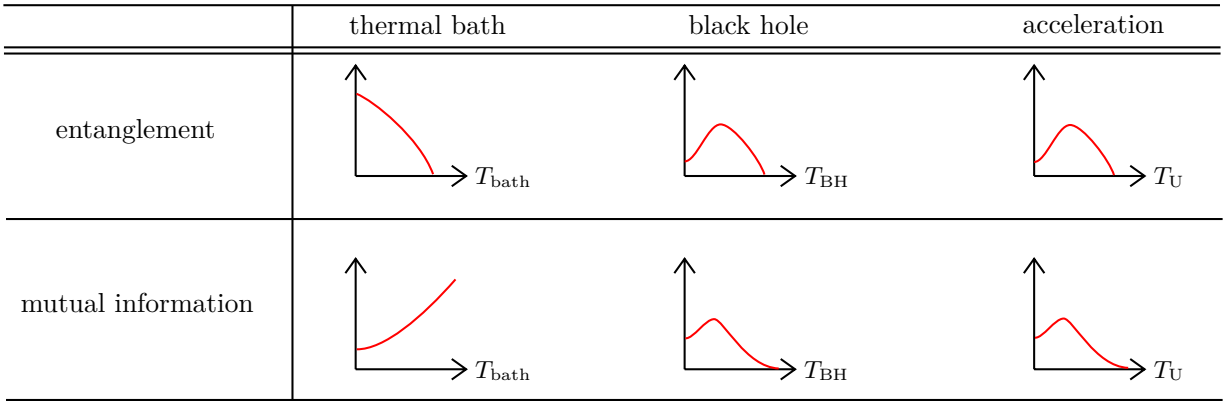

Figure 1.2: Temperature dependence of entanglement and mutual information in different scenarios.

This thesis primarily focuses on the influence of Unruh and Hawking effects on correlation harvesting. As mentioned above, the Unruh effect [15] refers to the phenomenon that a uniformly accelerating UDW detector experiences thermal equilibrium at the Unruh temperature $T_{\text{U}} = \hbar a/2\pi k_{\text{B}} c$ in the Minkowski vacuum, whereas the Hawking effect [3] claims that a black hole surrounded by a quantum field radiates Hawking quanta, which in turn thermalizes a stationary UDW detector hovering outside of the black hole. It was pointed out by Cliche and Kempf in 2011 [56] that high Hawking temperature would act as noise that prevents the detectors from harvesting entanglement near a black hole. Indeed, it was numerically shown by Henderson *et al.* in 2018 [41] that this is the case for two stationary detectors in the Bañados-Teitelboim-Zanelli (BTZ) black hole spacetime. In particular, they showed that there is a region in the vicinity of a black hole called the *entanglement shadow* where detectors cannot extract entanglement at all once one of them enters it. Uniformly accelerating detectors also behave in a similar way in the sense that high Unruh temperature T_{U} prevents them from harvesting entanglement [38].

However, the impact of thermal effects resulting from the Unruh and Hawking effects on correlation harvesting differs from that of a thermal state in a quantum field. It was shown [57, 1] that two detectors at rest in Minkowski spacetime interacting with a thermal quantum field monotonically decreases the amount of entanglement with temperature whereas the total correlation (quantum mutual information) monotonically increases. This result suggests that thermality in a thermal quantum field actually enhances total correlation at high temperatures, contrary to our intuition that thermality acts as noise. See Fig. 1.2 for the comparison.

In this thesis, we investigate the temperature dependence of harvested correlations by

filling out the missing pieces in Fig. 1.2. We first consider quantum mutual information (i.e., the total correlation) harvested by two uniformly accelerating UDW detectors in Minkowski spacetime in Ch. 3. We obtain the temperature dependence of quantum mutual information and show that the detectors are unable to harvest any correlation at $T_{\mathrm{U}} \to \infty$ as opposed to the thermal bath case in [57, 1]. In fact, entanglement harvested by uniformly accelerating detectors behaves in a similar manner [38], though it cannot be extracted at a finite Unruh temperature. Hence, in the high Unruh temperature regime, either classical correlation or non-distillable entanglement can be extracted.

Chapter 4 examines quantum mutual information harvested by two stationary detectors situated outside a BTZ black hole. Since Unruh and Hawking effects show a similar property, we expect that correlation harvesting is prohibited at infinite local temperatures observed by a detector as in Ch. 3. We show that this is the case; the total correlation vanishes at infinite temperatures while entanglement becomes zero with a finite temperature. This suggests that a "quantum mutual information shadow" does not exist. Furthermore, we reveal that only Hawking temperature is responsible for prohibiting correlation harvesting and gravitational redshift does not contribute to it.

As an extension of Ch. 4, we introduce a third UDW detector to the BTZ black hole spacetime and consider tripartite entanglement harvesting in Ch. 5. We place the three detectors around the black hole in an equilateral triangular configuration so that each detector feels the same gravitational redshift and local temperature, which simplifies the calculation. Here, we employ a tripartite entanglement measure called π-tangle. Although the π-tangle of a mixed state does not reflect the true amount of tripartite entanglement, it provides a lower bound. We demonstrate that harvesting tripartite entanglement is easier than harvesting bipartite entanglement and thereby, detectors can extract tripartite entanglement even from the bipartite entanglement shadow. Since bipartite entanglement is absent, the harvested tripartite entanglement is of the GHZ type.

Until now, the detectors in BTZ spacetime are stationary, namely, they are hovering at a constant proper distance from an event horizon. It is then intriguing to see how freely falling detectors extract correlations from the field. We uncover this in Ch. 6 by carrying out the (bipartite) correlation harvesting protocol in $(1+1)$-dimensional Schwarzschild spacetime. Here, three kinds of detector motions are considered: two static detectors as in the previous chapters, one detector is freely falling into a black hole from infinity while the other detector is stationary, and both detectors are free-falling. As expected, the entanglement shadow is present for the two static-detectors case. One would expect that if one of the detectors is in free fall, then the entanglement shadow is absent since the free-faller will not encounter the infinite temperature when crossing the horizon. However, this is not the case since the relative velocity of the free-faller with respect to the static

detector causes degradation of entanglement extraction. Nevertheless, quantum mutual information is less affected by this effect, especially near the horizon, and the free-faller and static detectors can extract correlations across the horizon. Finally, two free-fallers can always harvest correlations due to the fact that their local temperatures remain finite throughout their journey to the singularity.

All the basic ingredients needed in this thesis are provided in Ch. 2. The detailed description of QFT in BTZ spacetime is given in Appendix B. Throughout this thesis, we use the natural units, $\hbar = c = k_{\rm B} = 1$, where c and $k_{\rm B}$ are the speed of light and the Boltzmann constant. We also use the most-plus convention for metric and a point in spacetime is denoted by x.

Chapter 2

Quantum fields and particle detectors in curved spacetime

In this chapter, we introduce the concept of quantum field theory (QFT) in curved spacetime, which is based on [2, 58].

2.1 Quantum fields in curved spacetime

2.1.1 Classical field on a manifold

Let $(\mathcal{M}, g)$ be a pseudo-Riemannian manifold, where g is a pseudo-Riemannian metric. For example, $(\mathbb{R}^4, \eta)$ can be regarded as a $(3+1)$-dimensional Minkowski spacetime with $\eta = \mathrm{diag}(-1, 1, 1, 1)$. In QFT in curved spacetime, the manifold $(\mathcal{M}, g)$ is treated classically and the fields are defined on this manifold.

Before quantizing a field, consider a classical real scalar field (i.e., Klein-Gordon field), $\phi(\mathsf{x})$, which is defined on a point in a manifold: $\mathsf{x} \in \mathcal{M}$.[1] The action $S_\phi[\phi, g]$, for this classical scalar field is given by

$$S_\phi[\phi, g] = \frac{1}{2} \int_{\mathcal{M}} \mathrm{dvol}_g \left[g^{\mu\nu} \partial_\mu \phi(\mathsf{x}) \partial_\nu \phi(\mathsf{x}) - (m^2 + \xi R(\mathsf{x})) \phi^2(\mathsf{x}) \right] , \tag{2.1}$$

[1] Technically speaking, it is appropriate to define ϕ as $\phi : C_0^\infty(\mathcal{M}) \to \mathbb{R}$, where $C_0^\infty(\mathcal{M})$ is a space of smooth functions with compact support on $\mathcal{M}$.

where dvol_g is a volume element, $m \geq 0$ is the mass of the field, $\xi \in \mathbb{R}$ is a constant describing a coupling between the field and the Ricci curvature scalar $R(\mathsf{x})$. In $(n+1)$-dimensions, the volume element dvol_g is expressed as $\mathrm{dvol}_g = \mathrm{d}^{n+1}x\sqrt{-g}$, where $g \coloneqq \det g_{\mu\nu}$ is the metric determinant. The action S_ϕ is manifestly covariant, i.e., it is independent of coordinate transformations.

From the action principle, $\delta S_\phi[\phi, g] = 0$, one can obtain the Euler-Lagrange equation:

$$(\Box - m^2 - \xi R)\phi(\mathsf{x}) = 0\,, \tag{2.2}$$

where

$$\Box \coloneqq \frac{1}{\sqrt{-g}}\partial_\mu(g^{\mu\nu}\sqrt{-g}\partial_\nu) \tag{2.3}$$

is the d'Alembert operator. Equation (2.2) is known as the Klein-Gordon equation. Note that the Klein-Gordon equation depends on the background geometry (i.e., the curved spacetime on which the field is defined) even when $\xi = 0$ since the d'Alembert operator (2.3) contains $g_{\mu\nu}$, which has the information of the geometry.

The final task is to solve (2.2) and obtain an explicit form for $\phi(\mathsf{x})$. Since the d'Alembert operator (2.3) is a second-order, hyperbolic partial differential operator, the Klein-Gordon equation (2.2) is a second-order differential equation. This means that one can solve the equation once two initial conditions are specified. However, the existence of the solution $\phi(\mathsf{x})$ to the Klein-Gordon equation depends on the causal structure of the manifold $(\mathcal{M}, g)$. Specifically, the solution $\phi(\mathsf{x})$ is well-defined everywhere in a manifold if $(\mathcal{M}, g)$ is globally hyperbolic (namely, there exists a Cauchy slice). In this section, we will assume that the manifold is globally hyperbolic, so the solutions to the Klein-Gordon equation are well-defined.

2.1.2 Quantum field in curved spacetime

Formulation

So far, we have considered a *classical* Klein-Gordon field in curved spacetime. We now proceed to quantize this field and obtain a *quantum* field defined on curved spacetime.

Typically, the quantization of a field is done in the canonical quantization scheme, which promotes $\phi(\mathsf{x})$ and its canonical conjugate $\pi(\mathsf{x})$ to operator-valued quantities $\hat{\phi}(\mathsf{x})$ and $\hat{\pi}(\mathsf{x})$, respectively, and imposes canonical commutation relations (CCRs). That is,

$\hat{\phi}(\mathsf{x})$ and $\hat{\pi}(\mathsf{x})$ must obey the following three conditions.

(1) Hermiticity: $\hat{\phi}^\dagger(\mathsf{x}) = \hat{\phi}(\mathsf{x})$.
(2) CCR: $[\hat{\phi}(t,\boldsymbol{x}), \hat{\pi}(t,\boldsymbol{y})] = \mathsf{i}\delta^{(n)}(\boldsymbol{x}-\boldsymbol{y})$ in $(n+1)$-dimensions.[2]
(3) Heisenberg equations of motion:

$$\mathsf{i}\partial_t \hat{\phi}(t,\boldsymbol{x}) = [\hat{\phi}(t,\boldsymbol{x}), \hat{H}]\,, \tag{2.4}$$
$$\mathsf{i}\partial_t \hat{\pi}(t,\boldsymbol{x}) = [\hat{\pi}(t,\boldsymbol{x}), \hat{H}]\,, \tag{2.5}$$

or equivalently,

$$(\Box - m^2 - \xi R)\hat{\phi}(\mathsf{x}) = 0\,, \tag{2.6}$$
$$\hat{\pi}(\mathsf{x}) = \sqrt{-g}g^{0\nu}\partial_\nu \hat{\phi}(\mathsf{x})\,. \tag{2.7}$$

Hence, the goal is to find a solution $\hat{\phi}(\mathsf{x})$ that satisfies these conditions.

To do this, let us assume that spacetime possesses a timelike Killing vector field (which we will introduce later). Then, one can perform a mode-decomposition of $\hat{\phi}$ as

$$\hat{\phi}(\mathsf{x}) = \int_{\mathbb{R}^n} \mathrm{d}^n k \, \left(\hat{a}_{\boldsymbol{k}} u_{\boldsymbol{k}}(\mathsf{x}) + \hat{a}^\dagger_{\boldsymbol{k}} u^*_{\boldsymbol{k}}(\mathsf{x})\right)\,. \tag{2.8}$$

Here, $u_{\boldsymbol{k}}(\mathsf{x}) \in \mathbb{C}$ is the mode function, and $\hat{a}_{\boldsymbol{k}}$ and $\hat{a}^\dagger_{\boldsymbol{k}}$ are annihilation and creation operators, respectively. The vacuum state $|0\rangle$ is defined as $\hat{a}_{\boldsymbol{k}}|0\rangle = 0$ for all $\boldsymbol{k}$ (we will explain this later). The three conditions for $\hat{\phi}$ are now translated as follows. The Hermiticity condition (1) is manifest in this expression. The CCR condition (2) is obeyed if the following two conditions are satisfied:

$$[\hat{a}_{\boldsymbol{k}}, \hat{a}^\dagger_{\boldsymbol{k}'}] = \delta^{(n)}(\boldsymbol{k}-\boldsymbol{k}')\,, \tag{2.9}$$
$$\sqrt{-g}g^{0\nu}\int_{\mathbb{R}^n} \mathrm{d}^n k \, [u_{\boldsymbol{k}}(t,\boldsymbol{x})\partial_\nu u^*_{\boldsymbol{k}}(t,\boldsymbol{y}) - u^*_{\boldsymbol{k}}(t,\boldsymbol{x})\partial_\nu u_{\boldsymbol{k}}(t,\boldsymbol{y})] = \mathsf{i}\delta^{(n)}(\boldsymbol{x}-\boldsymbol{y})\,. \tag{2.10}$$

The second equation (2.10) is known as the Wronskian condition. Finally, the equation of motion is satisfied if $u_{\boldsymbol{k}}(\mathsf{x})$ obeys the Klein-Gordon equation,

$$(\Box - m^2 - \xi R)u_{\boldsymbol{k}}(\mathsf{x}) = 0\,, \tag{2.11}$$

[2]Technically, one has to specify a foliation of $\mathcal{M}$ as $\mathcal{M} = \mathbb{R}\times\Sigma$, where $\mathbb{R}$ is the time direction and Σ is a Cauchy surface. Such a decomposition is always possible in a globally hyperbolic spacetime.

since if this is the case, $u^*_{\boldsymbol{k}}(\mathsf{x})$ is a solution to the Klein-Gordon equation, and a linear combination $\hat{a}_{\boldsymbol{k}} u_{\boldsymbol{k}}(\mathsf{x}) + \hat{a}^\dagger_{\boldsymbol{k}} u^*_{\boldsymbol{k}}(\mathsf{x})$ is also a solution to the Klein-Gordon equation due to its linearity, and thus $\hat{\phi}(\mathsf{x})$ expressed in (2.8) can be a solution to the equation of motion. As mentioned in the previous subsection, globally hyperbolic spacetimes are useful. This is due to the fact that if $(\mathcal{M}, g)$ is globally hyperbolic, then there exist solutions $\{u_{\boldsymbol{k}}(\mathsf{x})\}$ to the Klein-Gordon equations satisfying the Wronskian condition (2.10).

We now introduce the Klein-Gordon product. Let $f, g \in \mathbb{R}$ be real-valued solutions to the Klein-Gordon equations (2.11), and denote $\mathrm{Sol}_{\mathbb{R}}(\mathcal{M})$ the solution space (a vector space), that is, $f, g \in \mathrm{Sol}_{\mathbb{R}}(\mathcal{M})$. We then promote $\mathrm{Sol}_{\mathbb{R}}(\mathcal{M})$ to a symplectic vector space $(\mathrm{Sol}_{\mathbb{R}}(\mathcal{M}), (\cdot,\cdot))$ by introducing a bi-linear symplectic form,

$$\begin{aligned} &(\cdot,\cdot) : \mathrm{Sol}_{\mathbb{R}}(\mathcal{M}) \times \mathrm{Sol}_{\mathbb{R}}(\mathcal{M}) \to \mathbb{R}\,, \\ &(\cdot,\cdot) : f_1, f_2 \mapsto (f_1, f_2) \coloneqq \int_\Sigma \mathrm{d}\Sigma^\mu \left(f_1 \partial_\mu f_2 - f_2 \partial_\mu f_1\right), \end{aligned} \tag{2.12}$$

where Σ is any Cauchy hypersurface in the manifold $\mathcal{M}$ and $\mathrm{d}\Sigma_\mu = \mathrm{d}\Sigma n_\mu$ with n_μ being a unit normal vector to Σ and $\mathrm{d}\Sigma$ is the volume element on that hypersurface. It is known that such a bi-linear form is independent of the choice of Σ, and is non-degenerate (i.e., non-zero if $f_1, f_2 \neq 0$). Moreover, one can easily check that it is anti-symmetric: $(f_1, f_2) = -(f_2, f_1)$.

We now extend this to $\mathrm{Sol}_{\mathbb{C}}(\mathcal{M})$, the solution space of the Klein-Gordon equation over $\mathbb{C}$. We define the Klein-Gordon product as

$$\begin{aligned} &(\cdot,\cdot)_{\mathrm{KG}} : \mathrm{Sol}_{\mathbb{C}}(\mathcal{M}) \times \mathrm{Sol}_{\mathbb{C}}(\mathcal{M}) \to \mathbb{R}\,, \\ &(\cdot,\cdot)_{\mathrm{KG}} : f_1, f_2 \mapsto (f_1, f_2)_{\mathrm{KG}} \coloneqq \mathsf{i}(f_1^*, f_2) = \mathsf{i} \int_\Sigma \mathrm{d}\Sigma^\mu \left[f_1^* \partial_\mu f_2 - (\partial_\mu f_1^*) f_2\right]. \end{aligned} \tag{2.13}$$

Here, the symplectic form $(\cdot,\cdot)$ is extended to the complex-valued solutions, $\mathrm{Sol}_{\mathbb{C}}(\mathcal{M})$. Then, by using the properties of the bi-linear symplectic form of the symplectic bases, the Klein-Gordon product of $u_{\boldsymbol{k}}(\mathsf{x}) \in \mathrm{Sol}_{\mathbb{C}}(\mathcal{M})$ satisfies the following.

$$(u_{\boldsymbol{k}}(\mathsf{x}), u_{\boldsymbol{k}'}(\mathsf{x}))_{\mathrm{KG}} = \delta^{(n)}(\boldsymbol{k} - \boldsymbol{k}')\,, \tag{2.14a}$$

$$(u^*_{\boldsymbol{k}}(\mathsf{x}), u^*_{\boldsymbol{k}'}(\mathsf{x}))_{\mathrm{KG}} = -\delta^{(n)}(\boldsymbol{k} - \boldsymbol{k}')\,, \tag{2.14b}$$

$$(u_{\boldsymbol{k}}(\mathsf{x}), u^*_{\boldsymbol{k}'}(\mathsf{x}))_{\mathrm{KG}} = 0\,. \tag{2.14c}$$

Note that the Klein-Gordon product is not an inner product since it is not positive semi-definite. However, it becomes an inner product if we divide the solution space $\mathrm{Sol}_{\mathbb{C}}(\mathcal{M})$ into the subspaces of positive and negative frequency modes, which we will define in the following.

The interesting part of QFT in curved spacetime is that the expression for $\hat{\phi}(\mathsf{x})$ is not unique. That is, one can find more than two sets of mode functions $\{u_{\boldsymbol{k}}(\mathsf{x})\}$ that satisfy all the conditions for a scalar field, and these can be unitarily inequivalent. So how can we find a vacuum state that is physically reasonable? One way is to use the symmetries of a background spacetime. If spacetime does not change its geometry with time, an observer would not see particle creation so long as the observer is stationary with the spacetime.

Let $K \in T_{\mathsf{x}}\mathcal{M}$ be a timelike Killing vector field. Then $u_{\boldsymbol{k}}(\mathsf{x})$ is called the positive frequency mode with respect to K if it satisfies

$$\mathcal{L}_K u_{\boldsymbol{k}}(\mathsf{x}) = -\mathsf{i}\omega_{\boldsymbol{k}} u_{\boldsymbol{k}}(\mathsf{x})\,, \quad \omega_{\boldsymbol{k}} > 0 \tag{2.15}$$

where $\mathcal{L}_K$ is the Lie derivative associated to K. The negative frequency modes, on the other hand, are the complex conjugates, $u^*_{\boldsymbol{k}}(\mathsf{x})$, since they satisfy

$$\mathcal{L}_K u^*_{\boldsymbol{k}}(\mathsf{x}) = \mathsf{i}\omega_{\boldsymbol{k}} u^*_{\boldsymbol{k}}(\mathsf{x})\,, \quad \omega_{\boldsymbol{k}} > 0 \tag{2.16}$$

One can then use $u_{\boldsymbol{k}}(\mathsf{x})$ and $u^*_{\boldsymbol{k}}(\mathsf{x})$ to decompose the field operator $\hat{\phi}$ as in (2.8). Moreover, the solution space $\mathrm{Sol}_{\mathbb{C}}(\mathcal{M})$ can be decomposed into the subspaces of positive and negative frequency solutions, denoted by $\mathcal{H}_{\mathrm{sol}}$ and $\mathcal{H}^*_{\mathrm{sol}}$, respectively, as

$$\mathrm{Sol}_{\mathbb{C}}(\mathcal{M}) = \mathcal{H}_{\mathrm{sol}} \oplus \mathcal{H}^*_{\mathrm{sol}}\,. \tag{2.17}$$

Since the Klein-Gordon product, $(\cdot,\cdot)_{\mathrm{KG}}$, becomes positive semi-definite in the subspace $\mathcal{H}_{\mathrm{sol}}$, a space $(\mathcal{H}_{\mathrm{sol}}, (\cdot,\cdot)_{\mathrm{KG}})$ turns out to be a Hilbert space of solutions to the Klein-Gordon equation.[3] The nice thing about the positive/negative frequency modes with respect to the timelike Killing vector field K is that the decomposition (2.17) remains the same under the flow generated by K. That is, the mode functions $\{u_{\boldsymbol{k}}(\mathsf{x}), u^*_{\boldsymbol{k}}(\mathsf{x})\}$ on a Cauchy surface Σ_0 will not be mixed on another surface Σ_1 after some time and therefore, the vacuum state defined by $\hat{a}_{\boldsymbol{k}}\,|0\rangle = 0$ will not change along the flow generated by K.

As a side note, the definition of positive/negative frequency modes given above is applicable only if timelike Killing vector fields exist. In a generic curved spacetime, there is no guarantee that such vector fields exist. Nevertheless, we can collect all possible elements in $\mathrm{Sol}_{\mathbb{C}}(\mathcal{M})$ that give a positive semi-definite Klein-Gordon product $(\cdot,\cdot)_{\mathrm{KG}}$ and claim such a subspace of $\mathrm{Sol}_{\mathbb{C}}(\mathcal{M})$ as $\mathcal{H}_{\mathrm{sol}}$. In QFT, the choice of $\mathcal{H}_{\mathrm{sol}}$ is not unique and thereby, the choice of vacuum is not unique.

States like $|0\rangle$ and $|1\rangle$, which we typically use in QFT, can be defined as states in the symmetric Fock space $\mathcal{F}_{\mathrm{s}}(\mathcal{H}_{\mathrm{sol}})$ of the Hilbert space $(\mathcal{H}_{\mathrm{sol}}, (\cdot,\cdot)_{\mathrm{KG}})$. The symmetric Fock

[3] Cauchy-completion with respect to $(\cdot,\cdot)_{\mathrm{KG}}$ is required to make $(\mathcal{H}_{\mathrm{sol}}, (\cdot,\cdot)_{\mathrm{KG}})$ a Hilbert space.

space is also a Hilbert space constructed as

$$\mathcal{F}_{\mathrm{s}}(\mathcal{H}_{\mathrm{sol}}) \coloneqq \bigoplus_{n=0}^{\infty} \mathcal{H}_{\mathrm{sol}}^{\otimes_{\mathrm{s}} n} = \mathbb{C} \oplus \mathcal{H}_{\mathrm{sol}} \oplus (\mathcal{H}_{\mathrm{sol}} \otimes_{\mathrm{s}} \mathcal{H}_{\mathrm{sol}}) \oplus \cdots , \tag{2.18}$$

where $\otimes_{\mathrm{s}}$ is the symmetric part of the tensor product $\otimes$ (symmetric because $\hat{\phi}$ is bosonic). Then, $|0\rangle \in \mathbb{C}$ (one-dimensional subspace), $|1\rangle \in \mathcal{H}_{\mathrm{sol}}$, and so on.

A simple example of a positive frequency mode can be seen in the scalar field in Minkowski spacetime. In the Minkowski coordinates (t, x, y, z), ∂_t is a Killing vector field. One can then consider positive frequency mode functions

$$u_{\boldsymbol{k}}(\mathsf{x}) = \frac{1}{\sqrt{(2\pi)^3 2\omega_{\boldsymbol{k}}}} e^{-\mathrm{i}\omega_{\boldsymbol{k}} t + \mathrm{i}\boldsymbol{k}\cdot\boldsymbol{x}} , \tag{2.19}$$

where $\omega_{\boldsymbol{k}} = \sqrt{|\boldsymbol{k}|^2 + m^2}$ with m being the mass of the scalar field. Therefore, the mode decomposition (2.8) reads

$$\hat{\phi}(\mathsf{x}) = \int_{\mathbb{R}^3} \frac{\mathrm{d}^3 k}{\sqrt{(2\pi)^3 2\omega_{\boldsymbol{k}}}} \left(\hat{a}_{\boldsymbol{k}} e^{-\mathrm{i}\omega_{\boldsymbol{k}} t + \mathrm{i}\boldsymbol{k}\cdot\boldsymbol{x}} + \hat{a}_{\boldsymbol{k}}^\dagger e^{\mathrm{i}\omega_{\boldsymbol{k}} t - \mathrm{i}\boldsymbol{k}\cdot\boldsymbol{x}} \right) , \tag{2.20}$$

and the Minkowski vacuum $|0_{\mathrm{M}}\rangle$ is defined as $\hat{a}_{\boldsymbol{k}} |0_{\mathrm{M}}\rangle = 0$ for all $\boldsymbol{k}$. One can easily check that $u_{\boldsymbol{k}}(\mathsf{x})$ is a positive frequency mode with respect to a timelike Killing vector field ∂_t.

Conformal vacuum

In certain cases, it is useful to introduce a different type of vacuum state called the *conformal vacuum*. This state applies when our spacetime is conformally related to another spacetime.

Let $(\mathcal{M}, g)$ and $(\tilde{\mathcal{M}}, \tilde{g})$ be two manifolds. These two are said to be conformally equivalent if the metrics are related by

$$\tilde{g}_{\mu\nu} = \Omega^2(\mathsf{x}) g_{\mu\nu} , \tag{2.21}$$

where $\Omega(\mathsf{x}) > 0$ is a smooth function. In particular, if $g_{\mu\nu}$ in above definition is flat (e.g., Minkowski metric $\eta_{\mu\nu}$) then $\tilde{g}_{\mu\nu}$ is said to be conformally flat, and any $(1+1)$-dimensional (pseudo-)Riemannian manifold is locally conformally flat, namely, one can always find $\Omega(\mathsf{x})$ such that $\tilde{g}_{\mu\nu} = \Omega^2(\mathsf{x})\eta_{\mu\nu}$ at each point in the spacetime. Note that the causal structures

of conformally related spacetimes are the same in the sense that if a vector v^μ on $g_{\mu\nu}$ is timelike (spacelike) then it is also timelike (spacelike) in $\tilde{g}_{\mu\nu}$.

Conformally related spacetimes are of particular interest in QFT in curved spacetime if the behavior of quantum fields is well-known in one of the two manifolds. For example, if $\tilde{g}$ is a conformally flat spacetime, then the behavior of a quantum field in $(\tilde{\mathcal{M}}, \tilde{g})$ can be approximately understood by considering QFT in Minkowski spacetime, since the two cases share some similarities due to the conformal flatness of $(\tilde{\mathcal{M}}, \tilde{g})$.

Consider two conformally related spacetimes in (2.21). Let $S_\phi[\hat{\phi}, g]$ be a quantized version of the action given by (2.1), and $S_{\tilde{\phi}}[\hat{\tilde{\phi}}, \tilde{g}]$ the action of another scalar field $\hat{\tilde{\phi}}$ on $\tilde{g}$. Then $S_{\tilde{\phi}}[\hat{\tilde{\phi}}, \tilde{g}]$ is said to be conformally invariant to $S_\phi[\hat{\phi}, g]$ if $S_{\tilde{\phi}}[\hat{\tilde{\phi}}, \tilde{g}] = S_\phi[\hat{\phi}, g]$. This means that the behavior of $\hat{\tilde{\phi}}$ on $\tilde{g}$ is the same as $\hat{\phi}$ on g. However, this does not always hold. One particular case in which two scalar field theories are conformally invariant is when we choose $m = 0$ and $\xi = (n-1)/4n$ in $(n+1)$-dimensional spacetime in (2.1). Such a coupling ξ is known as a conformal coupling. A massless, conformally coupled scalar field theory $S_{\tilde{\phi}}[\hat{\tilde{\phi}}, \tilde{g}]$ is conformally invariant to $S_\phi[\hat{\phi}, g]$ if $\hat{\tilde{\phi}}$ transforms as

$$\hat{\tilde{\phi}}(\mathsf{x}) = \Omega^{\frac{1-n}{2}}(\mathsf{x})\hat{\phi}(\mathsf{x})\,. \quad (n+1)\text{-dimension} \tag{2.22}$$

If we understand $\hat{\phi}$ in g to have a vacuum state $|0\rangle$, then the conformally invariant theory in $\tilde{g}$ can be obtained simply by multiplying $\Omega^{\frac{1-n}{2}}(\mathsf{x})$. The vacuum state $|\tilde{0}\rangle$ in $\tilde{g}$ can be obtained from $|0\rangle$ and this new vacuum $|\tilde{0}\rangle$ is called a conformal vacuum.

Correlation functions

One of the important quantities in entanglement harvesting is *the Wightman function*. Let ρ_ϕ be a quantum state of the field. Then the Wightman function (or two-point correlation function) $W(\mathsf{x}, \mathsf{x}') \in \mathbb{C}$ is defined as

$$W(\mathsf{x}, \mathsf{x}') \coloneqq \langle \hat{\phi}(\mathsf{x})\hat{\phi}(\mathsf{x}')\rangle_{\rho_\phi}\,. \tag{2.23}$$

In particular, if the field is in the vacuum state $\rho_\phi = |0\rangle\langle 0|$ then $W(\mathsf{x}, \mathsf{x}') = \langle 0|\hat{\phi}(\mathsf{x})\hat{\phi}(\mathsf{x}')|0\rangle$, which is sometimes referred to the vacuum two-point correlation function.

The Wightman function has three important properties:

(1) $W^*(\mathsf{x},\mathsf{x}') = W(\mathsf{x}',\mathsf{x})$,
(2) $\mathrm{Im}[W(\mathsf{x},\mathsf{x}')] = \frac{1}{2\mathsf{i}} \langle[\hat{\phi}(\mathsf{x}),\hat{\phi}(\mathsf{x}')]\rangle_{\rho_\phi}$,
(3) $\mathrm{Re}[W(\mathsf{x},\mathsf{x}')] = \frac{1}{2} \langle\{\hat{\phi}(\mathsf{x}),\hat{\phi}(\mathsf{x}')\}\rangle_{\rho_\phi}$.

The properties (2) and (3) are related to the causal relationship between two points x and x'. Micro-causality tells us that if x and x' are spacelike separated, then $[\hat{\phi}(\mathsf{x}),\hat{\phi}(\mathsf{x}')] = 0$. On the other hand, the anti-commutator $\{\hat{\phi}(\mathsf{x}),\hat{\phi}(\mathsf{x}')\}$ is non-zero in general. Therefore, the causal relations of x and x' are relevant to the value of the Wightman function, and it is useful to decompose it into the following form.

$$W(\mathsf{x},\mathsf{x}') = \frac{1}{2}W_{\mathrm{H}}(\mathsf{x},\mathsf{x}') + \frac{\mathsf{i}}{2}W_{\mathrm{PJ}}(\mathsf{x},\mathsf{x}')\,, \tag{2.24}$$

where $W_{\mathrm{H}}(\mathsf{x},\mathsf{x}')$ and $W_{\mathrm{PJ}}(\mathsf{x},\mathsf{x}')$ are *Hadamard* and *Pauli-Jordan* functions, respectively, defined as

$$W_{\mathrm{H}}(\mathsf{x},\mathsf{x}') \coloneqq 2\mathrm{Re}[W(\mathsf{x},\mathsf{x}')] = \langle\{\hat{\phi}(\mathsf{x}),\hat{\phi}(\mathsf{x}')\}\rangle_{\rho_\phi}\,, \tag{2.25}$$

$$W_{\mathrm{PJ}}(\mathsf{x},\mathsf{x}') \coloneqq 2\mathrm{Im}[W(\mathsf{x},\mathsf{x}')] = \frac{1}{\mathsf{i}}\langle[\hat{\phi}(\mathsf{x}),\hat{\phi}(\mathsf{x}')]\rangle_{\rho_\phi}\,. \tag{2.26}$$

We will use these functions in Sec. 2.3.

KMS state

The Kubo-Martin-Schwinger (KMS) state [59, 60, 61] is a generalized version of a thermal state (Gibbs state) that can be used in QFT. The rationale for defining this state is as follows. In quantum mechanics, the Gibbs state is given by

$$\rho_{\mathrm{th}} = \frac{1}{Z}e^{-\beta\hat{H}}\,, \tag{2.27}$$

where $Z \coloneqq \mathrm{Tr}[e^{-\beta\hat{H}}]$ is the partition function, $\beta \coloneqq 1/T$ is the inverse temperature of the bath, and $\hat{H}$ is the Hamiltonian of the bath. This is well-defined as long as the trace, $\mathrm{Tr}[\cdot]$, is well-defined. If the Hamiltonian allows eigenbases $\{|n\rangle\}$, then the trace can be concretely evaluated by $\mathrm{Tr}[\hat{A}] = \sum_n \langle n|\hat{A}|n\rangle$. However, this is tricky when it comes to the thermal state of a quantum field due to the fact that the Hilbert space of a field is, in general, non-separable (i.e., the basis is uncountable), and therefore a trace is ill-defined. In other words, $\mathrm{Tr}[\cdot] < \infty$ is not guaranteed.

One can generalize the notion of thermality to non-separable Hilbert spaces by extracting the essential features of the thermal state $\rho_{\rm th}$ in quantum mechanics. For any (bounded) operator $\hat{A}(t), \hat{B}(t)$ in the Heisenberg picture, the Gibbs state $\rho_{\rm th}$ always satisfies

$$\langle \hat{A}(0)\hat{B}(t+\mathrm{i}\beta)\rangle_{\rho_{\rm th}} = \langle \hat{B}(t)\hat{A}(0)\rangle_{\rho_{\rm th}} \ , \tag{2.28}$$

where $\hat{B}(t) = \hat{U}^\dagger(t)\hat{B}\hat{U}(t)$ is a time-evolved operator. Here, we used the definition $\langle \hat{A}\rangle_\rho := \mathrm{Tr}[\hat{A}\rho]$ and its cyclic property $\mathrm{Tr}[\hat{A}\hat{B}\hat{C}] = \mathrm{Tr}[\hat{B}\hat{C}\hat{A}] = \mathrm{Tr}[\hat{C}\hat{A}\hat{B}]$. In a nutshell, we employ the equality (2.28) as an axiom for thermality and call this the KMS condition.[4]

More specifically, let $\hat{H}$ be a Hamiltonian that is a generator of time-translation parametrized by t. ρ is a KMS state with respect to time t if the following conditions are satisfied.

(i) The expectation values $\langle \hat{A}\hat{B}(z)\rangle_\rho$ and $\langle \hat{B}(z)\hat{A}\rangle_\rho$, where $z \in \mathbb{C}$, are holomorphic (i.e., no poles) in $0 < \mathrm{Im}[z] < \beta$ and $-\beta < \mathrm{Im}[z] < 0$, respectively.
(ii) Eq. (2.28) is satisfied for $\beta > 0$.

The basic idea of condition (i) is to make both sides of (2.28) well-defined quantities (i.e., they converge in the respective regions) in the complex plane. Then, condition (ii) just states that we adopt (2.28) as the definition of thermality in a generic system.

It is crucial that the KMS condition is compatible with the Gibbs state in quantum mechanics [63]. That is, if the Hilbert space of a system is separable, then the KMS condition uniquely recovers the Gibbs state $\rho_{\rm th}$.

In this thesis, we are particularly interested in the Wightman function, $W_\rho(\mathsf{x},\mathsf{x}') = \langle \hat{\phi}(\mathsf{x})\hat{\phi}(\mathsf{x}')\rangle_\rho$. Let $W_\rho(\tau,\tau') \equiv \langle \hat{\phi}(\mathsf{x}(\tau))\hat{\phi}(\mathsf{x}'(\tau'))\rangle_\rho$ be the pullback of the Wightman function along a trajectory $\mathsf{x}(\tau) = (t(\tau), \boldsymbol{x}(\tau))$. If ρ is a KMS state with respect to τ then $W_\rho(\tau,\tau')$ satisfies [64]:

- Time-translational invariance with respect to τ: $W_\rho(\tau,\tau') = W_\rho(\Delta\tau)$;
- $W_\rho(\Delta\tau + \mathrm{i}\beta) = W_\rho(-\Delta\tau)$.

[4] The KMS condition is formally stated using the language of C^*-algebra, which we will not explore in depth. See [62, 63] for details.

2.2 Unruh-DeWitt particle detector model

We are interested in the scenario where quantum-mechanical atoms interact with a quantum field. As a realistic example, one can think of an atom (such as a Hydrogen atom) coupled to photons. In relativistic quantum information (RQI), such systems are commonly modeled by the so-called Unruh-DeWitt (UDW) particle detector model coupled to a quantum scalar field [15, 16]. In the literature, people use two types of UDW detectors: monopole and harmonic-oscillator type detectors. The monopole-type UDW detector consists of ground and excited states, $|g\rangle$ and $|e\rangle$ respectively, so it can be thought of as a qubit interacting with a quantum field. On the other hand, the harmonic oscillator-type UDW detector is described by the Hamiltonian for a harmonic oscillator and it can be thought of as a multi-level atom interacting with a quantum field. The benefit of using harmonic oscillator-type detectors is that one can solve the Heisenberg equation of motion and examine the back-reaction effect of the detectors on the field (see for example [65]).

Here, we will employ the monopole-type UDW detectors. We denote the ground and excited states for detector-j (say, detector-A, B, C) by $|g_j\rangle$ and $|e_j\rangle$, respectively, with the energy gap Ω_j between them in each detector's reference frame.

2.2.1 Single detector

Consider a single UDW detector linearly coupled to the scalar quantum field. In the Schrödinger picture, the total Hamiltonian, $\hat{H}_{\rm S,tot}$ is given by [66, 67]

$$\hat{H}_{\rm S,tot} = \hat{H}_{\rm S,d0} + \hat{H}_{\rm S,\phi 0} + \hat{H}_{\rm S,int}\,, \tag{2.29}$$

where

$$\hat{H}_{\rm S,d0} = \Omega \hat{\sigma}^+ \hat{\sigma}^- \otimes \mathbb{1}_\phi\,, \tag{2.30a}$$

$$\hat{H}_{\rm S,int} = \lambda \chi(\tau)(\hat{\sigma}^+ + \hat{\sigma}^-) \otimes \hat{\phi}(\boldsymbol{x}(\tau))\,, \tag{2.30b}$$

with $\hat{\sigma}^+ \equiv |e\rangle\langle g|$ and $\hat{\sigma}^- \equiv |g\rangle\langle e|$ being the raising and lowering operators, respectively, acting on the Hilbert space of the UDW detector, $\mathcal{H}_{\rm d}$.

Let us now transform the Hamiltonians from the Schrödinger picture to the interaction picture. In general, given that $\hat{H}_{\rm S,tot} = \hat{H}_{\rm S,0} + \hat{H}_{\rm S,int}$, an operator $\hat{A}_{\rm S}$ in the Schrödinger picture can be transformed into an operator $\hat{A}_{\rm I}$ in the interaction picture by

$$\hat{A}_{\rm I}(t) = \hat{U}_0^\dagger \hat{A}_{\rm S} \hat{U}_0\,, \tag{2.31}$$

where

$$\hat{U}_0 = \mathcal{T}_t \exp\left(-\mathsf{i}\int_{\mathbb{R}} \mathrm{d}t\, \hat{H}_{\mathrm{S},0}\right) , \tag{2.32}$$

with $\mathcal{T}_t$ being a time-ordering symbol with respect to t. In our case, $\hat{H}_{\mathrm{S},0}$ corresponds to $\hat{H}_{\mathrm{S,d}0} + \hat{H}_{\mathrm{S},\phi 0}$ and therefore, the interaction Hamiltonian in the interaction picture, $\hat{H}_{\mathrm{I}}$ can be obtained by

$$\begin{aligned}
\hat{H}^{\tau}_{\mathrm{I}}(\tau) &= \hat{U}_0^{\dagger}\hat{H}_{\mathrm{S,int}}\hat{U}_0 && (2.33)\\
&= \lambda\chi(\tau)e^{\mathsf{i}\hat{H}_{\mathrm{S,d}0}t}(\hat{\sigma}^{+} + \hat{\sigma}^{-})e^{-\mathsf{i}\hat{H}_{\mathrm{S,d}0}t} \otimes e^{\mathsf{i}\hat{H}_{\mathrm{S},\phi 0}t}\hat{\phi}(\boldsymbol{x})e^{-\mathsf{i}\hat{H}_{\mathrm{S},\phi 0}t} && (2.34)\\
&= \lambda\chi(\tau)\hat{m}(\tau) \otimes \hat{\phi}(\mathsf{x}(\tau)) , && (2.35)
\end{aligned}$$

where

$$\hat{m}(\tau) \equiv e^{\mathsf{i}\Omega\tau}\hat{\sigma}^{+} + e^{-\mathsf{i}\Omega\tau}\hat{\sigma}^{-} \tag{2.36}$$

is the monopole moment in the interaction picture. The superscript τ in $\hat{H}^{\tau}_{\mathrm{I}}(\tau)$ indicates that it is a generator of time-translation with respect to τ. The field operator $\hat{\phi}$ is defined along a trajectory of the detector $\mathsf{x}(\tau)$ (i.e., it is a pullback of the field operator along the trajectory). Therefore, the detector is *locally* interacting with the field at its location.

Before proceeding to a perturbative analysis, let us comment on modified versions of UDW detectors. The qubit-type UDW detector model we have introduced so far has no size, and it is often called a pointlike UDW detector. One may think of a UDW detector with a finite size. This can be implemented in the formulation by introducing a smearing function, which specifies the size and shape of the detector. Although we will use only pointlike detectors in this thesis, readers who are interested can refer to [66, 67, 68]

2.2.2 Two detectors

Let us now consider two pointlike UDW detectors A and B. In this case, the whole Hilbert space can be written as $\mathcal{H}_{\mathrm{A}} \otimes \mathcal{H}_{\mathrm{B}} \otimes \mathcal{H}_{\phi}$. The interaction Hamiltonian describing both detectors is given by

$$\hat{H}^{t}_{\mathrm{I}}(t) = \frac{\mathrm{d}\tau_{\mathrm{A}}}{\mathrm{d}t}\hat{H}^{\tau_{\mathrm{A}}}_{\mathrm{A}}(\tau_{\mathrm{A}}(t)) \otimes \mathbb{1}_{\mathrm{B}} + \mathbb{1}_{\mathrm{A}} \otimes \frac{\mathrm{d}\tau_{\mathrm{B}}}{\mathrm{d}t}\hat{H}^{\tau_{\mathrm{B}}}_{\mathrm{B}}(\tau_{\mathrm{B}}(t)) , \tag{2.37}$$

where

$$\hat{H}^{\tau_j}_{j}(\tau_j) = \lambda_j\chi_j(\tau_j)\hat{m}_j(\tau_j) \otimes \hat{\phi}(\mathsf{x}_j(\tau_j)) \,.\; j \in \{\mathrm{A},\mathrm{B}\} \tag{2.38}$$

Notice that we have three variables representing time: $\tau_{\rm A}, \tau_{\rm B}$, and t. Since the proper time τ_j only parametrizes detector-j's trajectory, we used a common time t to write the total interaction Hamiltonian, $\hat{H}^t_{\rm I}(t)$. In what follows, we assume that the coupling constant λ_j and the energy gap Ω_j for the both detectors are the same: $\lambda \equiv \lambda_{\rm A} = \lambda_{\rm B}$, $\Omega \equiv \Omega_{\rm A} = \Omega_{\rm B}$.

The time-evolution operator $\hat{U}_{\rm I}$ in the interaction picture is known to be

$$\hat{U}_{\rm I} = \mathcal{T}_t \exp\left(-\mathsf{i}\int_{\mathbb{R}} \mathrm{d}t\, \hat{H}^t_{\rm I}(t)\right), \tag{2.39}$$

where $\mathcal{T}_t$ is a time-ordering symbol with respect to t [66, 67]. We emphasize that this time-ordering is performed in terms of the common time t, rather than proper times τ_j since t specifies both the detectors' time. One can perform the Dyson series expansion by assuming the coupling constant λ is small:[5]

$$\hat{U}_{\rm I} = \mathbb{1} + \hat{U}^{(1)}_{\rm I} + \hat{U}^{(2)}_{\rm I} + \mathcal{O}(\lambda^3)\,, \tag{2.40a}$$

$$\hat{U}^{(1)}_{\rm I} = -\mathsf{i}\int_{-\infty}^{\infty} \mathrm{d}t\, \hat{H}^t_{\rm I}(t)\,, \tag{2.40b}$$

$$\hat{U}^{(2)}_{\rm I} = -\int_{-\infty}^{\infty} \mathrm{d}t_1 \int_{-\infty}^{t_1} \mathrm{d}t_2\, \hat{H}^t_{\rm I}(t_1)\hat{H}^t_{\rm I}(t_2)\,. \tag{2.40c}$$

Let ρ_0 be the initial state of the whole system (i.e., two UDW detectors and the field). The final state $\rho_{\rm tot}$ for the total system is then

$$\begin{aligned}\rho_{\rm tot} &= \hat{U}_{\rm I}\rho_0\hat{U}^\dagger_{\rm I} \\ &= \rho_0 + \rho^{(0,1)} + \rho^{(1,0)} + \rho^{(1,1)} + \rho^{(2,0)} + \rho^{(0,2)} + \mathcal{O}(\lambda^3)\,,\end{aligned} \tag{2.41}$$

where $\rho^{(i,j)} = \hat{U}^{(i)}_{\rm I}\rho_0\hat{U}^{(j)\dagger}_{\rm I}$. Since $\hat{U}^{(j)}_{\rm I}$ contains λ^j, $\rho^{(i,j)}$ is a λ^{i+j} term in the expansion. In particular, if one chooses the initial state to be $\rho_0 = \rho_{\rm AB,0} \otimes |0\rangle\langle 0|$, where $|0\rangle$ is a vacuum state of the quantum field, then the odd-power terms of λ vanish in $\rho_{\rm tot}$ [28]:

$$\rho_{\rm tot} = \rho_0 + \rho^{(1,1)} + \rho^{(2,0)} + \rho^{(0,2)} + \mathcal{O}(\lambda^4)\,. \tag{2.42}$$

Let us further assume that the detectors are both initially in their ground state: $\rho_{\rm AB,0} = |g_{\rm A}\rangle\langle g_{\rm A}| \otimes |g_{\rm B}\rangle\langle g_{\rm B}|$. One can then explicitly calculate each $\rho^{(i,j)}$ and obtains the final density matrix of the detectors, $\rho_{\rm AB}$, by tracing out the field degree of freedom: $\rho_{\rm AB} =$

[5] In natural units, λ has units of $[\text{Length}]^{(n-3)/2}$ in $(n+1)$-dimensional spacetime when detectors are linearly coupled to the field. Therefore, one needs to make this a unitless quantity $\tilde{\lambda} := \lambda\sigma^{-(n-3)/2}$, where σ is a length scale, and then make an assumption that $\tilde{\lambda} \ll 1$.

$\mathrm{Tr}_\phi[\rho_{\mathrm{tot}}]$. In the basis $\{|g_{\mathrm{A}}g_{\mathrm{B}}\rangle, |g_{\mathrm{A}}e_{\mathrm{B}}\rangle, |e_{\mathrm{A}}g_{\mathrm{B}}\rangle, |e_{\mathrm{A}}e_{\mathrm{B}}\rangle\}$, namely, $|g_{\mathrm{A}}, g_{\mathrm{B}}\rangle = [1,0,0,0]^\top$, $|g_{\mathrm{A}}, e_{\mathrm{B}}\rangle = [0,1,0,0]^\top$, $|e_{\mathrm{A}}, g_{\mathrm{B}}\rangle = [0,0,1,0]^\top$, and $|e_{\mathrm{A}}, e_{\mathrm{B}}\rangle = [0,0,0,1]^\top$, the final density matrix for the detectors, ρ_{AB}, reads (see Appendix A)

$$\rho_{\mathrm{AB}} = \begin{bmatrix} 1-P_{\mathrm{A}}-P_{\mathrm{B}} & 0 & 0 & X^*_{\mathrm{AB}} \\ 0 & P_{\mathrm{B}} & C^*_{\mathrm{AB}} & 0 \\ 0 & C_{\mathrm{AB}} & P_{\mathrm{A}} & 0 \\ X_{\mathrm{AB}} & 0 & 0 & 0 \end{bmatrix} + \mathcal{O}(\lambda^4) \tag{2.43}$$

where

$$P_j = \lambda^2 \int_{\mathbb{R}} \mathrm{d}\tau_j \int_{\mathbb{R}} \mathrm{d}\tau'_j \, \chi_j(\tau_j)\chi_j(\tau'_j) e^{-\mathrm{i}\Omega(\tau_j - \tau'_j)} W(\mathsf{x}_j(\tau_j), \mathsf{x}_j(\tau'_j)) \,, \tag{2.44a}$$

$$C_{\mathrm{AB}} = \lambda^2 \int_{\mathbb{R}} \mathrm{d}\tau_{\mathrm{A}} \int_{\mathbb{R}} \mathrm{d}\tau_{\mathrm{B}} \, \chi_{\mathrm{A}}(\tau_{\mathrm{A}})\chi_{\mathrm{B}}(\tau_{\mathrm{B}}) e^{-\mathrm{i}\Omega(\tau_{\mathrm{A}} - \tau_{\mathrm{B}})} W(\mathsf{x}_{\mathrm{A}}(\tau_{\mathrm{A}}), \mathsf{x}_{\mathrm{B}}(\tau_{\mathrm{B}})) \,, \tag{2.44b}$$

$$\begin{aligned} X_{\mathrm{AB}} = -\lambda^2 \int_{\mathbb{R}} \mathrm{d}\tau_{\mathrm{A}} \int_{\mathbb{R}} \mathrm{d}\tau_{\mathrm{B}} \, \chi_{\mathrm{A}}(\tau_{\mathrm{A}})\chi_{\mathrm{B}}(\tau_{\mathrm{B}}) e^{\mathrm{i}\Omega(\tau_{\mathrm{A}} + \tau_{\mathrm{B}})} \\ \times \Big[\Theta(t(\tau_{\mathrm{A}}) - t(\tau_{\mathrm{B}})) W(\mathsf{x}_{\mathrm{A}}(\tau_{\mathrm{A}}), \mathsf{x}_{\mathrm{B}}(\tau_{\mathrm{B}})) + \Theta(t(\tau_{\mathrm{B}}) - t(\tau_{\mathrm{A}})) W(\mathsf{x}_{\mathrm{B}}(\tau_{\mathrm{B}}), \mathsf{x}_{\mathrm{A}}(\tau_{\mathrm{A}})) \Big] \,, \end{aligned} \tag{2.44c}$$

where $\Theta(t)$ is the Heaviside step function and the quantity $W(\mathsf{x},\mathsf{y}) \coloneqq \langle 0| \hat{\phi}(\mathsf{x})\hat{\phi}(\mathsf{y}) |0\rangle$ is the Wightman function (i.e., vacuum two-point correlation function). The elements P_j, $j \in \{\mathrm{A},\mathrm{B}\}$ are known as transition probabilities (or response functions) from the ground $|g_j\rangle$ to excited $|e_j\rangle$ states. The off-diagonal elements X_{AB} and C_{AB} contribute to bipartite entanglement and quantum mutual information, respectively.

We point out that one has to pay sufficient attention to the Heaviside step functions in X_{AB}. Notice that the integrals are defined in terms of the proper times τ_j, but the argument of the Heaviside step function is of the form $t(\tau)$. This means that one needs to know the relationship between the common time t and the proper times: $t = t(\tau)$. One simple example is when the trajectory of each detector is given by $\mathsf{x}_{\mathrm{A}} = (\gamma_{\mathrm{A}}\tau_{\mathrm{A}}, \boldsymbol{x}_{\mathrm{A}})$ and $\mathsf{x}_{\mathrm{B}} = (\gamma_{\mathrm{B}}\tau_{\mathrm{B}}, \boldsymbol{x}_{\mathrm{B}})$, where γ_j is the redshift factor. In this case,

$$\Theta(t(\tau_{\mathrm{A}}) - t(\tau_{\mathrm{B}})) = \Theta(\gamma_{\mathrm{A}}\tau_{\mathrm{A}} - \gamma_{\mathrm{B}}\tau_{\mathrm{B}}) \,, \tag{2.45}$$

and so the double integral containing this particular Heaviside step function reads

$$\int_{\mathbb{R}} \mathrm{d}\tau_{\mathrm{A}} \int_{\mathbb{R}} \mathrm{d}\tau_{\mathrm{B}} \, \Theta(t(\tau_{\mathrm{A}}) - t(\tau_{\mathrm{B}})) = \int_{\mathbb{R}} \mathrm{d}\tau_{\mathrm{A}} \int_{-\infty}^{(\gamma_{\mathrm{A}}/\gamma_{\mathrm{B}})\tau_{\mathrm{A}}} \mathrm{d}\tau_{\mathrm{B}} \,. \tag{2.46}$$

Of course, in general, the argument of the Heaviside step function could be very complicated. In this thesis, this will be the case when we deal with detectors freely falling into a black hole.

In summary, the calculations provided above state as follows. First, we initially ($t \to -\infty$) prepare two UDW detectors in the ground state and assume that the field is in a vacuum state. At this stage, there is no correlation at all. Then the detectors are turned on according to their switching functions $\chi_j(\tau_j)$ so that they locally interact with the quantum field. At some point the interaction is turned off, and we obtain the final state of the detectors ρ_{AB}, which may be entangled with each other.

2.2.3 Three detectors

Finally, consider three UDW detectors, A, B, and C. One can obtain the final density matrix ρ_{ABC} of the detectors in the same way as before. The interaction Hamiltonian $\hat{H}_{\mathrm{I}}^{t}(t)$ for the three detectors is

$$\begin{aligned}&\hat{H}_{\mathrm{I}}^{t}(t)\\&=\frac{\mathrm{d}\tau_{\mathrm{A}}}{\mathrm{d}t}\hat{H}_{\mathrm{A}}^{\tau_{\mathrm{A}}}(\tau_{\mathrm{A}}(t))\otimes\mathbb{1}_{\mathrm{B}}\otimes\mathbb{1}_{\mathrm{C}}+\mathbb{1}_{\mathrm{A}}\otimes\frac{\mathrm{d}\tau_{\mathrm{B}}}{\mathrm{d}t}\hat{H}_{\mathrm{B}}^{\tau_{\mathrm{B}}}(\tau_{\mathrm{B}}(t))\otimes\mathbb{1}_{\mathrm{C}}+\mathbb{1}_{\mathrm{A}}\otimes\mathbb{1}_{\mathrm{B}}\otimes\frac{\mathrm{d}\tau_{\mathrm{C}}}{\mathrm{d}t}\hat{H}_{\mathrm{C}}^{\tau_{\mathrm{C}}}(\tau_{\mathrm{C}}(t))\,.\end{aligned}\tag{2.47}$$

Assume that the detectors are all initially in their ground states and the field is in the vacuum $|0\rangle$. The initial density operator is

$$\rho_0=|g\rangle_{\mathrm{A}}\langle g|\otimes|g\rangle_{\mathrm{B}}\langle g|\otimes|g\rangle_{\mathrm{C}}\langle g|\otimes|0\rangle\langle 0|\,,\tag{2.48}$$

and the time-evolution operator $\hat{U}_{\mathrm{I}}$ (2.39) gives us the final density operator:

$$\rho_{\mathrm{ABC}}=\mathrm{Tr}_{\phi}[\rho_{\mathrm{tot}}]=\mathrm{Tr}_{\phi}[\hat{U}_{\mathrm{I}}\rho_0\hat{U}_{\mathrm{I}}^{\dagger}]\,.\tag{2.49}$$

Introducing the basis $\{|g_{\mathrm{A}}g_{\mathrm{B}}g_{\mathrm{C}}\rangle, |g_{\mathrm{A}}g_{\mathrm{B}}e_{\mathrm{C}}\rangle, |g_{\mathrm{A}}e_{\mathrm{B}}g_{\mathrm{C}}\rangle, |e_{\mathrm{A}}g_{\mathrm{B}}g_{\mathrm{C}}\rangle, |g_{\mathrm{A}}e_{\mathrm{B}}e_{\mathrm{C}}\rangle, |e_{\mathrm{A}}g_{\mathrm{B}}e_{\mathrm{C}}\rangle, |e_{\mathrm{A}}e_{\mathrm{B}}g_{\mathrm{C}}\rangle, |e_{\mathrm{A}}e_{\mathrm{B}}e_{\mathrm{C}}\rangle\}$, namely, $|g_{\mathrm{A}}g_{\mathrm{B}}g_{\mathrm{C}}\rangle=[1,0,0,0,0,0,0,0]^{\top}$, $|g_{\mathrm{A}}g_{\mathrm{B}}e_{\mathrm{C}}\rangle=[0,1,0,0,0,0,0,0]^{\top},\cdots$, ρ_{ABC} takes the form [32]

$$\rho_{\mathrm{ABC}}=\begin{bmatrix}r_{11}&0&0&0&r_{51}^{*}&r_{61}^{*}&r_{71}^{*}&0\\0&r_{22}&r_{32}^{*}&r_{42}^{*}&0&0&0&r_{82}^{*}\\0&r_{32}&r_{33}&r_{43}^{*}&0&0&0&r_{83}^{*}\\0&r_{42}&r_{43}&r_{44}&0&0&0&r_{84}^{*}\\r_{51}&0&0&0&r_{55}&r_{65}^{*}&r_{75}^{*}&0\\r_{61}&0&0&0&r_{65}&r_{66}&r_{76}^{*}&0\\r_{71}&0&0&0&r_{75}&r_{76}&r_{77}&0\\0&r_{82}&r_{83}&r_{84}&0&0&0&r_{88}\end{bmatrix},\tag{2.50}$$

with a constraint $\sum_i r_{ii} = 1$. Here, r^*_{ij} is a complex conjugate of $r_{ij} \in \mathbb{C}$ and $r_{ii} \in \mathbb{R}$. Note that ρ_{ABC} takes this form even before applying the perturbative expansion. For our perturbative analysis, ρ_{ABC} to the leading order in λ reads

$$\rho_{\mathrm{ABC}} = \begin{bmatrix} 1-(P_{\mathrm{A}}+P_{\mathrm{B}}+P_{\mathrm{C}}) & 0 & 0 & 0 & X^*_{\mathrm{BC}} & X^*_{\mathrm{AC}} & X^*_{\mathrm{AB}} & 0 \\ 0 & P_{\mathrm{C}} & C^*_{\mathrm{BC}} & C^*_{\mathrm{AC}} & 0 & 0 & 0 & 0 \\ 0 & C_{\mathrm{BC}} & P_{\mathrm{B}} & C^*_{\mathrm{AB}} & 0 & 0 & 0 & 0 \\ 0 & C_{\mathrm{AC}} & C_{\mathrm{AB}} & P_{\mathrm{A}} & 0 & 0 & 0 & 0 \\ X_{\mathrm{BC}} & 0 & 0 & 0 & 0 & 0 & 0 & 0 \\ X_{\mathrm{AC}} & 0 & 0 & 0 & 0 & 0 & 0 & 0 \\ X_{\mathrm{AB}} & 0 & 0 & 0 & 0 & 0 & 0 & 0 \\ 0 & 0 & 0 & 0 & 0 & 0 & 0 & 0 \end{bmatrix} + \mathcal{O}(\lambda^4)\,, \tag{2.51}$$

where P_j, C_{jk}, and X_{jk} are the same as (2.44).

One can obtain the reduced bipartite density matrices $\rho_{\mathrm{AB}}, \rho_{\mathrm{BC}}$, and ρ_{CA}, by tracing out one of the detectors:

$$\rho_{jk} = \begin{bmatrix} 1-P_j-P_k & 0 & 0 & X^*_{jk} \\ 0 & P_k & C^*_{jk} & 0 \\ 0 & C_{jk} & P_j & 0 \\ X_{jk} & 0 & 0 & 0 \end{bmatrix} + \mathcal{O}(\lambda^4)\,. \tag{2.52}$$

To make sure that the density matrix ρ_{ABC} given by (2.51) is an actual density matrix, one needs to impose some conditions. That is, a density matrix has to be hermitian with $\mathrm{Tr}[\rho_{\mathrm{AB}}] = 1$, and all the eigenvalues of ρ_{ABC} are positive. The first two conditions are already satisfied by construction, though the positivity of eigenvalues is yet to be imposed. However, some of the eigenvalues of ρ_{ABC} cannot be analytically obtained. Instead, if we simplify this density matrix by setting

$$C_{\mathrm{AB}} = C_{\mathrm{BC}} = C_{\mathrm{CA}} \equiv C\,, \tag{2.53a}$$
$$X_{\mathrm{AB}} = X_{\mathrm{BC}} = X_{\mathrm{CA}} \equiv X\,, \tag{2.53b}$$
$$P_{\mathrm{A}} = P_{\mathrm{B}} = P_{\mathrm{C}} \equiv P\,, \tag{2.53c}$$

and assuming $C \in \mathbb{R}$, the positivity conditions read

$$P \geq C\,, \tag{2.54a}$$
$$2C + P \geq 0\,, \tag{2.54b}$$
$$\frac{1}{2}\left(1 - 3P \pm \sqrt{(1-3P)^2 + 12|X|^2}\right) \geq 0\,. \tag{2.54c}$$

We will use these conditions in Sec. 2.4.2.

We point out that the calculations provided above are all within perturbation theory. However, one can carry out non-perturbative approaches by sacrificing some aspects of UDW detectors. As an example, the *delta-switching approach* [69] employs smeared UDW detectors with $\chi_j(\tau_j) = \delta(\tau_j/\eta_j)$, where η_j is a constant with a dimension of time. Physically, such a switching function corresponds to an instantaneous interaction, i.e., the detectors interact with the field just for a moment. Such treatment allows us to use a non-perturbative analysis since it removes the time-ordering symbol, $\mathcal{T}_t$, in the time-evolution operator $\hat{U}_{\rm I}$ in (2.39). However, unlike other kinds of switching, two delta-switched detectors are unable to extract entanglement from the field if each of them switches once [69, 70, 71] (but other types of correlation can be extracted [72]). Here are other references using the delta-switching approach: [73, 74, 75, 76, 77, 13, 78].

Another non-perturbative approach is the *gapless detector approach* (also known as the *degenerate detector approach*), which sets the energy of a UDW detector to be $\Omega = 0$. If one instead uses the Magnus expansion of (2.39), the higher-order terms will all vanish because of this. Note that this approach uses a pointlike UDW detector with an arbitrary switching function $\chi(\tau)$. As in the delta-switching approach, the gapless detectors also cannot extract entanglement from the field [70, 71]. See other references such as [11, 12, 79].

2.3 Entanglement harvesting in a nutshell

As mentioned earlier, entanglement harvesting (or broadly, correlation harvesting) is a protocol, where one employs multiple UDW detectors and extracts entanglement from a quantum field. Specifically, initially uncorrelated UDW detectors become entangled at the end of the operation. This is due to the fact that a quantum field is already an entangled state even in its vacuum. Although the harvesting protocol primarily considers a relativistic quantum field, a quantum mechanical system such as a chain of coupled harmonic oscillators allows probes to be entangled. Here, we first show how entanglement harvesting works by looking at a chain of harmonic oscillators, and then extend this to a relativistic quantum field theory.

Consider a chain of coupled harmonic oscillators in one dimension, in which the system is governed by a Hamiltonian,

$$\hat{H}_{\rm tot} = \hat{H}_0 + \hat{H}_{\rm int}\,, \tag{2.55}$$

where $\hat{H}_0$ is the free Hamiltonian and $\hat{H}_{\rm int}$ is the interaction Hamiltonian of the form

$$\hat{H}_0 = \sum_i \hat{H}_0^{(i)} \equiv \sum_i \frac{\hat{p}_i^2}{2m}\,, \tag{2.56}$$

$$\hat{H}_{\rm int} = \frac{1}{2}\sum_i k_{\rm s}(\hat{x}_{i+1} - \hat{x}_i)^2\,, \tag{2.57}$$

where m and $k_{\rm s}$ are the mass and spring constant of a harmonic oscillator. One notices that the free and the interaction Hamiltonians do not commute, $[\hat{H}_0, \hat{H}_{\rm int}] \neq 0$, which leads to $[\hat{H}_{\rm tot}, \hat{H}_0] \neq 0$, and so they cannot be simultaneously diagonalized. Consequently, the harmonic chain is in an entangled state, even in its vacuum. To see this, let $|0_i\rangle$ be a vacuum state of the i-th harmonic oscillator, $\hat{H}_0^{(i)}$. Assuming each harmonic oscillator is in the vacuum state, the fact $[\hat{H}_{\rm tot}, \hat{H}_0] \neq 0$ leads to

$$|0\rangle \neq \bigotimes_k |0_k\rangle\ , \tag{2.58}$$

where $|0\rangle$ is the vacuum state of the total Hamiltonian. Then, the density matrix of a joint system of the i-th and j-th sites, $\rho_{i,j}$ is a non-separable state:

$$\rho_{i,j} = {\rm Tr}_{k\neq i,j}[|0\rangle\langle 0|] \tag{2.59}$$

$$\neq {\rm Tr}_{k\neq i,j}\left[\,|0_1, 0_2, \cdots\rangle\langle 0_1, 0_2, \cdots|\,\right] \tag{2.60}$$

$$= |0_i\rangle\langle 0_i| \otimes |0_j\rangle\langle 0_j|\ . \tag{2.61}$$

Since this is true for any other sites, we say the chain is entangled even in a vacuum state due to $[\hat{H}_{\rm tot}, \hat{H}_0] \neq 0$. Therefore, if one brings a probe (such as a UDW detector) and lets it interact with one of the sites, the probe and the chain become entangled. Subsequently, if another probe interacts with a different site, the second probe entangles with the chain and hence, the two probes entangle with each other. Note that this is due to the pre-existent entanglement in the chain.

This argument can be extended to quantum fields since a quantum field can be thought of as a continuum limit of a harmonic chain [80]. In addition, the fact that QFT is compatible with Relativity allows us to examine how causality affects entanglement harvesting. For example, two causally disconnected UDW detectors still can be entangled, thanks to the pre-existed entanglement in the field. One can mathematically see this from the Wightman function [30]. Recall that the Wightman function $W(\mathsf{x},\mathsf{x}')$ can be decomposed into the Pauli-Jordan and the Hadamard functions [see (2.24)]:

$$W(\mathsf{x},\mathsf{x}') = \frac{1}{2}W_{\rm H}(\mathsf{x},\mathsf{x}') + \frac{\mathsf{i}}{2}W_{\rm PJ}(\mathsf{x},\mathsf{x}')\,. \tag{2.62}$$

The Pauli-Jordan function, $W_{\rm PJ}(\mathsf{x},\mathsf{x}')$, is the commutator part in the Wightman function (i.e., $W_{\rm PJ}(\mathsf{x},\mathsf{x}') \sim \langle[\hat{\phi}(\mathsf{x}),\hat{\phi}(\mathsf{x}')]\rangle_\rho$). Therefore, if two points x and x' are spacelike then micro-causality tells you that $W_{\rm PJ}(\mathsf{x},\mathsf{x}')=0$. In the context of entanglement harvesting, this tells you that if two UDW detectors cannot communicate at all, then $W_{\rm PJ}(\mathsf{x},\mathsf{x}')$ does not contribute at all. However, the Hadamard function, $W_{\rm H}(\mathsf{x},\mathsf{x}')$, is non-vanishing even if x,x' are spacelike, and so two causally disconnected detectors are able to be entangled. Of course, if detectors can communicate through a quantum field then the Pauli-Jordan function also contributes to $P_j, X_{\rm AB}$, and $C_{\rm AB}$ in (2.43).

We now comment on the term 'harvesting' in the literature. Some papers implicitly claim that entanglement is 'harvested' if two detectors entangle at the end of a procedure, regardless of how much of the entanglement is coming from $W_{\rm H}$ and $W_{\rm PJ}$. In this sense, their claim can be summarized as 'entanglement is said to be harvested if it comes from the Wightman function $W(\mathsf{x},\mathsf{x}')$'. On the other hand, Ref. [30] claims that 'entanglement is said to be harvested if it comes purely from the Hadamard function $W_{\rm H}(\mathsf{x},\mathsf{x}')$'. This is due to the fact that the Pauli-Jordan function is state-independent; Since it does not depend on the state of the field ρ_ϕ, detectors still can be entangled even if ρ_ϕ does not contain any entanglement, which defeats the idea of 'extraction of the *pre-existing* entanglement from a quantum field'. In contrast, the Hadamard function is state-dependent, so the only way to acquire entanglement from the entanglement pre-existing in the field is through this function.

For this reason, it is important to know where the correlation comes from. First, let us define the term 'communication' or 'signaling' as follows (see also [81]).

Terminology: communication and signaling
We say detector-A is *communicating* or *signaling* to detector-B if the Pauli-Jordan contribution in $C_{\rm AB}$ and $X_{\rm AB}$ in the density matrix $\rho_{\rm AB}$ is non-zero. As a physical interpretation, detectors can communicate by exchanging field quanta.

Then, we define 'harvesting' as follows.

Terminology: harvesting
We say that a correlation such as entanglement is *harvested* or *extracted* from a quantum field if the resulting entanglement between two detectors has the non-zero Hadamard contribution in $C_{\rm AB}$ and $X_{\rm AB}$. That is, entanglement can be harvested even with the help of communication as long as the Hadamard contribution is non-vanishing. In particular, if two detectors cannot signal to each other (i.e., zero Pauli-Jordan contribution) then we say the correlation is *genuinely harvested*. Moreover, we say that the harvested entanglement is *assisted by communication* to emphasize that the Pauli-Jordan function is contributing to the entanglement harvesting, and if the Hadamard contribution is zero then the obtained

entanglement is *not harvested*.

The rationale for the terminology for 'harvesting' is as follows. The Hadamard function contributes to the entanglement between two detectors most of the time. If the detectors cannot communicate at all then only the Hadamard function gives rise to the extracted entanglement; otherwise, both functions *could* contribute to the entanglement. It "*could*" be so since it is possible to find a case where only the Pauli-Jordan part contributes to the entanglement [30]. However, this is not always the case. This indicates that the Hadamard and Pauli-Jordan contributions are not mutually exclusive in general. Therefore, it is reasonable to give the name 'harvesting' to the phenomenon in which particle detectors become entangled whenever the Hadamard contribution in $X_{\rm AB}$ is non-zero, and particularly call 'genuine harvesting' when entanglement is purely coming from the Hadamard function.[6]

To illustrate this point, consider two detectors A and B in (3+1)-dimensional Minkowski spacetime as depicted in Fig. 2.1. We fix detector-A's timing of interaction with the field (red curve) and consider three cases for detector-B's interaction (blue curves). Assuming a massless scalar field, it is known that the Pauli-Jordan function is non-vanishing if two points x, x' are lightlike-separated. Moreover, the Hadamard contribution becomes zero (at least for a Gaussian switching) when the detectors are exactly lightlike separated for a large detector separation [30]. Note that quantum mutual information behaves in a slightly different way. One can numerically check that both Hadamard and Pauli-Jordan parts almost equally contribute to the mutual information when detectors are lightlike separated, and so the region in which the Hadamard contribution vanishes (the grey region in Fig. 2.1) does not exist.

If detector-B interacts with the field during the case (i), there is no way that two detectors exchange quanta, in which case the Wightman function only depends on the Hadamard part. This is also true for case (iii), and we say that the detectors genuinely harvest entanglement. On the other hand, case (ii) indicates that detector-B receives quanta emitted from detector-A. Mathematically, this can be seen from the fact that $W_{\rm PJ} \neq 0$. The harvested entanglement comes from both the Hadamard and the Pauli-Jordan functions. In this case, we say the harvested entanglement is assisted by communication.

[6] If this were a mutually exclusive property such like "Hadamard-only" or "Pauli-Jordan-only" then it would be reasonable to call the former 'harvesting' and the latter 'non-harvesting'.

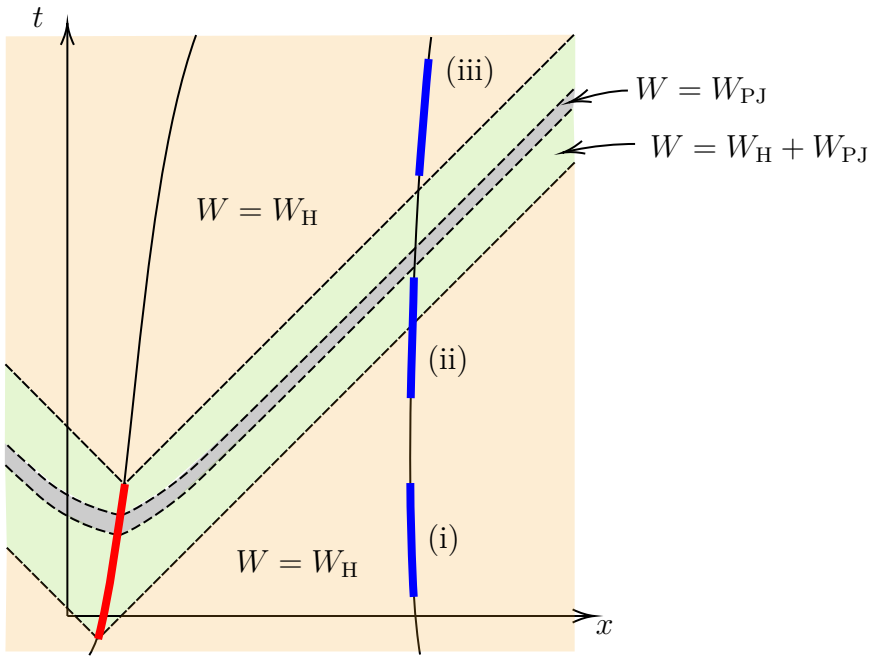

Figure 2.1: A spacetime diagram representing an entanglement harvesting protocol performed by detector-A (red) and B (blue). The red and blue stripes indicate the interaction of the detectors with the field. Based on [30], the green region suggests the domain of communication, i.e., if detector-B enters this region during the interaction, it receives a signal from detector-A [scenario (ii)]. The grey region, on the other hand, is dominated by the Pauli-Jordan function and the Hadamard contribution is zero if the center of B's switching is in this region. Outside of these regions there is no Pauli-Jordan contribution [e.g., cases (i) and (iii)].

2.4 Correlation among UDW detectors

We are particularly interested in the correlation between two or three detectors extracted from the field. We will focus on two correlations: quantum mutual information (the total correlation including classical and quantum) and entanglement, which is contained in the quantum mutual information.

For *bipartite qubit systems in a mixed state*, entanglement between the two qubits can be quantified by using the so-called *concurrence* or *negativity of entanglement*. In addition, entanglement in *tripartite qubit systems in a pure state* can be examined by the π*-tangle*, which is defined by using the negativity of entanglement. See [82] for a review.

2.4.1 Correlations between two qubits

Quantum mutual information

Quantum mutual information is the total correlation including both classical and quantum. Therefore, entanglement is part of quantum mutual information.

Let S_{AB} be the von Neumann entropy of the systems A and B, which is defined by [83]

$$S_{\mathrm{AB}} \coloneqq -\operatorname{Tr}[\rho_{\mathrm{AB}} \ln \rho_{\mathrm{AB}}] \,. \tag{2.63}$$

One can also introduce the von Neumann entropy of the subsystems by $S_{\mathrm{A}} \coloneqq -\operatorname{Tr}[\rho_{\mathrm{A}} \ln \rho_{\mathrm{A}}]$, where $\rho_{\mathrm{A}} = \operatorname{Tr}_{\mathrm{B}}[\rho_{\mathrm{AB}}]$. The quantum mutual information between systems A and B, denoted by I_{AB}, is then defined as [83]

$$I_{\mathrm{AB}} \coloneqq S_{\mathrm{A}} + S_{\mathrm{B}} - S_{\mathrm{AB}} \,. \tag{2.64}$$

Quantum mutual information is non-negative, $I_{\mathrm{AB}} \geq 0$, with equality if and only if $S_{\mathrm{A}} + S_{\mathrm{B}} = S_{\mathrm{AB}}$. Quantum mutual information is said to be the total correlation since it is the upper bound of a correlation function and so if $I_{\mathrm{AB}} = 0$ then it is guaranteed that no correlations exist between A and B [84].

In our particular case where the density matrix ρ_{AB} is given by (2.43), I_{AB} up to second order in λ is known to be [28]

$$I_{\mathrm{AB}} = \mathcal{L}_+ \ln \mathcal{L}_+ + \mathcal{L}_- \ln \mathcal{L}_- - P_{\mathrm{A}} \ln P_{\mathrm{A}} - P_{\mathrm{B}} \ln P_{\mathrm{B}} + \mathcal{O}(\lambda^4) \,, \tag{2.65}$$

where

$$\mathcal{L}_{\pm} \coloneqq \frac{1}{2}\left(P_{\rm A} + P_{\rm B} \pm \sqrt{(P_{\rm A} - P_{\rm B})^2 + 4|C_{\rm AB}|^2}\right). \tag{2.66}$$

One can easily check that mutual information vanishes when $|C_{\rm AB}| = 0$. In addition, from the condition $P_{\rm A}P_{\rm B} \geq |C_{\rm AB}|^2$ [29], if one of the transition probabilities are $P_j = 0$ then $|C_{\rm AB}| = 0$, thereby $I_{\rm AB} = 0$.

It is also instructive when two detectors have identical transition probabilities. Let us consider the case when $P \equiv P_{\rm A} = P_{\rm B}$, which leads us to $\mathcal{L}_{\pm} = P \pm |C_{\rm AB}|$. In the case where the transition probability P is large, $P \gg |C_{\rm AB}|$, mutual information becomes negligible $I_{\rm AB} \approx 0$ since $\mathcal{L}_{\pm} \approx P$. This observation will be useful when we examine the quantum mutual information of detectors near an event horizon since their transition probabilities become large.

Concurrence

Concurrence [85, 86] is a measure of bipartite entanglement based on the entanglement of formation [87] and its minimization. Here, we present the basic idea behind concurrence.

Suppose we have a density matrix $\rho_{\rm AB}$ of a joint system $\mathcal{H}_{\rm A} \otimes \mathcal{H}_{\rm B}$. We can perform a pure-state decomposition of $\rho_{\rm AB}$ as $\rho_{\rm AB} = \sum_i p_i \left|\psi_i\right\rangle \left\langle\psi_i\right|$. Then, the entanglement of formation $E(\rho_{\rm AB})$ is defined as

$$E(\rho_{\rm AB}) \coloneqq \min_{\{p_i, |\psi_i\rangle\}} \sum_i p_i S(\psi_i)\,, \tag{2.67}$$

where $S(\psi_i)$ is the von Neumann entropy of the reduced density matrix of $\left|\psi_i\right\rangle \left\langle\psi_i\right|$, i.e., $\mathrm{Tr}_{\rm A}[\left|\psi_i\right\rangle \left\langle\psi_i\right|]$ or equivalently $\mathrm{Tr}_{\rm B}[\left|\psi_i\right\rangle \left\langle\psi_i\right|]$. The entanglement of formation (2.67) is thus the minimization of the average of all possible pure-state decompositions of $\rho_{\rm AB}$.

Although this is not so practical in general since one has to find all possible decompositions and then minimize their average, the expression for $E(\rho_{\rm AB})$ can be found if $\dim(\mathcal{H}_{\rm A}) \times \dim(\mathcal{H}_{\rm B}) = 2 \times 2$ (i.e., a two-qubit system). To see how this works, consider a pure state $\left|\psi\right\rangle \in \mathcal{H}_{\rm A} \otimes \mathcal{H}_{\rm B}$. People tend to use a basis $\{\left|00\right\rangle, \left|01\right\rangle, \left|10\right\rangle, \left|11\right\rangle\}$, which is constructed from the eigenvectors of $\hat{\sigma}_z$, but it is known that the so-called magic basis $\{\left|e_1\right\rangle, \left|e_2\right\rangle, \left|e_3\right\rangle, \left|e_4\right\rangle\}$ is useful in this case. The magic basis is defined by

$$\left|e_1\right\rangle = \frac{1}{2}(\left|00\right\rangle + \left|11\right\rangle), \left|e_2\right\rangle = \frac{\mathsf{i}}{2}(\left|00\right\rangle - \left|11\right\rangle), \left|e_3\right\rangle = \frac{\mathsf{i}}{2}(\left|01\right\rangle + \left|10\right\rangle), \left|e_4\right\rangle = \frac{1}{2}(\left|01\right\rangle - \left|10\right\rangle), \tag{2.68}$$

and they are orthonormal to each other. We then change the basis to the magic basis and write $|\psi\rangle$ as

$$|\psi\rangle = \sum_{i=1}^{4} \alpha_i |e_i\rangle \ . \tag{2.69}$$

The entanglement of formation can be written as

$$E(|\psi\rangle) = H_{\text{bin}}\left(\frac{1}{2} + \frac{1}{2}\sqrt{1 - \mathcal{C}^2(|\psi\rangle)}\right) \ , \tag{2.70}$$

where $H_{\text{bin}}(x) \coloneqq -x \log_2 x - (1-x)\log_2(1-x)$ is the binary Shannon entropy [83], and $\mathcal{C}(|\psi\rangle) \in [0,1]$ is the concurrence defined by

$$\mathcal{C}(|\psi\rangle) \coloneqq \left|\sum_{i=1}^{4} \alpha_i^2\right| \ . \tag{2.71}$$

The concurrence can be thought of as an entanglement measure since the entanglement of formation monotonically increases with $\mathcal{C}$.

The point one should be aware of is that the concurrence is written as a sum of the squares of coefficients of $|\psi\rangle$ in the magic basis. Therefore, once ρ_{AB} is given in the $\hat{\sigma}_z$-basis, one should change the basis to the magic basis and compute the concurrence. It turns out that one can make use of $\hat{\sigma}_y$ to compute $\mathcal{C}$ easily in the $\hat{\sigma}_z$-basis. To see this, we use the fact that the concurrence can be written as $\mathcal{C}(|\psi\rangle) = |\langle\psi^*|\psi\rangle|$, where $|\psi^*\rangle = \sum_i \alpha_i^* |e_i\rangle$.[7]

Suppose $|\psi\rangle$ is given in the $\hat{\sigma}_z$-basis, such as $|\psi\rangle = c_{00}|00\rangle + c_{01}|01\rangle + c_{10}|10\rangle + c_{11}|11\rangle$. We then change the basis to $\{|e_i\rangle\}$ and then take a complex conjugate, $|\psi^*\rangle$. One can check that the resulting concurrence, $\mathcal{C}(|\psi\rangle) = |\langle\psi^*|\psi\rangle|$ is equivalent to the expression $|\langle\psi|\tilde{\psi}\rangle|$, where $|\tilde{\psi}\rangle$ is constructed as follows. *Instead of* changing the basis to the magic basis, take a complex conjugate so that $|\psi^*\rangle = c_{00}^*|00\rangle + c_{01}^*|01\rangle + c_{10}^*|10\rangle + c_{11}^*|11\rangle$, and then apply $\hat{\sigma}_y \otimes \hat{\sigma}_y$:

$$|\tilde{\psi}\rangle \coloneqq (\hat{\sigma}_y \otimes \hat{\sigma}_y)|\psi^*\rangle \ . \tag{2.72}$$

The nice thing about the equality, $\mathcal{C}(|\psi\rangle) = |\langle\psi|\tilde{\psi}\rangle|$, is that applying $\hat{\sigma}_y$ allows us to compute $\mathcal{C}$ in the $\hat{\sigma}_z$-basis, and this is much easier than changing the basis to the magic basis.

[7] Notice that the expression for the concurrence (2.71) is not $\sum_i |\alpha_i|^2$.

This expression allows us to generalize the concurrence to that of mixed states: $\mathcal{C}(\rho_{\rm AB})$. Define (in the $\hat{\sigma}_z$-basis)

$$\tilde{\rho}_{\rm AB} \coloneqq (\hat{\sigma}_y \otimes \hat{\sigma}_y)\rho^*_{\rm AB}(\hat{\sigma}_y \otimes \hat{\sigma}_y)\,, \tag{2.73}$$

which is the mixed-state generalization of $|\tilde{\psi}\rangle$. Since $\mathcal{C}(|\psi\rangle) = |\,\langle\psi|\tilde{\psi}\rangle\,|$ can be seen as a fidelity [83] between $|\psi\rangle$ and $|\tilde{\psi}\rangle$, we introduce a Hermitian operator $\sqrt{\sqrt{\rho_{\rm AB}}\tilde{\rho}_{\rm AB}\sqrt{\rho_{\rm AB}}}$. The concurrence of $\rho_{\rm AB}$ is found to be [86]

$$\mathcal{C}(\rho_{\rm AB}) \coloneqq \max\{0, w_1 - w_2 - w_3 - w_4\}\,, \qquad (w_1 \geq w_2 \geq w_3 \geq w_4) \tag{2.74}$$

where w_i are the eigenvalues of the aforementioned Hermitian operator, (or equivalently, the square roots of the eigenvalues of $\rho_{\rm AB}\tilde{\rho}_{\rm AB}$).

For a density matrix of the form

$$\rho_{\rm AB} = \begin{bmatrix} r_{11} & 0 & 0 & r_{14} \\ 0 & r_{22} & r_{23} & 0 \\ 0 & r^*_{23} & r_{33} & 0 \\ r^*_{14} & 0 & 0 & r_{44} \end{bmatrix}, \tag{2.75}$$

which is known as the X-state, w_i read

$$w_i \in \{\sqrt{r_{11}r_{44}} \pm |r_{14}|,\ \sqrt{r_{22}r_{33}} \pm |r_{23}|\,\}, \tag{2.76}$$

and so the concurrence is either

$$\mathcal{C}(\rho_{\rm AB}) = 2\max\{0,\ |r_{14}| - \sqrt{r_{22}r_{33}}\}\,, \quad (\text{when } w_1 = \sqrt{r_{11}r_{44}} + |r_{14}|) \tag{2.77}$$

$$\mathcal{C}(\rho_{\rm AB}) = 2\max\{0,\ |r_{23}| - \sqrt{r_{11}r_{44}}\}\,. \quad (\text{when } w_1 = \sqrt{r_{22}r_{33}} + |r_{23}|) \tag{2.78}$$

It turns out that our density matrix (2.43) always satisfies (2.77) and so

$$\mathcal{C}_{\rm AB} \equiv \mathcal{C}(\rho_{\rm AB}) = 2\max\{0,\ |X_{\rm AB}| - \sqrt{P_{\rm A}P_{\rm B}}\}\,. \tag{2.79}$$

It provides a nice interpretation for $X_{\rm AB}$ and P_j. The off-diagonal element $X_{\rm AB}$ is responsible for entanglement since two systems A and B entangle if and only if $|X_{\rm AB}| > \sqrt{P_{\rm A}P_{\rm B}}$. Likewise, the transition probabilities P_j can be thought of as noise since they tend to prevent the systems from being entangled.

Negativity

The idea behind the *negativity of entanglement* [88] is the so-called Peres-Horodecki criterion [89, 90]. The Peres separability criterion [89], also known as the positive partial transpose (PPT) criterion, states that if a state ρ is separable, then all the eigenvalues of a partial-transposed density matrix, $\rho^{\top_{\mathrm{B}}}$, are positive. By contraposition, this also means that if at least one of the eigenvalues of a partial-transposed density matrix, $\rho^{\top_{\mathrm{B}}}$, is negative then the state ρ is entangled. Soon after, the Horodecki family showed [90] that the above statement becomes a necessary and sufficient condition for $\dim(\mathcal{H}_{\mathrm{A}}) \times \dim(\mathcal{H}_{\mathrm{B}}) = 2 \times 2$ and 2×3 cases, which we refer to the Peres-Horodecki criterion [82]. The negativity of entanglement utilizes this fact and quantifies entanglement by computing the negative eigenvalues of $\rho^{\top_{\mathrm{B}}}$.

Suppose the system $\mathcal{H}_{\mathrm{A}} \otimes \mathcal{H}_{\mathrm{B}}$ is 2×2. Let us perform a partial transpose $\top_{\mathrm{B}}$ to the subsystem $\mathcal{H}_{\mathrm{B}}$. This is a map

$$\top_{\mathrm{B}} : |a_{\mathrm{A}}\rangle \langle b_{\mathrm{A}}| \otimes |\mu_{\mathrm{B}}\rangle \langle \nu_{\mathrm{B}}| \mapsto |a_{\mathrm{A}}\rangle \langle b_{\mathrm{A}}| \otimes |\mu_{\mathrm{B}}\rangle \langle \nu_{\mathrm{B}}|^{\top_{\mathrm{B}}} \coloneqq |a_{\mathrm{A}}\rangle \langle b_{\mathrm{A}}| \otimes |\nu_{\mathrm{B}}\rangle \langle \mu_{\mathrm{B}}| \, . \tag{2.80}$$

The Peres-Horodecki criterion states that ρ_{AB} is entangled if and only if there exists at least one negative eigenvalue of $\rho_{\mathrm{AB}}^{\top_{\mathrm{B}}}$. Let λ_i, $i \in \{1, 2, 3, 4\}$ be the eigenvalues of $\rho_{\mathrm{AB}}^{\top_{\mathrm{B}}}$. There are four of them since ρ_{AB} (and thereby $\rho_{\mathrm{AB}}^{\top_{\mathrm{B}}}$) is a 4×4 matrix. The negativity of entanglement $\mathcal{N}_{\mathrm{A(B)}}$ is given by [88]

$$\mathcal{N}_{\mathrm{A(B)}} \coloneqq \frac{||\rho_{\mathrm{AB}}^{\top_{\mathrm{B}}}|| - 1}{2} = \left| \sum_{\lambda_i < 0} \lambda_i \right| . \tag{2.81}$$

Here $||\rho_{\mathrm{AB}}^{\top_{\mathrm{B}}}|| \coloneqq \mathrm{Tr}\, |\rho_{\mathrm{AB}}^{\top_{\mathrm{B}}}|$ is the trace norm of an operator $\rho_{\mathrm{AB}}^{\top_{\mathrm{B}}}$. This definition is telling us that the negativity is the (absolute value of) sum of all possible negative eigenvalues of $\rho_{\mathrm{AB}}^{\top_{\mathrm{B}}}$, and if there are no such eigenvalues, entanglement is zero, which is consistent with the PPT criterion.

Let us restrict our density matrix ρ_{AB} to the X-state (2.75). The partial transposition $\top_{\mathrm{B}}$ swaps the off-diagonal elements in ρ_{AB}:

$$\rho_{\mathrm{AB}}^{\top_{\mathrm{B}}} = \begin{bmatrix} r_{11} & 0 & 0 & r_{23} \\ 0 & r_{22} & r_{14} & 0 \\ 0 & r_{14}^* & r_{33} & 0 \\ r_{23}^* & 0 & 0 & r_{44} \end{bmatrix} , \tag{2.82}$$

which has the following eigenvalues.

$$\lambda_1 = \frac{r_{22}+r_{33}}{2} - \sqrt{\left(\frac{r_{22}-r_{33}}{2}\right)^2 + |r_{14}|^2}\,, \tag{2.83a}$$

$$\lambda_2 = \frac{r_{22}+r_{33}}{2} + \sqrt{\left(\frac{r_{22}-r_{33}}{2}\right)^2 + |r_{14}|^2}\,, \tag{2.83b}$$

$$\lambda_3 = \frac{r_{11}+r_{44}}{2} - \sqrt{\left(\frac{r_{11}-r_{44}}{2}\right)^2 + |r_{23}|^2}\,, \tag{2.83c}$$

$$\lambda_4 = \frac{r_{11}+r_{44}}{2} + \sqrt{\left(\frac{r_{11}-r_{44}}{2}\right)^2 + |r_{23}|^2}\,. \tag{2.83d}$$

Note that the diagonal elements r_{ii} are positive-reals and the off-diagonal elements are complex numbers. Therefore, λ_1 and λ_3 are the only possible eigenvalues to be negative. The conditions to be negative are [29]

$$\lambda_1 < 0 \Leftrightarrow |r_{14}|^2 > r_{22}r_{33}\,, \tag{2.84}$$

$$\lambda_3 < 0 \Leftrightarrow |r_{23}|^2 > r_{11}r_{44}\,. \tag{2.85}$$

Since the only possible negative eigenvalues are λ_1 and λ_3, we will use the following formula.

$$\mathcal{N}_{\mathrm{A(B)}} = \left|\min\{0,\lambda_1\} + \min\{0,\lambda_3\}\right|\,. \tag{2.86}$$

It turns out that our perturbative density matrix (2.43) has only one negative eigenvalue λ_1. Therefore, the negativity for (2.43) is

$$\mathcal{N}_{\mathrm{A(B)}} = \sqrt{\left(\frac{P_{\mathrm{B}}-P_{\mathrm{A}}}{2}\right)^2 + |X_{\mathrm{AB}}|^2} - \frac{P_{\mathrm{B}}+P_{\mathrm{A}}}{2}\,. \tag{2.87}$$

Note that if two detectors are identical and have $P_{\mathrm{A}} = P_{\mathrm{B}}$, then the negativity can be related to the concurrence as $\mathcal{N}_{\mathrm{A(B)}} = \mathcal{C}_{\mathrm{AB}}/2$. From this, one can see that the negativity has a range $0 \le \mathcal{N}_{\mathrm{A(B)}} \le 1/2$ since $0 \le \mathcal{C}_{\mathrm{AB}} \le 1$. Indeed, concurrence and negativity are related by [91]

$$\sqrt{(1-\mathcal{C}_{\mathrm{AB}})^2 + \mathcal{C}_{\mathrm{AB}}^2} - (1-\mathcal{C}_{\mathrm{AB}}) \le 2\mathcal{N}_{\mathrm{A(B)}} \le \mathcal{C}_{\mathrm{AB}}\,. \tag{2.88}$$

2.4.2 Correlation in three qubits

The harvested tripartite entanglement can be quantified by the *π-tangle* [92]. Consider three qubits A, B, and C. The π-tangle is defined by using the negativity:

$$\pi := \frac{\pi_{\mathrm{A}} + \pi_{\mathrm{B}} + \pi_{\mathrm{C}}}{3}\,, \tag{2.89}$$

where

$$\pi_{\rm A} = \mathcal{N}^2_{\rm A(BC)} - \mathcal{N}^2_{\rm A(B)} - \mathcal{N}^2_{\rm A(C)}\,, \tag{2.90a}$$

$$\pi_{\rm B} = \mathcal{N}^2_{\rm B(AC)} - \mathcal{N}^2_{\rm B(A)} - \mathcal{N}^2_{\rm B(C)}\,, \tag{2.90b}$$

$$\pi_{\rm C} = \mathcal{N}^2_{\rm C(AB)} - \mathcal{N}^2_{\rm C(B)} - \mathcal{N}^2_{\rm C(A)}\,, \tag{2.90c}$$

and by definition,

$$\mathcal{N}_{\rm A(BC)} = \frac{||\rho^{\top_{\rm A}}_{\rm ABC}|| - 1}{2}\,, \quad \mathcal{N}_{\rm B(CA)} = \frac{||\rho^{\top_{\rm B}}_{\rm ABC}|| - 1}{2}\,, \quad \mathcal{N}_{\rm C(AB)} = \frac{||\rho^{\top_{\rm C}}_{\rm ABC}|| - 1}{2}\,. \tag{2.91}$$

Note that $\mathcal{N}_{\rm A(BC)}$ does not reflect the entanglement between detector-A and the rest, (BC), since it is $\dim(\mathcal{H}_{\rm A}) \times \dim(\mathcal{H}_{\rm BC}) = 2 \times 4$ and therefore, only the PPT criterion is valid. In other words, if the negativity is positive, $\mathcal{N}_{\rm A(BC)} > 0$, then there is entanglement between A and (BC), whereas $\mathcal{N}_{\rm A(BC)} = 0$ *does not guarantee* that there does not exist entanglement between A and (BC); it only provides the lower bound for entanglement.

Nevertheless, the π-tangle (2.89) quantifies the tripartite entanglement in the system when $\rho_{\rm ABC}$ is a pure state. This is supported by a monogamy relation called the Coffman-Kundu-Wootters (CKW) inequality for negativity [92]:

$$\mathcal{N}^2_{\rm A(B)} + \mathcal{N}^2_{\rm A(C)} \leq \mathcal{N}^2_{\rm A(BC)}\,. \tag{2.92}$$

In general, however, this inequality will not hold when $\rho_{\rm ABC}$ is mixed. In such a case, the π-tangle defined in (2.89) and (2.90) is only a lower bound for the tripartite entanglement. To obtain genuine tripartite entanglement for a mixed state, one needs to generalize the inequality as [92]

$$\mathcal{N}^2_{\rm A(B)} + \mathcal{N}^2_{\rm A(C)} \leq \min\left[\mathcal{N}^2_{\rm A(BC)}\right]\,, \tag{2.93}$$

where the minimization is performed over all possible pure-state decompositions [93, 92].

Concretely, suppose $\rho_{\rm ABC}$ can be decomposed into $\rho_{\rm ABC} = \sum_i p_i \left|\psi_i\right\rangle \left\langle\psi_i\right|$. Then the expectation value of $\mathcal{N}^2_{\rm A(BC)}$ can be written as

$$\left\langle \mathcal{N}^2_{\rm A(BC)} \right\rangle_\psi \coloneqq \sum_i p_i \mathcal{N}^2_{\rm A(BC)}(\psi_i)\,, \tag{2.94}$$

where $\mathcal{N}^2_{\rm A(BC)}(\psi_i)$ is the square of negativity of the pure state $\left|\psi_i\right\rangle \in \mathcal{H}_{\rm A} \otimes \mathcal{H}_{\rm B} \otimes \mathcal{H}_{\rm C}$. Since the CKW inequality (2.92) is satisfied for a pure state $\left|\psi_i\right\rangle$, we have

$$\mathcal{N}^2_{\rm A(B)}(\psi_i) + \mathcal{N}^2_{\rm A(C)}(\psi_i) \leq \mathcal{N}^2_{\rm A(BC)}(\psi_i)\,. \tag{2.95}$$

The left-hand side of the inequality is understood as

$$\mathcal{N}_{\mathrm{A(B)}}(\psi_i) \coloneqq \frac{||\,\mathrm{Tr_C}[|\psi_i\rangle\langle\psi_i|]^{\top_\mathrm{A}}|| - 1}{2}\,. \tag{2.96}$$

The weighted-sum, $\sum_i p_i$, of this inequality reads

$$\sum_i p_i \mathcal{N}^2_{\mathrm{A(B)}}(\psi_i) + \sum_i p_i \mathcal{N}^2_{\mathrm{A(C)}}(\psi_i) \leq \sum_i p_i \mathcal{N}^2_{\mathrm{A(BC)}}(\psi_i) (= \langle \mathcal{N}^2_{\mathrm{A(BC)}} \rangle_\psi)\,. \tag{2.97}$$

Since negativity has the convexity property, $\mathcal{N}(\sum_i p_i \rho) \leq \sum_i p_i \mathcal{N}(\rho)$, one can apply this to the left-hand side of the inequality. The resulting inequality becomes

$$\mathcal{N}^2_{\mathrm{A(B)}}(\rho_{\mathrm{AB}}) + \mathcal{N}^2_{\mathrm{A(C)}}(\rho_{\mathrm{AC}}) \leq \langle \mathcal{N}^2_{\mathrm{A(BC)}} \rangle_\psi\,, \tag{2.98}$$

where the left-hand side is understood as

$$\mathcal{N}_{\mathrm{A(B)}}(\rho_{\mathrm{AB}}) \coloneqq \frac{||\,\mathrm{Tr_C}[\rho_{\mathrm{ABC}}]^{\top_\mathrm{A}}|| - 1}{2}\,. \tag{2.99}$$

This is the CKW inequality for a pure-state decomposition. However, the pure-state decomposition of ρ_{ABC} is not unique and there are many ways to decompose it (e.g., $\rho_{\mathrm{ABC}} = \sum_i q_i |\phi_i\rangle\langle\phi_i|$). This means the right-hand side of (2.98) is not unique for a given ρ_{ABC}. We choose the decomposition that minimizes the right-hand side of (2.98), which is (2.93). We also remark that the π-tangle for a mixed state ρ_{ABC} is the lower bound of the 'pure-state decomposed π-tangle.' This is due to the fact that the negativity is a convex function and so the right-hand side of (2.98) has the following relationship:

$$\forall\{p_i, |\psi_i\rangle\} \;:\; \langle \mathcal{N}^2_{\mathrm{A(BC)}} \rangle_\psi \geq \mathcal{N}^2_{\mathrm{A(BC)}}(\sum_i p_i |\psi_i\rangle\langle\psi_i|) = \mathcal{N}^2_{\mathrm{A(BC)}}(\rho_{\mathrm{ABC}})\,. \tag{2.100}$$

By subtracting the left-hand side of (2.98), we obtain $\pi_{\mathrm{A}}(\rho_{\mathrm{ABC}}) \leq \pi_{\mathrm{A}}(\{p_i, |\psi_i\rangle\})$, where

$$\pi_{\mathrm{A}}(\{p_i, |\psi_i\rangle\}) \coloneqq \langle \mathcal{N}^2_{\mathrm{A(BC)}} \rangle_\psi - \mathcal{N}^2_{\mathrm{A(B)}}(\rho_{\mathrm{AB}}) - \mathcal{N}^2_{\mathrm{A(C)}}(\rho_{\mathrm{AC}})\,. \tag{2.101}$$

Since minimization of negativity is tedious, we will use the π-tangle (2.89) as a lower bound for mixed tripartite entanglement. However, one needs to keep in mind that the π-tangle could be negative due to the violation of the CKW inequality (2.92) even for non-perturbative approaches.

Let us now consider an explicit form of the π-tangle for our density matrix ρ_{ABC} in (2.51). The bipartite negativities, $\mathcal{N}_{j(k)}$, are already known as (2.87). However, the tripartite negativities, $\mathcal{N}_{j(kl)}$, have slightly complicated forms. As a concrete example, let us compute $\mathcal{N}_{\mathrm{A(BC)}}$. The partial transpose $\top_{\mathrm{A}}$ yields

$$\rho_{\mathrm{ABC}}^{\top_{\mathrm{A}}} = \begin{bmatrix} 1-(P_{\mathrm{A}}+P_{\mathrm{B}}+P_{\mathrm{C}}) & 0 & 0 & 0 & X_{\mathrm{BC}}^{*} & C_{\mathrm{AC}} & C_{\mathrm{AB}} & 0 \\ 0 & P_{\mathrm{C}} & C_{\mathrm{BC}}^{*} & X_{\mathrm{AC}} & 0 & 0 & 0 & 0 \\ 0 & C_{\mathrm{BC}} & P_{\mathrm{B}} & X_{\mathrm{AB}} & 0 & 0 & 0 & 0 \\ 0 & X_{\mathrm{AC}}^{*} & X_{\mathrm{AB}}^{*} & P_{\mathrm{A}} & 0 & 0 & 0 & 0 \\ X_{\mathrm{BC}} & 0 & 0 & 0 & 0 & 0 & 0 & 0 \\ C_{\mathrm{AC}}^{*} & 0 & 0 & 0 & 0 & 0 & 0 & 0 \\ C_{\mathrm{AB}}^{*} & 0 & 0 & 0 & 0 & 0 & 0 & 0 \\ 0 & 0 & 0 & 0 & 0 & 0 & 0 & 0 \end{bmatrix} + \mathcal{O}(\lambda^4)\,, \tag{2.102}$$

and its eigenvalues are

$$\mathrm{eigen}(\rho_{\mathrm{ABC}}^{\top_{\mathrm{A}}}) = \{0,\, 0,\, 0,\, \varrho_1^{\pm},\, \varrho_2\}\,, \tag{2.103}$$

where

$$\varrho_1^{\pm} \coloneqq \frac{1}{2}\left(1-P_{\mathrm{A}}-P_{\mathrm{B}}-P_{\mathrm{C}} \pm \sqrt{(1-P_{\mathrm{A}}-P_{\mathrm{B}}-P_{\mathrm{C}})^2+4(|C_{\mathrm{AB}}|^2+|C_{\mathrm{AC}}|^2+|X_{\mathrm{BC}}|^2)}\right)\,, \tag{2.104}$$

and ϱ_2 are the three solutions to the following cubic equation.

$$\begin{aligned} &\varrho_2^3-(P_{\mathrm{A}}+P_{\mathrm{B}}+P_{\mathrm{C}})\varrho_2^2+(P_{\mathrm{A}}+P_{\mathrm{B}}+P_{\mathrm{C}}-|C_{\mathrm{BC}}|^2-|X_{\mathrm{AB}}|^2-|X_{\mathrm{AC}}|^2)\varrho_2 \\ &\quad +P_{\mathrm{A}}|C_{\mathrm{BC}}|^2+P_{\mathrm{B}}|X_{\mathrm{AC}}|^2+P_{\mathrm{C}}|X_{\mathrm{AB}}|^2-P_{\mathrm{A}}P_{\mathrm{B}}P_{\mathrm{C}}-2\mathrm{Re}[C_{\mathrm{BC}}X_{\mathrm{AB}}^{*}X_{\mathrm{AC}}]=0\,. \end{aligned} \tag{2.105}$$

For $\varrho_1^{\pm}$, because $\tilde{\lambda}^2 \ll 1$,

$$\varrho_1^{\pm} = \frac{1}{2}\left(1 - P_{\rm A} - P_{\rm B} - P_{\rm C} \pm (1 - P_{\rm A} - P_{\rm B} - P_{\rm C})\sqrt{1 + \frac{4(|C_{\rm AB}|^2 + |C_{\rm AC}|^2 + |X_{\rm BC}|^2)}{(1 - P_{\rm A} - P_{\rm B} - P_{\rm C})^2}}\right) \tag{2.106}$$

$$\simeq \frac{1}{2}\left[1 - P_{\rm A} - P_{\rm B} - P_{\rm C} \pm (1 - P_{\rm A} - P_{\rm B} - P_{\rm C})\left(1 + \frac{2(|C_{\rm AB}|^2 + |C_{\rm AC}|^2 + |X_{\rm BC}|^2)}{(1 - P_{\rm A} - P_{\rm B} - P_{\rm C})^2}\right)\right] \tag{2.107}$$

$$= \begin{cases} 1 - P_{\rm A} - P_{\rm B} - P_{\rm C} + \dfrac{|C_{\rm AB}|^2 + |C_{\rm AC}|^2 + |X_{\rm BC}|^2}{1 - P_{\rm A} - P_{\rm B} - P_{\rm C}} \approx 1 \\ -\dfrac{|C_{\rm AB}|^2 + |C_{\rm AC}|^2 + |X_{\rm BC}|^2}{1 - P_{\rm A} - P_{\rm B} - P_{\rm C}} \approx -(|C_{\rm AB}|^2 + |C_{\rm AC}|^2 + |X_{\rm BC}|^2) = \mathcal{O}(\lambda^4) \end{cases} . \tag{2.108}$$

Therefore, $\varrho_1^{\pm}$ contribute only to the negativity in $\mathcal{O}(\lambda^4)$.

Since the solutions to the cubic equation above are complicated in general, we are interested in the simplest scenario where

$$C_{\rm AB} = C_{\rm BC} = C_{\rm CA} \equiv C\,, \tag{2.109a}$$
$$X_{\rm AB} = X_{\rm BC} = X_{\rm CA} \equiv X\,, \tag{2.109b}$$
$$P_{\rm A} = P_{\rm B} = P_{\rm C} \equiv P\,. \tag{2.109c}$$

Such a simplification is possible if the detectors are placed in an appropriate way. An equilateral triangle configuration in Minkowski spacetime is one example, as long as the detectors are identical and they switch at the same time. Another example that is relevant to this thesis is an equilateral triangle configuration in a BTZ black hole spacetime. In this case, the center of the black hole is aligned with the center of the equilateral triangle, so that each detector experiences the same redshift effect from the black hole. We will describe this in Ch. 5 in more detail.

In the simplified scenario described above, the three solutions to the quartic equation are

$$\varrho_2 = P - C\,,\ \frac{1}{2}\left(C + 2P \pm \sqrt{C^2 + 8|X|^2}\right)\,, \tag{2.110}$$

and so the negativities can be simply written as [32]

$$\mathcal{N}_{\rm A(BC)} = \mathcal{N}_{\rm B(CA)} = \mathcal{N}_{\rm C(AB)} = \max\left\{0,\ \frac{\sqrt{C^2 + 8|X|^2}}{2} - \frac{C}{2} - P\right\} + \mathcal{O}(\lambda^4)\,, \tag{2.111}$$

$$\mathcal{N}_{\rm A(B)} = \mathcal{N}_{\rm A(C)} = \mathcal{N}_{\rm B(C)} = \mathcal{N}_{\rm B(A)} = \mathcal{N}_{\rm C(A)} = \mathcal{N}_{\rm C(B)} = \max\{0,\ |X| - P\} + \mathcal{O}(\lambda^4)\,. \tag{2.112}$$

Here, we used the fact that $P - C \geq 0$ from (2.54). The π-tangle (2.89) is then

$$\pi = \max\left\{0,\, \frac{\sqrt{C^2 + 8|X|^2}}{2} - \frac{C}{2} - P\right\}^2 - 2\max\{0,\, |X| - P\}^2 + \mathcal{O}(\lambda^6)\,. \tag{2.113}$$

Unlike the bipartite negativity, which is positive if $|X| > P$, the tripartite negativity (and so the π-tangle) also depends on C. Also note that the π-tangle can be positive even when the bipartite entanglement is 0. Such tripartite entanglement with vanishing bipartite entanglement is known as the Greenberger-Horne-Zeilinger (GHZ) state [94].

Chapter 3

Extraction of correlation by uniformly accelerated particle detectors

This thesis aims to show how Unruh and Hawking effects affect the correlation harvesting protocols. In particular, a single particle detector under uniform acceleration responds as if it is at rest in a thermal bath. This is due to the fact that the Wightman function along the accelerating trajectory takes the same form as that of a detector at rest in a thermal bath. On the other hand, if two detectors are uniformly accelerating in the Minkowski vacuum, the harvested entanglement behaves in a very different way compared to the case of two inertial detectors in a thermal bath. In this chapter, we examine the mutual information harvesting protocol with two uniformly accelerating detectors (see Fig. 1.2) and show how it is different from the thermal bath scenario.

This chapter is organized as follows. We first specify three kinds of detector trajectories, parallel, anti-parallel, and perpendicular, and obtain the corresponding Wightman functions in Sec. 3.1. We then show the mutual information harvested by these detectors and compare this to the result provided by [1] in Sec. 3.2.

3.1 Accelerating detectors' trajectories

Let us consider two uniformly accelerating detectors in $(3+1)$-dimensional Minkowski spacetime. The quantum scalar field $\hat{\phi}(\mathsf{x})$ is assumed to be massless ($m = 0$) and minimally

coupled ($\xi = 0$) in Eq. (2.1). One can perform a mode expansion as

$$\hat{\phi}(\mathsf{x}) = \int_{\mathbb{R}^3} \frac{\mathrm{d}^3 k}{\sqrt{(2\pi)^3 2|\boldsymbol{k}|}} \left(\hat{a}_{\boldsymbol{k}} e^{-\mathsf{i}|\boldsymbol{k}|t+\mathsf{i}\boldsymbol{k}\cdot\boldsymbol{x}} + \hat{a}^\dagger_{\boldsymbol{k}} e^{\mathsf{i}|\boldsymbol{k}|t-\mathsf{i}\boldsymbol{k}\cdot\boldsymbol{x}}\right) . \tag{3.1}$$

See Sec. 2.1.2 for a detail. The vacuum state associated with these mode functions is the Minkowski vacuum $|0_{\mathrm{M}}\rangle$ satisfying $\hat{a}_{\boldsymbol{k}}|0_{\mathrm{M}}\rangle = 0$ for all $\boldsymbol{k}$. The creation and annihilation operators obey the canonical commutation relations,

$$[\hat{a}_{\boldsymbol{k}}, \hat{a}^\dagger_{\boldsymbol{k}'}] = \delta^{(3)}(\boldsymbol{k} - \boldsymbol{k}') , \tag{3.2a}$$

$$[\hat{a}_{\boldsymbol{k}}, \hat{a}_{\boldsymbol{k}'}] = 0 , \quad [\hat{a}^\dagger_{\boldsymbol{k}}, \hat{a}^\dagger_{\boldsymbol{k}'}] = 0 . \tag{3.2b}$$

The Wightman function in the Minkowski vacuum state $|0_{\mathrm{M}}\rangle$ is then known to be

$$W(\mathsf{x}, \mathsf{x}') = \lim_{\epsilon\to 0^+} -\frac{1}{4\pi^2} \frac{1}{(t - t' - \mathsf{i}\epsilon)^2 - |\boldsymbol{x} - \boldsymbol{x}'|^2} , \tag{3.3}$$

where ϵ is a UV regulator.

In this chapter, we wish to compute the mutual information harvested by two uniformly accelerated UDW detectors. Therefore, from (2.65), we need to have P_j and C_{AB}. To evaluate these density matrix elements, one needs to specify the trajectories of detectors A and B in this Wightman function. In what follows, we will consider three different acceleration scenarios: parallel, anti-parallel, and perpendicular.

Parallel acceleration

The *parallel acceleration scenario* refers to the case where a pair of UDW detectors A and B is accelerating in the same direction along x. In particular, their spatial separation on the $t = const$ slice is L for all times, as shown in Fig. 3.1(a). The detectors' trajectories can be written as

$$\mathsf{x}_{\mathrm{A}} = \left\{t = \frac{1}{a}\sinh(a\tau_{\mathrm{A}}), x = \frac{1}{a}[\cosh(a\tau_{\mathrm{A}}) - 1] + \frac{L}{2}, y = 0, z = 0\right\} , \tag{3.4a}$$

$$\mathsf{x}_{\mathrm{B}} = \left\{t = \frac{1}{a}\sinh(a\tau_{\mathrm{B}}), x = \frac{1}{a}[\cosh(a\tau_{\mathrm{B}}) - 1] - \frac{L}{2}, y = 0, z = 0\right\} , \tag{3.4b}$$

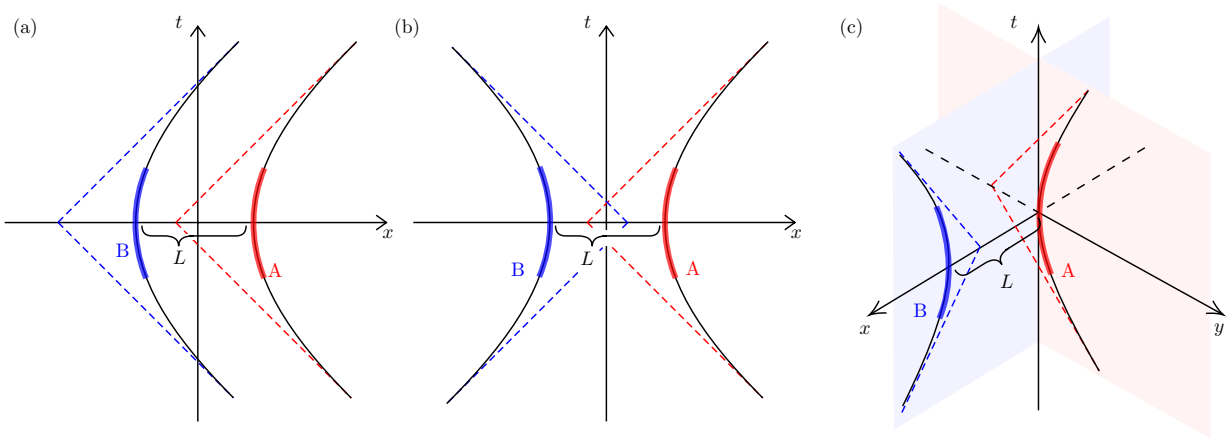

Figure 3.1: Three configurations of acceleration: (a) parallel, (b) anti-parallel, and (c) perpendicular. The red and blue stripes indicate the interaction duration of detectors A and B, respectively. In all cases, the detectors are separated by L at $t = 0$, at which their Gaussian switching peaks. Note that the separation in the parallel configuration is L for all times.

where a (≥ 0) is the proper acceleration of a detector. The Wightman functions (3.3) along these trajectories are

$$W_a(\mathsf{x}_j(\tau_j), \mathsf{x}'_j(\tau'_j)) = -\frac{a^2}{16\pi^2} \frac{1}{\sinh^2[a(\tau_j - \tau'_j)/2 - \mathrm{i}\epsilon]}, \quad j \in \{\mathrm{A}, \mathrm{B}\} \tag{3.5}$$

$$W_{\mathrm{para}}(\mathsf{x}_{\mathrm{A}}(\tau_{\mathrm{A}}), \mathsf{x}_{\mathrm{B}}(\tau_{\mathrm{B}})) = -\frac{a^2}{4\pi^2} \frac{1}{[\sinh(a\tau_{\mathrm{A}}) - \sinh(a\tau_{\mathrm{B}}) - \mathrm{i}\epsilon]^2 - |\cosh(a\tau_{\mathrm{A}}) - \cosh(a\tau_{\mathrm{B}}) + aL|^2}, \tag{3.6}$$

where the subscript a indicates that the Wightman function is defined along an accelerated trajectory. Here, $\lim_{\epsilon \to 0^+}$ is implied. The first Wightman function (3.5) is defined along a single trajectory, whereas the second one (3.6) is along the two trajectories of A and B.

As explained before, we employ a Gaussian switching function. In this chapter, we will use

$$\chi_j(\tau_j) = e^{-\tau_j^2/2\sigma^2}, \tag{3.7}$$

where $\sigma (> 0)$ is the typical duration of interaction, or in other words, the typical width of the Gaussian function. Note that the peak of the Gaussian is at $t = 0$.

Let us consider the transition probabilities $P_{\rm A}$ and $P_{\rm B}$. For the Gaussian switching (3.7), the transition probability P_j can be simplified to [38]

$$P_j = \underbrace{\frac{\lambda^2}{4\pi}[e^{-\Omega^2\sigma^2} - \sqrt{\pi}\Omega\sigma\mathrm{erfc}(\Omega\sigma)]}_{\text{at rest}} + \frac{\lambda^2 a\sigma}{4\pi^{3/2}}\int_0^\infty \mathrm{d}s\, \frac{\cos(\beta s)e^{-\alpha s^2}(\sinh^2 s - s^2)}{s^2\sinh^2 s}\,, \tag{3.8}$$

where $\beta \equiv 2\Omega/a, \alpha \equiv 1/(a\sigma)^2$, and $\mathrm{erfc}(x) \coloneqq 1 - \mathrm{erf}(x)$ is the so-called complementary error function, and $\mathrm{erf}(x)$ is the error function defined by

$$\mathrm{erf}(x) \coloneqq \frac{2}{\sqrt{\pi}}\int_0^x \mathrm{d}s\, e^{-s^2}\,. \tag{3.9}$$

We remark that the first term in P_j is the transition probability of a detector at rest in $(3+1)$-dimensional Minkowski spacetime. Moreover, this expression for P_j is the same for both A and B (i.e., $P_{\rm A} = P_{\rm B}$) since their trajectories are the same up to the spatial translation.

Anti-parallel acceleration

The anti-parallel configuration, shown in Fig. 3.1(b), is the case where two detectors accelerate toward each other and after momentarily stopping (at which point the detector separation is L), they accelerate away. Unlike the parallel acceleration configuration, the distance between the detectors is not fixed. In addition to the parallel configuration, we consider the anti-parallel and perpendicular configurations to make a comparison to the entanglement harvesting scenario examined in [38].

The trajectories are given by

$$\mathsf{x}_{\rm A} = \left\{t = \frac{1}{a}\sinh(a\tau_{\rm A}), x = \frac{1}{a}[\cosh(a\tau_{\rm A}) - 1] + \frac{L}{2}, y = 0, z = 0\right\}, \tag{3.10a}$$

$$\mathsf{x}_{\rm B} = \left\{t = \frac{1}{a}\sinh(a\tau_{\rm B}), x = -\frac{1}{a}[\cosh(a\tau_{\rm B}) - 1] - \frac{L}{2}, y = 0, z = 0\right\}. \tag{3.10b}$$

The Wightman function along a single detector trajectory is the same as the parallel acceleration case (3.5), and so is the transition probability P_j (3.8). On the other hand, the Wightman function along both the trajectories, $W(\mathsf{x}_{\rm A}, \mathsf{x}_{\rm B})$, differs from (3.6) and therefore, the off-diagonal elements $C_{\rm AB}$ and $X_{\rm AB}$ in the density matrix (2.43) are different from those in the parallel case. Note that the detectors, as long as L is small, can in general communicate with each other by exchanging field quanta when the detectors are lightlike separated. See Fig. 3.1(b).

Perpendicular acceleration

As depicted in Fig. 3.1(c), the perpendicular acceleration configuration is similar to the anti-parallel configuration, but now detectors are traveling along different axes x and y. That is, detector-A and B accelerate along y and x axes, respectively; they accelerate toward and away from each other with a 90° angle. The minimum distance between them at which they stop momentarily is L. The trajectories are

$$\mathsf{x}_{\rm A} = \left\{ t = \frac{1}{a}\sinh(a\tau_{\rm A}), x = 0, y = \frac{1}{a}[\cosh(a\tau_{\rm A}) - 1], z = 0 \right\}, \tag{3.11a}$$

$$\mathsf{x}_{\rm B} = \left\{ t = \frac{1}{a}\sinh(a\tau_{\rm B}), x = \frac{1}{a}[\cosh(a\tau_{\rm B}) - 1] + L, y = 0, z = 0 \right\}. \tag{3.11b}$$

As before, the transition probability P_j of each detector is the same as (3.8).

3.2 Results: thermality and Unruh effect

We now examine the correlation harvested by two uniformly accelerated UDW detectors in the Minkowski vacuum. The main message of this section is that, although a single accelerating detector observes thermality, the correlation between two detectors after the interaction is very different from that of inertial detectors in a thermal bath. To show this, we first revisit the correlation harvesting protocol by two detectors at rest in a thermal bath in [1]. We then provide our results.

3.2.1 Review: harvesting correlations from a thermal bath

Here, we briefly review [1] and obtain their results summarized in Fig. 1.2.

Consider $(n+1)$-dimensional Minkowski spacetime with a massive quantum field in a KMS state $\rho_{\rm th}$. One can calculate the thermal Wightman function at the inverse temperature β as

$$W_{\rm th}(\mathsf{x},\mathsf{x}') = W_{\rm vac}(\mathsf{x},\mathsf{x}') + W_\beta(\mathsf{x},\mathsf{x}'), \tag{3.12}$$

where

$$W_{\rm vac}(\mathsf{x},\mathsf{x}') = \int_{\mathbb{R}^3} \frac{{\rm d}^n k}{(2\pi)^n 2\omega_{\boldsymbol{k}}} e^{-{\rm i}\omega_{\boldsymbol{k}}(t-t')+{\rm i}\boldsymbol{k}\cdot(\boldsymbol{x}-\boldsymbol{x}')}, \tag{3.13a}$$

$$W_\beta(\mathsf{x},\mathsf{x}') = \int_{\mathbb{R}^3} \frac{{\rm d}^n k}{(2\pi)^n 2\omega_{\boldsymbol{k}}} \frac{e^{-{\rm i}\omega_{\boldsymbol{k}}(t-t')+{\rm i}\boldsymbol{k}\cdot(\boldsymbol{x}-\boldsymbol{x}')} + {\rm c.c.}}{e^{\beta\omega_{\boldsymbol{k}}} - 1}, \tag{3.13b}$$

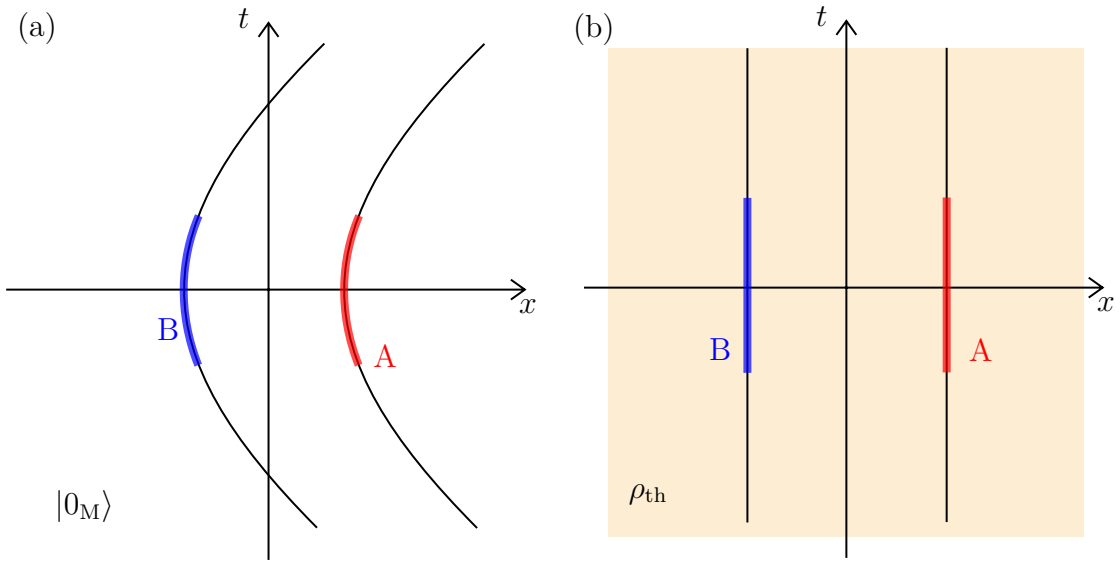

Figure 3.2: (a) Uniformly accelerating UDW detectors A and B in the Minkowski vacuum $|0_{\rm M}\rangle$. (b) Detectors at rest in a thermal bath (depicted in orange). The field is in the KMS state $\rho_{\rm th}$.

are the vacuum Wightman function and the thermal contribution to the Wightman function, respectively.[1] One can then evaluate the elements of the density matrix (2.43) from this Wightman function $W_{\rm th}(\mathsf{x},\mathsf{x}')$ and show that for identical UDW detectors, the non-local elements $X^{\rm th}_{\rm AB}(T_1)$ and $X^{\rm th}_{\rm AB}(T_2)$ for any temperatures obeying $T_1 < T_2$ satisfies $|X^{\rm th}_{\rm AB}(T_2)| \leq |X^{\rm th}_{\rm AB}(T_1)|$, and consequently the concurrences are [1]

$$\mathcal{C}^{\rm th}_{\rm AB}(T_2) \leq \mathcal{C}^{\rm th}_{\rm AB}(T_1)\,. \tag{3.14}$$

This means that the ability to harvest entanglement downgrades monotonically with the temperature $T(=\beta^{-1})$ of the thermal bath.

One can also numerically show that the harvested quantum mutual information behaves in an opposite manner. Consider $(3+1)$-dimensional Minkowski spacetime, in which the two detectors are at rest in a single reference frame [Fig. 3.2(b)]. By employing Gaussian switching $\chi(\tau) = e^{-\tau^2/2\sigma^2}$, Fig. 3.3 depicts the temperature dependence of (a) transition probability P and correlation element $|C_{\rm AB}|$, and (b) quantum mutual information $I_{\rm AB}$

[1] In fact, this is the same result as those obtained by using the Gibbs thermal state $\rho = e^{-\beta\hat{H}_\phi}/Z$, where $Z = {\rm Tr}[e^{-\beta\hat{H}_\phi}]$ is the partition function [1].

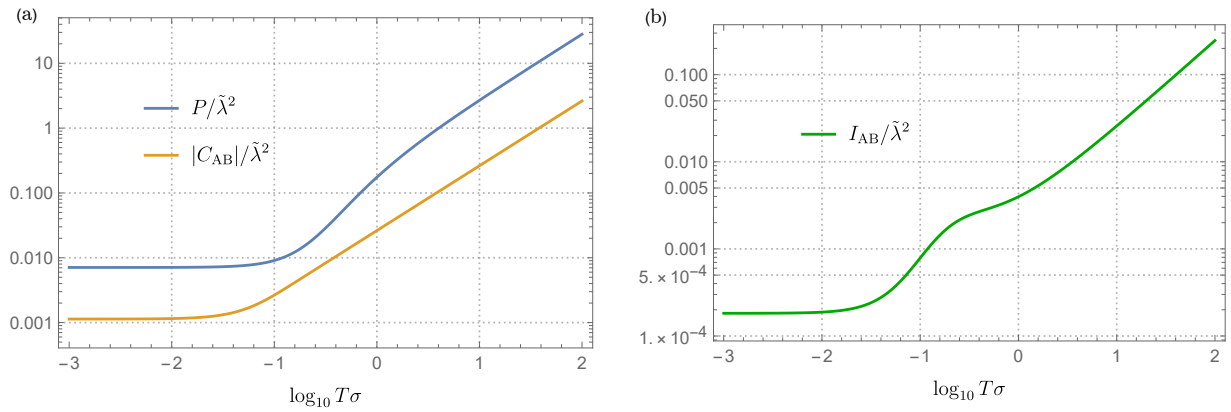

Figure 3.3: Harvesting protocol considered in [1]. (a) Transition probability P and the correlation element $|C_{\rm AB}|/\tilde{\lambda}^2$ as a function of the temperature of the field. Here, $\Omega\sigma = 1, L/\sigma = 7$. Unlike $|X_{\rm AB}|$, the element $|C_{\rm AB}|$ increases with temperature. (b) Using the elements in (a), quantum mutual information $I_{\rm AB}/\tilde{\lambda}^2$ is plotted as a function of $T\sigma$.

examined in [1]. Unlike concurrence, quantum mutual information increases with temperature T. This is due to the fact that $|C_{\rm AB}|$ also increases with $T\sigma$. We point out that the quantum mutual information is not monotonic with T in some cases. Nevertheless, $I_{\rm AB}$ never decreases at the high-temperature regime.

3.2.2 Correlations harvested by accelerating detectors

Figure 3.4 shows the effect of acceleration on mutual information harvesting for each of the scenarios in Fig. 3.1, plotting mutual information $I_{\rm AB}$ as a function of acceleration $a\sigma$ (which is proportional to the Unruh temperature $T_{\rm U} = a/2\pi$). The diagrams depict different energy gaps Ω and detector separations L at $t = 0$. Figures 3.4(a) and (b) depict $I_{\rm AB}$ with $\Omega\sigma = 0.5$ and 2, respectively, when the separation is small ($L/\sigma = 1$), whereas (c) and (d) have a large separation: $L/\sigma = 7$ for the same two gaps. Note that the effect of communication between the two detectors is negligible when $L/\sigma = 7$, which suggests that the harvested mutual information predominantly comes from the Hadamard contribution and it is genuine quantum mutual information. On the other hand, both the Hadamard and Pauli-Jordan parts of the Wightman function contribute to the case of $L/\sigma = 1$, and so this is the communication-assisted mutual information.

We see that high acceleration suppresses mutual information harvesting in all three

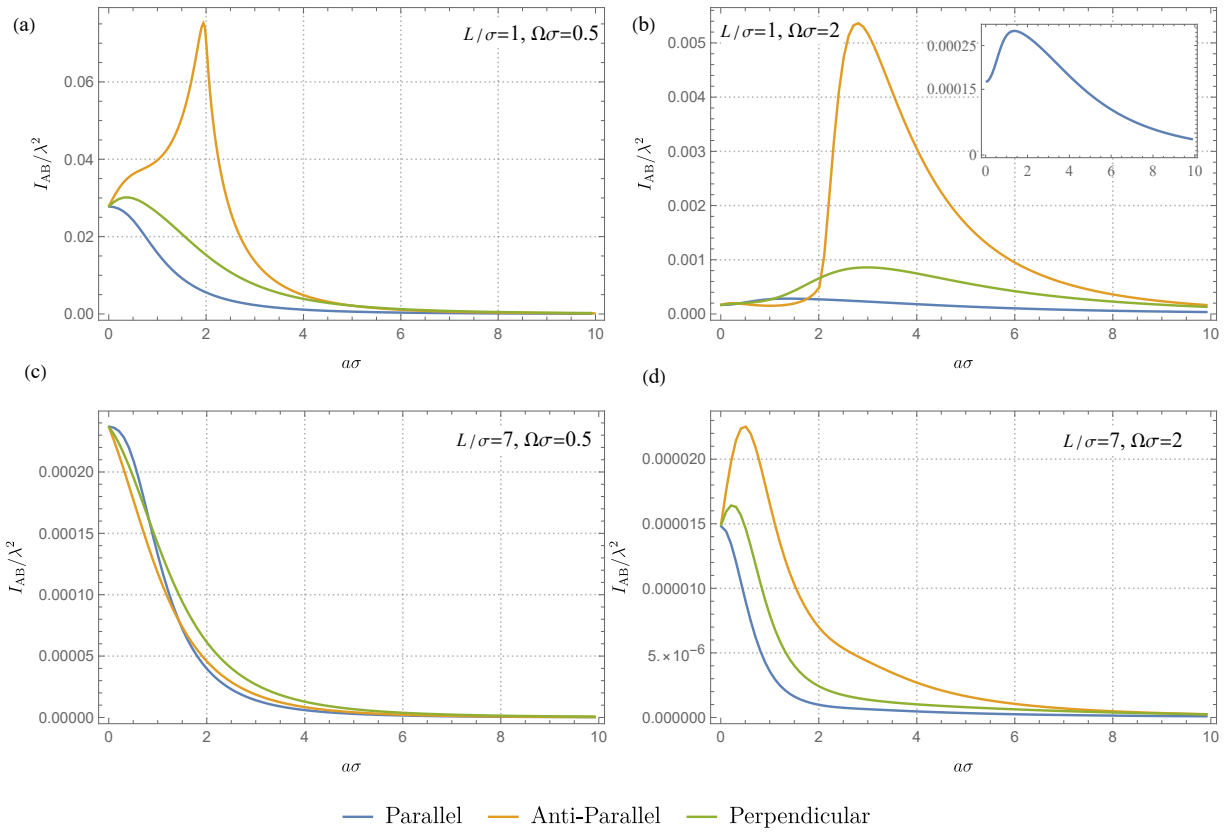

Figure 3.4: Mutual Information as a function of acceleration $a\sigma$ in three acceleration scenarios (parallel, anti-parallel, and perpendicular). (a) $L/\sigma = 1, \Omega\sigma = 0.5$, (b) $L/\sigma = 1, \Omega\sigma = 2$, (c) $L/\sigma = 7, \Omega\sigma = 0.5$, and (d) $L/\sigma = 7, \Omega\sigma = 2$.

acceleration scenarios regardless of the energy gap $\Omega\sigma$ and separation L/σ. This characteristic property of mutual information can be explained as follows. Since the two detectors have the same transition probabilities, $P_{\mathrm{A}} = P_{\mathrm{B}} \equiv P$, then $\mathcal{L}_{\pm}$ in (2.66) becomes

$$\mathcal{L}_{\pm} = P \pm |C_{\mathrm{AB}}| \,. \tag{3.15}$$

The reason that I_{AB} vanishes at high acceleration (or equivalently, high temperatures $T_{\mathrm{U}} \to \infty$) is that the transition probability P monotonically increases with $a\sigma$ while $|C_{\mathrm{AB}}|$ remains small, which leads to $P \gg |C_{\mathrm{AB}}|$ and so $\mathcal{L}_{\pm} \approx P$. Thus, the mutual information $I_{\mathrm{AB}} \approx 0$. However, for a thermal bath (Fig. 1.2) [1], the mutual information between two inertial detectors increases with T because both P and $|C_{\mathrm{AB}}|$ increase with temperature T; consequently the mutual information monotonically increases with T.

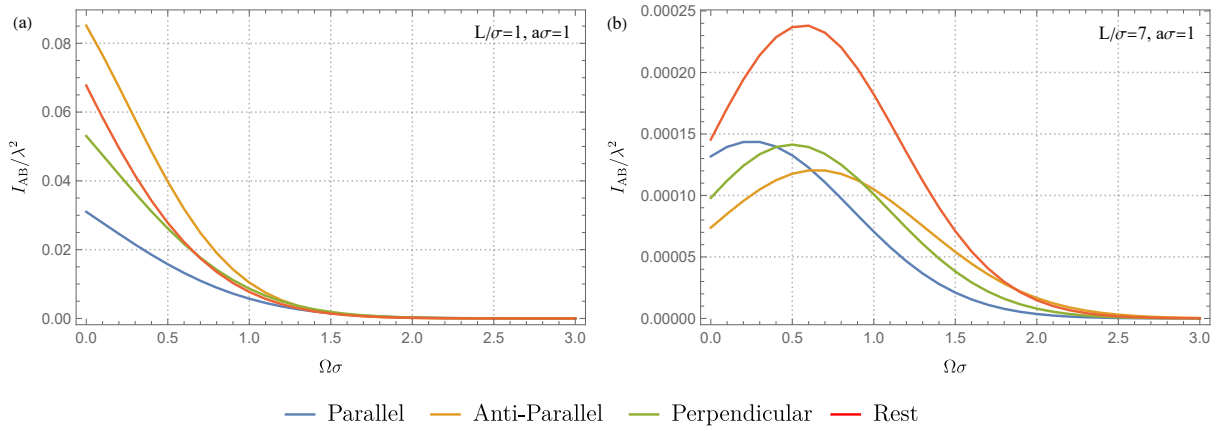

Figure 3.5: Mutual Information as a function of energy gap $\Omega\sigma$ in three acceleration scenarios (parallel, anti-parallel, and perpendicular) with $a\sigma = 1$ and (a) $L/\sigma = 1$, (b) $L/\sigma = 7$. The red curve represents the harvested mutual information by two inertial detectors in the Minkowski vacuum, which corresponds to $a\sigma = 0$.

By contrast, small acceleration seems to affect mutual information harvesting differently depending on the type of acceleration, energy gap, and detectors' separation. In the case of small energy gap and small detector separation, shown in Fig. 3.4(a), we find that small acceleration enhances mutual information for anti-parallel and perpendicular configurations with higher harvested mutual information in the anti-parallel scenario, while harvested mutual information monotonically decreases with $a\sigma$ in the parallel acceleration case. Nevertheless, as the energy gap Ω changes from 0.5 to 2, the acceleration dependence of $I_{\rm AB}$ changes, as shown in Fig. 3.4(b). In particular, the parallel acceleration case no longer monotonically decreases with $a\sigma$, and smaller acceleration could enhance mutual information harvesting. This is also true for $L/\sigma = 7$ in Figs. 3.4(c) and (d). We also examine how harvested mutual information changes with the energy gap by plotting $I_{\rm AB}$ as a function of $\Omega\sigma$ in Fig. 3.5. Here, we fix the value of acceleration to be $a\sigma = 1$, and plot the energy gap dependence when $L/\sigma = 1$ and 7 in Figs. 3.5(a) and (b), respectively. For entanglement harvesting reported in [38], any accelerating detectors (as well as inertial detectors) with small energy gaps cannot extract entanglement when the detector separation L is large. However, this is not the case for mutual information; we find that for both $L/\sigma = 1$ and 7 in Fig. 3.5, mutual information $I_{\rm AB}$ is non-vanishing near $\Omega = 0$, which suggests that the harvested correlation with small Ω is either classical correlation or non-distillable entanglement.

3.2.3 Comparison to previous studies

As we have shown in the previous section, harvested quantum mutual information $I_{\rm AB}$ behaves in a manner similar to harvested entanglement [38]. From Fig. 1.2, we can now discuss how different the temperature dependence among various scenarios is. Here, we focus on the difference between the accelerating detector scenarios and the thermal bath scenario in [95, 1].

Recall that the concurrence for detectors in a thermal bath, $\mathcal{C}^{\rm th}_{\rm AB}(T)$, monotonically decreased with the temperature as in (3.14) [1]. This is distinct from the case of uniformly accelerating detectors [38], where entanglement is either enhanced before vanishing at high temperature or monotonically decreases, depending on parameters such as the energy gap Ω. It is difficult to analytically show the behavior of quantum mutual information due to its logarithmic definition. However one can numerically check that the mutual information in a thermal bath increases at the high-temperature regime [1] as depicted in Fig. 3.3(b), whereas our result (Fig. 3.4) shows similar behavior to that in the entanglement harvesting scenario with accelerating detectors [38].

Although an accelerating single detector experiences a thermal bath, two detectors exhibit remarkably different behavior. This can be explained by looking at their Wightman functions (3.12) and (3.6). One can examine this difference by, for example, performing a series expansion around $T = 0$:

$$W_{\rm th}(\mathsf{x},\mathsf{x}') = W_{\rm vac}(\mathsf{x},\mathsf{x}') + \frac{T^2}{12} + \mathcal{O}(T^4)\,, \tag{3.16}$$

$$W_a(\mathsf{x},\mathsf{x}') = W_{\rm vac}(\mathsf{x},\mathsf{x}') + c_1(\mathsf{x},\mathsf{x}')T_{\rm U} + c_2(\mathsf{x},\mathsf{x}')T_{\rm U}^2 + \mathcal{O}(T_{\rm U}^3)\,, \tag{3.17}$$

where the $c_j(\mathsf{x},\mathsf{x}')$ are expansion coefficients that depend on the spacetime points. Note that $W_{\rm th}(\mathsf{x},\mathsf{x}')$ has an expansion in even-powers of T for two arbitrary points x and x', and thereby along a single detector trajectory. On the other hand, for a single accelerating detector, these functions become $c_1(\mathsf{x},\mathsf{x}') = 0$ and $c_2(\mathsf{x},\mathsf{x}') = 1/12$, and so $W_a(\mathsf{x},\mathsf{x}')$ reduces to

$$W_a(\mathsf{x},\mathsf{x}') = W_{\rm vac}(\mathsf{x},\mathsf{x}') + \frac{T_{\rm U}^2}{12} + \mathcal{O}(T_{\rm U}^4)\,, \tag{3.18}$$

which is equivalent to $W_{\rm th}(\mathsf{x},\mathsf{x}')$. Apparently, the Wightman functions along two trajectories differ, whereas the ones on a single trajectory match. It is not so surprising that two distinct Wightman functions give different correlations. If we specify the state of the field and the trajectories of the detectors in such a way that two Wightman functions match,

the corresponding quantities such as concurrence or transition probability behave in the same way, which is the case for a single accelerating detector.

As an application of this observation, consider two UDW detectors in an expanding universe considered in [49, 96]. The line element of the de Sitter spacetime in the planar coordinates is

$$\mathrm{d}s^2 = -\mathrm{d}t^2 + e^{2\kappa t}(\mathrm{d}x^2 + \mathrm{d}y^2 + \mathrm{d}z^2)\,, \tag{3.19}$$

where κ is the expansion rate of the universe. We employ a conformally coupled, massless scalar field in the conformal vacuum. In this case, a single inertial detector also sees a thermal bath at temperature $T_{\rm GH} \coloneqq \kappa/2\pi$ (the Gibbons-Hawking effect [97]). This can be seen from the Wightman function [2],

$$\begin{aligned} W_{\rm dS}(\mathsf{x},\mathsf{x}') = -\frac{1}{4\pi^2}\frac{1}{\dfrac{\sinh^2(\pi T_{\rm GH}\Delta t - \mathrm{i}\epsilon)}{\pi^2 T_{\rm GH}^2} - e^{2\pi T_{\rm GH}\Delta_+ t}L^2}\,, \\ (\Delta t \equiv t - t',\, \Delta_+ t \equiv t + t')\,, \end{aligned} \tag{3.20}$$

by pulling it back to a single inertial trajectory, $L = 0$, which yields the same form as (3.5).

Nevertheless, a series expansion of $W_{\rm dS}(\mathsf{x},\mathsf{x}')$ around $T_{\rm GH} = 0$ reads

$$W_{\rm dS}(\mathsf{x},\mathsf{x}') = W_{\rm M}(\mathsf{x},\mathsf{x}') + c_1^{\rm dS}(\mathsf{x},\mathsf{x}')T_{\rm GH} + c_2^{\rm dS}(\mathsf{x},\mathsf{x}')T_{\rm GH}^2 + \mathcal{O}(T_{\rm GH}^3)\,, \tag{3.21}$$

and this obviously differs from $W_{\rm th}(\mathsf{x},\mathsf{x}')$ in (3.16).

In summary, harvested correlations do not necessarily show the same behavior even if two scenarios give the same transition probability. This is simply because the Wightman functions are different in general between distinct spacetime points on different trajectories. These quantities, including transition probability, show identical features if the Wightman functions in two scenarios happen to be the same.

3.2.4 General argument

So far, we have considered the properties of quantum mutual information extracted from both inertial detectors in a thermal bath and from linearly accelerating detectors in the Minkowski vacuum. Although their response functions are identical, the matrix element $C_{\rm AB}$ is different in these cases, resulting in differences in quantum mutual information. Here, we provide a general argument for why such different behavior should be expected.

As shown in Appendix A, C_{AB} can be obtained from

$$\int_{\mathbb{R}} \mathrm{d}\tau_{\mathrm{A}} \int_{\mathbb{R}} \mathrm{d}\tau_{\mathrm{B}}\ \mathrm{Tr}_{\phi}\left[\hat{H}_{\mathrm{B}}(\tau_{\mathrm{B}})\rho_0 \hat{H}_{\mathrm{A}}(\tau_{\mathrm{A}})\right] . \tag{3.22}$$

By using the expressions

$$\hat{H}_j(\tau_j) = \lambda \chi_j(\tau_j)\hat{m}(\tau_j) \otimes \hat{\phi}(\mathsf{x}) , \tag{3.23}$$

$$\hat{\phi}(\mathsf{x}) = \int \frac{\mathrm{d}^n k}{\sqrt{(2\pi)^n 2\omega_{\boldsymbol{k}}}} \left(\hat{a}_{\boldsymbol{k}} e^{\mathsf{i}k\cdot x} + \hat{a}^{\dagger}_{\boldsymbol{k}} e^{-\mathsf{i}k\cdot x}\right) , \tag{3.24}$$

where $\mathsf{i}k\cdot x \equiv -\mathsf{i}\omega_{\boldsymbol{k}} t + \mathsf{i}\boldsymbol{k}\cdot\boldsymbol{x}$ and $\omega^2_{\boldsymbol{k}} = |\boldsymbol{k}|^2 + m^2$, Eq. (3.22) reads

$$\mathrm{Tr}_{\phi}\left[\left(I^{+}_{\mathrm{B},\boldsymbol{k}}\hat{\sigma}^{+}_{\mathrm{B}}\hat{a}_{\boldsymbol{k}} + I^{-}_{\mathrm{B},\boldsymbol{k}}\hat{\sigma}^{+}_{\mathrm{B}}\hat{a}^{\dagger}_{\boldsymbol{k}} + \mathrm{h.c.}\right)(\rho_{\mathrm{AB},0}\otimes\rho_{\phi})\left(I^{+}_{\mathrm{A},\boldsymbol{k}'}\hat{\sigma}^{+}_{\mathrm{A}}\hat{a}_{\boldsymbol{k}'} + I^{-}_{\mathrm{A},\boldsymbol{k}'}\hat{\sigma}^{+}_{\mathrm{A}}\hat{a}^{\dagger}_{\boldsymbol{k}'} + \mathrm{h.c.}\right)\right] , \tag{3.25}$$

where

$$I^{\pm}_{j,\boldsymbol{k}} \coloneqq \lambda \int_{\mathbb{R}} \mathrm{d}\tau_j\, \chi_j(\tau_j) \int \frac{\mathrm{d}^n k}{\sqrt{(2\pi)^n 2\omega_{\boldsymbol{k}}}} e^{\mathsf{i}\Omega\tau_j \pm \mathsf{i}k\cdot x_j} . \tag{3.26}$$

The terms $\hat{\sigma}^{+}_j\hat{a}_{\boldsymbol{k}}$ and $\hat{\sigma}^{-}_j\hat{a}^{\dagger}_{\boldsymbol{k}}$ correspond to the rotating wave terms, whereas $\hat{\sigma}^{+}_j\hat{a}^{\dagger}_{\boldsymbol{k}}$ and $\hat{\sigma}^{-}_j\hat{a}_{\boldsymbol{k}}$ are the counter-rotating wave terms. Therefore, $I^{+}_{j,\boldsymbol{k}}$ and $I^{-}_{j,\boldsymbol{k}}$ respectively correspond to the rotation and counter-rotation terms.

We now assume that the detectors' initial state is $\rho_{\mathrm{AB},0} = |g_{\mathrm{A}}\rangle\langle g_{\mathrm{A}}| \otimes |g_{\mathrm{B}}\rangle\langle g_{\mathrm{B}}|$, which further simplifies (3.25) as

$$\begin{aligned}
&\mathrm{Tr}_{\phi}\left[\left(I^{+}_{\mathrm{B},\boldsymbol{k}}\hat{\sigma}^{+}_{\mathrm{B}}\hat{a}_{\boldsymbol{k}} + I^{-}_{\mathrm{B},\boldsymbol{k}}\hat{\sigma}^{+}_{\mathrm{B}}\hat{a}^{\dagger}_{\boldsymbol{k}}\right)(\rho_{\mathrm{AB},0}\otimes\rho_{\phi})\left(I^{+*}_{\mathrm{A},\boldsymbol{k}'}\hat{\sigma}^{-}_{\mathrm{A}}\hat{a}^{\dagger}_{\boldsymbol{k}'} + I^{-*}_{\mathrm{A},\boldsymbol{k}'}\hat{\sigma}^{-}_{\mathrm{A}}\hat{a}_{\boldsymbol{k}'}\right)\right] \\
&= \mathrm{Tr}_{\phi}\left[\left(I^{+}_{\mathrm{B},\boldsymbol{k}}\hat{a}_{\boldsymbol{k}} + I^{-}_{\mathrm{B},\boldsymbol{k}}\hat{a}^{\dagger}_{\boldsymbol{k}}\right)\rho_{\phi}\left(I^{+*}_{\mathrm{A},\boldsymbol{k}'}\hat{a}^{\dagger}_{\boldsymbol{k}'} + I^{-*}_{\mathrm{A},\boldsymbol{k}'}\hat{a}_{\boldsymbol{k}'}\right)\right]\hat{\sigma}^{+}_{\mathrm{B}}\rho_{\mathrm{AB},0}\hat{\sigma}^{-}_{\mathrm{A}} \\
&= \underbrace{\left(I^{+}_{\mathrm{B},\boldsymbol{k}}I^{+*}_{\mathrm{A},\boldsymbol{k}'}\langle\hat{a}^{\dagger}_{\boldsymbol{k}'}\hat{a}_{\boldsymbol{k}}\rangle_{\rho_{\phi}} + I^{+}_{\mathrm{B},\boldsymbol{k}}I^{-*}_{\mathrm{A},\boldsymbol{k}'}\langle\hat{a}_{\boldsymbol{k}'}\hat{a}_{\boldsymbol{k}}\rangle_{\rho_{\phi}} + I^{-}_{\mathrm{B},\boldsymbol{k}}I^{+*}_{\mathrm{A},\boldsymbol{k}'}\langle\hat{a}^{\dagger}_{\boldsymbol{k}'}\hat{a}^{\dagger}_{\boldsymbol{k}}\rangle_{\rho_{\phi}} + I^{-}_{\mathrm{B},\boldsymbol{k}}I^{-*}_{\mathrm{A},\boldsymbol{k}'}\langle\hat{a}_{\boldsymbol{k}'}\hat{a}^{\dagger}_{\boldsymbol{k}}\rangle_{\rho_{\phi}}\right)}_{C_{\mathrm{AB}}} \\
&\quad\times \hat{\sigma}^{+}_{\mathrm{B}}\rho_{\mathrm{AB},0}\hat{\sigma}^{-}_{\mathrm{A}} .
\end{aligned} \tag{3.27}$$

Let us consider a specific field state ρ_{ϕ}. If the detectors are inertial in the Minkowski vacuum $\rho_{\phi} = |0_{\mathrm{M}}\rangle\langle 0_{\mathrm{M}}|$, then $\hat{a}_{\boldsymbol{k}}|0_{\mathrm{M}}\rangle = 0$ for all $\boldsymbol{k}$, which leads to

$$C_{\mathrm{AB}} = I^{-}_{\mathrm{B},\boldsymbol{k}}I^{-*}_{\mathrm{A},\boldsymbol{k}'}\langle 0_{\mathrm{M}}|\hat{a}_{\boldsymbol{k}'}\hat{a}^{\dagger}_{\boldsymbol{k}}|0_{\mathrm{M}}\rangle . \tag{3.28}$$

This means that the only contribution is from the counter-rotating terms.

Now, instead of the Minkowski vacuum, let us consider the inertial detectors in a thermal state $\rho_\phi = \rho_{\rm th}$. In this case, it is known that $\langle \hat{a}_{\boldsymbol{k}'} \hat{a}_{\boldsymbol{k}} \rangle_{\rho_{\rm th}} = \langle \hat{a}^\dagger_{\boldsymbol{k}'} \hat{a}^\dagger_{\boldsymbol{k}} \rangle_{\rho_{\rm th}} = 0$ [1] and so

$$C_{\rm AB} = I^{+}_{{\rm B},\boldsymbol{k}} I^{+*}_{{\rm A},\boldsymbol{k}'} \langle \hat{a}^\dagger_{\boldsymbol{k}'} \hat{a}_{\boldsymbol{k}} \rangle_{\rho_{\rm th}} + I^{-}_{{\rm B},\boldsymbol{k}} I^{-*}_{{\rm A},\boldsymbol{k}'} \langle \hat{a}_{\boldsymbol{k}'} \hat{a}^\dagger_{\boldsymbol{k}} \rangle_{\rho_{\rm th}} \ . \tag{3.29}$$

This expression has contributions from both the rotating and counter-rotating terms.

One could ask how this is different from the linearly accelerating detectors in the Minkowski vacuum. In this case, the field operator $\hat{\phi}(\mathsf{x})$ is written in terms of the Rindler modes $\hat{b}_{\boldsymbol{k}}$ with $\hat{b}_{\boldsymbol{k}} |0_{\rm M}\rangle \neq 0$. The operators $\hat{b}_{\boldsymbol{k}}$ and $\hat{b}^\dagger_{\boldsymbol{k}}$ are related to the Minkowski modes $\hat{a}_{\boldsymbol{k}}$ and $\hat{a}^\dagger_{\boldsymbol{k}}$ by a Bogoliubov transformation. For this reason, all four terms in (3.27) are non-vanishing, which leads to the difference between the cases of the thermal bath and linear acceleration.

Chapter 4

Extraction of bipartite correlation from BTZ black hole spacetime

In this chapter, we consider the quantum mutual information harvesting protocol in a black hole spacetime and examine how the Hawking and Unruh effects affect the extraction of correlations. Realistic black hole spacetimes, such as the (3+1)-dimensional Schwarzschild black hole, are of great interest. However, their computations involve mode sums, which can be extremely tedious if one tries a brute force calculation. However, see the recent advancement, for example, [98, 99] for the transition probability and [47] for entanglement harvesting. Here, we instead consider simplified black hole spacetimes: the Bañados-Teitelboim-Zanelli (BTZ) spacetime in Ch. 4 and the $(1 + 1)$-dimensional Schwarzschild black hole (Ch. 6) spacetimes.

The lesson we will learn in this chapter is that an extreme temperature caused by the Hawking and Unruh effects will prevent two detectors from harvesting correlations from the field. This is somewhat different from the case of detectors at rest in a thermal bath as described in Ch. 3 (also see Fig. 1.2). In [1], it is shown that extracted correlations from a quantum scalar field in the KMS state by two inertial detectors in Minkowski spacetime have the following properties: (i) extracted entanglement monotonically decreases with increasing temperature; and (ii) extracted mutual information increases with temperature. However, as we will see in this chapter, high temperatures due to Hawking and Unruh effects forbid the extraction of correlation of *any* type.

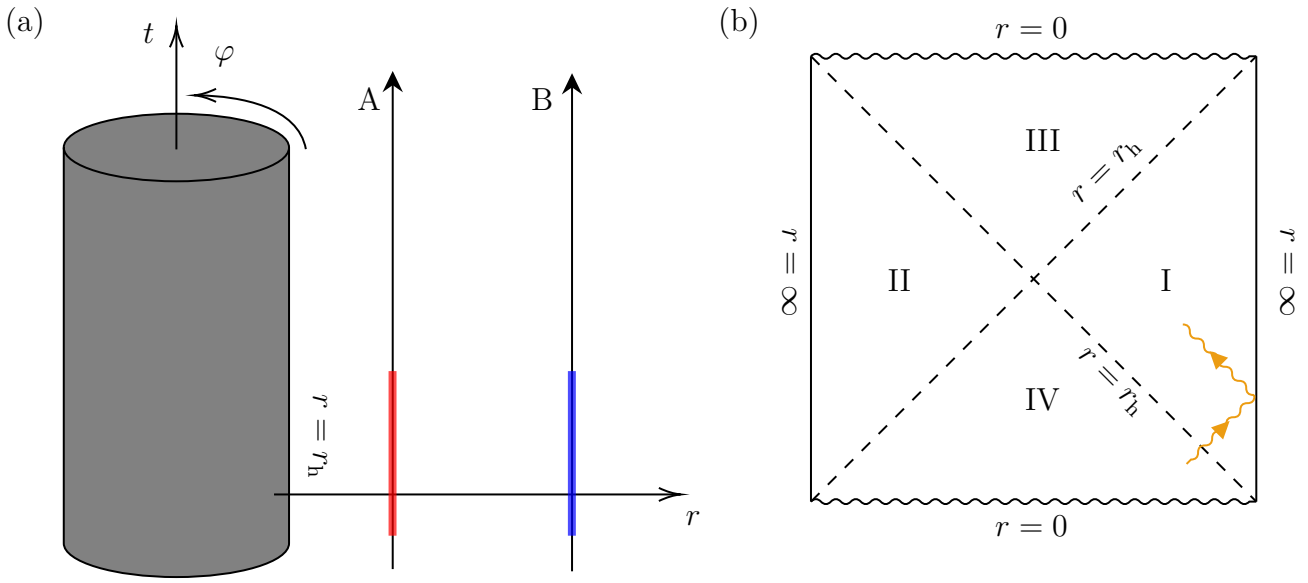

Figure 4.1: (a) A schematic diagram of a BTZ black hole with two detectors A and B floating outside of it. The red and blue stripes indicate when the detectors interact with the quantum field. (b) A Penrose diagram of BTZ spacetime. Regions I and II are the exteriors of the black hole while III is the interior of the black hole. Region IV is the white hole. The orange wiggling line represents a photon traveling toward the boundary $r = \infty$, bouncing off, and traveling toward the black hole.

4.1 Static detectors in BTZ black hole spacetime

4.1.1 Quantum field in BTZ spacetime

BTZ spacetime

The BTZ black hole spacetime [100, 101] is a $(2+1)$-dimensional spacetime and can be obtained as a solution to the Einstein field equations with a negative cosmological constant $\Lambda = -1/\ell^2$, where $\ell(\geq 0)$ is the so-called AdS (anti-de Sitter) length. See Appendix B for details. The line-element for a non-rotating BTZ spacetime reads

$$\mathrm{d}s^2 = -f(r)\mathrm{d}t^2 + \frac{\mathrm{d}r^2}{f(r)} + r^2\mathrm{d}\varphi^2\,, \quad f(r) = \frac{r^2}{\ell^2} - M \tag{4.1}$$

where $t \in \mathbb{R}, r \in (0,\infty)$, and $\varphi \in [0, 2\pi)$. One can think of (r, φ) as a polar coordinate system. M is the mass of the black hole, which is dimensionless in this case. The event horizon is located at $r = r_{\rm h} \equiv \ell\sqrt{M}$. See Fig. 4.1.

We note that the BTZ spacetime can be obtained from $(2+1)$-dimensional AdS_3 spacetime by a topological identification and thereby BTZ spacetime is conformally equivalent to AdS_3. That is, BTZ spacetime locally looks like AdS_3 and shares similar properties. This fact allows us to write the Wightman function $W_{\rm BTZ}(\mathsf{x}, \mathsf{x}')$, in BTZ spacetime as a sum of correlators in AdS_3, $W_{\rm AdS_3}(\mathsf{x}, \mathsf{x}')$. See Appendix B for details.

Since we will be considering two static detectors sitting outside the black hole [see Fig. 4.1(a) for the illustration], let us introduce the proper time τ of such detectors and the proper distance between two spatial points at a constant time. By a static detector, we mean a pointlike detector following a timelike Killing vector field ∂_t at a fixed point (r, φ). Thus, the proper time of such a detector can be obtained from the line-element (4.1) by setting $\mathrm{d}r = 0$ and $\mathrm{d}\varphi = 0$:

$$\mathrm{d}\tau = \sqrt{f(r)}\mathrm{d}t\,. \tag{4.2}$$

We impose that $\tau = 0$ when $t = 0$ so that $\tau = \sqrt{f(r)}t$. The quantity $\sqrt{f(r)}$ is called the redshift factor, and we denote this by

$$\gamma(r) \equiv \sqrt{f(r)} = \frac{\sqrt{r^2 - r_{\rm h}^2}}{\ell} \qquad (r \geq r_{\rm h})\,. \tag{4.3}$$

Note that $\gamma(r) \to 0$ as $r \to r_{\rm h}$.

Let us introduce a (radial) proper distance on a time-slice $\mathrm{d}t = 0$. The proper distance, $d(r_1, r_2)$, between two spacetime points (t, r_1, φ) and (t, r_2, φ) with $r_2 > r_1 \geq r_{\rm h}$ can be obtained from the line-element (4.1) by setting $\mathrm{d}t = 0$ and $\mathrm{d}\varphi = 0$:

$$d(r_1, r_2) = \ell \ln\left(\frac{r_2 + \sqrt{r_2^2 - r_{\rm h}^2}}{r_1 + \sqrt{r_1^2 - r_{\rm h}^2}}\right)\,. \tag{4.4}$$

For simplicity, we will denote the proper distance between the horizon and detector-j by $d_j \equiv d(r_{\rm h}, r_j)$ with $r_j (\geq r_{\rm h})$ being the radial coordinate of detector-j, and proper distance between detectors A and B by $d_{\rm AB} \equiv d(r_{\rm A}, r_{\rm B})$.

The Hawking temperature $T_{\rm H}$ of a BTZ black hole (seen from $r = \infty$) is known as [100] $T_{\rm H} = r_{\rm h}/2\pi\ell^2$ and the local temperature $T_j \equiv T(r_j)$ at radial position $r = r_j$ can be

derived from the KMS condition as [102]

$$T_j = \frac{T_{\rm H}}{\gamma(r_j)}\,, \tag{4.5}$$

which is equivalent to the Tolman relation [103]. For $r_{\rm B} > r_{\rm A} > r_{\rm h}$, the redshift factors for detectors A and B can be written in terms of the proper distances:

$$\gamma_{\rm A} \equiv \gamma(r_{\rm A}) = \frac{r_{\rm h}}{\ell} \sinh \frac{d_{\rm A}}{\ell}\,, \tag{4.6a}$$

$$\gamma_{\rm B} \equiv \gamma(r_{\rm B}) = \frac{r_{\rm h}}{\ell} \sinh \frac{d_{\rm AB} + d_{\rm A}}{\ell}\,. \tag{4.6b}$$

QFT in BTZ spacetime

Let us now consider a quantum scalar field $\hat{\phi}(\mathsf{x})$ defined on this spacetime. In particular, a massless conformally coupled scalar field satisfying the Klein-Gordon equation,

$$(\Box - R/8)\hat{\phi}(\mathsf{x}) = 0\,, \tag{4.7}$$

where $\Box$ is the d'Alembert operator and R is the Ricci scalar. Since BTZ spacetime is conformally equivalent to AdS_3, the conformally coupled quantum field in BTZ can be constructed from that of AdS_3.

Let $W_{\rm BTZ}(\mathsf{x},\mathsf{x}') \coloneqq \langle 0_{\rm H}|\hat{\phi}(\mathsf{x})\hat{\phi}(\mathsf{x}')|0_{\rm H}\rangle$ be the Wightman function in the Hartle-Hawking vacuum $|0_{\rm H}\rangle$ in the BTZ spacetime so that the BTZ black hole is in thermal equilibrium with its exterior. $W_{\rm BTZ}(\mathsf{x},\mathsf{x}')$ can be expressed as an image sum of the correlation function in AdS_3 spacetime [102, 104]:

$$\begin{aligned} W_{\rm BTZ}(\mathsf{x},\mathsf{x}') &= \sum_{n=-\infty}^{\infty} W_{\mathrm{AdS}_3}(\mathsf{x},\Gamma^n\mathsf{x}') \\ &= \frac{1}{4\pi\sqrt{2}\ell} \sum_{n=-\infty}^{\infty} \left[\frac{1}{\sqrt{\sigma_\epsilon(\mathsf{x},\Gamma^n\mathsf{x}')}} - \frac{\zeta}{\sqrt{\sigma_\epsilon(\mathsf{x},\Gamma^n\mathsf{x}')+2}} \right], \end{aligned} \tag{4.8}$$

where $\Gamma : (t, r, \varphi) \mapsto (t, r, \varphi + 2\pi)$ is a topological identification of an event in AdS_3 and

$$\sigma_\epsilon(\mathsf{x},\Gamma^n\mathsf{x}') = \frac{rr'}{r_{\rm h}^2}\cosh\left[\frac{r_{\rm h}}{\ell}(\Delta\varphi - 2\pi n)\right] - 1 - \frac{\sqrt{(r^2-r_{\rm h}^2)(r'^2-r_{\rm h}^2)}}{r_{\rm h}^2}\cosh\left(\frac{r_{\rm h}}{\ell^2}\Delta t - \mathrm{i}\epsilon\right)$$

with $\Delta\varphi \coloneqq \varphi - \varphi'$, $\Delta t \coloneqq t - t'$, and ϵ is a UV cutoff. As shown in Fig. 4.1(b), the spatial infinity ($r \to \infty$) of BTZ spacetime is timelike, and so one needs to impose a boundary condition, which is characterized by $\zeta \in \mathbb{R}$.

4.1.2 Mutual information harvested from BTZ spacetime

In this section, we investigate how a black hole affects the extraction of quantum mutual information. We assume the following:

- Detectors A and B are both static outside the black hole as depicted in Fig. 4.1(a). Their trajectories are respectively described by $(t, r_{\rm A}, \varphi_0)$ and $(t, r_{\rm B}, \varphi_0)$, where $r_{\rm B} > r_{\rm A} > r_{\rm h}$ and φ_0 is a constant.
- Both detectors have the same Gaussian switching function $\chi(\tau_j) = e^{-\tau_j^2/2\sigma^2}$, where σ is the Gaussian width. All quantities will be expressed in units of σ to make them adimensional. For example, $\tilde{\lambda} \coloneqq \lambda\sqrt{\sigma}$ denotes a dimensionless coupling constant.
- The proper separation between A and B, $d_{\rm AB}/\sigma$, is always fixed so that the change in correlation comes from the black hole and not from the change in $d_{\rm AB}/\sigma$. Specifically, we set $d_{\rm AB}/\sigma = 7$ so that the contribution coming from the Pauli-Jordan function (2.26) is very small.

We remind the reader that we are examining quantum mutual information (2.65) by computing P_j and $C_{\rm AB}$ by substituting the Wightman function (4.8) into Eqs. (2.44a) and (2.44b). Therefore, in general, the mutual information is a function of $d_j, d_{\rm AB}, \Omega, \ell$, and M: $I_{\rm AB} = I_{\rm AB}(d_{\rm A}/\sigma, d_{\rm B}/\sigma, d_{\rm AB}/\sigma, \Omega\sigma, \ell/\sigma, M)$. Also note that the Wightman function in (4.8) has a square root, leading to branch cuts in the complex plane. It turns out that one of the branch cuts resides along the real axis, and one has to take this into account when evaluating (2.44). We explicitly deal with this issue in Appendix B.2.

Let us first analyze the dependence on the energy gap of the detectors, Ω, and the proper distance $d_{\rm A} \equiv d(r_{\rm h}, r_{\rm A})$ between detector-A and the event horizon in Fig. 4.2. Here, we fix $\ell/\sigma = 10, M = 10^{-2}$ (which gives $r_{\rm h}/\sigma = 1$) and $d_{\rm AB}/\sigma = 7$. Since $d_{\rm B} = d_{\rm A} + d_{\rm AB}$, mutual information becomes a function of $d_{\rm A}$ and Ω: $I_{\rm AB} = I_{\rm AB}(d_{\rm A}/\sigma, \Omega\sigma)$. Figure 4.2(a) is a 3D plot of quantum mutual information, $I_{\rm AB}/\tilde{\lambda}^2$, as a function of $d_{\rm A}/\sigma$ and $\Omega\sigma$, and Figs. 4.2(b) and (c) are the slices of (a) with constant $d_{\rm A}/\sigma$ and $\Omega\sigma$, respectively. From Figs. 4.2(a) and (b), one finds that there exists an optimal value of $\Omega\sigma$ for mutual information harvesting.

Figure 4.2(c) displays quantum mutual information as a function of $d_{\rm A}/\sigma$ for various values of $\Omega\sigma$. For a given value of $\Omega\sigma$, a point on the curve represents the amount of harvested value $I_{\rm AB}/\tilde{\lambda}^2$ after the interaction, with detectors A and B placed at distances $d_{\rm A}$ and $d_{\rm B} = d_{\rm A} + d_{\rm AB}$ from the horizon, respectively. Overall, as the detectors move away

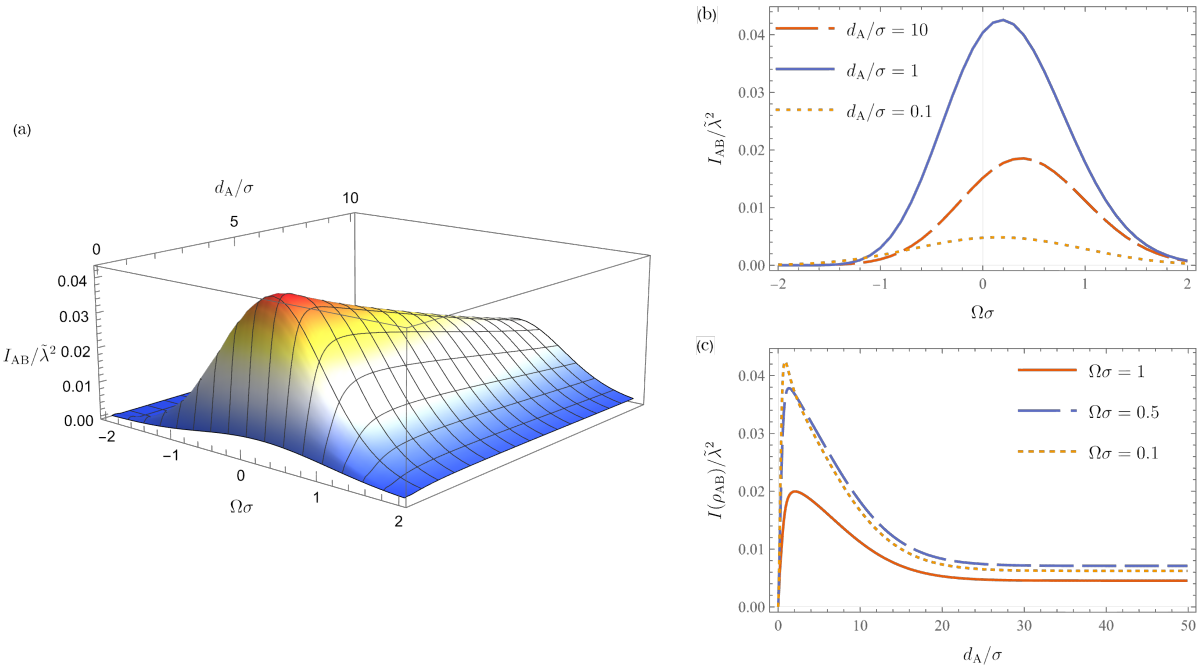

Figure 4.2: (a) 3D plot of quantum mutual information $I_{AB}/\tilde{\lambda}^2$ as a function of energy gap $\Omega\sigma$ and proper distance d_A/σ. The parameters are chosen to be $\ell/\sigma = 10, M = 10^{-2}$, and $d_{AB}/\sigma = 7$. (b) Some slices of (a) with constant $d_A/\sigma = 10, 1$, and 0.1. (c) Slices of (a) with constant $\Omega\sigma = 1, 0.5$, and 0.1.

from the horizon, the mutual information initially grows very quickly, reaches a maximum, and then asymptotes to a constant corresponding to detectors in AdS_3 spacetime.

Henderson *et al.* [41] showed that two static detectors cannot harvest entanglement when one of them is close to the black hole. That is, if one plots the concurrence $\mathcal{C}_{AB}/\tilde{\lambda}^2$ as a function of d_A/σ as in Fig. 4.2(c), then $\mathcal{C}_{AB}/\tilde{\lambda}^2 = 0$ for some d_A/σ near $d_A/\sigma = 0$. Such a region is known as the "entanglement shadow," and Ref. [41] concluded that this is due to extreme Hawking radiation and gravitational redshift.

By contrast, our mutual information $I_{AB}/\tilde{\lambda}^2$ depicted in Fig. 4.2(c) is non-zero everywhere except at $d_A/\sigma = 0$, namely, a "quantum mutual information shadow" does not exist. In other words, detectors are able to harvest mutual information from the region arbitrarily close to the horizon. Since the detectors can harvest mutual information but not entanglement near the horizon, the extracted correlation in the entanglement shadow is either the classical correlation or non-distillable entanglement. As we will see in the next chapter, this statement holds true even in the $(1+1)$-dimensional Schwarzschild spacetime [43, 44].

One would expect that the decline of correlation near the horizon and its death at $d_{\rm A}/\sigma = 0$ are attributed to the gravitational redshift and the intense Hawking radiation as suggested in Ref. [41]. In fact, we will show that it is not the gravitational redshift but rather Hawking radiation that kills the correlation at $d_{\rm A}/\sigma = 0$. To this end, we examine how these two factors contribute by treating detector A's redshift factor $\gamma_{\rm A}$ and local temperature $T_{\rm A}$ as independent variables, and write quantum mutual information as well as concurrence as a function of them: $I_{\rm AB} = I_{\rm AB}(T_{\rm A}\sigma, \gamma_{\rm A}), \mathcal{C}_{\rm AB} = \mathcal{C}_{\rm AB}(T_{\rm A}\sigma, \gamma_{\rm A})$. To do this, let us express the event horizon $r_{\rm h}$ and the proper distance $d_{\rm A}$ in terms of $T_{\rm A}$ and $\gamma_{\rm A}$ as follows.

$$r_{\rm h} = 2\pi\ell^2 T_{\rm A}\gamma_{\rm A}\,, \tag{4.9}$$

$$d_{\rm A} = \ell \ln \frac{1+\sqrt{1+(2\pi\ell T_{\rm A})^2}}{2\pi\ell T_{\rm A}}\,. \tag{4.10}$$

One notices that the scenarios where $T_{\rm A} = const$ and $\gamma_{\rm A} = const$ are different. As illustrated in Fig. 4.3(a-i), fixing $T_{\rm A}$ while varying $\gamma_{\rm A}$ corresponds to the case where the size of the black hole is varied while fixing the proper distances of the detectors from the horizon. This is because the proper distance (4.10) only depends on the local temperature $T_{\rm A}$. Note that the local temperature detected by detector B, $T_{\rm B}$, is also fixed. On the other hand, setting $\gamma_{\rm A}$ a constant and changing $T_{\rm A}$ corresponds to the case where both $r_{\rm h}$ and $d_{\rm A}$ change with $T_{\rm A}$ [Fig. 4.3(b-i)]. High temperature with constant $\gamma_{\rm A}$ means the detectors are very close to a large black hole.

Let us first take a look at the matrix elements $P_{\rm A}$ and $C_{\rm AB}$ and see how they depend on $\gamma_{\rm A}$ and $T_{\rm A}$. We also decompose these functions into the AdS-Rindler ($n = 0$) and BTZ ($n \neq 0$) to see how a black hole plays a role in the correlation harvesting protocol.

Figures 4.3(a-ii) and (a-iii) are respectively $P_{\rm A}/\tilde{\lambda}^2$ and $C_{\rm AB}/\tilde{\lambda}^2$ when the local KMS temperature of detector-A, $T_{\rm A}$, is fixed as shown in (a-i). Here, $T_{\rm A}\sigma = 1$. One can observe that the AdS-Rindler term in both $P_{\rm A}$ and $C_{\rm AB}$ is independent of $\gamma_{\rm A}$, whereas the BTZ part is non-vanishing only when $\gamma_{\rm A} \ll 1$. The fact that $P_{\rm A}^{(n=0)}$ and $C_{\rm AB}^{(n=0)}$ are constant for all $\gamma_{\rm A}$ tells us that the AdS-Rindler contribution remains unaffected by the black hole. In fact, for a larger black hole (with fixed $T_{\rm A}$), only the AdS-Rindler part is contributing to these matrix elements. Hence, $P_{\rm A} = P_{\rm A}^{(n=0)} + P_{\rm A}^{(n\neq 0)}$ and $C_{\rm AB} = C_{\rm AB}^{(n=0)} + C_{\rm AB}^{(n\neq 0)}$ are non-zero for all $\gamma_{\rm A}$, indicating that quantum mutual information will not vanish because of the gravitational redshift in the AdS-Rindler part.

On the other hand, Figs. 4.3(b) depict the matrix elements $P_{\rm A}$ and $C_{\rm AB}$ when the gravitational redshift factor $\gamma_{\rm A}$ is fixed but the local temperature is varied. We first note that the transition probability $P_{\rm A}$ of detector A [Fig. 4.3(b-ii)] decreases as the temperature

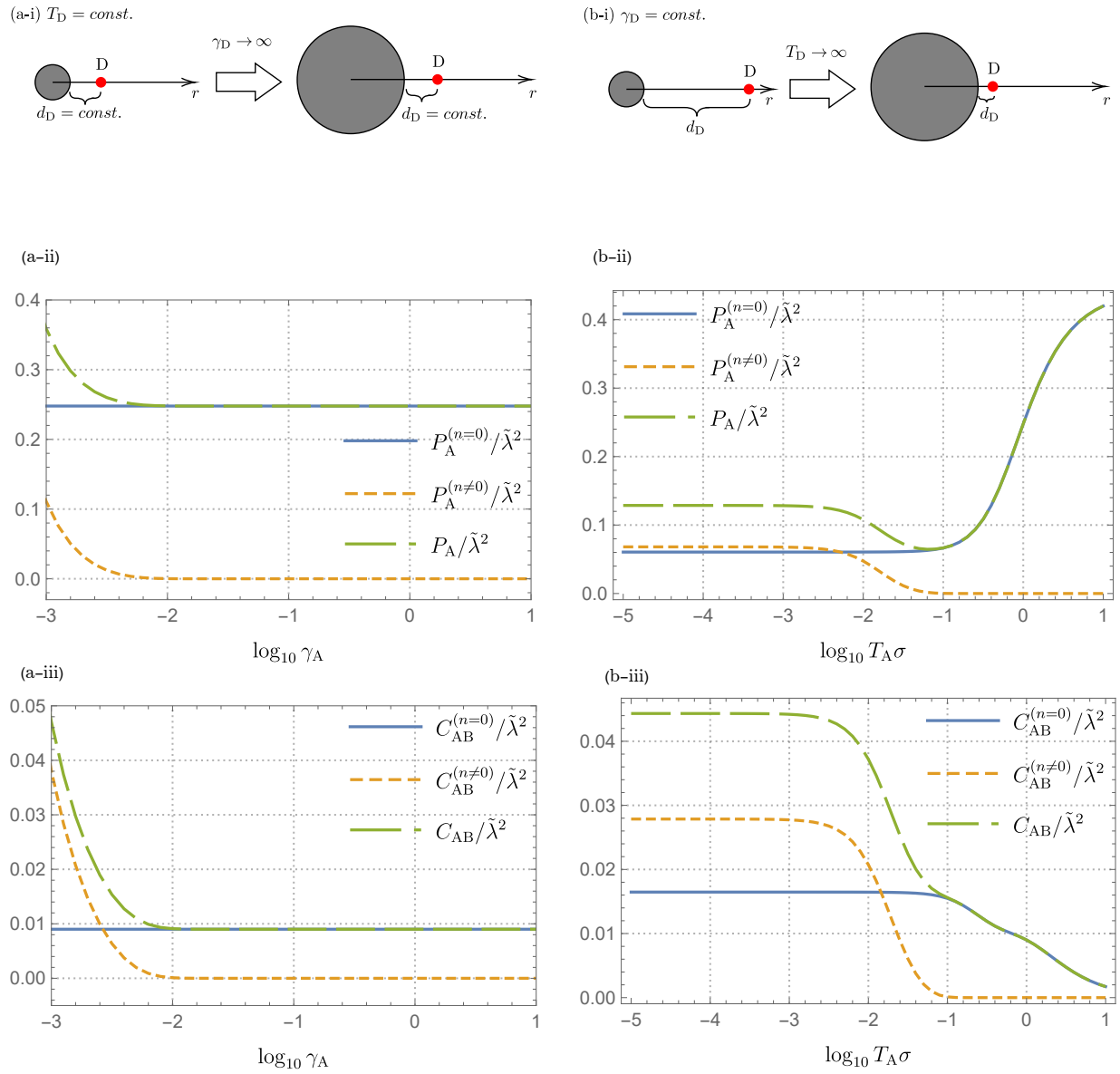

Figure 4.3: AdS-Rindler and BTZ contributions in P_A and C_{AB} with $\ell/\sigma = 10, d_{AB}/\sigma = 7$, and $\Omega\sigma = 1$. (a-i)-(a-iii): Varying γ_A while $T_A\sigma = 1$ is fixed. For both P_A and C_{AB}, the AdS-Rindler part ($n = 0$) is independent of γ_A and the BTZ part ($n \neq 0$) is non-zero only for $\gamma_A \ll 1$. (b-i)-(b-iii): Varying T_A with fixed $\gamma_A = 1/10$. For C_{AB}, both AdS-Rindler and BTZ terms vanish at $T_A\sigma \to \infty$.

increases. In a nutshell, one expects the contrary: that a detector's transition probability increases monotonically as the local temperature increases. However, this turns out to be not necessarily true; even a carefully switched detector with an infinite interaction duration experiences "cool down" as temperature increases. More precisely, writing $\mathcal{F}(\Omega) \equiv P_j/\tilde{\lambda}^2$, the conditions

$$\frac{\mathrm{d}\mathcal{F}(\Omega)}{\mathrm{d}T_{\mathrm{KMS}}} < 0 \quad \text{weak} \tag{4.11}$$

$$\frac{\partial T_{\mathrm{EDR}}}{\partial T_{\mathrm{KMS}}} < 0 \quad \text{strong} \tag{4.12}$$

in the presence of a black hole are respectively referred to as the weak and strong anti-Hawking effects [105] (see also [106, 107, 108, 109]), where

$$T_{\mathrm{EDR}} = -\frac{\Omega}{\ln \mathcal{R}} \tag{4.13}$$

with

$$\mathcal{R} = \frac{\mathcal{F}(\Omega)}{\mathcal{F}(-\Omega)}\,, \tag{4.14}$$

being the excitation-to-de-excitation ratio of the detector. For an accelerating detector in a flat spacetime these effects are respectively referred to as weak and strong anti-Unruh phenomena [110, 64], and will not be present in a situation where an inertial detector is in a thermal bath.

Since there is a range of temperature in which $P_{\mathrm{A}}/\tilde{\lambda}^2$ decreases, the detector exhibits the weak anti-Hawking effect and the redshift is not involved. Also note that (under the Dirichlet boundary condition, $\zeta = 1$) this originates from the BTZ part of the Wightman function, as demonstrated in [105].

Figure 4.3(b-iii) shows that the off-diagonal term $C_{\mathrm{AB}}/\tilde{\lambda}^2$ asymptotes to 0 as $T_{\mathrm{A}}\sigma \to \infty$. This suggests that it is the extreme temperature that inhibits detectors from harvesting mutual information. Hence, the fact that the detectors cannot extract correlations when one of them is at the event horizon [Figs. 4.2(a), (c)] is purely due to the extremity of the local Unruh/Hawking effects there, which is a combination of increasing black hole mass with decreasing d_{A} so as to ensure constant redshift.

Finally, we plot mutual information $I_{\mathrm{AB}}/\tilde{\lambda}^2$ as a function of detector A's local temperature, T_{A}, and the redshift factor, γ_{A}, in Fig. 4.4(a). Here we fix $\ell/\sigma = 10$, $d_{\mathrm{AB}}/\sigma = 7$, and $\Omega\sigma = 1$. One can observe from Fig. 4.4(a) that the detectors easily harvest mutual

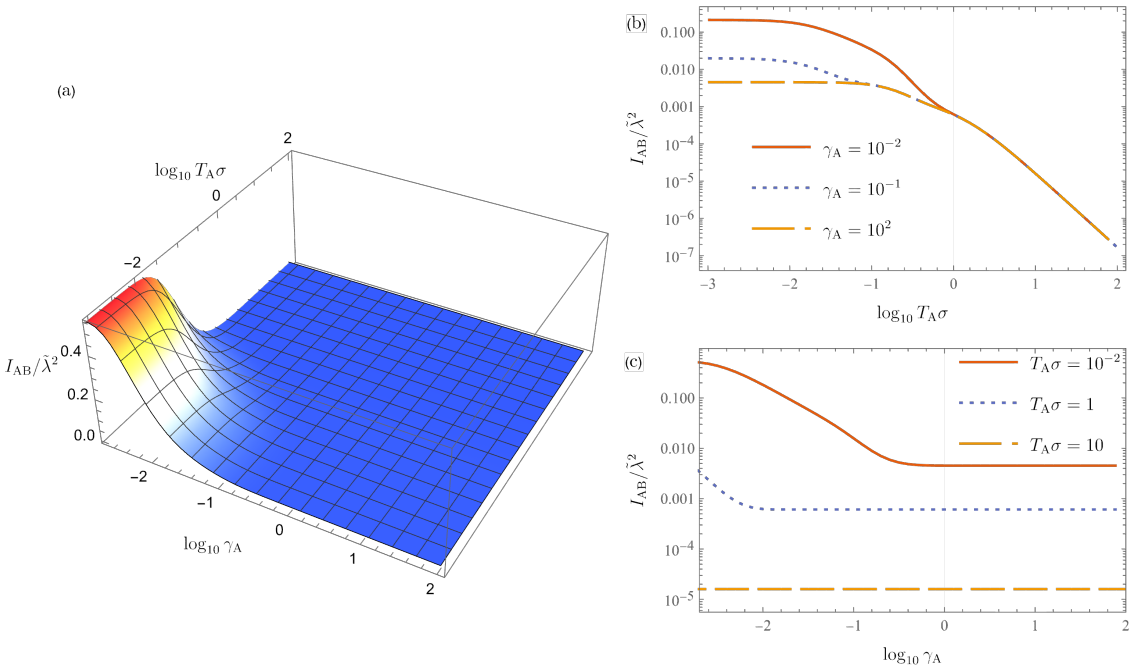

Figure 4.4: (a) 3D plot of mutual information $I_{AB}/\tilde{\lambda}^2$ as a function of local temperature T_A and redshift factor γ_A of detector A. Here, $\ell/\sigma = 10, \Omega\sigma = 1$, and $d_{AB}/\sigma = 7$. (b) Slices of (a) at constant γ_A in a logarithmic scale. The curves at lower temperature show the scenario of static detectors in AdS_3 spacetime without radiation, and the higher temperature regime represents how Unruh and/or Hawking radiations "attack" the detectors. (c) Slices of (a) at constant $T_A\sigma$ in a logarithmic scale. The contribution coming from the black hole can be seen in $\gamma_A \ll 1$ regime. As $\gamma_A \to \infty$, the Hawking effect becomes negligible and only Unruh effect survives.

information when the temperature T_A and redshift γ_A are both small. This corresponds to a case where two detectors are located far away ($d_A/\sigma \gg 1$) from a tiny black hole ($r_h/\sigma \ll 1$). On the other hand, high temperature or large redshift factor, which corresponds to $r_h/\sigma \gg 1$ and $d_A/\sigma \ll 1$, suppress the extraction of correlation.

Figure 4.4(b) depicts slices of Fig. 4.4(a) with constant γ_A in a logarithmic scale to analyze the relationship of mutual information with the Unruh and Hawking effects. As the figure indicates, the colder the temperature, the more the correlation harvested, whereas $I_{AB}/\tilde{\lambda}^2 \to 0$ as the temperature gets large. This indicates that the radiation from the black hole acts as noise that inhibits extraction of correlation by the detectors, and this is true no matter what the value of redshift is.

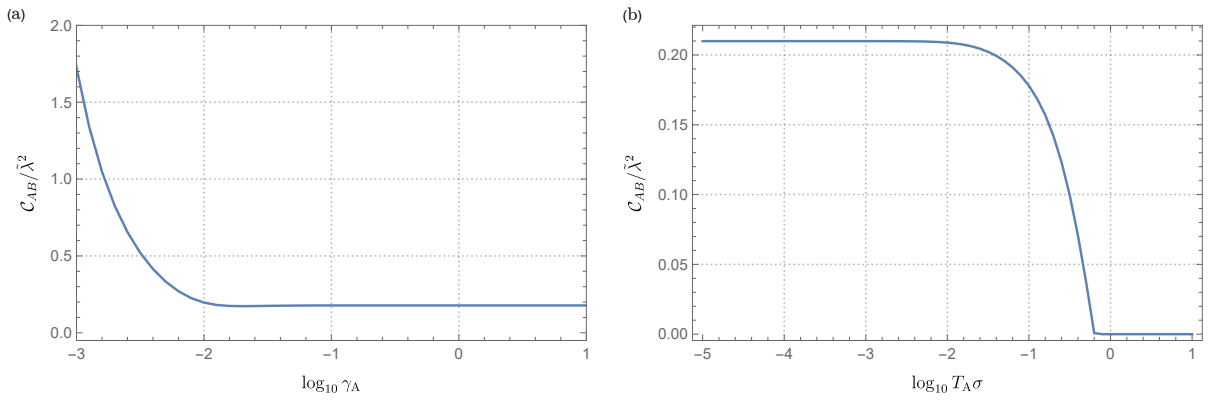

Figure 4.5: Concurrence harvested by two detectors in BTZ black hole spacetime. Here, $\ell/\sigma = 10, \Omega\sigma = 1$, and $d_{\rm AB}/\sigma = 1$. (a) Fixing $T_{\rm A}\sigma = 0.1$, the concurrence is plotted as a function of $\log_{10}\gamma_{\rm A}$. (b) Fixing $\gamma_{\rm A} = 1$, this figure depicts the temperature dependence of the concurrence.

Conversely, Fig. 4.4(c) exhibits the influence of redshift $\gamma_{\rm A}$ while the temperature $T_{\rm A}$ is fixed. In contrast to Fig. 4.4(b), mutual information does not go to 0 as $\gamma_{\rm A} \to \infty$. Instead, it asymptotes to a finite value that is characterized by the temperature $T_{\rm A}$. As we saw in Fig. 4.3(a-ii) and (a-iii), the BTZ part of P_j and $C_{\rm AB}$ vanishes at large $\gamma_{\rm A}$, leading us to conclude that the asymptotic values in Fig. 4.4(c) coincide with mutual information harvested by *accelerating* detectors in AdS_3 spacetime with corresponding accelerations that give local temperature $T_{\rm A}$. From these figures, we conclude that the death of mutual information in a black hole spacetime is purely due to the Unruh and Hawking effects. We have checked that this feature holds for other boundary conditions ($\zeta = 0, -1$).

We finally revisit [41] and see how entanglement harvested around a black hole is influenced by $\gamma_{\rm A}$ and $T_{\rm A}$. In Fig. 4.5(a) and (b), we plot the concurrence $\mathcal{C}_{\rm AB}/\tilde{\lambda}^2$ as a function of $\log_{10}\gamma_{\rm A}$ (with fixed $T_{\rm A}\sigma = 0.1$) and $\log_{10} T_{\rm A}\sigma$ (with fixed $\gamma_{\rm A} = 1$), respectively, when $\ell/\sigma = 10, \Omega\sigma = 1$, and $d_{\rm AB}/\sigma = 1$. Note that the proper distance between the detectors, $d_{\rm AB}/\sigma$, is small for the sake of reliable numerical calculations. Figure 4.5(a) tells us that the concurrence $\mathcal{C}_{\rm AB}/\tilde{\lambda}^2$ is non-vanishing for all $\gamma_{\rm A}$, indicating that the previously known entanglement shadow is not caused by the redshift. On the other hand, Fig. 4.5(b) explicitly shows that the concurrence dies if a detector feels a high black hole temperature, and this is the very reason that the entanglement shadow occurs.

In conclusion, by studying the temperature and gravitational redshift dependence of harvested correlations, we find that the high black hole temperature prevents the detec-

tors from harvesting correlations. Both entanglement and quantum mutual information do not vanish for all γ_{A} due to the fact that the AdS-Rindler contribution is constant. While entanglement cannot be harvested above some *finite* black hole temperature, quantum mutual information only vanishes at the *infinite* temperature limit, indicating that quantum mutual information can be extracted from the field arbitrarily close to the event horizon.

Chapter 5

Extraction of tripartite correlation from BTZ black hole spacetime

In this chapter we investigate the tripartite correlation harvesting protocol in BTZ black hole spacetime. The tripartite harvesting protocol was first examined by Silman and Reznik [111], who showed that the harvested entanglement by three UDW detectors can be distilled into a W state [112] (on which we will elaborate later). Other investigations of tripartite entanglement harvesting in flat spacetime can be found in [113, 32, 77]. These papers found that tripartite entanglement is relatively easier to extract from the vacuum than bipartite entanglement.

Tripartite entanglement is interesting in its own right due to the richness of its entanglement structure. Unlike bipartite entanglement, which only has two classes of states (entangled and separable states), tripartite entanglement can be characterized into four classes: Greenberger-Horne-Zeilinger (GHZ), W, bi-separable, and fully separable states [112, 114]. These four are described as follows.

- Fully separable: a state that is not entangled at all, such as $|g_{\rm A}\rangle \otimes |g_{\rm B}\rangle \otimes |g_{\rm C}\rangle$.
- Bi-separable: it is an entangled state but one of the subsystems is separable from the rest. For instance, $|g_{\rm A}\rangle \otimes (|g_{\rm B}g_{\rm C}\rangle + |e_{\rm B}e_{\rm C}\rangle)/\sqrt{2}$.
- W state [112]: three subsystems are all entangled with each other (genuinely entangled). As an example, $|W\rangle = (|g_{\rm A}g_{\rm B}e_{\rm C}\rangle + |g_{\rm A}e_{\rm B}g_{\rm C}\rangle + |e_{\rm A}g_{\rm B}g_{\rm C}\rangle)/\sqrt{3}$. If one measures one of the subsystems (e.g., subsystem C) of $|W\rangle$,then the resulting bipartite state remains entangled. The W state cannot be transformed into the GHZ state via stochastic local operations and classical communication (SLOCC) protocols.

- GHZ state [94]: this is also a genuine entanglement, though distinct from the W state (since it cannot be converted into the W state via SLOCC). An example of GHZ state is $|\mathrm{GHZ}\rangle = (|g_\mathrm{A} g_\mathrm{B} g_\mathrm{C}\rangle + |e_\mathrm{A} e_\mathrm{B} e_\mathrm{C}\rangle)/\sqrt{2}$, and it becomes a separable bipartite state once one of the subsystems is measured.

In this chapter, we examine the influence of the Hawking effect on the extraction of tripartite entanglement by considering three static detectors in BTZ spacetime. Specifically, we investigate whether tripartite entanglement can be extracted in the bipartite entanglement shadow, and whether a tripartite entanglement shadow exists. We will show that the tripartite entanglement shadow exists and it is "narrower" than the bipartite entanglement shadow, indicating that tripartite entanglement can be extracted even if the extraction of bipartite entanglement is prohibited.

Although tripartite harvesting and its classification are intriguing, our current tool is too limited to fully investigate this matter. As described in Sec. 2.4.2, the π-tangle, which is the entanglement measure we will use, is well-defined only for pure states. On the other hand, our final state is a mixed state and thus the π-tangle does not necessarily reflect the true amount of entanglement. Nevertheless, the π-tangle for mixed states can be thought of as the lower bound of the "true" π-tangle, and so it will provide us with some insightful information on tripartite entanglement harvesting. Specifically, if the π-tangle is positive then it is guaranteed that the true π-tangle is also positive. However, if the π-tangle is either zero or negative, then we cannot say anything about the existence of tripartite entanglement since the true π-tangle still could be positive.

5.1 Equilateral configuration

For three UDW detectors, the simplest spatial configuration is an equilateral triangle configuration, when one detector is located at each corner (see Fig. 5.1). In Ref. [32], entanglement harvesting with detectors in an equilateral triangle configuration in Minkowski spacetime was investigated. In flat spacetimes (so long as the detectors are at rest in a single reference frame), the transition probabilities P_j and correlation elements C_{jk}, X_{jk} simplify to (2.53):

$$\begin{aligned} &C_\mathrm{AB} = C_\mathrm{BC} = C_\mathrm{CA} \equiv C\,, \\ &X_\mathrm{AB} = X_\mathrm{BC} = X_\mathrm{CA} \equiv X\,, \\ &P_\mathrm{A} = P_\mathrm{B} = P_\mathrm{C} \equiv P\,. \end{aligned} \qquad (2.53)$$

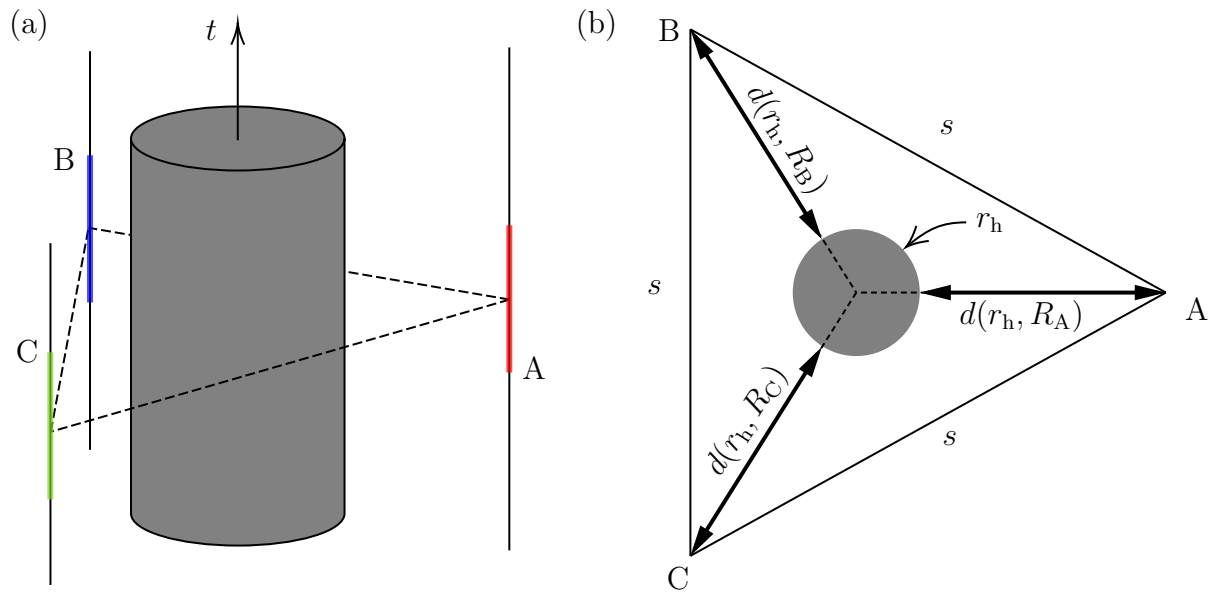

Figure 5.1: (a) Showing a BTZ black hole and static trajectories of three UDW detectors A, B, and C. The colored stripes indicate when the detectors interact with the quantum field. (b) A time-slice of (a). The detectors are located at the corners of the equilateral triangle, and therefore, $d(r_{\rm h}, R_j)/\sigma$ are all the same.

In general spacetimes, the equilateral triangle configuration does not necessarily simplify the density matrix elements in the aforementioned manner. For example, if one of them experiences a redshift effect then the transition probability and non-local elements will be different. In the BTZ black hole case, we can simplify as (2.53) by aligning the centers of the equilateral triangle and the black hole, so that the proper distance of each detector from the horizon, $d(r_{\rm h}, r_j)$, is the same (Fig. 5.1).

We then consider a conformally coupled massless scalar field in the Hartle-Hawking vacuum as in Ch. 4 and see how the Hawking effect influences the tripartite entanglement. Since the detectors are now in the equilateral triangle configuration, we set $\Delta\varphi = 2\pi/3$ in the Wightman function (4.8). By calculating $P, C_{\rm AB}$, and $X_{\rm AB}$, one can obtain the

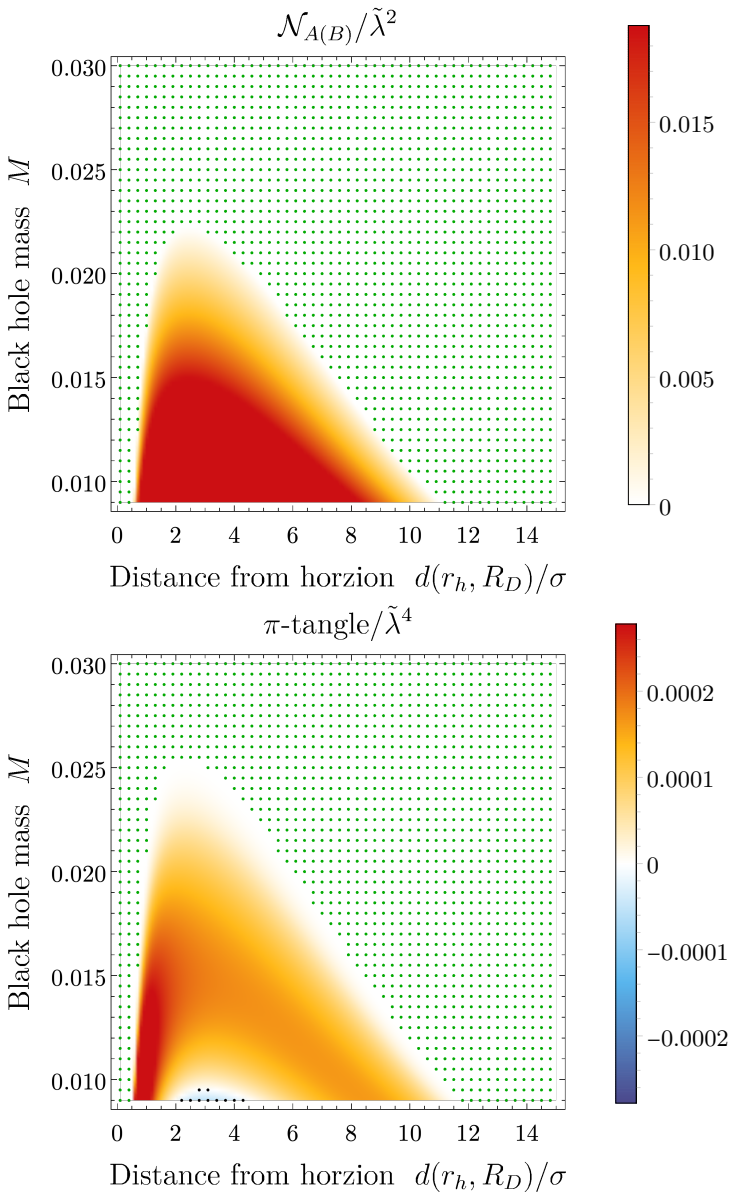

Figure 5.2: *(Top:)* The bipartite negativity, $\mathcal{N}_{\mathrm{D(D')}}$, between two of the detectors, and *(bottom:)* the extracted π-tangle in the case of the equilateral triangle configuration depicted in Fig. 5.1 as a function of the mass of the black hole M and the proper distance $d(r_{\mathrm{h}}, R_{\mathrm{D}})/\sigma$ of the detectors from the horizon. Here, the energy gap $\Omega\sigma = 1$. In the top figure, the green dots indicate the region where $\mathcal{N}_{\mathrm{D(D')}} = 0$ and in the bottom figure the green dots indicate the region where the π-tangle is zero. Black dots indicate the region where the $\pi < 0$.

bipartite negativity $\mathcal{N}_{\mathrm{D(D')}}$ and the π-tangle by (2.112) and (2.113), respectively:

$$\mathcal{N}_{\mathrm{D(D')}} = \max\{0,\, |X| - P\} + \mathcal{O}(\lambda^4)\,, \qquad (2.112)$$

$$\pi = \max\left\{0,\, \frac{\sqrt{C^2 + 8|X|^2}}{2} - \frac{C}{2} - P\right\}^2 - 2\max\{0,\, |X| - P\}^2 + \mathcal{O}(\lambda^6)\,. \qquad (2.113)$$

In Fig. 5.2(top), we plot the bipartite negativity $\mathcal{N}_{\mathrm{D(D')}}$ between two of the three detectors in the equilateral triangle configuration as a function of the black hole mass M and the proper distance of the detectors from the horizon, $d(r_{\mathrm{h}}, R_{\mathrm{D}})/\sigma$. We find that bipartite entanglement harvesting by detectors with an energy gap of $\Omega\sigma = 1$ is only possible, at any distance from the horizon, if the mass of the black hole is smaller than $M \approx 0.0225$. This is likely due to the fact that as the mass M of the black hole increases, the proper separation $d(R_{\mathrm{D}}, R_{\mathrm{D'}})/\sigma$ between the two detectors also increases if one fixes the distance from the horizon, $d(r_{\mathrm{h}}, R_{\mathrm{D}})/\sigma$. Since greater detector separations, $d(R_{\mathrm{D}}, R_{\mathrm{D'}})/\sigma$, decrease the correlations between the detectors, greater black hole masses will decrease the maximum distance from the horizon where entanglement harvesting is possible.

Moreover, the bipartite entanglement is zero when the detectors are very close to the horizon, which is caused by the high black hole temperature [41, 45]. The term $|X_{\mathrm{AB}}|$ in (2.112) sharply decreases while the transition probability P increases with temperature. Hence, the entanglement shadow still exists even when detectors are located at a different angle φ_j.

However, we see from Fig. 5.2 (bottom), where we now consider the π-tangle between all three detectors, that harvesting tripartite entanglement is indeed possible for black hole masses larger than those that allow for bipartite entanglement harvesting. The fact that the detectors can extract tripartite entanglement when the bipartite one is vanishing can be seen from (2.113). We also find it is possible to extract tripartite entanglement at larger distances from the horizon than is possible in the bipartite case, which corresponds to greater detector separations, in agreement with previous results in flat spacetime [32]. We note that for this particular value of energy gap, $\Omega\sigma = 1$, the π-tangle becomes zero for all detector distances from the horizon when the black hole mass is larger than $M \approx 0.0255$. Furthermore, we find that when the black hole mass is less than $M \approx 0.01$, the π-tangle becomes negative for moderate detector distances, despite being positive for both smaller and larger distances. Since the π-tangle (2.89) puts a lower bound on the tripartite entanglement, we are unable to gain any information about multivariate correlations between the three detectors in this region (where $\pi \leq 0$) of the parameter space, and instead focus our attention on regions where the π-tangle is positive. For this reason, we do not explore black holes with smaller masses.

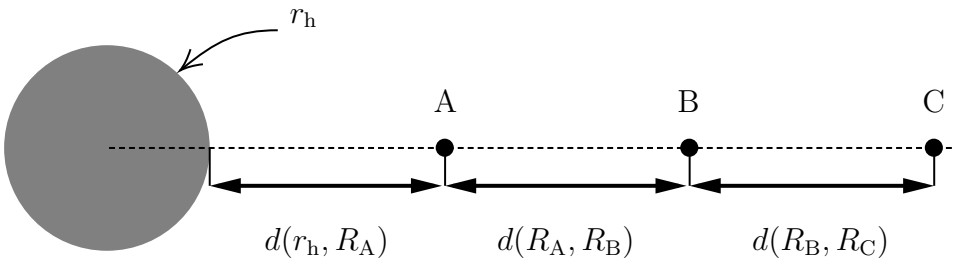

Figure 5.3: The straight line configuration.

In summary, detectors can extract tripartite entanglement from the field even when bipartite entanglement cannot be harvested. This can be seen from Eqs. (2.112) and (2.113). Bipartite entanglement can be harvested whenever $|X| > P$ and otherwise, the noise P prevents the detectors from extraction. On the other hand, the first term in the π-tangle (2.113) can be positive. As a demonstration, suppose $|X| = P$: in this case the bipartite negativity is 0. Then it is straightforward to show that the first term in the π-tangle is positive.

5.2 Straight line configuration

By placing the three detectors along a line intersecting the center of the black hole (Fig. 5.3), we gain further insight into the distinctions between the bipartite and tripartite cases. In the bipartite case the entanglement shadow was manifest when one of the detectors was placed close to the horizon [41]. However, we find that the situation is very different in the tripartite case.

In Fig. 5.4, we fix the proper distance between the detectors to be $d(R_{\rm A}, R_{\rm B})/\sigma = d(R_{\rm B}, R_{\rm C})/\sigma = 1$ and plot the π-tangle as a function of the proper distance from the black hole horizon to the nearest detector for $M = 0.01$ and differing energy gaps. We find that, provided the energy gap of the detectors is large enough, tripartite entanglement can be harvested at distances arbitrarily close to the black hole horizon. In striking distinction to the bipartite case, tripartite entanglement often has no entanglement shadow in the line configuration, and, unlike in the case of the equilateral triangle configuration, it is quite easy to find regions in parameter space where this occurs. The minimum value of the detector energy gap guaranteeing near horizon tripartite entanglement harvesting depends on the mass of the black hole. Specifically, we find that for $M = 0.01$ and $\Omega\sigma = 0.01$ the

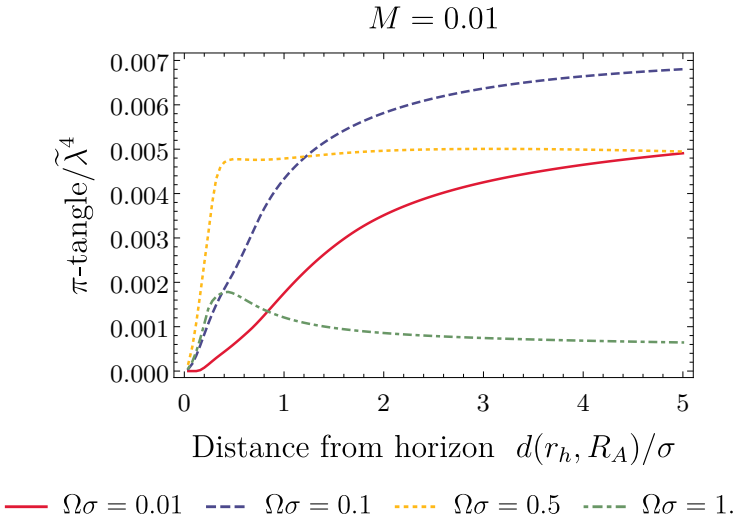

Figure 5.4: The π-tangle harvested by detectors in the straight line configuration as a function of the proper distance of the closest detector A to the horizon, $d(r_{\rm h}, R_{\rm A})/\sigma$. Here, $M = 0.01$ and $d(R_{\rm A}, R_{\rm B})/\sigma = d(R_{\rm B}, R_{\rm C})/\sigma = 1$.

π-tangle becomes zero when the first detector is very close at $d(r_{\rm h}, R_{\rm A})/\sigma \lesssim 0.08$. We also note that the π-tangle asymptotes to a constant value, which depends on Ω and M, in the limit $d(r_{\rm h}, R_{\rm A})/\sigma \to \infty$, as expected since the BTZ spacetime is asymptotically AdS_3.

We now explicitly show that the π-tangle is positive where the bipartite entanglement is zero. Choosing two cases $(M, \Omega\sigma) = (0.01, 0.01)$ and $(0.01, 0.1)$ in Fig. 5.4, we plot their bipartite and tripartite negativities in (2.90) as a function of the proper distance of detector A from the horizon in Fig. 5.5. For both values of the energy gap $\Omega\sigma$ considered, we find that each π_j ($j \in \{\rm A, B, C\}$) in (2.89) is positive even when some of the bipartite negativities $\mathcal{N}_{\rm D(D')}$ vanish. Consider $\pi_{\rm A}$ (2.90a) as an example. We see that $\mathcal{N}_{\rm A(BC)}$ remains positive while $\mathcal{N}_{\rm A(B)} = \mathcal{N}_{\rm A(C)} = 0$, which suggests that $\pi_{\rm A} > 0$ in the bipartite entanglement shadow. This is also true for $\pi_{\rm B}$ and $\pi_{\rm C}$ if they possess the bipartite entanglement shadow, and therefore the π-tangle is positive.[1] We point out that $\mathcal{N}_{\rm B(C)}$ does not vanish in Fig. 5.4 (bottom) since detectors B and C are still far away from the horizon when $d(r_{\rm h}, R_{\rm A})/\sigma = 0$. Nevertheless, for a sufficiently large $\Omega\sigma$, tripartite entanglement can be extracted in the

[1]Since the tripartite negativity is a lower bound, $\mathcal{N}_{\rm A(BC)} = 0$ does not mean that there is no entanglement between detector A and the (BC) subsystem; there is very likely to be some, since detector B is more entangled with (AC) and detector C is more entangled with (AB) then detector B is entangled with detector C alone.

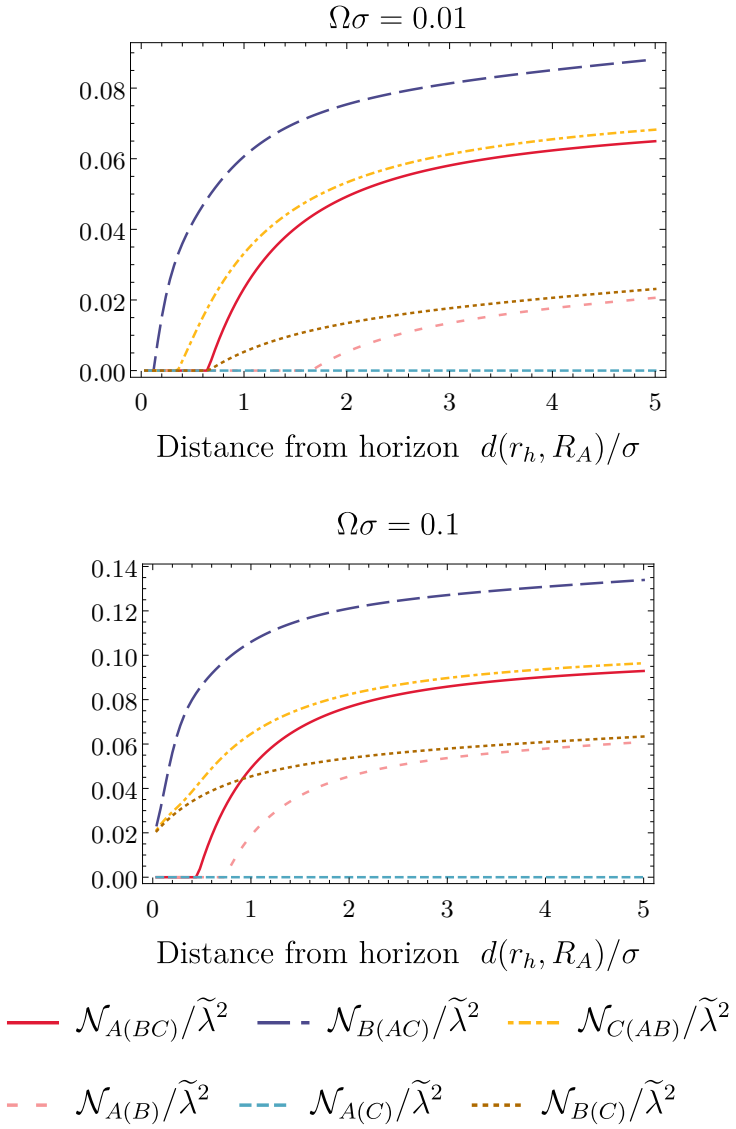

Figure 5.5: In the case of three detectors placed along a straight line outside of a BTZ black hole (Fig. 5.3), the three tripartite and three bipartite negativities are calculated as a function of $d(r_{\rm h}, R_{\rm A})/\sigma$ for a detector energy gap of *Top:* $\Omega\sigma = 0.01$ and *Bottom:* $\Omega\sigma = 0.1$. Here, the proper distance between the detectors remains constant at $d(R_{\rm A}, R_{\rm B})/\sigma = d(R_{\rm B}, R_{\rm C})/\sigma = 1$. The AdS length $\ell/\sigma = 10$, the boundary condition $\zeta = 1$, and the mass of the black hole $M = 0.01$.

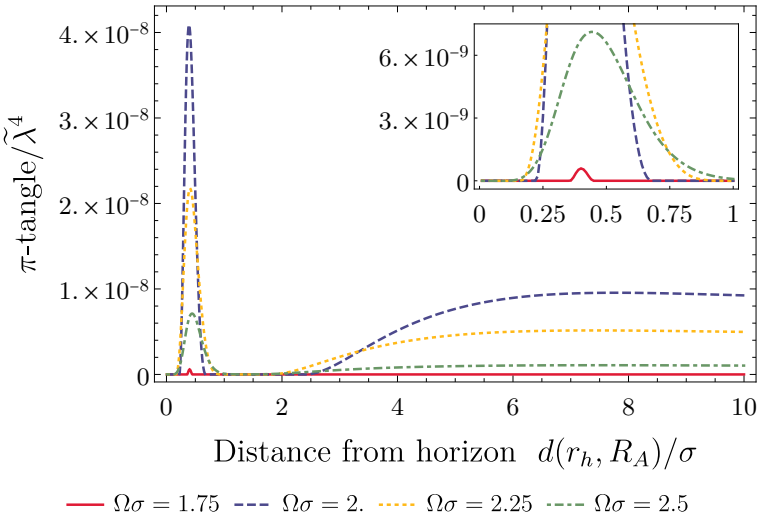

Figure 5.6: The π-tangle extracted by detectors in the straight line configuration in Fig. 5.3. Here, the proper distance between the detectors remains constant at $d(R_{\rm A}, R_{\rm B})/\sigma = d(R_{\rm B}, R_{\rm C})/\sigma = 5$. The AdS length $\ell/\sigma = 10$, the boundary condition $\zeta = 1$, and the mass of the black hole $M = 0.01$. The inset shows details of the near horizon spike in π-tangle for $\Omega\sigma = 1.75$ and $\Omega\sigma = 2$.

bipartite entanglement shadow, which suggests that the harvested entanglement is of the GHZ type.

We note from Fig. 5.4 that a local maximum exists in $\pi/\tilde{\lambda}^2$ for some $\Omega\sigma$. In fact, for some choices of parameters, this maximum leads to an interesting result.

In Fig. 5.6 we again plot the π-tangle of the detectors in the straight line configuration as a function of the proper distance of the nearest detector from the horizon, but now for larger detector separation $d(R_{\rm A}, R_{\rm B})/\sigma = d(R_{\rm B}, R_{\rm C})/\sigma = 5$. Unlike the previous case, as the detectors move towards the horizon, the π-tangle becomes zero followed by a sharp spike before it drops to zero again. These spikes in the π-tangle are larger in magnitude than its asymptotic value at $d(r_{\rm h}, R_{\rm A})/\sigma \to \infty$.

To better understand the origin and properties of the near-horizon spike in the π-tangle, we plot the bipartite and tripartite negativities in Fig. 5.7. We first note that the large spike in the π-tangle occurs at values of $d(r_{\rm h}, R_{\rm A})$ where the bipartite negativities are zero, i.e. inside the bipartite entanglement shadow of all three detectors, meaning that the tripartite entanglement extracted from the field in this region of the spacetime is of the GHZ type. Consequently, the π-tangle results from the tripartite negativities, and when

the energy gap of the detectors is small enough, only from $\mathcal{N}_{\mathrm{B(AC)}}$, which puts a lower bound on the entanglement between detector B and the (AC) subsystem. As the energy gap of the detector is increased, the remaining two tripartite negativities also contribute to near-horizon π-tangle.

The bipartite and tripartite negativities are functions of the matrix elements of Eq. (2.51), which we plot in Fig. 5.8 for the same detector configuration as in Fig. 5.6. We find that as detector A approaches the horizon, both the detector correlations $C_{\mathrm{DD}'}$ and the non-local correlations $|X_{\mathrm{DD}'}|$ between detectors A and B and between A and C also show a near-horizon spike. Here, the spike in the detector correlations $C_{\mathrm{DD}'}$ is smaller and occurs closer to the horizon than that of the non-local correlations $|X_{\mathrm{DD}'}|$. The correlations between detectors B and C do not exhibit spikes, as they are still relativity far from the horizon, $d(r_{\mathrm{h}}, R_{\mathrm{B}})/\sigma = d(r_{\mathrm{h}}, R_{\mathrm{A}})/\sigma + 5$. This spike in pairwise correlations is directly responsible for the spike in the tripartite negativities shown in Fig. 5.7. Such a spike is not seen in the bipartite negativities, since the transition probability of detector A, $P_{\mathrm{A}}/\tilde{\lambda}^2$, is very large near the horizon, due to the local field temperature, which will prevent any entanglement between detector A and B (or C). Since detectors B and C remain far from the horizon, their transition probabilities remain small, and as a result, the three detectors can have tripartite entanglement. We also note that a near horizon spike does not appear in the pairwise correlations when $\Omega\sigma < 1$.

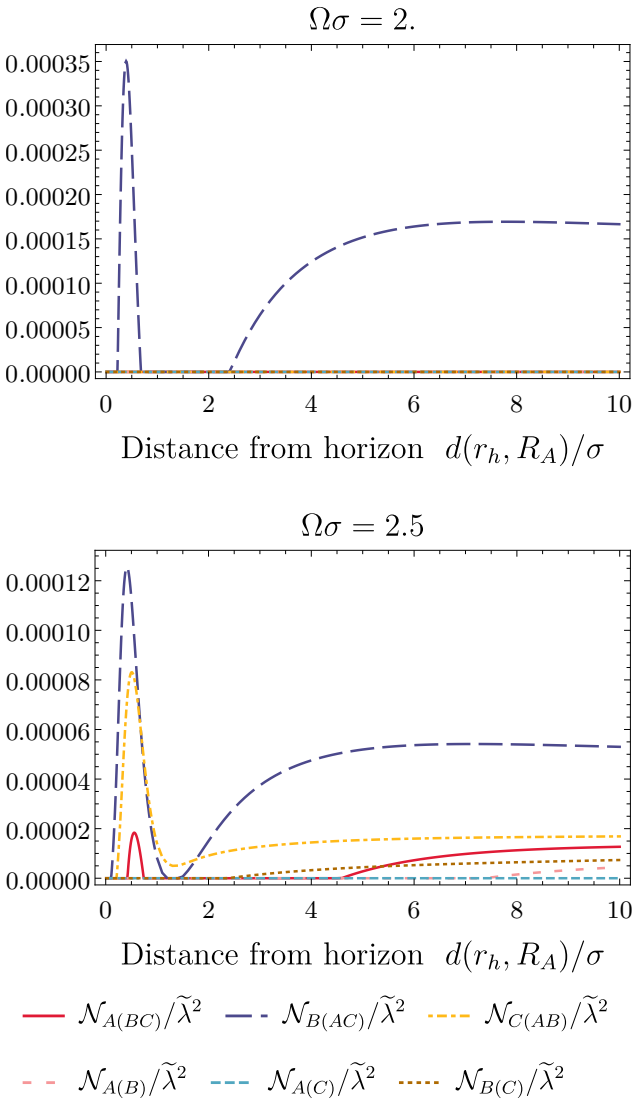

Figure 5.7: In the case of three detectors placed along a straight line outside of a BTZ black hole (Fig. 5.3), the three tripartite and three bipartite negativities are plotted as a function of the proper distance $d(r_{\rm h}, R_{\rm A})/\sigma$ for a detector energy gap of *Top:* $\Omega\sigma = 2$ and *Bottom:* $\Omega\sigma = 2.5$. Here, the proper distance between the detectors remains constant at $d(R_{\rm A}, R_{\rm B})/\sigma = d(R_{\rm B}, R_{\rm C})/\sigma = 5$. Here, the mass of the black hole is $M = 0.01$.

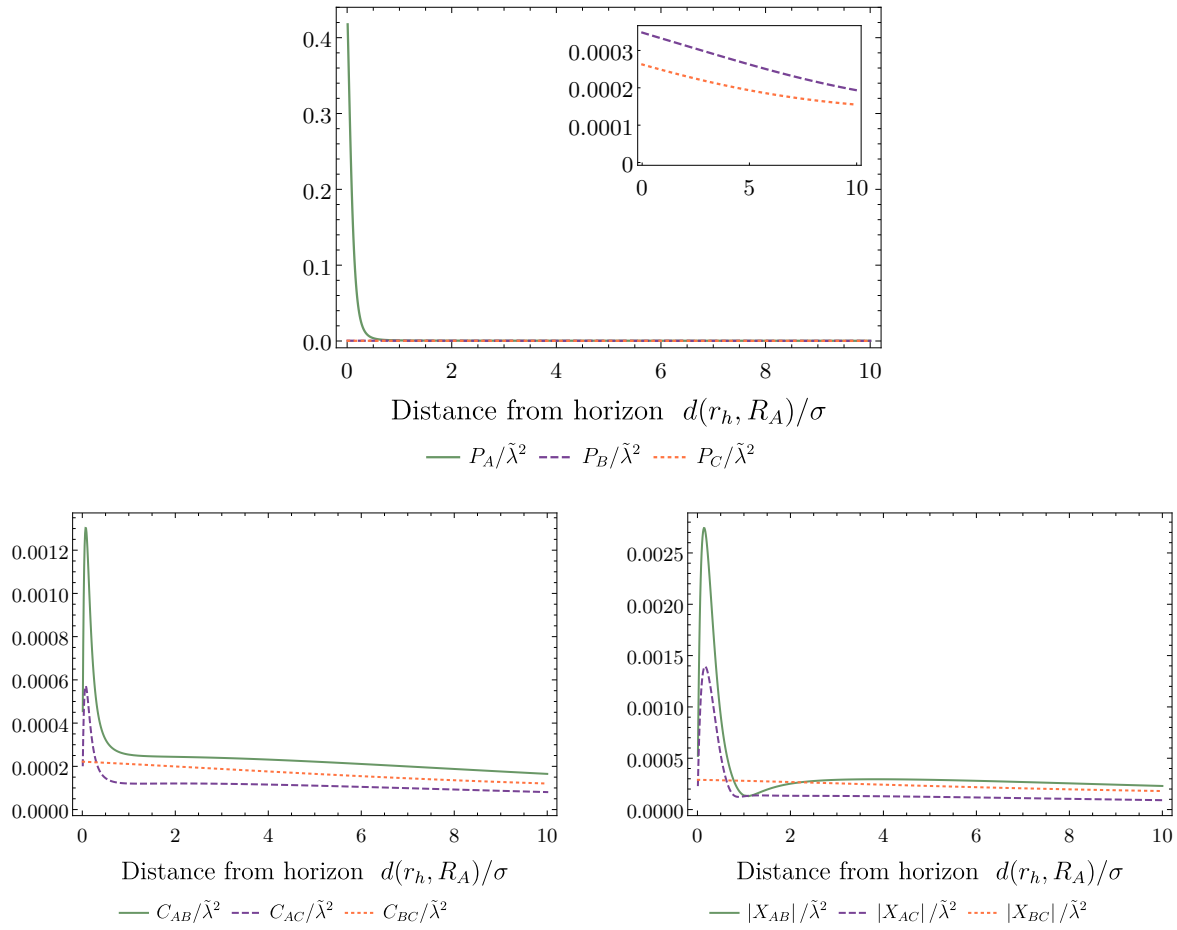

Figure 5.8: In the case of three detectors placed along a straight line outside of a BTZ black hole (Fig. 5.3) with $\ell/\sigma = 10$, and $M = 0.01$, the matrix elements of Eq. (2.51) are calculated as a function of $d(r_{\rm h}, R_{\rm A})/\sigma$, for *top:* the transition probabilities $P_{\rm D}/\tilde{\lambda}^2$, *bottom-left:* the pairwise detector correlations $C_{\rm DD'}/\tilde{\lambda}^2$, and *bottom-right:* the pairwise non-local correlations $|X_{\rm DD'}|/\tilde{\lambda}^2$. Here, the proper distance between the detectors remains constant at $d(R_{\rm A}, R_{\rm B})/\sigma = d(R_{\rm B}, R_{\rm C})/\sigma = 5$ and the energy gap of the detectors is $\Omega\sigma = 2.5$. The inset in the left figure shows details of $P_{\rm B}$ and $P_{\rm C}$.

Chapter 6

Extraction of bipartite correlation from Schwarzschild black hole spacetime

We finally examine the correlation harvesting protocol in (1+1)-dimensional Schwarzschild spacetime. So far in Ch. 4, we have learned that the high black hole temperature is responsible for the entanglement shadow and vanishing quantum mutual information at the horizon. Here, we first confirm that this is also the case for two static detectors in Schwarzschild spacetime. We then let one of the detectors free-fall into the black hole. While the free faller does not encounter infinite temperature upon crossing the horizon, the relative velocity between the free faller and the static observer diminishes the ability to extract correlations. Finally, we let two detectors fall into the black hole from infinity and see that there is no problem for the detectors to harvest correlations across the event horizon due to finite black hole temperature.

6.1 Quantum field in (1+1)-dimensional Schwarzschild spacetime

6.1.1 Schwarzschild spacetime and a free-faller's trajectory

In the next two sections we first review the geometrical and quantum field-theoretic aspects of a quantum massless scalar field in a Schwarzschild background spacetime, following dis-

cussion in [115, 43]. We will review three coordinate systems that are naturally associated with the three standard vacua — Boulware, Unruh, and Hartle-Hawking states — and also a coordinate system adapted to a class of free-falling observers.

Schwarzschild geometry

Consider a $(3+1)$-dimensional Schwarzschild spacetime described by the metric

$$\mathrm{d}s^2 = -f(r)\mathrm{d}t_{\mathrm{s}}^2 + \frac{1}{f(r)}\mathrm{d}r^2 + r^2(\mathrm{d}\theta^2 + \sin^2\theta\mathrm{d}\varphi^2)\,, \quad f(r) = 1 - \frac{r_{\mathrm{h}}}{r} \tag{6.1}$$

where $r_{\mathrm{h}} = 2G_{\mathrm{N}}\mathsf{M}$ is the event horizon and $\mathsf{M} \geq 0$ is the ADM mass. In what follows, we write $M = G_{\mathrm{N}}\mathsf{M}$ so that r_{h} has units of length. The coordinate system $(t_{\mathrm{s}}, r, \theta, \varphi)$ is known as the Schwarzschild coordinates, where the subscript 'S' will be useful to distinguish it from other coordinate systems. The metric (6.1) is valid only for $r > r_{\mathrm{h}}$ due to the coordinate singularity at $r = r_{\mathrm{h}}$.

We can extend the coordinate system by first introducing the tortoise coordinate $r_\star$ defined by

$$r_\star \coloneqq r + r_{\mathrm{h}} \ln\left|\frac{r}{r_{\mathrm{h}}} - 1\right|\,, \tag{6.2}$$

and then defining the null coordinates $v \coloneqq t_{\mathrm{s}} + r_\star$, $u \coloneqq t_{\mathrm{s}} - r_\star$. With this, the metric now reads

$$\mathrm{d}s^2 = -\frac{r_{\mathrm{h}}}{r}e^{-\frac{r}{r_{\mathrm{h}}}}e^{\frac{v-u}{2r_{\mathrm{h}}}}\mathrm{d}u\,\mathrm{d}v + r^2\left(\mathrm{d}\theta^2 + \sin^2\theta\mathrm{d}\varphi^2\right)\,. \tag{6.3}$$

Finally, introducing new coordinates

$$U \coloneqq -2r_{\mathrm{h}}e^{-u/2r_{\mathrm{h}}}\,,\ V \coloneqq 2r_{\mathrm{h}}e^{v/2r_{\mathrm{h}}}\,, \tag{6.4}$$

the extension to region II in Fig. 6.1 is obtained by considering the coordinate system (U, v, θ, φ) where $U, v \in \mathbb{R}$ and the metric reads

$$\mathrm{d}s^2 = -\frac{2r_{\mathrm{h}}^2}{r}e^{-\frac{r}{r_{\mathrm{h}}}+\frac{v}{2r_{\mathrm{h}}}}\mathrm{d}U\mathrm{d}v + r^2\left(\mathrm{d}\theta^2 + \sin^2\theta\mathrm{d}\varphi^2\right)\,. \tag{6.5}$$

Note that here r is an implicit function of U and v. The maximal analytic extension is obtained by considering the coordinate system (U, V, θ, φ) where $U, V \in \mathbb{R}$ and the metric reads

$$\mathrm{d}s^2 = -\frac{r_{\mathrm{h}}}{r}e^{-r/r_{\mathrm{h}}}\mathrm{d}V\mathrm{d}U + r^2\left(\mathrm{d}\theta^2 + \sin^2\theta\mathrm{d}\varphi^2\right)\,. \tag{6.6}$$

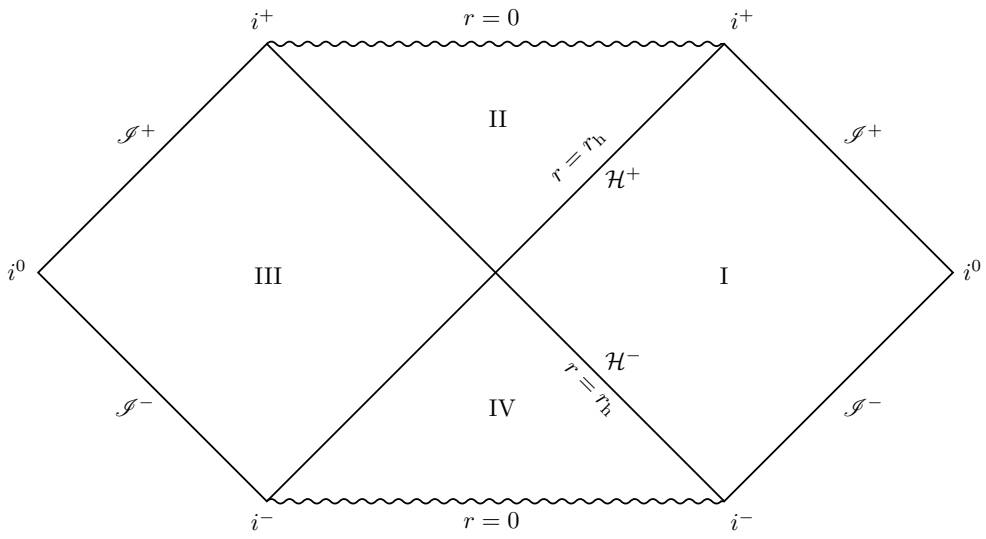

Figure 6.1: Penrose diagram for Schwarzschild spacetime.

Thus we have obtained three distinct coordinate systems for the Schwarzschild black hole spacetime: *Schwarzschild coordinates* with metric (6.1), *Eddington-Finkelstein coordinates*[1] with metric (6.5), and *Kruskal-Szekeres coordinates* with metric (6.6). These three coordinate systems are naturally adapted for definitions of the three standard vacuum states of quantum fields in this background spacetime, as we will see in the next subsection.

Finally, we will consider a class of free-falling observers that are infalling from infinity towards the curvature singularity at $r = 0$. For this purpose, it will not be sufficient for us to simply solve for radial geodesics in Schwarzschild coordinates because the coordinate systems do not apply for free-fallers inside the horizon. The coordinate system we need for this class of observers that is also regular at the event horizon $r = r_\mathrm{h}$ is the Painlevé-Gullstrand (PG) coordinate system (see [116] and references therein), which is constructed based on a free-falling observer's proper time.

The PG coordinate system is adapted to free-falling observers starting at rest at spatial infinity, with metric given by

$$\mathrm{d}s^2 = -f(r)\mathrm{d}t_\mathrm{PG}^2 + 2\sqrt{1-f(r)}\mathrm{d}t_\mathrm{PG}\mathrm{d}r + \mathrm{d}r^2 + r^2(\mathrm{d}\theta^2 + \sin^2\theta\mathrm{d}\varphi^2), \tag{6.7}$$

[1]Strictly speaking Eddington-Finkelstein coordinates refer to coordinates (u, r, θ, φ) or (v, r, θ, φ), but we will borrow this name because they share the same region of validity (regions I and II) without any analytic extension.

where $t_{\rm PG}$ is the PG coordinate time. The PG coordinates $(t_{\rm PG}, r, \theta, \varphi)$ for infalling observers are obtained from the Schwarzschild metric (6.1) by using the coordinate transformation

$$t_{\rm PG} = t_{\rm s} + 2r_{\rm h}\left(\sqrt{\frac{r}{r_{\rm h}}} + \frac{1}{2}\ln\left|\frac{\sqrt{r/r_{\rm h}}-1}{\sqrt{r/r_{\rm h}}+1}\right|\right) . \tag{6.8}$$

Time reparametrization invariance allows us to fix $t_{\rm PG} = 0$ at the singularity $r = 0$ and so $t_{\rm PG} < 0$ for all $r > 0$. A remarkable property of the PG coordinates is that the induced metric at constant $t_{\rm PG}$ slices (i.e., $\mathrm{d}t_{\rm PG} = 0$) are flat; thus proper distances between two fixed radial coordinates r_1, r_2 on a $t_{\rm PG} = \textit{constant}$ surface will be given simply by $\Delta r = |r_2 - r_1|$.

In what follows, we will consider the (1+1)-dimensional reduction of the Schwarzschild spacetime, by truncating the angular part. While we will lose the physics that depends on angular variables such as the graybody factors due to the gravitational potential (associated with spherical harmonic parts of the wave equation) and the physics associated with orbital motion, much of the essential features of quantum field theory in curved spacetimes will remain. For example, the detailed balance condition associated with detector thermalization in the Hartle-Hawking state can be obtained [115, 43]. This dimensional reduction allows us to borrow conformal techniques and obtain closed-form expressions for the two-point functions of the quantum field, thus simplifying the setup considerably.

Klein-Gordon field and Wightman functions

Let $\phi(\mathsf{x})$ be a massless Klein-Gordon field in $(1+1)$-dimensional Schwarzschild spacetime, satisfying the Klein-Gordon equation (2.2). After canonical quantization, the quantum field admits Fourier mode decomposition of the form

$$\hat{\phi}(\mathsf{x}) = \int_{\mathbb{R}} \mathrm{d}k \, \left(\hat{a}_k u_k(\mathsf{x}) + \hat{a}_k^\dagger u_k^*(\mathsf{x})\right) , \tag{6.9}$$

with the mode functions $\{u_k(\mathsf{x})\}$ satisfying the conditions given by (2.14).

The definition of a vacuum state of the field depends on the choice of timelike Killing vector field with respect to which the positive frequency modes $u_k(\mathsf{x})$ are defined [2, 115, 43]. There are three standard choices of vacuum states that are unitarily inequivalent and are associated with different regions of spacetime:

- Boulware vacuum $|0_{\rm B}\rangle$: The corresponding mode functions $u_k(\mathsf{x})$ are positive frequency modes with respect to $\partial_{t_{\rm s}}$. The state is defined on the exterior region I of Fig. 6.1.
- Unruh vacuum $|0_{\rm U}\rangle$: The corresponding mode functions $u_k(\mathsf{x})$ are positive frequency modes with respect to ∂_U on $\mathcal{H}^-$ and ∂_v on $\mathscr{I}^-$. The state is defined in regions I and II of Fig. 6.1.
- Hartle-Hawking vacuum $|0_{\rm H}\rangle$: The corresponding mode functions $u_k(\mathsf{x})$ are positive frequency modes with respect to ∂_U and ∂_V. The state is defined on the full maximally extended Schwarzschild spacetime regions I–IV of Fig. 6.1.

The Boulware vacuum is the vacuum state that reproduces the Minkowski vacuum in $r \to \infty$ limit, whereas the Hartle-Hawking vacuum is the vacuum state that reproduces a thermal state in flat space in the large r limit. The Unruh vacuum is, by construction, one that mimics radiation outflux, effectively by replacing the ingoing Hartle-Hawking modes with ingoing Boulware modes.

In terms of field observables, the distinct vacua (denoted $|0_\alpha\rangle$ where $\alpha = \rm B, U, H$) can be specified by the vacuum Wightman functions:

$$W_\alpha(\mathsf{x},\mathsf{x}') \coloneqq \langle 0_\alpha|\hat{\phi}(\mathsf{x})\hat{\phi}(\mathsf{x}')|0_\alpha\rangle \ . \tag{6.10}$$

For each vacuum state, we have

$$W_{\rm B}(\mathsf{x},\mathsf{x}') = -\frac{1}{4\pi}\ln\left[-\Lambda^2(\Delta u - \mathsf{i}\epsilon)(\Delta v - \mathsf{i}\epsilon)\right] \ , \tag{6.11a}$$

$$W_{\rm U}(\mathsf{x},\mathsf{x}') = -\frac{1}{4\pi}\ln\left[-\Lambda^2(\Delta U - \mathsf{i}\epsilon)(\Delta v - \mathsf{i}\epsilon)\right] \ , \tag{6.11b}$$

$$W_{\rm H}(\mathsf{x},\mathsf{x}') = -\frac{1}{4\pi}\ln\left[-\Lambda^2(\Delta U - \mathsf{i}\epsilon)(\Delta V - \mathsf{i}\epsilon)\right] \ , \tag{6.11c}$$

where $\Lambda > 0$ is an infrared (IR) cutoff inherent in $(1+1)$ massless scalar field theory.

We make a parenthetical remark that in principle, one could try to perform canonical quantization with respect to the PG coordinates where the vacuum state (which we may call PG vacuum $|0_{\rm PG}\rangle$) is associated with a freely falling observer (see e.g., [117, 118, 119] for related discussions). This will be slightly more involved due to the cross-term in the metric. However by construction this state will be regular across the horizon and is well-defined on regions I and II of the Schwarzschild spacetime. We expect that essential qualitative features of our results in the context of entanglement harvesting will be similar to Hartle-Hawking and Unruh vacua.

Following [120, 115, 43], we shall use a particular model of detector-field interaction known as the *derivative coupling* detector model. The reason for this choice is that the Wightman functions (6.11a)-(6.11c) have two shortcomings; they do not possess the Hadamard short-distance property [121, 122], and they have an IR ambiguity associated with massless fields in two-dimensional QFT with no boundary conditions. Instead, since we are interested only in the two-point functions evaluated along the support of each detector, we will only need to calculate the pullback of the two-point functions along the detectors' trajectories, and consider the proper time derivatives associated with the two trajectories $\mathsf{x}(\tau)$ and $\mathsf{x}'(\tau')$:

$$\mathcal{A}_\alpha(\mathsf{x}(\tau),\mathsf{x}'(\tau')) = \langle 0_\alpha|\partial_\tau\hat{\phi}(\mathsf{x}(\tau))\partial_{\tau'}\hat{\phi}(\mathsf{x}'(\tau'))|0_\alpha\rangle \ . \tag{6.12}$$

The proper time derivatives remove the IR ambiguity from the Wightman function and the resulting two-point functions mimic the short-distance behavior of the Wightman distribution in (3+1) dimensions. It also retains all other essential features such as invariance under time translation generated by the respective timelike Killing vector fields that define each vacuum state. Past results have suggested that qualitatively similar results to the linear coupling model are obtained in flat space and $(1+1)$-dimensional spacetimes with moving mirrors [25, 39].

More explicitly, the proper time derivative two-point function reads

$$\mathcal{A}_{\rm B}(\tau,\tau') = -\frac{1}{4\pi}\left[\frac{\dot{u}\dot{u}'}{(u-u'-\mathsf{i}\epsilon)^2}+\frac{\dot{v}\dot{v}'}{(v-v'-\mathsf{i}\epsilon)^2}\right] , \tag{6.13a}$$

$$\mathcal{A}_{\rm U}(\tau,\tau') = -\frac{1}{4\pi}\left[\frac{\dot{U}\dot{U}'}{(U-U'-\mathsf{i}\epsilon)^2}+\frac{\dot{v}\dot{v}'}{(v-v'-\mathsf{i}\epsilon)^2}\right] , \tag{6.13b}$$

$$\mathcal{A}_{\rm H}(\tau,\tau') = -\frac{1}{4\pi}\left[\frac{\dot{U}\dot{U}'}{(U-U'-\mathsf{i}\epsilon)^2}+\frac{\dot{V}\dot{V}'}{(V-V'-\mathsf{i}\epsilon)^2}\right] , \tag{6.13c}$$

where we used the shorthand $\mathcal{A}_\alpha(\tau,\tau') \equiv \mathcal{A}_\alpha(\mathsf{x}(\tau),\mathsf{x}'(\tau'))$, $\dot{y} \equiv \partial_\tau[y(\tau)]$, and $\dot{y}' \equiv \partial_{\tau'}[y(\tau')]$. We stress that in general τ and τ' in the derivative coupling Wightman functions are proper times associated with *distinct trajectories* $\mathsf{x}(\tau)$ and $\mathsf{x}'(\tau')$; thus in general $\mathrm{d}\tau/\mathrm{d}\tau' \neq 1$ due to relative gravitational and kinematic redshifts of the two trajectories. For the rest of this chapter we will refer to $\mathcal{A}_\alpha(\tau,\tau') \equiv \mathcal{A}_\alpha(\mathsf{x}(\tau),\mathsf{x}'(\tau'))$ in Eqs. (6.13a)-(6.13c) as the Wightman functions, and not the original Wightman functions (6.11a)-(6.11c).

Let us comment on the choice of coordinate systems. The coordinate system x^μ is chosen in such a way that it specifies the coordinates of two detectors. In $(1+1)$-dimensional Schwarzschild spacetime, such a coordinate system could be the Schwarzschild, Eddington-Finkelstein, Kruskal-Szekeres, PG coordinate systems, etc. For the two static detectors

case considered in [43], any one of the coordinate systems above can be used. However, this is not true when one of the detectors is free-falling and enters the black hole; Schwarzschild coordinates cannot be used since it prevents us from analyzing the horizon-crossing moment. For this purpose, the coordinate system adapted to free-falling observers will be the simplest for our purposes both conceptually and numerically. The calculations of the geodesic equation for the free-falling trajectories in terms of the double null coordinates are given in Appendix C.1.

In what follows, we will employ the PG coordinate system to examine the harvesting protocol, that is, the time parameter t used in (2.39) will be $t_{\rm PG}$, and so the Heaviside step functions in (2.44) become

$$\Theta(t_{\rm PG}(\tau_{\rm A}) - t_{\rm PG}(\tau_{\rm B})),\ \Theta(t_{\rm PG}(\tau_{\rm B}) - t_{\rm PG}(\tau_{\rm A}))\,. \tag{6.14}$$

This choice is possible since the time-ordering is preserved when the detectors have negligible spatial extent [68].

6.2 Correlations harvested from Schwarzschild spacetime

In this section, we present our main results for entanglement and quantum mutual correlation harvesting for various parameter choices and detector trajectories. We define $d(r_i, r_j)$ to be the proper distance between two coordinate radii r_i, r_j, and write $d_{\rm AB} \coloneqq d(r_{\rm A}, r_{\rm B})$ for the proper separation between two detectors A and B.

It is clear that for two static detectors, the proper distance $d_{\rm AB}$ is unambiguous, but for free-falling detectors the proper distance between them changes with time. Therefore, there is a need to find some sort of effective proper distance that works for free-falling scenarios. For this purpose, we use the locations of the peaks of Alice and Bob's Gaussian switching functions, that is, we employ Gaussian switching functions

$$\chi_j(\tau_j) = \exp\left[-\frac{(\tau_j - \tau_{j,0})^2}{\sigma^2}\right], \tag{6.15}$$

where $\tau_{j,0}$ is the peak proper time of the Gaussian, and use $\tau_{\rm A,0}$ and $\tau_{\rm B,0}$ as reference points as follows.

(a) If Alice and Bob are static as depicted in Fig. 6.2(a) (we will call this the **SS scenario**), we take $d_{\rm AB}$ to be measured when both peaks are at some constant-$t_{\rm PG}$ slice. Since

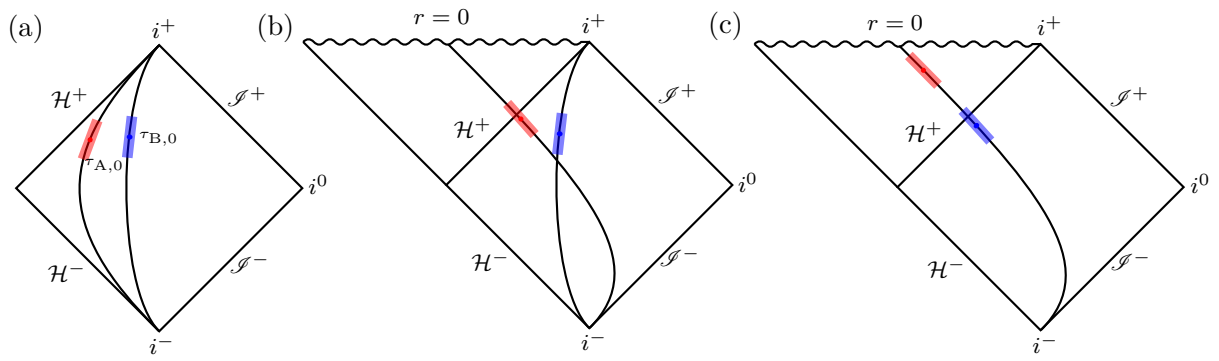

Figure 6.2: Penrose diagrams for three cases: (a) SS, (b) FS, and (c) FF.

both are static, their separation $d_{\rm AB}$ computed this way is also valid even if the switching peaks are translated along their respective trajectories.

(b) If Alice is free-falling and Bob is static [Fig. 6.2(b)] (we will call this the **FS scenario**), we take $d_{\rm AB}$ to be measured with respect to the peaks of their Gaussian switching, thus effectively locating Alice at $r_{\rm A} = r(\tau_{\rm A,0})$ and Bob at some fixed $r_{\rm B}$. We stress that both detector trajectories are parametrized by different proper times due to gravitational redshift, i.e., $\mathrm{d}\tau_{\rm A}/\mathrm{d}\tau_{\rm B} \neq 1$.

(c) If both detectors are free-falling from infinity [Fig. 6.2(c)] (we will call this the **FF scenario**) initially at rest, then the proper distance is given by $d_{\rm AB} = |r(\tau_{\rm A,0}) - r(\tau_{\rm A,0} + \text{const.})|$ with the constant to be determined. This is because in this case both detector trajectories can be parametrized by the same proper time and hence the proper distance is completely controlled by the difference $\tau_{\rm B,0} - \tau_{\rm A,0} = \text{constant}$.

We will compute all quantities in units of the switching width σ as before. Concurrence and quantum mutual information were evaluated as $\mathcal{C}_{\rm AB}/\tilde{\lambda}^2$ and $I_{\rm AB}/\tilde{\lambda}^2$ in Ch. 4, where $\tilde{\lambda}$ is the unitless coupling constant given by $\tilde{\lambda} := \lambda\sigma^{(n-3)/2}$ for *linear coupling* $\sim \hat{m}_j \otimes \hat{\phi}$ in $(n+1)$-dimensional spacetime. For the derivative coupling, this becomes $\tilde{\lambda} := \lambda\sigma^{(n-1)/2}$, and so in $(1+1)$ dimensions, this gives $\tilde{\lambda} = \lambda$ (i.e., λ is already dimensionless) but we will use $\tilde{\lambda}$ in this section to remind ourselves that the coupling strength of the (derivative) UDW model is dimension dependent.

Unlike in the BTZ spacetime case, the numerical calculations in Schwarzschild spacetime are more involved since the double integrals in (2.44) cannot be simplified to single integrals. For this reason, we use the technique involving numerical contour integration outlined in [43], with a modification for the evaluation of the non-local term $X_{\rm AB}$ in (2.44):

the free-falling trajectory introduces some numerical instability that makes it difficult to work with the Heaviside step function directly. Consequently, the computation is done by approximating the step function using a smooth analytic function: for our purposes we use the fact that

$$\Theta(z) = \lim_{k\to\infty} \left(\frac{1}{2} + \frac{1}{2}\tanh kz\right) , \tag{6.16}$$

and define an *approximate step function*[2] to be

$$\Theta_k(z) \coloneqq \frac{1}{2} + \frac{1}{2}\tanh kz \tag{6.17}$$

where k is fixed but sufficiently large. The choice of k will in fact be dependent on the choice of the contour size (i.e. the value of ϵ in the $i\epsilon$ prescription), which for generic situations requires small ϵ for large k.

6.2.1 Free-falling Alice, static Bob (FS)

In Fig. 6.3 we plot the concurrence and quantum mutual information as functions of Alice's proper distance from the horizon, $d(r_{\rm A}, r_{\rm h})/\sigma$, at the exterior of the black hole for both Unruh and Hartle-Hawking vacuum states and we compare the free-falling-static (FS) and static-static (SS) scenarios.

We observe that the SS scenario has a larger concurrence than the FS scenario, and this is true even when both detectors are far from the black hole. The entanglement shadow near the horizon is wider for the FS case, whereas for the SS case the shadow is much smaller in comparison [see inset in Fig. 6.3(a)]. The generic result here is that when one detector is free-falling, the bipartite entanglement harvesting is less potent than the static case. We will revisit this issue later in order to see to what extent this can be explained by relative velocities between the two detectors. We remark that the results for the SS case differ somewhat from those a previous study of harvesting in a $(1+1)$-dimensional collapsing shell spacetime [43] because the protocols are implemented slightly differently; here the switching peaks of the detectors are turned on at the same constant $t_{\rm PG}$ slices, while in [43] the detectors are turned on at the same constant proper time τ_0 (in their own

[2]The analysis of this technique is given in [123], which includes the performance of this approximation along with other possible choices of analytic functions and variations of the contour. We also note that the numerical evaluation is done using *Mathematica* 10 [124], as it is (surprisingly) more stable than the newer versions and in some cases the newer versions may even compute the wrong answers on physical grounds.

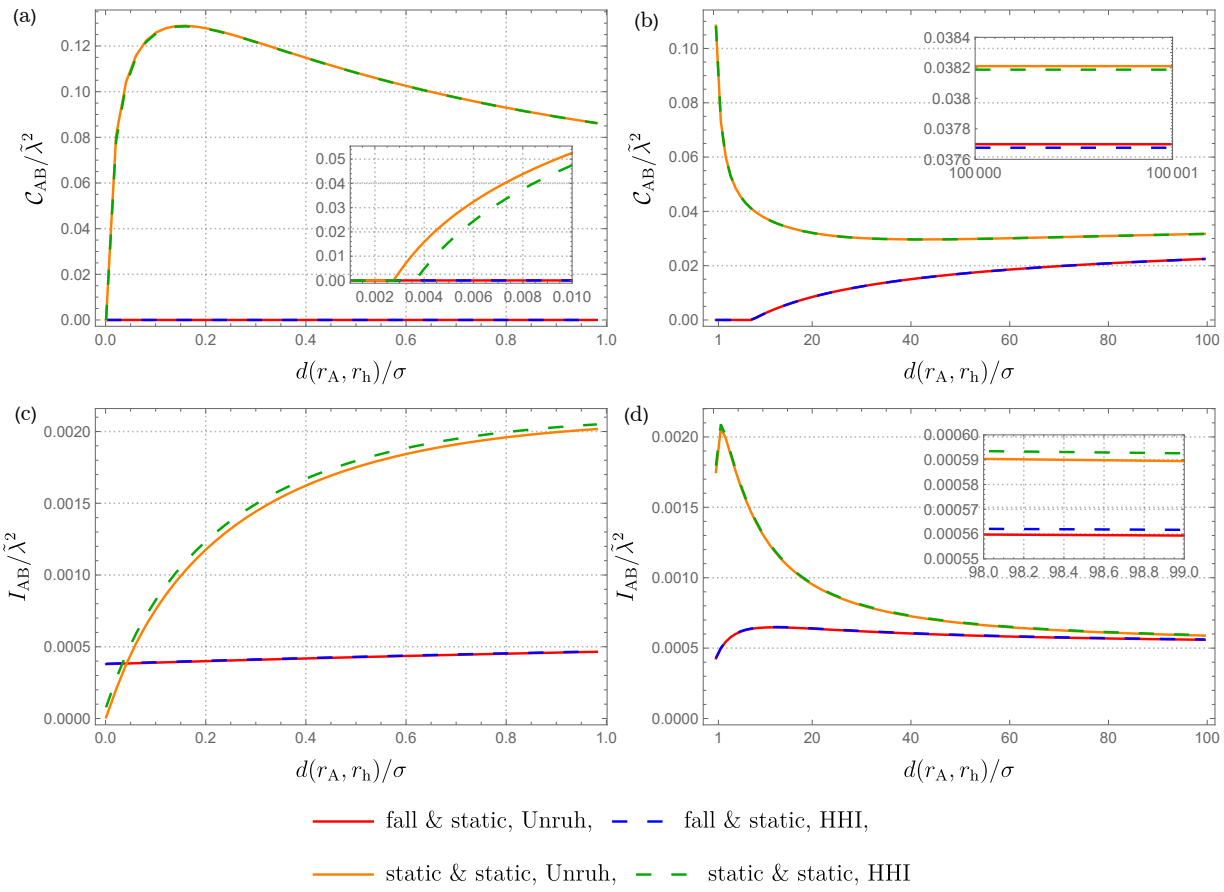

Figure 6.3: Concurrence and mutual information are plotted as a function of the effective proper distance of Alice from the horizon for both the SS and FS scenarios. Here we chose $\Omega\sigma = 2, M/\sigma = 5, d_{AB}/\sigma = 2$. (a) Concurrence near the horizon, where $d(r_A, r_h)/\sigma \in [0.001, 1]$. (b) Concurrence further away from the horizon at $d(r_A, r_h)/\sigma \in [1, 100]$ with the inset covering very far regime $d(r_A, r_h)/\sigma \in [10^5, 10^5+1]$. (c) Quantum mutual information near the horizon, where $d(r_A, r_h)/\sigma \in [0.001, 1]$. (d) Mutual information further away from the horizon at $d(r_A, r_h)/\sigma \in [1, 100]$.

frames). The relative redshift factor is markedly different, and hence the entanglement shadow size is different [very small in Fig. 6.3(a) inset].

However, for quantum mutual information harvesting, notably the FS scenario can outperform the SS case very near to the horizon, as we show in Fig. 6.3(c). The overall behavior for mutual information harvesting is similar to concurrence in that the FS case is less efficient in extracting correlations from the field, although there is non-zero mutual information in general. This behavior is consistent with the results presented in Ch. 4, where the harvested quantum mutual information does not have a shadow.

Next, we consider how the harvesting protocol depends on the black hole masses, as we show in Fig. 6.4. In general, we see that the smaller mass black holes allow for better harvesting efficiency for both concurrence and mutual information. However, due to non-trivial roles of curvature and communication between two detectors, the variation of concurrence and mutual information as we vary detector distances from the horizon is generally not monotonic. This is especially so for mutual information, where we see that sufficiently far from the horizon, the behavior flips and detectors harvest mutual information less for smaller masses; we verified at large distances [see inset of Fig. 6.4(d)] that the curves flip again, and we again obtain the result that larger mass leads to less correlation harvested.

A natural question that arises is to what extent the results obtained thus far depend only on the kinematic properties of the detectors (i.e., their velocities) and how much of it comes from the intrinsic properties of the background spacetime (i.e., the curvature). As it turns out, the UDW formalism is not very sensitive to spacetime curvature and much of the results here can be simulated using the corresponding flat space result, at least in the exterior geometry of the black hole sufficiently distant from the horizon. In order to better understand this kinematical aspect of the harvesting protocol, we will consider concurrence and mutual information for the Boulware vacuum and compare the results with the Minkowski vacuum analog.[3]

For this comparison to work, we will use the notion of intrinsic relative velocities in general relativity. The idea is that since in curved spacetimes $(\mathcal{M}, g)$ the connection is not flat, one cannot compare vectors belonging to tangent spaces at different points directly. Consequently, in the presence of curvature, one cannot naïvely compute relative velocities between two observers at two different events $p, q \in \mathcal{M}$ because a vector u^a in $T_p\mathcal{M}$ is not *a priori* related to vectors in $T_q\mathcal{M}$. However, for spacetimes with well-defined spacelike foliations, one can generalize the notion of relative velocities by making use of

[3] A similar comparison has been carried out between Rindler and Schwarzschild spacetimes [125].

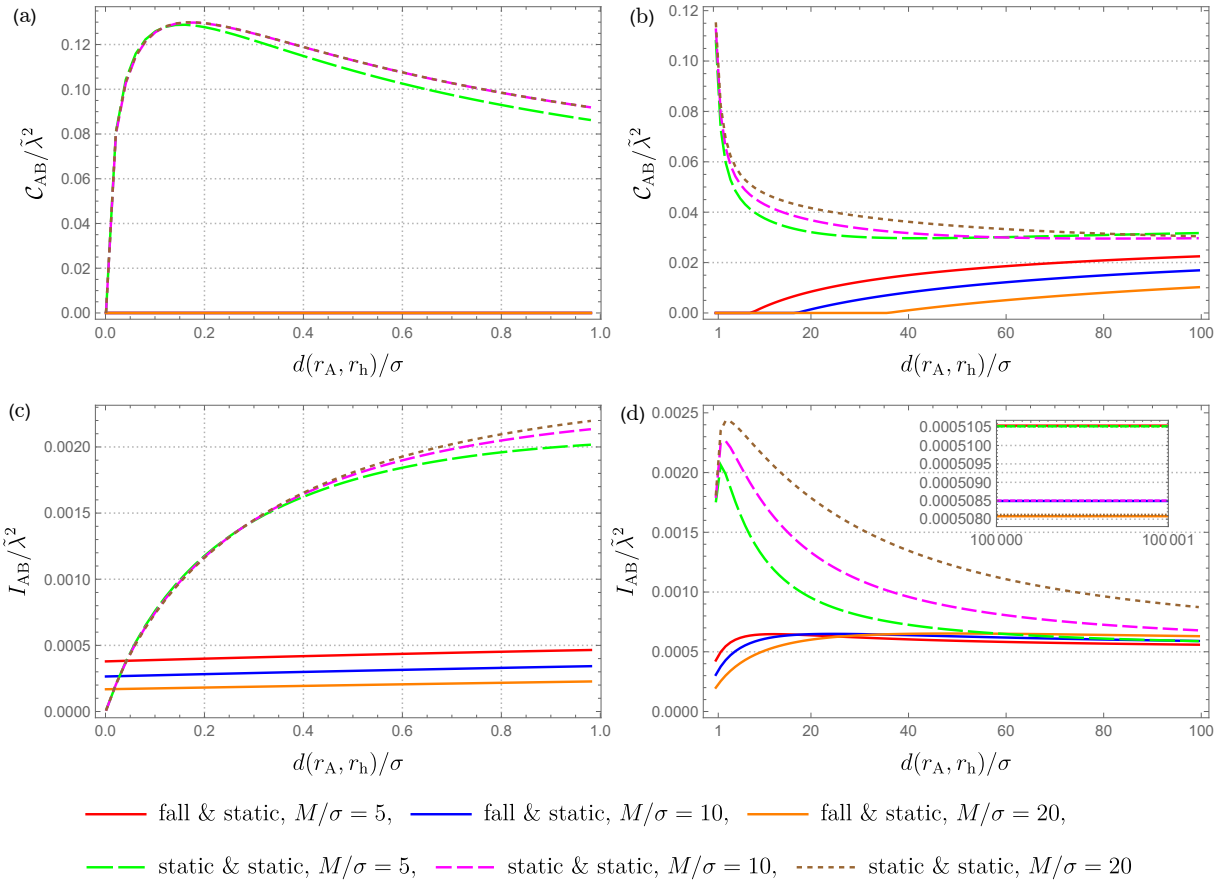

Figure 6.4: Concurrence and mutual information are plotted for various black hole masses in both the FS and SS scenarios as a function of Alice's proper distance from the horizon. As a benchmark, we use the Unruh vacuum and we consider three different masses $M/\sigma = 5, 10, 20$. We fix the other parameters as $\Omega\sigma = 2, d_{\rm AB}/\sigma = 2$. (a) Concurrence near the horizon at $d(r_{\rm A}, r_{\rm h})/\sigma \in [0.001, 1]$. We see that the FS case vanishes close to the horizon. (b) Concurrence further away at $d(r_{\rm A}, r_{\rm h})/\sigma \in [1, 100]$. The entanglement shadow in the SS case increases with increasing M [43]. (c) Mutual information near the horizon at $d(r_{\rm A}, r_{\rm h})/\sigma \in [0.001, 1]$. (d) Mutual information further away at $d(r_{\rm A}, r_{\rm h})/\sigma \in [1, 100]$.

the generalized version of spacelike simultaneity in flat space. Such a relative velocity is called the kinematic relative velocity (KRV), which is described in Appendix C.2.

For Schwarzschild geometry, the notion of KRV boils down to a simple formula in terms of the metric function $f(r)$. If Alice and Bob are both static observers at fixed radii, the KRV is zero. For the FS scenario where Alice is free-falling from infinity, her KRV relative to Bob is given by [126]

$$V_{\mathrm{A,kin}}\big|_{\mathrm{B}} = -f(r_{\mathrm{B}})\sqrt{1-\frac{f(r_{\mathrm{A}})^2}{E^2}}\frac{\partial}{\partial r}\bigg|_{\mathrm{B}}\,, \tag{6.18}$$

where $E = \sqrt{1-2M/r_0}$ and r_0 is the initial radius of the free-falling trajectory at rest [127]. In our FS scenario, we have $r_0 \to \infty$ so that $E = 1$ and the magnitude of the KRV is given simply $V_{\mathrm{AB}} \coloneqq |V_{\mathrm{A,kin}}| = f(r_{\mathrm{B}})\sqrt{1-f(r_{\mathrm{A}})^2}$. Note that V_{AB} depends on τ_{A} since a free-falling detector has non-zero proper acceleration; in this case, Alice's proper acceleration can be shown to be [see Eq. (C.3) in Appendix C.1]

$$a(\tau_{\mathrm{A}}) \coloneqq \sqrt{a_\mu a^\mu} = -\frac{M}{r(\tau_{\mathrm{A}})^2}\,. \tag{6.19}$$

If the detectors are far enough from the black hole and/or the support of the Gaussian is sufficiently small, then the variation of Alice's radial velocity across the Gaussian support can be considered approximately constant, equal to the value at Alice's Gaussian peak. In this case, the KRV is given approximately by $V_{\mathrm{AB},0} \coloneqq f(r_{\mathrm{B}})\sqrt{1-f(r(\tau_{\mathrm{A},0}))^2}$ where $\tau_{\mathrm{A},0}$ is the Gaussian peak of Alice. We can then compare the concurrence and mutual information of the corresponding scenario in Minkowski space where Alice has relative velocity V_{AB} with respect to Bob for the same derivative coupling UDW model.[4]

We compare the concurrence and mutual information in the FS scenario in the Boulware vacuum against the corresponding Minkowski vacuum scenario with the same constant relative velocity $V_{\mathrm{AB},0}$ in Fig. 6.5. The flat space version (shown in orange in Fig. 6.5) corresponds to Bob at rest in an inertial frame and Alice boosted away from Bob, with $d_{\mathrm{AB}}/\sigma = 2$ measured from the peaks of both Gaussian switching functions. The relevant scale is given by $a(\tau_{\mathrm{A},0})\sigma \approx 10^{-5} \ll 1$ (thus the constant velocity approximation is valid across the Gaussian support) and $V_{\mathrm{AB},0} \lesssim 0.08$ which is almost in the relativistic regime. Observe that for this setup, most of the correlations at $d(r_{\mathrm{A}}, r_{\mathrm{h}})/\sigma \sim 300 - 500$ can be accounted for by the correct relative velocity alone (hence purely kinematic). Therefore, the

[4] All we need to change is the definition of the null coordinates into $u, v = t \mp r$ in the definition of Wightman distribution for the Boulware vacuum (6.13a).

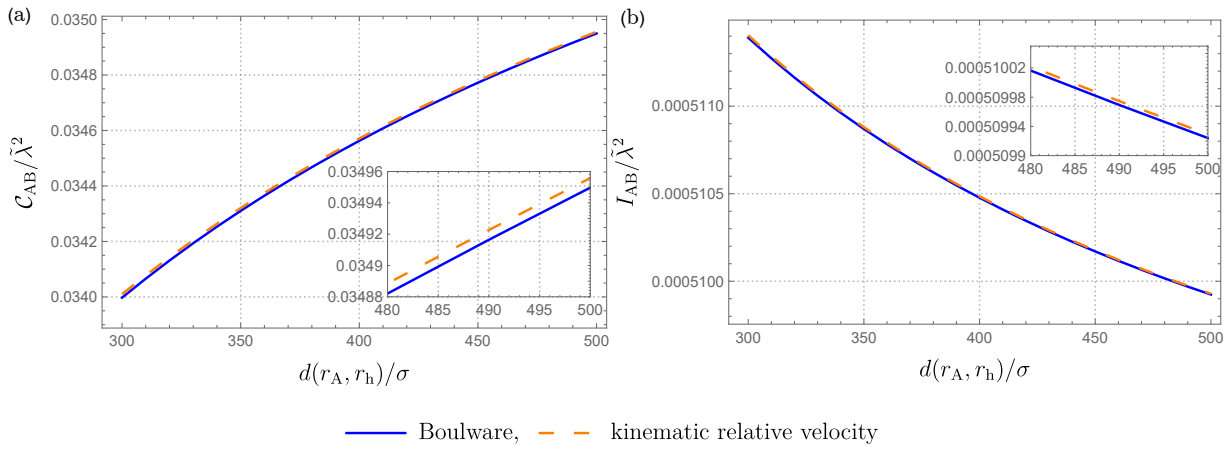

Figure 6.5: Concurrence and mutual information for the FS scenario are plotted for the Boulware vacuum and compared to the KRV in the Minkowski vacuum. $\Omega\sigma = 2, M/\sigma = 1, d_{\rm AB}/\sigma = 2$, and stationary and boosted inertial detectors in (1+1)-dimensional Minkowski spacetime with $\Omega\sigma = 2, d_{\rm AB}/\sigma = 2$.

relative motion between the detectors (measured by KRV) is the most relevant physics that explains why correlations in the FS scenario are consistently lower than the SS counterpart in Figs. 6.3 and 6.4. At distances much farther than 500σ, the concurrence and mutual information harvesting are practically indistinguishable from flat space. As we approach the horizon the correlation harvested will start to be different for fixed σ as more non-uniformity in the accelerated motion is captured by the Gaussian support.

We remark that this does not mean the effect of the gravitational field is absent from the harvesting protocol; in fact, our analysis based on the kinematic relative velocity is a manifestation of local flatness and the equivalence principle, since a small enough Gaussian support is equivalent to looking at a small enough region of spacetime (the detector is already pointlike). The fact that the black hole is present will be manifest in other ways: for instance, insofar as Alice cannot signal to detectors near future null infinity $\mathscr{I}^+$ once Alice falls into the black hole, or that Alice will hit the singularity in finite proper time. Also, by putting Bob in a static trajectory such that the switching peak is sufficiently near future timelike infinity i^+ while Alice is inside the black hole, it is guaranteed that any correlation harvested is from the Hadamard contribution since they are both causally disconnected by the future horizon $\mathcal{H}^+$. In [43] it was shown how the signaling estimator for static detectors is already generally non-trivial in some finite region in the exterior: since the field commutator is state-independent, the non-trivial signaling is gravitational

in nature as the classical solutions to the Klein-Gordon equation depend on curvature (reflected by the non-trivial wave operator $\nabla_\mu \nabla^\mu$).

6.2.2 Dependence of harvesting with signaling between detectors

Our analysis so far has been focused on the detector trajectories, regardless of whether the detectors harvest correlations purely from the vacuum or potentially assisted by communication. We would like to understand to what extent the harvesting protocol in this particular setup is assisted by communication between the detectors mediated by the quantum field.

Although a direct way of showing how much of the harvested correlation comes from the quantum field is to decompose the matrix elements X_{AB} and C_{AB} into the Hadamard and Pauli-Jordan contributions as done in [30], it could be tedious to do this in a generic curved spacetime. Here, we instead employ a measure of how causally disconnected the two detectors are: the *signaling estimator* $\mathcal{E}$ [81, 43]. We take the signaling estimator to be[5]

$$\mathcal{E} := \frac{\lambda^2}{2}\mathrm{Im}\left(\int_{-\infty}^{\infty} \mathrm{d}\tau_{\mathrm{A}} \int_{-\infty}^{\infty} \mathrm{d}\tau_{\mathrm{B}}\, \chi(\tau_{\mathrm{A}})\chi(\tau_{\mathrm{B}}) \langle 0| \left[\partial_{\tau_{\mathrm{A}}}\hat{\phi}(\mathsf{x}_{\mathrm{A}}(\tau_{\mathrm{A}})), \partial_{\tau_{\mathrm{B}}}\hat{\phi}(\mathsf{x}_{\mathrm{B}}(\tau_{\mathrm{B}}))\right] |0\rangle \right). \tag{6.20}$$

We have removed the subscript α from the vacuum state since the field commutators are state-independent. This estimator is useful for the following reason: due to finite switching times for both detectors, it is classically challenging to determine if Alice is in the causal complement of Bob or not since it will require non-trivial ray tracing for the entire spatiotemporal support of both detectors, even if the detectors are pointlike. This provides us with a relatively cheap measure of how spacelike/timelike two detectors are; the main drawback is that it does not allow us to clearly quantify how much of the correlations harvested are due to communication-assisted contributions and how much are coming from the pre-existent entanglement in the field as done in [30].

A cautionary note is in order here. The signaling estimator is crude insofar as it is not quite an entanglement monotone; this will become apparent in what follows. Thus non-zero $\mathcal{E}$ can only indicate that some of the concurrence is due to the field-mediated communication channel between Alice and Bob. Conversely, if two detectors are causally disconnected then $\mathcal{E}$ is guaranteed to be zero. Likewise, small $\mathcal{E}$ is indicative that most of the harvested entanglement is not due to a communication channel. The sign of $\mathcal{E}$ is

[5]Strictly speaking we only need the modulus $|\mathcal{E}|$ since what is more relevant is the spatial interval or region where $\mathcal{E}$ is approximately zero: the non-zero value of $\mathcal{E}$ itself is secondary.

secondary[6] and in what follows we shall plot $|\mathcal{E}|$ whenever it is conceptually clearer to do so.

Note that the signaling estimator $\mathcal{E}$ is in terms of the commutator of the proper time derivative of the field along the two detectors' trajectories instead of the field commutator $[\hat{\phi}(\mathsf{x}_{\rm A}(\tau_{\rm A})), \hat{\phi}(\mathsf{x}_{\rm B}(\tau_{\rm B}))]$. This is because, for the derivative-coupling UDW model, one can show that the leading order correction[7] to Bob's density matrix $\rho_{\rm B}^{(2)} := \mathrm{Tr}_{\rm A}\, \rho_{\rm AB}^{(2)}$ due to Alice's detector depends only on the commutator $[\partial_{\tau_{\rm A}}\hat{\phi}(\mathsf{x}_{\rm A}(\tau_{\rm A})), \partial_{\tau_{\rm B}}\hat{\phi}(\mathsf{x}_{\rm B}(\tau_{\rm B}))]$. The calculation proceeds analogously up to Eq. (24) in [81]. Furthermore, since the signaling component depends on proper time derivatives, it means that the communication contribution of the harvesting protocol mimics the $(3+1)$-dimensional setting, in that the commutator only has support on the light cone. Therefore, communication mediated by the massless scalar field will only occur if the supports of the switching functions of Bob's detector overlap with the lightlike boundary of Alice's causal past/future and vice versa. This means that they only can communicate via the scalar field if the support of the Gaussian of one detector intersects the causal past/future of the other detector.

Finally, we remark that the Gaussian switching can be effectively taken to have compact support despite the infinite exponential tails. We define *strong support* to be the interval $[-5\sigma+\tau_{j,0}, 5\sigma+\tau_{j,0}]$, where $\tau_{j,0}$ are the Gaussian peaks defined in each detector's rest frame. The switching function $\chi(\tau_j)$ can be taken to be negligible outside of this interval. This sort of strong support approximation has been shown to be reasonable for detector-field interaction studies [81, 43].

To this end, we consider the signaling estimator for Alice and Bob's trajectories, as shown in Fig. 6.6. The orange lines in 6.6(a) represent the light rays that can reach or emanate from the endpoints of Alice's Gaussian support, indicating the region along Bob's trajectory at which Bob can send or receive signals from Alice. We divide the regions along Bob's trajectory into four parts, shown in Fig. 6.6. Regions (i) and (iii) do not allow signaling between both detectors: this is expected from the fact that the commutator of $\partial_{\tau_{\rm A}}\hat{\phi}(\mathsf{x}_{\rm A})$ and $\partial_{\tau_{\rm B}}\hat{\phi}(\mathsf{x}_{\rm B})$ has support only on the lightlike region. Region (ii) is where Bob can signal to Alice when the Gaussian support of Bob's detector intersects the orange lines, whereas region (iv) is where Alice can signal to Bob. Notice that region (iv) is wider than region (ii).

For a given choice of Alice and Bob's detector parameters, the signaling region between Alice and Bob mediated by the detector-field interaction can be quantified by a single parameter δ and the PG coordinates. As depicted in Fig. 6.6(a), we first find the constant

[6] Indeed, the absolute value $|\mathcal{E}|$ is the definition of signaling estimator in [81].

[7] Here $\rho_{\rm AB}^{(2)}$ contains all terms of order λ^2 in Eq. (2.43).

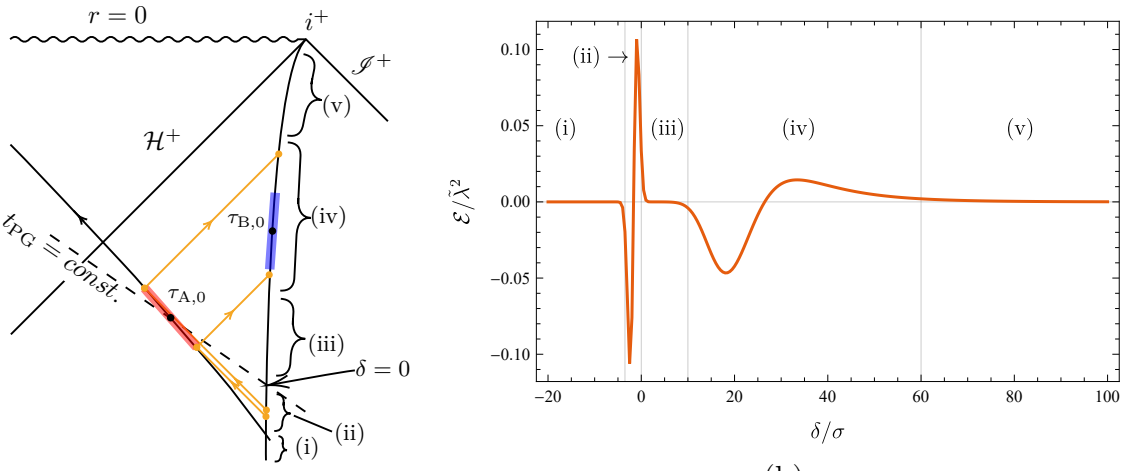

Figure 6.6: (a) Penrose diagram of the schematics of Alice (red) and Bob's (blue) positions, and (b) the corresponding signaling estimator between Alice and Bob as a function of the "time-delay" parameter, δ/σ, for the FS scenario. Here we choose $M/\sigma = 5, d_{\rm AB}/\sigma = 5$ and $d(r_{\rm A}, r_{\rm h})/\sigma = 1$. The red and blue stripes in (a) denote the strong support of Alice's and Bob's Gaussian switching, and the orange lines in denote the light rays that emanate or arrive at the endpoints of Alice's strong support.

$t_{\rm PG}$ slice that crosses Alice's Gaussian peak $\tau_{\rm A,0}$. This is simply given by $t_{\rm PG} = \tau_{\rm A,0}$. Bob is stationary at the radial coordinate[8] $r_{\rm B} = r_{\rm h} + d(r_{\rm A}, r_{\rm h}) + d_{\rm AB}$ and we suppose that Bob has the freedom to decide when to switch the detector on (for fixed width σ). The parameter δ gives a measure of time delay of Bob's switching away from the $t_{\rm PG} = \tau_{\rm A,0}$ line (the constant-$t_{\rm PG}$ slice that matches Alice's Gaussian peak) and it is given by

$$\delta := \tau_{\rm B,0} - \sqrt{f(r_{\rm B})}\left(\tau_{\rm A,0} - 2r_{\rm h}\sqrt{\frac{r_{\rm B}}{r_{\rm h}}} - r_{\rm h}\ln\frac{\sqrt{r_{\rm B}/r_{\rm h}}-1}{\sqrt{r_{\rm B}/r_{\rm h}}+1}\right). \tag{6.21}$$

Note that $\delta > 0$ if the Gaussian peak $\tau_{\rm B,0}$ is located in the future of the constant $t_{\rm PG} = \tau_{\rm A,0}$ line.

The signaling estimator between the two detectors as a function of δ/σ is given in Fig. 6.6(b); we see that it is not an entanglement monotone, as expected. By comparing

[8]Recall that in PG coordinates, the spatial slices are flat. Thus the coordinate separation between two radial coordinates r_i, r_j is equivalently given by the proper separation $\Delta r = |r_i - r_j| = d(r_i, r_j)$. This is not true for Schwarzschild coordinates $(t_{\rm s}, r)$.

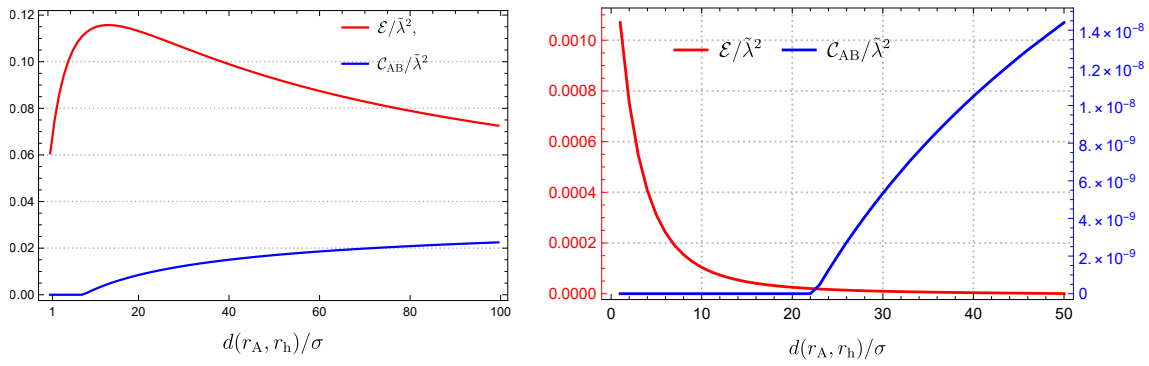

Figure 6.7: Concurrence and signaling estimator as a function of proper distance from the horizon for FS scenario. **Left:** $\Omega\sigma = 2, M/\sigma = 5, d_{\rm AB}/\sigma = 2$, as done in Fig. 6.3. **Right:** $M/\sigma = 5, \Omega\sigma = 5, d_{\rm AB}/\sigma = 5$ (larger distance between two detectors). Here we chose $\delta/\sigma = 1$ so that two detectors cannot communicate at large $d(r_{\rm A}, r_{\rm h})/\sigma$. In these cases, $\mathcal{E} > 0$.

with Fig. 6.6(a), we see that as δ varies from regions (i)-(iv), the communication between Alice and Bob can be precisely captured using the signaling estimator $\mathcal{E}$ (or rather the absolute value $|\mathcal{E}|$). Indeed the signaling estimator $|\mathcal{E}|$ is very sharp and narrow in region (ii) because the support of Bob's Gaussian switching crosses the small region where Bob can send signals to Alice via the field. Region (iv), where Bob can receive signals from Alice, is very wide compared to (ii), and this is manifest in $|\mathcal{E}| \neq 0$ for a wide range of δ. Regions (i) and (iii) have vanishing $|\mathcal{E}|$ because Bob is outside the signaling region. In region (v) δ is large enough that Bob is again causally disconnected from Alice.

We can now clarify whether the harvesting protocol we studied earlier is communication-assisted or not. By computing the signaling estimator for the results in Fig. 6.3, we conclude that indeed the harvesting protocol *is* communication-assisted because $|\mathcal{E}| \neq 0$, as we show in the left plot of Fig. 6.7. In the language of Fig. 6.6, this also means that for $d_{\rm AB}/\sigma = 2$, region (iii) is so small that it cannot completely contain the Gaussian support of Bob; hence the commutator cannot vanish as δ/σ increases from (ii) to (iv).

In view of this, we can ask whether the protocol still allows for entanglement harvesting with free-falling Alice when Bob is causally disconnected from Alice; the answer is yes, as we show in the right plot of Fig. 6.7. In this case, we have chosen the setup parameters and manipulated the time-delay parameter δ/σ such that the detectors are causally discon-

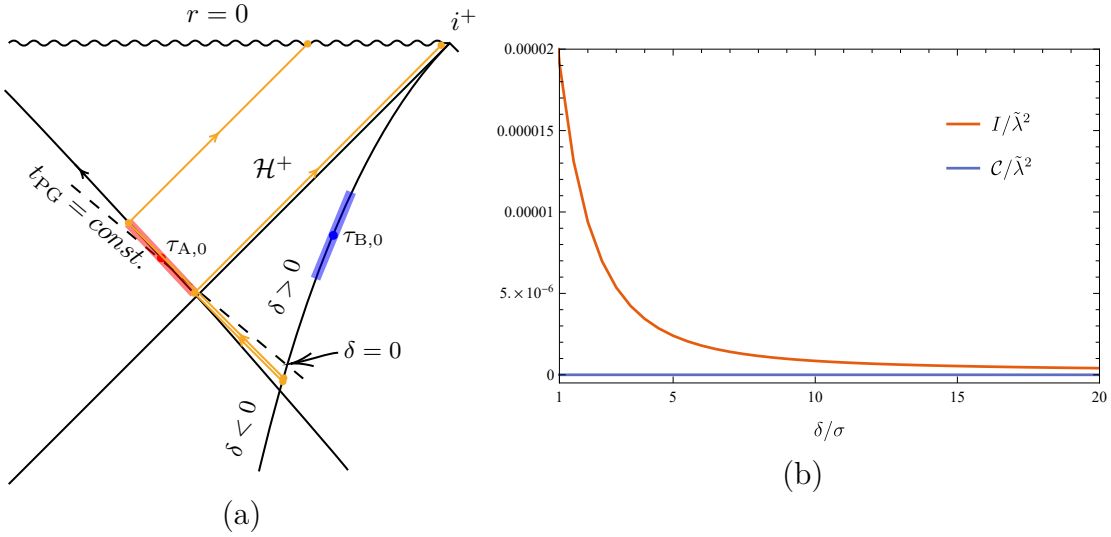

Figure 6.8: Schematics of the FS scenario when Alice's strong support is completely contained in the black hole interior. Here we chose $\Omega\sigma = 2, M/\sigma = 10, d(r_{\rm A}, 0)/\sigma = 14$, and $d(r_{\rm B}, r_{\rm h})/\sigma = 7$. Alice turns her detector on after she enters the black hole while Bob is staying outside. For this choice of parameters, mutual information harvested between the causally disconnected detectors is still manifestly non-zero, although the concurrence is zero in this case.

nected. Indeed, we see that the two detectors can still have non-zero concurrence without communication, indicating that the harvested entanglement is a genuine entanglement. Conversely, from the left diagram in Fig. 6.7, we also see that communication does not necessarily assist entanglement harvesting.

Last but not least, we consider the final FS scenario when Alice's Gaussian support is completely contained inside the black hole, as shown in Fig. 6.8(a). Here the crucial point is that Alice can never send a signal to Bob because her causal future is completely contained in the black hole interior, although there are values of $\delta < 0$ where Bob can still signal to Alice. The black hole mass needs to be large enough relative to the Gaussian width for Alice's strong support to fit inside. An example that fits such a requirement is given by $\Omega\sigma = 2, M/\sigma = 10, d(r_{\rm A}, 0)/\sigma = 14$, and $d(r_{\rm B}, r_{\rm h})/\sigma = 7$. For this choice, the concurrence is zero but the quantum mutual information is still non-zero, as seen from Fig. 6.8(b).

One may ask if two detectors causally disconnected by a horizon can harvest entanglement. Although we do not have an answer to this question, we provide an intuition

in the following. For two detectors at rest in Minkowski vacuum, it was shown [49, 28] that, for any detector separation L, there exists a minimum energy gap $\Omega_{\rm min}$ such that $|X_{\rm AB}| - \sqrt{P_{\rm A}P_{\rm B}} > 0$ for $\Omega \geq \Omega_{\rm min}$ for a Gaussian switching. However, if the detectors are immersed in a thermal bath caused by the Gibbons-Hawking effect [49] or the Unruh effect [128], the statement above about the detectors at rest does not hold; The detectors cannot be entangled if their separation L is large enough, no matter how large Ω is. Unfortunately, due to the highly oscillatory phase in the non-local matrix element $X_{\rm AB}$, we are unable to plot the results for $\Omega\sigma \gtrsim 4.6$. Since the detector static outside of the black hole experiences the Hawking effect, it could be possible that the detectors in the FS scenario cannot extract entanglement. This argument differs from the paper [44] on which this chapter is based.

In Fig. 6.8, the quantum mutual information harvested decreases with increasing δ/σ. Thus it seems that the harvesting protocol depends on how late Bob's detector is turned on even though the proper separation between the two detectors is the same. This can be traced to the fact that while the Wightman functions are stationary with respect to coordinate t (Schwarzschild or PG), it is *not* stationary with respect to the respective proper times $\tau_{\rm A}$ and $\tau_{\rm B}$, i.e., $\mathcal{A}_\alpha(\tau_{\rm A}, \tau_{\rm B}) \neq \mathcal{A}_\alpha(\tau_{\rm A} - \tau_{\rm B})$, since there is relative gravitational and kinematical redshift between the two trajectories. This is true even for two static detectors at two different radii and hence is also true for any FS scenarios where the two trajectories do not share the same proper time parametrization. In that sense, the harvesting protocol is sensitive to the relative proper time delay between both detectors, i.e., making one of the detectors turn on much later in the future generically decreases the mutual information and concurrence between them.[9]

We comment on the implementation of the harvesting protocol when Alice is inside the black hole. Strictly speaking, since Alice and Bob are causally disconnected by the horizon, there is no physical procedure for checking the entanglement by themselves. This is because neither party can collect the other party's detectors and perform state tomography of the joint system. For this particular scenario, we can follow similar principle as outlined in e.g. [49]: essentially, one has to consider a third party, say Charlie, who follows a trajectory that is contained in the causal futures of *both* Alice and Bob's detectors. Charlie will then collect information from both parties and perform state tomography on their behalf. Note that Charlie also needs to fall *inside* the black hole, since Alice's causal future is contained in the black hole interior. In contrast, when both detectors are outside, Alice and Bob

[9] Generically this is because, by varying δ/σ, there will be a value $\delta_{\rm max}$ where it attains a maximum for both concurrence and mutual information since the same reasoning should hold if Bob is turned on "too early" in the asymptotic past. For derivative coupling, the lightlike support of the commutator implies that switching on too early also disables communication.

can simply reconvene after the interactions have been turned off, although they can also employ a third party to do the joint state tomography.

6.2.3 Alice and Bob free-falling (FF)

We close the section by briefly analyzing the FF scenario, i.e. when both Alice and Bob are free-falling towards the black hole. Here, we only consider the free-falling trajectory initially at rest at spatial infinity since the adapted coordinate system is precisely the PG coordinates. Thus for this FF setup, Alice and Bob follow the same timelike trajectory but with different switching peaks. This simpler setup has the advantage that the derivative-coupling Wightman functions are expressible in relatively simple terms, since the radially infalling geodesics are relatively straightforward to implement. Note that due to the derivative coupling with the field, the support of $[\partial_{\tau_\mathrm{A}}\hat{\phi}(\mathsf{x}_\mathrm{A}(\tau_\mathrm{A})), \partial_{\tau_\mathrm{B}}\hat{\phi}(\mathsf{x}_\mathrm{B}(\tau_\mathrm{B}))]$ is lightlike. Thus being along the same timelike trajectory does not guarantee field-mediated communication between them.

As shown in Fig. 6.9(a), without loss of generality we set Bob's detector to switch on earlier than Alice's. This simulates the effect of Alice free-falling ahead of Bob. The effective proper separation d_AB between the detectors is fixed with respect to their Gaussian peaks. That is, given Alice's Gaussian peak at $\tau_{\mathrm{A},0}$ and a fixed proper distance d_AB, we can work out at what proper time $\tau_{\mathrm{B},0}$ Bob's Gaussian peak should be. More explicitly, given Alice's (effective) proper distance from the horizon $d_\mathrm{A} \coloneqq d(r_\mathrm{A}, 0)$, their Gaussian peaks can be written purely in geometric terms as

$$\tau_{\mathrm{A},0} = -\frac{d_\mathrm{A}}{3}\sqrt{\frac{2d_\mathrm{A}}{M}}\,, \tag{6.22}$$

$$\tau_{\mathrm{B},0} = -\frac{d_\mathrm{A}+d_\mathrm{AB}}{3}\sqrt{\frac{2(d_\mathrm{A}+d_\mathrm{AB})}{M}}\,. \tag{6.23}$$

We can study the harvesting protocol in a manner analogous to the SS or FS scenarios for any choice of d_A and d_AB. Fig. 6.9(b) depicts the signaling estimator and the concurrence between two freely falling detectors when $\Omega\sigma = 5, M/\sigma = 50, d_\mathrm{AB}/\sigma = 5$.

We immediately notice from Fig. 6.9(b) that the previously known entanglement shadow near the horizon [41, 43] is absent; the freely falling detectors can harvest entanglement from the interior and exterior of the black hole. First, note that in the SS scenario, the closer the detectors are to the horizon, the lower the value of $|X_\mathrm{AB}| - \sqrt{P_\mathrm{A}P_\mathrm{B}}$ as the noise term P_j dominates the non-local term $|X_\mathrm{AB}|$ [41, 43]. On general grounds, it can be

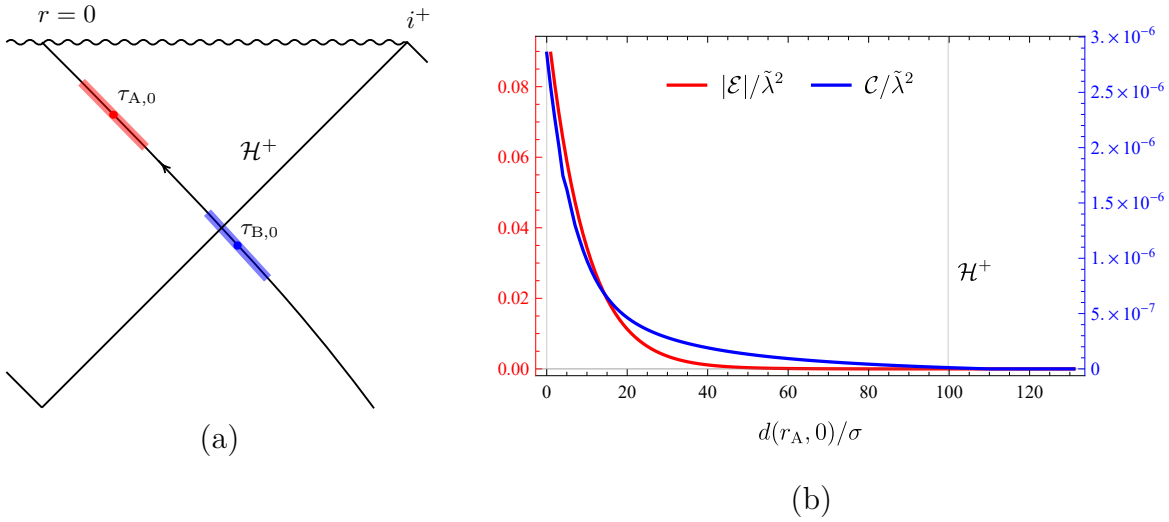

Figure 6.9: Schematics of two detectors in the FF scenario. Here we set $\Omega\sigma = 5, M/\sigma = 50, d_{\rm AB}/\sigma = 5$. (a) The Penrose diagram of freely falling detectors, with Alice infalling first towards the singularity followed by Bob. The horizontal axis is Alice's proper distance from the singularity, and the event horizon is at $r_{\rm h}/\sigma = 2M/\sigma = 100$. Alice cannot signal to Bob via the coupling to the field but can receive signals from Bob when they are close to the singularity. (b) The modulus of signaling estimator $|\mathcal{E}|/\tilde{\lambda}^2$ (red) and the concurrence (blue) between the two free-falling observers.

shown that for fixed proper separation $d_{\rm AB}$, $|X_{\rm AB}|$ remains finite as Alice (and hence Bob) is brought closer to the horizon (in fact vanishes in this limit), whilst $P_{\rm A} > |X_{\rm AB}|$ (for sufficiently small $d_{\rm AB}$ we have $P_{\rm A} \sim P_{\rm B}$). This behavior is a generic result of the fact that static detectors cannot remain static at the horizon, manifest as an infinite gravitational redshift factor. By contrast, the equivalence principle requires that free-falling observers (or detectors) experience nothing peculiar across the horizon. Free-falling detectors do not experience divergent gravitational redshift at the horizon, and so in generic FF situations the entanglement shadow is absent as both detectors cross the horizon along a radial geodesic.

Moreover, Fig. 6.9(b) shows that the amount of harvested entanglement (in blue) increases as the detectors reach the singularity. At early stages after horizon crossing, $|\mathcal{E}|$ is small and most of the entanglement harvested is from the vacuum. As the singularity is

approached, we can (using analogous ray-tracing analysis from previous subsections) see that as the singularity is approached, Bob becomes able to signal to Alice, which is manifest as increasing non-zero $|\mathcal{E}|$ (in red). Therefore, up until the point at which Alice's Gaussian tail approaches the singularity (beyond which we cannot make any conclusions at a semi-classical level), entanglement harvesting becomes increasingly communication-assisted for this particular setup.

Finally we make a comment regarding the generality of this FF scenario. There are extra complications in both analytic and numerical evaluation of the detectors' reduced density matrix if we consider generalized free-falling coordinates associated with free-falling observers initially at rest at finite radial coordinate r_0 (see [116] for the generalized coordinates adapted to different free-falling observers). This modified scenario is very useful in principle because we can minimize the effect of relative velocities of the detectors when they are very close to the black hole or even inside: our current setup necessarily requires that Alice has non-negligible (possibly relativistic) velocities that may by itself suppress the quality of the harvesting protocol. We leave this finite-radius free-falling scenario for future work.

Chapter 7

Conclusion

In this thesis, we investigated the influence of Unruh and Hawking effects on the correlation harvesting protocol. Previously Ref. [1] showed that two detectors at rest interacting with a thermal quantum field in Minkowski spacetime extract correlations from the field in such a way that entanglement monotonically decreases with temperature while quantum mutual information increases at the high-temperature regime (Sec. 3.2.1). In this thesis, we demonstrated that this is not the case for the thermal baths resulting from the Unruh and Hawking effects.

For uniformly accelerating Unruh-DeWitt (UDW) detectors with fixed proper separation between them, the harvested entanglement can be enhanced for some Unruh temperature T_{U}, and vanishes at high temperatures [38] (Sec. 3.2.2). This is due to the fact that the transition probability monotonically increases with temperature, and the concurrence (a measure of entanglement) becomes 0 whenever the transition probability P exceeds the non-local elements X_{AB} in the density matrix ρ_{AB} of the detectors: $|X_{\mathrm{AB}}| \leq P$. Quantum mutual information can also be enhanced for some T_{U} and decreases with higher temperatures, but it asymptotes to 0 at $T_{\mathrm{U}} \to \infty$, instead of suddenly vanishing. Therefore, high (but finite) Unruh temperatures prevent the detectors from extracting entanglement and other types of correlations such as classical and non-distillable entanglement in the $T_{\mathrm{U}} \to \infty$ limit.

We then examined the harvesting protocol in black hole spacetimes. In Ch. 4, detectors in Bañados-Teitelboim-Zanelli (BTZ) black hole spacetime were considered. The quantum field is in the Hartle-Hawking vacuum, which gives a thermal equilibrium of Hawking radiation. In Ref. [41], the harvested entanglement between two static detectors hovering outside of the black hole was shown to vanish when one of the detectors are close enough to

the event horizon. They claimed that this is caused by the high black hole temperature and gravitational redshift. Here, we wrote the concurrence and quantum mutual information in terms of the local temperature T and the gravitational redshift γ of the detector closest to the horizon and showed that the high temperature is responsible for the "death" of correlation near the horizon. To be more precise, at finite but high temperatures, entanglement can no longer be harvested while the extraction of mutual information is prohibited only in the limit $T \to \infty$, just as in the case of accelerating detectors.

The influence of black hole temperature on tripartite entanglement was also investigated in Ch. 5. Unlike bipartite entanglement, tripartite entanglement has a rich structure consisting of four classes of entanglement: Greenberger-Horne-Zeilinger (GHZ), W, biseparable, and fully separable states. It is of interest that which states can be generated from the field. We found that tripartite entanglement is less affected by high black hole temperature compared to bipartite entanglement. This leads us to the case where the π-tangle (a measure of tripartite entanglement) is non-zero while all the bipartite entanglement is vanishing. Hence, we claimed that such tripartite entanglement is of GHZ type.

We make two remarks here. First, the π-tangle is a measure of tripartite entanglement for *pure* states, while our final density matrix is mixed. One has to appropriately optimize the π-tangle in order to apply it to mixed states, though a concrete procedure for such an optimization is not known as far as we know. However, the π-tangle we used in this thesis is the lower bound of the optimized π-tangle; thereby whenever the π-tangle is positive, it is guaranteed that the optimized one is also positive. Nevertheless, such optimization is required for a thorough investigation of tripartite entanglement harvesting. Second, it is questionable that we are actually "harvesting" tripartite entanglement from the field since the three-point correlation function, $\langle 0|\hat{\phi}(\mathsf{x}_1)\hat{\phi}(\mathsf{x}_2)\hat{\phi}(\mathsf{x}_3)|0\rangle$ is zero in the free theory. This means that our tripartite entanglement is not coming from the tripartite correlations in the field, but rather, it is from the two-point correlation function. In this sense, it is appropriate to call it "tripartite entanglement generation."

Finally, we considered two detectors in $(1+1)$-dimensional Schwarzschild spacetime in Ch. 6 and investigated the scenario where thermal equilibrium does not exist. This is implemented by introducing the Unruh vacuum, which is a mixture of the Hartle-Hawking and Boulware vacua, and by letting the detectors free-fall into the black hole. Along with [43] we found that the detectors in the Unruh vacuum behave similarly to the Hartle-Hawking vacuum case. If one of the detectors free-falls into the black hole, the entanglement shadow (the region in which detectors are prohibited to extract entanglement) becomes wider. In fact, the harvested entanglement by the free-faller and the static detector is always less than the entanglement extracted by two static detectors. This is counter-intuitive since a freely falling detector will see relatively lower temperatures near the horizon compared

to the static detectors. We revealed that the downgrade of the ability of entanglement harvesting by the free-faller is caused by the kinematic properties of UDW detectors; The Doppler redshift due to the relative velocity between the detectors will degrade the entanglement. Nevertheless, the quantum mutual information remains non-zero even when the free-faller crosses the horizon, which indicates that the absence of infinite temperature for the freely falling observer saves the correlation. We also looked at two freely falling detectors. Due to the absence of infinite temperature for both detectors, they manage to extract correlations without a problem.

We comment on entanglement harvesting in the Boulware vacuum in [43]. The Boulware vacuum is associated with the positive frequency mode with respect to ∂_{t_s}, where t_s is the Schwarzschild time. As a result, the black hole temperature is zero and in fact, the Boulware vacuum is identical to the Minkowski vacuum at spatial infinity. In Ref. [43], it was observed that the entanglement shadow is still present near the event horizon even in the Boulware vacuum. This observation appears to conflict with our claim that the shadow is a result of the high black hole temperature. However, we argue that the entanglement shadow manifest in the Boulware vacuum is a mere result of non-zero transition probability, which is a consequence of the interaction duration being finite. This phenomenon is also observed in the Minkowski vacuum. By extending the interaction duration, the transition probability can be reduced (indeed, for a detector with an infinitely long interaction time, the transition probability becomes zero). See [129] in the context of transition rate in $(3+1)$-dimensional Schwarzschild spacetime. Hence, if the interaction duration is long enough, the detectors can harvest entanglement from the field (in the Boulware vacuum) arbitrarily close to the event horizon.

We close this thesis by discussing potential avenues for future research. It is still unclear how to classify the tripartite entanglement generated among the detectors from the field. As mentioned above, this issue is due to the lack of a tripartite entanglement measure that can be properly applied to mixed states. It is, therefore, crucial to find such a measure (or a witness) for a three-qubit system. One can also think about the experimental realization of entanglement harvesting. In particular, it may be possible to verify the influence of the Unruh effect on harvested correlations from a Bose-Einstein condensate [130, 131, 132]. However, the entanglement harvesting protocol in this setup remains largely unexplored.

References

[1] Petar Simidzija and Eduardo Martín-Martínez. Harvesting correlations from thermal and squeezed coherent states. *Phys. Rev. D*, 98:085007, Oct 2018. doi: 10.1103/PhysRevD.98.085007. URL https://link.aps.org/doi/10.1103/PhysRevD.98.085007. vi, 3, 4, 5, 38, 42, 43, 44, 45, 47, 50, 51, 98

[2] N.D. Birrell and P.C.W. Davies. *Quantum Fields in Curved Space*. Cambridge Monographs on Mathematical Physics. Cambridge University Press, Cambridge, England, 1984. ISBN 9780521278584. URL https://books.google.ca/books?id=SEnaUnrqzrUC. 1, 7, 48, 78

[3] S. W. Hawking. Particle creation by black holes. *Commun. Math. Phys.*, 43(3): 199–220, 1975. doi: https://link.springer.com/article/10.1007/BF01608497. URL https://link.springer.com/article/10.1007/BF01608497. 1, 4

[4] Patrick Hayden and John Preskill. Black holes as mirrors: quantum information in random subsystems. *Journal of High Energy Physics*, 2007(09):120, sep 2007. doi: 10.1088/1126-6708/2007/09/120. URL https://dx.doi.org/10.1088/1126-6708/2007/09/120. 1

[5] Shinsei Ryu and Tadashi Takayanagi. Holographic Derivation of Entanglement Entropy from the anti–de Sitter Space/Conformal Field Theory Correspondence. *Phys. Rev. Lett.*, 96:181602, May 2006. doi: 10.1103/PhysRevLett.96.181602. URL https://link.aps.org/doi/10.1103/PhysRevLett.96.181602. 1

[6] David D. Blanco, Horacio Casini, Ling-Yan Hung, and Robert C. Myers. Relative entropy and holography. *J. High Energy Phys.*, 08(2013):060, 2013. URL https://doi.org/10.1007/JHEP08(2013)060. 1

[7] F. Verstraete, V. Murg, and J. I. Cirac. Matrix product states, projected entangled pair states, and variational renormalization group methods for quantum spin systems.

Advances in Physics, 57(2):143–224, 2008. doi: 10.1080/14789940801912366. URL https://doi.org/10.1080/14789940801912366. 1

[8] Thomas Faulkner, Thomas Hartman, Matthew Headrick, Mukund Rangamani, and Brian Swingle. Snowmass white paper: Quantum information in quantum field theory and quantum gravity. *arXiv e-prints*, art. arXiv:2203.07117, March 2022. URL https://arxiv.org/abs/2203.07117. 1

[9] John Goold, Marcus Huber, Arnau Riera, Lídia del Rio, and Paul Skrzypczyk. The role of quantum information in thermodynamics—a topical review. *Journal of Physics A Mathematical General*, 49(14):143001, April 2016. URL https://doi.org/10.1088/1751-8113/49/14/143001. 1

[10] M. Cliche and A. Kempf. Relativistic quantum channel of communication through field quanta. *Phys. Rev. A*, 81:012330, Jan 2010. doi: 10.1103/PhysRevA.81.012330. URL https://link.aps.org/doi/10.1103/PhysRevA.81.012330. 2

[11] André G. S. Landulfo. Nonperturbative approach to relativistic quantum communication channels. *Phys. Rev. D*, 93:104019, May 2016. doi: 10.1103/PhysRevD.93.104019. URL https://link.aps.org/doi/10.1103/PhysRevD.93.104019. 2, 22

[12] Ian Bernardes Barcellos and André G. S. Landulfo. Relativistic quantum communication: Energy cost and channel capacities. *Phys. Rev. D*, 104:105018, Nov 2021. doi: 10.1103/PhysRevD.104.105018. URL https://link.aps.org/doi/10.1103/PhysRevD.104.105018. 2, 22

[13] Erickson Tjoa and Kensuke Gallock-Yoshimura. Channel capacity of relativistic quantum communication with rapid interaction. *Phys. Rev. D*, 105:085011, Apr 2022. doi: 10.1103/PhysRevD.105.085011. URL https://link.aps.org/doi/10.1103/PhysRevD.105.085011. 2, 22

[14] T. Rick Perche and Eduardo Martín-Martínez. Role of quantum degrees of freedom of relativistic fields in quantum information protocols. *Phys. Rev. A*, 107:042612, Apr 2023. doi: 10.1103/PhysRevA.107.042612. URL https://link.aps.org/doi/10.1103/PhysRevA.107.042612. 2

[15] W. G. Unruh. Notes on black-hole evaporation. *Phys. Rev. D*, 14:870–892, Aug 1976. doi: 10.1103/PhysRevD.14.870. URL https://link.aps.org/doi/10.1103/PhysRevD.14.870. 2, 4, 16

[16] B. S. DeWitt. Quantum gravity: the new synthesis in General Relativity, edited by S. W. Hawking and W. Israel. *Cambridge University Press*, pages 680–745, 1979. 2, 16

[17] William G. Unruh and Robert M. Wald. What happens when an accelerating observer detects a Rindler particle. *Phys. Rev. D*, 29:1047–1056, Mar 1984. doi: 10.1103/PhysRevD.29.1047. URL https://link.aps.org/doi/10.1103/PhysRevD.29.1047. 2

[18] Stephen J. Summers and Reinhard Werner. The vacuum violates Bell's inequalities. *Phys. Lett.*, 110A(5):257 – 259, 1985. ISSN 0375-9601. doi: https://doi.org/10.1016/0375-9601(85)90093-3. URL http://www.sciencedirect.com/science/article/pii/0375960185900933. 2

[19] Stephen J. Summers and Reinhard Werner. Bell's inequalities and quantum field theory. I. General setting. *J. Math. Phys. (N.Y.)*, 28(10):2440–2447, 1987. doi: 10.1063/1.527733. URL https://doi.org/10.1063/1.527733. 2

[20] Antony Valentini. Non-local correlations in quantum electrodynamics. *Phys. Lett.*, 153A(6):321 – 325, 1991. ISSN 0375-9601. doi: https://doi.org/10.1016/0375-9601(91)90952-5. URL http://www.sciencedirect.com/science/article/pii/0375960191909525. 2

[21] Benni Reznik. Entanglement from the vacuum. *Found. Phys.*, 33(1):167–176, 2003. doi: https://doi.org/10.1023/A:1022875910744. URL https://doi.org/10.1023/A:1022875910744. 2

[22] Benni Reznik, Alex Retzker, and Jonathan Silman. Violating Bell's inequalities in vacuum. *Phys. Rev. A*, 71:042104, Apr 2005. doi: 10.1103/PhysRevA.71.042104. URL https://link.aps.org/doi/10.1103/PhysRevA.71.042104. 2

[23] Eduardo Martín-Martínez, Miguel Montero, and Marco del Rey. Wavepacket detection with the Unruh-DeWitt model. *Phys. Rev. D*, 87:064038, Mar 2013. doi: 10.1103/PhysRevD.87.064038. URL https://link.aps.org/doi/10.1103/PhysRevD.87.064038. 3

[24] Álvaro M. Alhambra, Achim Kempf, and Eduardo Martín-Martínez. Casimir forces on atoms in optical cavities. *Phys. Rev. A*, 89:033835, Mar 2014. doi: 10.1103/PhysRevA.89.033835. URL https://link.aps.org/doi/10.1103/PhysRevA.89.033835. 3

[25] Alejandro Pozas-Kerstjens and Eduardo Martín-Martínez. Entanglement harvesting from the electromagnetic vacuum with hydrogenlike atoms. *Phys. Rev. D*, 94:064074, Sep 2016. doi: 10.1103/PhysRevD.94.064074. URL https://link.aps.org/doi/10.1103/PhysRevD.94.064074. 3, 80

[26] Nicholas Funai, Jorma Louko, and Eduardo Martín-Martínez. $\hat{\boldsymbol{p}} \cdot \hat{\boldsymbol{A}}$ vs $\hat{\boldsymbol{x}} \cdot \hat{\boldsymbol{E}}$: Gauge invariance in quantum optics and quantum field theory. *Phys. Rev. D*, 99:065014, Mar 2019. doi: 10.1103/PhysRevD.99.065014. URL https://link.aps.org/doi/10.1103/PhysRevD.99.065014. 3

[27] Richard Lopp and Eduardo Martín-Martínez. Quantum delocalization, gauge, and quantum optics: Light-matter interaction in relativistic quantum information. *Phys. Rev. A*, 103:013703, Jan 2021. doi: 10.1103/PhysRevA.103.013703. URL https://link.aps.org/doi/10.1103/PhysRevA.103.013703. 3

[28] Alejandro Pozas-Kerstjens and Eduardo Martín-Martínez. Harvesting correlations from the quantum vacuum. *Phys. Rev. D*, 92:064042, Sep 2015. doi: 10.1103/PhysRevD.92.064042. URL https://link.aps.org/doi/10.1103/PhysRevD.92.064042. 3, 18, 27, 94

[29] Eduardo Martín-Martínez, Alexander R. H. Smith, and Daniel R. Terno. Spacetime structure and vacuum entanglement. *Phys. Rev. D*, 93:044001, Feb 2016. doi: 10.1103/PhysRevD.93.044001. URL https://link.aps.org/doi/10.1103/PhysRevD.93.044001. 3, 28, 32

[30] Erickson Tjoa and Eduardo Martín-Martínez. When entanglement harvesting is not really harvesting. *Phys. Rev. D*, 104:125005, Dec 2021. doi: 10.1103/PhysRevD.104.125005. URL https://link.aps.org/doi/10.1103/PhysRevD.104.125005. 3, 23, 24, 25, 26, 89

[31] C. Suryaatmadja, R. B. Mann, and W. Cong. Entanglement harvesting of inertially moving Unruh-DeWitt detectors in Minkowski spacetime. *Phys. Rev. D*, 106:076002, Oct 2022. doi: 10.1103/PhysRevD.106.076002. URL https://link.aps.org/doi/10.1103/PhysRevD.106.076002. 3

[32] Diana Mendez-Avalos, Laura J. Henderson, Kensuke Gallock-Yoshimura, and Robert B. Mann. Entanglement harvesting of three Unruh-DeWitt detectors. *General Relativity and Gravitation*, 54:87, 2022. doi: 10.1007/s10714-022-02956-x. URL https://doi.org/10.1007/s10714-022-02956-x. 3, 20, 36, 63, 64, 67

[33] Eric G. Brown. Thermal amplification of field-correlation harvesting. *Phys. Rev. A*, 88:062336, Dec 2013. doi: 10.1103/PhysRevA.88.062336. URL https://link.aps.org/doi/10.1103/PhysRevA.88.062336. 3

[34] Zhihong Liu, Jialin Zhang, and Hongwei Yu. Entanglement harvesting of accelerated detectors versus static ones in a thermal bath. *Phys. Rev. D*, 107:045010, Feb 2023. doi: 10.1103/PhysRevD.107.045010. URL https://link.aps.org/doi/10.1103/PhysRevD.107.045010. 3

[35] Grant Salton, Robert B Mann, and Nicolas C Menicucci. Acceleration-assisted entanglement harvesting and rangefinding. *New J. Phys.*, 17(3):035001, mar 2015. doi: 10.1088/1367-2630/17/3/035001. URL https://iopscience.iop.org/article/10.1088/1367-2630/17/3/035001. 3

[36] Jialin Zhang and Hongwei Yu. Entanglement harvesting for Unruh-DeWitt detectors in circular motion. *Phys. Rev. D*, 102:065013, Sep 2020. doi: 10.1103/PhysRevD.102.065013. URL https://link.aps.org/doi/10.1103/PhysRevD.102.065013. 3

[37] Zhihong Liu and Jialin Zhang. Entanglement harvesting in the presence of a reflecting boundary. *J. High Energy Phys.*, 08(2021):020, 2021. ISSN 1029-8479. doi: 10.1007/JHEP08(2021)020. URL https://doi.org/10.1007/JHEP08(2021)020. 3

[38] Zhihong Liu, Jialin Zhang, Robert B. Mann, and Hongwei Yu. Does acceleration assist entanglement harvesting? *Phys. Rev. D*, 105(8):085012, 2022. doi: 10.1103/PhysRevD.105.085012. URL https://journals.aps.org/prd/abstract/10.1103/PhysRevD.105.085012. 3, 4, 5, 41, 46, 47, 98

[39] Wan Cong, Erickson Tjoa, and Robert B Mann. Entanglement harvesting with moving mirrors. *J. High Energy Phys.*, 06(2019):021, 2019. URL https://doi.org/10.1007/JHEP06(2019)021. 3, 80

[40] Wan Cong, Chen Qian, Michael R.R. Good, and Robert B. Mann. Effects of horizons on entanglement harvesting. *J. High Energy Phys.*, 10(2020):67, Oct 2020. ISSN 1029-8479. doi: 10.1007/JHEP10(2020)067. URL https://doi.org/10.1007/JHEP10(2020)067. 3

[41] Laura J Henderson, Robie A Hennigar, Robert B Mann, Alexander R H Smith, and Jialin Zhang. Harvesting entanglement from the black hole vacuum. *Classical Quantum Gravity*, 35(21):21LT02, oct 2018. URL https://doi.org/10.1088/1361-6382/aae27e. 3, 4, 56, 57, 61, 67, 68, 95, 98, 131

[42] Matthew P. G. Robbins, Laura J. Henderson, and Robert B. Mann. Entanglement amplification from rotating black holes. *Classical Quantum Gravity*, 39(2):02LT01, 2022. URL https://doi.org/10.1088/1361-6382/ac08a8. 3

[43] Erickson Tjoa and Robert B Mann. Harvesting correlations in Schwarzschild and collapsing shell spacetimes. *J. High Energy Phys.*, 08(2020):155, 2020. URL https://doi.org/10.1007/JHEP08(2020)155. 3, 56, 76, 78, 80, 81, 82, 83, 86, 88, 89, 90, 95, 99, 100

[44] Kensuke Gallock-Yoshimura, Erickson Tjoa, and Robert B. Mann. Harvesting entanglement with detectors freely falling into a black hole. *Phys. Rev. D*, 104:025001, Jul 2021. doi: 10.1103/PhysRevD.104.025001. URL https://link.aps.org/doi/10.1103/PhysRevD.104.025001. 3, 56, 94

[45] Kendra Bueley, Luosi Huang, Kensuke Gallock-Yoshimura, and Robert B. Mann. Harvesting mutual information from BTZ black hole spacetime. *Phys. Rev. D*, 106:025010, Jul 2022. doi: 10.1103/PhysRevD.106.025010. URL https://link.aps.org/doi/10.1103/PhysRevD.106.025010. 3, 67

[46] Laura J. Henderson, Su Yu Ding, and Robert B. Mann. Entanglement harvesting with a twist. *AVS Quantum Sci.*, 4(1):014402, 2022. doi: 10.1116/5.0078314. URL https://doi.org/10.1116/5.0078314. 3

[47] João G. A. Caribé, Robert H. Jonsson, Marc Casals, Achim Kempf, and Eduardo Martín-Martínez. Lensing of Vacuum Entanglement near Schwarzschild Black Holes, 2023. URL https://doi.org/10.48550/arXiv.2303.01402. 3, 51

[48] Ireneo James Membrere, Kensuke Gallock-Yoshimura, Laura J. Henderson, and Robert B. Mann. Tripartite Entanglement Extraction from the Black Hole Vacuum. *arXiv preprint arXiv:2304.07847*, 2023. URL https://arxiv.org/abs/2304.07847. 3

[49] Greg Ver Steeg and Nicolas C. Menicucci. Entangling power of an expanding universe. *Phys. Rev. D*, 79:044027, Feb 2009. doi: 10.1103/PhysRevD.79.044027. URL https://link.aps.org/doi/10.1103/PhysRevD.79.044027. 3, 48, 94

[50] S. Kukita and Y. Nambu. Harvesting large scale entanglement in de Sitter space with multiple detectors. *Entropy*, 19(9):449, Aug 2017. ISSN 1099-4300. doi: 10.3390/e19090449. URL http://dx.doi.org/10.3390/e19090449. 3

[51] Keith K. Ng, Robert B. Mann, and Eduardo Martín-Martínez. Unruh-DeWitt detectors and entanglement: The anti–de Sitter space. *Phys. Rev. D*, 98:125005, Dec 2018. doi: 10.1103/PhysRevD.98.125005. URL https://link.aps.org/doi/10.1103/PhysRevD.98.125005. 3

[52] Laura J Henderson, Robie A Hennigar, Robert B Mann, Alexander RH Smith, and Jialin Zhang. Entangling detectors in anti-de Sitter space. *J. High Energy Phys.*, 05 (2019):178, 2019. URL https://doi.org/10.1007/JHEP05(2019)178. 3

[53] Qidong Xu, Shadi Ali Ahmad, and Alexander R. H. Smith. Gravitational waves affect vacuum entanglement. *Phys. Rev. D*, 102:065019, Sep 2020. doi: 10.1103/PhysRevD.102.065019. URL https://link.aps.org/doi/10.1103/PhysRevD.102.065019. 3

[54] Finnian Gray, David Kubizňák, Taillte May, Sydney Timmerman, and Erickson Tjoa. Quantum imprints of gravitational shockwaves. *J. High Energy Phys.*, 11(2021):054, 2021. URL https://doi.org/10.1007/JHEP11(2021)054. 3

[55] Dyuman Bhattacharya, Kensuke Gallock-Yoshimura, Laura J. Henderson, and Robert B. Mann. Extraction of entanglement from quantum fields with entangled particle detectors. *Phys. Rev. D*, 107:105008, May 2023. doi: 10.1103/PhysRevD.107.105008. URL https://link.aps.org/doi/10.1103/PhysRevD.107.105008. 3

[56] M. Cliche and A. Kempf. Vacuum entanglement enhancement by a weak gravitational field. *Phys. Rev. D*, 83:045019, Feb 2011. doi: 10.1103/PhysRevD.83.045019. URL https://link.aps.org/doi/10.1103/PhysRevD.83.045019. 4

[57] Eric G. Brown, Eduardo Martín-Martínez, Nicolas C. Menicucci, and Robert B. Mann. Detectors for probing relativistic quantum physics beyond perturbation theory. *Phys. Rev. D*, 87:084062, Apr 2013. doi: 10.1103/PhysRevD.87.084062. URL https://link.aps.org/doi/10.1103/PhysRevD.87.084062. 4, 5

[58] Robert M. Wald. *Quantum Field Theory in Curved Spacetime and Black Hole Thermodynamics*. The University of Chicago Press, Chicago, 1994. ISBN 0226870278. URL https://press.uchicago.edu/ucp/books/book/chicago/Q/bo3684008.html. 7

[59] Ryogo Kubo. Statistical-Mechanical Theory of Irreversible Processes. I. General Theory and Simple Applications to Magnetic and Conduction Problems. *Journal of the Physical Society of Japan*, 12(6):570–586, 1957. doi: 10.1143/JPSJ.12.570. URL https://doi.org/10.1143/JPSJ.12.570. 14

[60] Paul C. Martin and Julian Schwinger. Theory of Many-Particle Systems. I. *Phys. Rev.*, 115:1342–1373, Sep 1959. doi: 10.1103/PhysRev.115.1342. URL https://link.aps.org/doi/10.1103/PhysRev.115.1342. 14

[61] Rudolf Haag, Nicolaas Marinus Hugenholtz, and Marinus Winnink. On the equilibrium states in quantum statistical mechanics. *Communications in Mathematical Physics*, 5(3):215–236, 1967. URL https://doi.org/10.1007/BF01646342. 14

[62] Ola Bratteli and Derek William Robinson. *Operator algebras and quantum statistical mechanics 1: C^*-and W^*-Algebras, Symmetry Groups, Decomposition of States.* Springer Berlin, Heidelberg, 2002. URL https://link.springer.com/book/10.1007/978-3-662-02520-8. 15

[63] Ola Bratteli and Derek William Robinson. *Operator algebras and quantum statistical mechanics 2: Equilibrium States. Models in Quantum Statistical Mechanics.* Springer Berlin, Heidelberg, 2002. URL https://link.springer.com/book/10.1007/978-3-662-09089-3. 15

[64] Luis J. Garay, Eduardo Martín-Martínez, and José de Ramón. Thermalization of particle detectors: The Unruh effect and its reverse. *Phys. Rev. D*, 94:104048, Nov 2016. doi: 10.1103/PhysRevD.94.104048. URL https://link.aps.org/doi/10.1103/PhysRevD.94.104048. 15, 59

[65] Shih-Yuin Lin and B. L. Hu. Accelerated detector-quantum field correlations: From vacuum fluctuations to radiation flux. *Phys. Rev. D*, 73:124018, Jun 2006. doi: 10.1103/PhysRevD.73.124018. URL https://link.aps.org/doi/10.1103/PhysRevD.73.124018. 16

[66] Eduardo Martín-Martínez and Pablo Rodriguez-Lopez. Relativistic quantum optics: The relativistic invariance of the light-matter interaction models. *Phys. Rev. D*, 97:105026, May 2018. doi: 10.1103/PhysRevD.97.105026. URL https://link.aps.org/doi/10.1103/PhysRevD.97.105026. 16, 17, 18

[67] Eduardo Martín-Martínez, T. Rick Perche, and Bruno de S. L. Torres. General relativistic quantum optics: Finite-size particle detector models in curved spacetimes. *Phys. Rev. D*, 101:045017, Feb 2020. doi: 10.1103/PhysRevD.101.045017. URL https://link.aps.org/doi/10.1103/PhysRevD.101.045017. 16, 17, 18

[68] Eduardo Martín-Martínez, T. Rick Perche, and Bruno de S. L. Torres. Broken covariance of particle detector models in relativistic quantum information. *Phys.*

Rev. D, 103:025007, Jan 2021. doi: 10.1103/PhysRevD.103.025007. URL https://link.aps.org/doi/10.1103/PhysRevD.103.025007. 17, 81

[69] Petar Simidzija and Eduardo Martín-Martínez. Nonperturbative analysis of entanglement harvesting from coherent field states. *Phys. Rev. D*, 96:065008, Sep 2017. doi: 10.1103/PhysRevD.96.065008. URL https://link.aps.org/doi/10.1103/PhysRevD.96.065008. 22

[70] Alejandro Pozas-Kerstjens, Jorma Louko, and Eduardo Martín-Martínez. Degenerate detectors are unable to harvest spacelike entanglement. *Phys. Rev. D*, 95:105009, May 2017. doi: 10.1103/PhysRevD.95.105009. URL https://link.aps.org/doi/10.1103/PhysRevD.95.105009. 22

[71] Petar Simidzija, Robert H. Jonsson, and Eduardo Martín-Martínez. General no-go theorem for entanglement extraction. *Phys. Rev. D*, 97:125002, Jun 2018. doi: 10.1103/PhysRevD.97.125002. URL https://link.aps.org/doi/10.1103/PhysRevD.97.125002. 22

[72] Kensuke Gallock-Yoshimura and Robert B. Mann. Entangled detectors nonperturbatively harvest mutual information. *Phys. Rev. D*, 104:125017, Dec 2021. doi: 10.1103/PhysRevD.104.125017. URL https://link.aps.org/doi/10.1103/PhysRevD.104.125017. 22

[73] Nicholas Funai and Eduardo Martín-Martínez. Engineering negative stress-energy densities with quantum energy teleportation. *Phys. Rev. D*, 96:025014, Jul 2017. doi: 10.1103/PhysRevD.96.025014. URL https://link.aps.org/doi/10.1103/PhysRevD.96.025014. 22

[74] Laura J. Henderson and Nicolas C. Menicucci. Bandlimited entanglement harvesting. *Phys. Rev. D*, 102:125026, Dec 2020. doi: 10.1103/PhysRevD.102.125026. URL https://link.aps.org/doi/10.1103/PhysRevD.102.125026. 22

[75] Abhisek Sahu, Irene Melgarejo-Lermas, and Eduardo Martín-Martínez. Sabotaging the harvesting of correlations from quantum fields. *Phys. Rev. D*, 105:065011, Mar 2022. doi: 10.1103/PhysRevD.105.065011. URL https://link.aps.org/doi/10.1103/PhysRevD.105.065011. 22

[76] T. Rick Perche and Ahmed Shalabi. Spacetime curvature from ultrarapid measurements of quantum fields. *Phys. Rev. D*, 105:125011, Jun 2022. doi: 10.1103/PhysRevD.105.125011. URL https://link.aps.org/doi/10.1103/PhysRevD.105.125011. 22

[77] Diana Méndez Avalos, Kensuke Gallock-Yoshimura, Laura J Henderson, and Robert B Mann. Instant extraction of non-perturbative tripartite entanglement. *arXiv preprint arXiv:2204.02983*, 2022. URL https://arxiv.org/abs/2204.02983. 22, 63

[78] Ahmed Shalabi, Laura J. Henderson, and Robert B. Mann. Locally detecting UV cutoffs on a sphere with particle detectors. *Phys. Rev. D*, 107:045006, Feb 2023. doi: 10.1103/PhysRevD.107.045006. URL https://link.aps.org/doi/10.1103/PhysRevD.107.045006. 22

[79] Gabriel Cozzella, Stephen A. Fulling, André G. S. Landulfo, and George E. A. Matsas. Uniformly accelerated classical sources as limits of Unruh-DeWitt detectors. *Phys. Rev. D*, 102:105016, Nov 2020. doi: 10.1103/PhysRevD.102.105016. URL https://link.aps.org/doi/10.1103/PhysRevD.102.105016. 22

[80] Herbert Goldstein, Charles Poole, and John Safko. *Classical Mechanics*. Addison-Wesley, 2001. 23

[81] Eduardo Martín-Martínez. Causality issues of particle detector models in QFT and quantum optics. *Phys. Rev. D*, 92:104019, Nov 2015. doi: 10.1103/PhysRevD.92.104019. URL https://link.aps.org/doi/10.1103/PhysRevD.92.104019. 24, 89, 90

[82] Ryszard Horodecki, Paweł Horodecki, Michał Horodecki, and Karol Horodecki. Quantum entanglement. *Rev. Mod. Phys.*, 81:865–942, Jun 2009. doi: 10.1103/RevModPhys.81.865. URL https://link.aps.org/doi/10.1103/RevModPhys.81.865. 27, 31

[83] M.A. Nielsen and I.L. Chuang. *Quantum Computation and Quantum Information*. Cambridge Series on Information and the Natural Sciences. Cambridge University Press, Cambridge, England, 2000. ISBN 9780521635035. URL https://books.google.ca/books?id=65FqEKQOfP8C. 27, 29, 30

[84] Michael M. Wolf, Frank Verstraete, Matthew B. Hastings, and J. Ignacio Cirac. Area Laws in Quantum Systems: Mutual Information and Correlations. *Phys. Rev. Lett.*, 100:070502, Feb 2008. doi: 10.1103/PhysRevLett.100.070502. URL https://link.aps.org/doi/10.1103/PhysRevLett.100.070502. 27

[85] Sam A. Hill and William K. Wootters. Entanglement of a Pair of Quantum Bits. *Phys. Rev. Lett.*, 78:5022–5025, Jun 1997. doi: 10.1103/PhysRevLett.78.5022. URL https://link.aps.org/doi/10.1103/PhysRevLett.78.5022. 28

[86] William K. Wootters. Entanglement of formation of an arbitrary state of two qubits. *Phys. Rev. Lett.*, 80:2245–2248, Mar 1998. doi: 10.1103/PhysRevLett.80.2245. URL https://link.aps.org/doi/10.1103/PhysRevLett.80.2245. 28, 30

[87] Charles H. Bennett, David P. DiVincenzo, John A. Smolin, and William K. Wootters. Mixed-state entanglement and quantum error correction. *Phys. Rev. A*, 54:3824–3851, Nov 1996. doi: 10.1103/PhysRevA.54.3824. URL https://link.aps.org/doi/10.1103/PhysRevA.54.3824. 28

[88] G. Vidal and R. F. Werner. Computable measure of entanglement. *Phys. Rev. A*, 65:032314, Feb 2002. doi: 10.1103/PhysRevA.65.032314. URL https://link.aps.org/doi/10.1103/PhysRevA.65.032314. 31

[89] Asher Peres. Separability criterion for density matrices. *Phys. Rev. Lett.*, 77:1413–1415, Aug 1996. doi: 10.1103/PhysRevLett.77.1413. URL https://link.aps.org/doi/10.1103/PhysRevLett.77.1413. 31

[90] Michał Horodecki, Paweł Horodecki, and Ryszard Horodecki. Separability of mixed states: necessary and sufficient conditions. *Phys. Lett. A*, 223(1):1–8, 1996. ISSN 0375-9601. URL http://www.sciencedirect.com/science/article/pii/S0375960196007062. 31

[91] Frank Verstraete, Koenraad Audenaert, Jeroen Dehaene, and Bart De Moor. A comparison of the entanglement measures negativity and concurrence. *Journal of Physics A: Mathematical and General*, 34(47):10327, 2001. URL https://iopscience.iop.org/article/10.1088/0305-4470/34/47/329. 32

[92] Yong-Cheng Ou and Heng Fan. Monogamy inequality in terms of negativity for three-qubit states. *Phys. Rev. A*, 75:062308, Jun 2007. doi: 10.1103/PhysRevA.75.062308. URL https://link.aps.org/doi/10.1103/PhysRevA.75.062308. 32, 33

[93] Valerie Coffman, Joydip Kundu, and William K. Wootters. Distributed entanglement. *Phys. Rev. A*, 61:052306, Apr 2000. doi: 10.1103/PhysRevA.61.052306. URL https://link.aps.org/doi/10.1103/PhysRevA.61.052306. 33

[94] Daniel M Greenberger, Michael A Horne, and Anton Zeilinger. Going beyond Bell's theorem. *Bell's theorem, quantum theory and conceptions of the universe*, pages 69–72, 1989. URL https://doi.org/10.1007/978-94-017-0849-4_10. 37, 64

[95] Eric G. Brown, Eduardo Martín-Martínez, Nicolas C. Menicucci, and Robert B. Mann. Detectors for probing relativistic quantum physics beyond perturbation theory. *Phys. Rev. D*, 87:084062, Apr 2013. doi: 10.1103/PhysRevD.87.084062. URL https://link.aps.org/doi/10.1103/PhysRevD.87.084062. 47

[96] Yasusada Nambu and Yuji Ohsumi. Classical and quantum correlations of scalar field in the inflationary universe. *Phys. Rev. D*, 84:044028, Aug 2011. doi: 10.1103/PhysRevD.84.044028. URL https://link.aps.org/doi/10.1103/PhysRevD.84.044028. 48

[97] G. W. Gibbons and S. W. Hawking. Cosmological event horizons, thermodynamics, and particle creation. *Phys. Rev. D*, 15:2738–2751, May 1977. doi: 10.1103/PhysRevD.15.2738. URL https://link.aps.org/doi/10.1103/PhysRevD.15.2738. 48

[98] Keith K Ng, Chen Zhang, Jorma Louko, and Robert B Mann. A little excitement across the horizon. *New Journal of Physics*, 24(10):103018, oct 2022. doi: 10.1088/1367-2630/ac9547. URL https://dx.doi.org/10.1088/1367-2630/ac9547. 51

[99] Robert H. Jonsson, David Q. Aruquipa, Marc Casals, Achim Kempf, and Eduardo Martín-Martínez. Communication through quantum fields near a black hole. *Phys. Rev. D*, 101:125005, Jun 2020. doi: 10.1103/PhysRevD.101.125005. URL https://link.aps.org/doi/10.1103/PhysRevD.101.125005. 51

[100] Máximo Bañados, Claudio Teitelboim, and Jorge Zanelli. Black hole in three-dimensional spacetime. *Phys. Rev. Lett.*, 69:1849–1851, Sep 1992. doi: 10.1103/PhysRevLett.69.1849. URL https://link.aps.org/doi/10.1103/PhysRevLett.69.1849. 52, 53

[101] Máximo Bañados, Marc Henneaux, Claudio Teitelboim, and Jorge Zanelli. Geometry of the 2+1 black hole. *Phys. Rev. D*, 48:1506–1525, Aug 1993. doi: 10.1103/PhysRevD.48.1506. URL https://link.aps.org/doi/10.1103/PhysRevD.48.1506. 52

[102] Gilad Lifschytz and Miguel Ortiz. Scalar field quantization on the (2+1)-dimensional black hole background. *Phys. Rev. D*, 49:1929–1943, Feb 1994. doi: 10.1103/PhysRevD.49.1929. URL https://link.aps.org/doi/10.1103/PhysRevD.49.1929. 54, 127, 128

[103] Richard C. Tolman. On the Weight of Heat and Thermal Equilibrium in General Relativity. *Phys. Rev.*, 35:904–924, Apr 1930. doi: 10.1103/PhysRev.35.904. URL https://link.aps.org/doi/10.1103/PhysRev.35.904. 54

[104] Steven Carlip. The (2+1)-dimensional black hole. *Class. Quant. Grav.*, 12(12):2853, 1995. doi: 10.1088/0264-9381/12/12/005. URL https://iopscience.iop.org/article/10.1088/0264-9381/12/12/005. 54, 128

[105] Laura J. Henderson, Robie A. Hennigar, Robert B. Mann, Alexander R.H. Smith, and Jialin Zhang. Anti-Hawking phenomena. *Physics Letters B*, 809:135732, 2020. ISSN 0370-2693. doi: https://doi.org/10.1016/j.physletb.2020.135732. URL https://www.sciencedirect.com/science/article/pii/S0370269320305359. 59

[106] Lissa de Souza Campos and Claudio Dappiaggi. Ground and thermal states for the Klein-Gordon field on a massless hyperbolic black hole with applications to the anti-Hawking effect. *Phys. Rev. D*, 103:025021, Jan 2021. doi: 10.1103/PhysRevD.103.025021. URL https://link.aps.org/doi/10.1103/PhysRevD.103.025021. 59

[107] Lissa de Souza Campos and Claudio Dappiaggi. The anti-Hawking effect on a BTZ black hole with Robin boundary conditions. *Physics Letters B*, 816:136198, 2021. ISSN 0370-2693. doi: https://doi.org/10.1016/j.physletb.2021.136198. URL https://www.sciencedirect.com/science/article/pii/S0370269321001386. 59

[108] Matthew P. G. Robbins and Robert B. Mann. Anti-Hawking phenomena around a rotating BTZ black hole. *Phys. Rev. D*, 106:045018, Aug 2022. doi: 10.1103/PhysRevD.106.045018. URL https://link.aps.org/doi/10.1103/PhysRevD.106.045018. 59

[109] Aindriú Conroy and Peter Taylor. Response of an Unruh-DeWitt detector near an extremal black hole. *Phys. Rev. D*, 105:085001, Apr 2022. doi: 10.1103/PhysRevD.105.085001. URL https://link.aps.org/doi/10.1103/PhysRevD.105.085001. 59

[110] W.G. Brenna, Robert B. Mann, and Eduardo Martín-Martínez. Anti-Unruh phenomena. *Physics Letters B*, 757:307 – 311, 2016. ISSN 0370-2693. doi: https://doi.org/10.1016/j.physletb.2016.04.002. URL http://www.sciencedirect.com/science/article/pii/S0370269316300727. 59

[111] Jonathan Silman and Benni Reznik. Many-region vacuum entanglement: Distilling a W state. *Phys. Rev. A*, 71:054301, May 2005. doi: 10.1103/PhysRevA.71.054301. URL https://link.aps.org/doi/10.1103/PhysRevA.71.054301. 63

[112] W. Dür, G. Vidal, and J. I. Cirac. Three qubits can be entangled in two inequivalent ways. *Phys. Rev. A*, 62:062314, Nov 2000. doi: 10.1103/PhysRevA.62.062314. URL https://link.aps.org/doi/10.1103/PhysRevA.62.062314. 63

[113] Krzysztof Lorek, Daniel Pecak, Eric G. Brown, and Andrzej Dragan. Extraction of genuine tripartite entanglement from the vacuum. *Phys. Rev. A*, 90:032316, Sep 2014. doi: 10.1103/PhysRevA.90.032316. URL https://link.aps.org/doi/10.1103/PhysRevA.90.032316. 63

[114] A. Acín, D. Bruß, M. Lewenstein, and A. Sanpera. Classification of Mixed Three-Qubit States. *Phys. Rev. Lett.*, 87:040401, Jul 2001. doi: 10.1103/PhysRevLett.87.040401. URL https://link.aps.org/doi/10.1103/PhysRevLett.87.040401. 63

[115] Benito A. Juárez-Aubry and Jorma Louko. Quantum fields during black hole formation: How good an approximation is the Unruh state? *J. High Energy Phys.*, 05(2018):140, May 2018. ISSN 1029-8479. doi: 10.1007/JHEP05(2018)140. URL https://doi.org/10.1007/JHEP05(2018)140. 76, 78, 80

[116] Karl Martel and Eric Poisson. Regular coordinate systems for Schwarzschild and other spherical spacetimes. *Am. J. Phys.*, 69(4):476–480, 2001. doi: 10.1119/1.1336836. URL https://doi.org/10.1119/1.1336836. 77, 97

[117] Marvin Weinstein. Moving mirrors, black holes, hawking radiation and all that .... *Nucl. Phys. B, Proc. Suppl.*, 108:68–73, 2002. ISSN 0920-5632. doi: https://doi.org/10.1016/S0920-5632(02)01306-3. URL https://www.sciencedirect.com/science/article/pii/S0920563202013063. lignt-cone physics: Particles and strings Proceedings of the International Workshop TRENTO 2001. 79

[118] Kirill Melnikov and Marvin Weinstein. On the evolution of a massless scalar field in a Schwarzschild background: A new look at Hawking radiation and the information paradox. *Int. J. Mod. Phys. D*, 13(08):1595–1635, 2004. doi: 10.1142/S0218271804005249. URL https://doi.org/10.1142/S0218271804005249. 79

[119] Kanato Goto and Yoichi Kazama. On the observer dependence of the Hilbert space near the horizon of black holes. *Prog. Theor. Exp. Phys.*, 2019(2), 02 2019. ISSN 2050-3911. URL https://doi.org/10.1093/ptep/pty146. 023B01. 79

[120] Benito A Juárez-Aubry and Jorma Louko. Onset and decay of the 1+1 Hawking-Unruh effect: What the derivative-coupling detector saw. *Classical and Quantum Gravity*, 31(24):245007, nov 2014. doi: 10.1088/0264-9381/31/24/245007. URL https://doi.org/10.1088%2F0264-9381%2F31%2F24%2F245007. 80, 136

[121] Marek J. Radzikowski. Micro-local approach to the Hadamard condition in quantum field theory on curved space-time. *Commun. Math. Phys.*, 179(3):529–553, Sep 1996. ISSN 1432-0916. doi: 10.1007/BF02100096. URL https://doi.org/10.1007/BF02100096. 80

[122] Igor Khavkine and Valter Moretti. *Algebraic QFT in Curved Spacetime and Quasifree Hadamard States: An Introduction*, pages 191–251. Springer International Publishing, Cham, 2015. ISBN 978-3-319-21353-8. URL https://doi.org/10.1007/978-3-319-21353-8_5. 80

[123] Erickson Tjoa. Numerical contour integration. *The Mathematica Journal, 2021*. URL https://doi.org/10.3888/tmj.23-3. 83

[124] Wolfram Research, Inc. Mathematica, Version 10.0. URL https://www.wolfram.com/mathematica. Champaign, IL, 2020. 83

[125] Aida Ahmadzadegan, Eduardo Martín-Martínez, and Robert B. Mann. Cavities in curved spacetimes: The response of particle detectors. *Phys. Rev. D*, 89:024013, Jan 2014. doi: 10.1103/PhysRevD.89.024013. URL https://link.aps.org/doi/10.1103/PhysRevD.89.024013. 85

[126] Vicente J Bolós. Intrinsic definitions of "relative velocity" in general relativity. *Commun. Math. Phys.*, 273(1):217–236, 2007. URL https://doi.org/10.1007/s00220-007-0248-9. 87, 137

[127] S. Chandrasekhar. *The Mathematical Theory of Black Holes*. International Series of Monographs on Physics. Clarendon Press, Oxford, 1998. ISBN 9780198503705. URL https://books.google.ca/books?id=LBOVcrzFfhsC. 87

[128] Lana Bozanic, Manar Naeem, Kensuke Gallock-Yoshimura, and Robert B. Mann. To be published. 94

[129] Lee Hodgkinson, Jorma Louko, and Adrian C. Ottewill. Static detectors and circular-geodesic detectors on the Schwarzschild black hole. *Phys. Rev. D*, 89:104002, May 2014. doi: 10.1103/PhysRevD.89.104002. URL https://link.aps.org/doi/10.1103/PhysRevD.89.104002. 100

[130] A. Retzker, J. I. Cirac, M. B. Plenio, and B. Reznik. Methods for Detecting Acceleration Radiation in a Bose-Einstein Condensate. *Phys. Rev. Lett.*, 101:110402, Sep 2008. doi: 10.1103/PhysRevLett.101.110402. URL https://link.aps.org/doi/10.1103/PhysRevLett.101.110402. 100

[131] Cisco Gooding, Steffen Biermann, Sebastian Erne, Jorma Louko, William G. Unruh, Jörg Schmiedmayer, and Silke Weinfurtner. Interferometric Unruh Detectors for Bose-Einstein Condensates. *Phys. Rev. Lett.*, 125:213603, Nov 2020. doi: 10.1103/PhysRevLett.125.213603. URL https://link.aps.org/doi/10.1103/PhysRevLett.125.213603. 100

[132] Steffen Biermann, Sebastian Erne, Cisco Gooding, Jorma Louko, Jörg Schmiedmayer, William G. Unruh, and Silke Weinfurtner. Unruh and analogue Unruh temperatures for circular motion in $3+1$ and $2+1$ dimensions. *Phys. Rev. D*, 102:085006, Oct 2020. doi: 10.1103/PhysRevD.102.085006. URL https://link.aps.org/doi/10.1103/PhysRevD.102.085006. 100

[133] S.M. Carroll. *Spacetime and Geometry: An Introduction to General Relativity*. Cambridge University Press, Cambridge, England, 2019. ISBN 9781108775557. URL https://books.google.ca/books?id=1XSmDwAAQBAJ. 122, 135

[134] S. J. Avis, C. J. Isham, and D. Storey. Quantum field theory in anti-de Sitter spacetime. *Phys. Rev. D*, 18:3565–3576, Nov 1978. doi: 10.1103/PhysRevD.18.3565. URL https://link.aps.org/doi/10.1103/PhysRevD.18.3565. 127

[135] Kiyoshi Shiraishi and Takuya Maki. Quantum fluctuation of stress tensor and black holes in three dimensions. *Phys. Rev. D*, 49:5286–5294, May 1994. doi: 10.1103/PhysRevD.49.5286. URL https://link.aps.org/doi/10.1103/PhysRevD.49.5286. 128

[136] James Ward Brown and Ruel V Churchill. *Complex variables and applications*. McGraw-Hill Education, 2009. URL https://books.google.ca/books?id=ytJFAQAAIAAJ. 130

[137] *Introduction to Smooth Manifolds*. Springer New York, 2012. URL https://doi.org/10.1007/978-1-4419-9982-5. 138

APPENDICES

Appendix A

Elements in the density matrix

Here, we derive the density matrix (2.43). Let us begin with $\rho_{\rm tot}$ given by (2.42). The final density matrix for two detectors, $\rho_{\rm AB}$ is obtained by tracing out the field part:

$$\begin{aligned}\rho_{\rm AB} &= {\rm Tr}_\phi[\rho_{\rm tot}] \\ &= {\rm Tr}_\phi[\rho_0] + {\rm Tr}_\phi[\rho^{(1,1)}] + {\rm Tr}_\phi[\rho^{(2,0)}] + {\rm Tr}_\phi[\rho^{(0,2)}] + \mathcal{O}(\lambda^4) \qquad \text{(A.1)} \\ &= \rho_{\rm AB,0} + {\rm Tr}_\phi[\rho^{(1,1)}] + {\rm Tr}_\phi[\rho^{(2,0)}] + {\rm Tr}_\phi[\rho^{(0,2)}] + \mathcal{O}(\lambda^4)\,, \qquad \text{(A.2)}\end{aligned}$$

where $\rho_{\rm AB,0} = |g_{\rm A}\rangle\langle g_{\rm A}| \otimes |g_{\rm B}\rangle\langle g_{\rm B}|$.

$\underline{{\rm Tr}_\phi[\rho^{(1,1)}] \text{ term:}}$

$$\begin{aligned}{\rm Tr}_\phi[\rho^{(1,1)}] &= {\rm Tr}_\phi[\hat{U}^{(1)}\rho_0\hat{U}^{(1)\dagger}] \\ &= {\rm Tr}_\phi\left[\int_{\mathbb{R}} {\rm d}t_2 \left(\frac{{\rm d}\tau_{\rm A}}{{\rm d}t_2}\hat{H}_{\rm A}(\tau_{\rm A}(t_2)) + \frac{{\rm d}\tau_{\rm B}}{{\rm d}t_2}\hat{H}_{\rm B}(\tau_{\rm B}(t_2))\right)\rho_0 \right. \\ &\qquad \left. \times \int_{\mathbb{R}} {\rm d}t_1 \left(\frac{{\rm d}\tau_{\rm A}}{{\rm d}t_1}\hat{H}_{\rm A}(\tau_{\rm A}(t_1)) + \frac{{\rm d}\tau_{\rm B}}{{\rm d}t_1}\hat{H}_{\rm B}(\tau_{\rm B}(t_1))\right)\right] \\ &= \int {\rm d}t_1 {\rm d}t_2\, {\rm Tr}_\phi\left[\frac{{\rm d}\tau_{\rm A}}{{\rm d}t_1}\frac{{\rm d}\tau_{\rm A}}{{\rm d}t_2}\hat{H}_{\rm A}(\tau_{\rm A}(t_2))\rho_0\hat{H}_{\rm A}(\tau_{\rm A}(t_1))\right. \\ &\qquad + \frac{{\rm d}\tau_{\rm A}}{{\rm d}t_2}\frac{{\rm d}\tau_{\rm B}}{{\rm d}t_1}\hat{H}_{\rm A}(\tau_{\rm A}(t_2))\rho_0\hat{H}_{\rm B}(\tau_{\rm B}(t_1)) \\ &\qquad + \frac{{\rm d}\tau_{\rm A}}{{\rm d}t_1}\frac{{\rm d}\tau_{\rm B}}{{\rm d}t_2}\hat{H}_{\rm B}(\tau_{\rm B}(t_2))\rho_0\hat{H}_{\rm A}(\tau_{\rm A}(t_1)) \\ &\qquad \left. + \frac{{\rm d}\tau_{\rm B}}{{\rm d}t_1}\frac{{\rm d}\tau_{\rm B}}{{\rm d}t_2}\hat{H}_{\rm B}(\tau_{\rm B}(t_2))\rho_0\hat{H}_{\rm B}(\tau_{\rm B}(t_1))\right]. \qquad \text{(A.3)}\end{aligned}$$

Let us evaluate each term. For simplicity, we write $\tau_{j1} \equiv \tau_j(t_1)$ and $\tau_{j2} \equiv \tau_j(t_2)$.

$$
\begin{aligned}
&\bullet\ \mathrm{Tr}_\phi \left[\frac{\mathrm{d}\tau_\mathrm{A}}{\mathrm{d}t_1} \frac{\mathrm{d}\tau_\mathrm{A}}{\mathrm{d}t_2} \hat{H}_\mathrm{A}(\tau_{\mathrm{A}2}) \rho_0 \hat{H}_\mathrm{A}(\tau_{\mathrm{A}1}) \right] \\
&= \frac{\mathrm{d}\tau_\mathrm{A}}{\mathrm{d}t_1} \frac{\mathrm{d}\tau_\mathrm{A}}{\mathrm{d}t_2} \lambda_\mathrm{A}^2 \chi_\mathrm{A}(\tau_{\mathrm{A}1}) \chi_\mathrm{A}(\tau_{\mathrm{A}2}) \,\mathrm{Tr}_\phi \left[\hat{\phi}(\mathsf{x}_{\mathrm{A}2}) \left|0\right\rangle \left\langle 0\right| \hat{\phi}(\mathsf{x}_{\mathrm{A}1}) \right] \hat{m}_\mathrm{A}(\tau_{\mathrm{A}2}) \rho_{\mathrm{AB},0} \hat{m}_\mathrm{A}(\tau_{\mathrm{A}1}) \\
&= \frac{\mathrm{d}\tau_\mathrm{A}}{\mathrm{d}t_1} \frac{\mathrm{d}\tau_\mathrm{A}}{\mathrm{d}t_2} \lambda_\mathrm{A}^2 \chi_\mathrm{A}(\tau_{\mathrm{A}1}) \chi_\mathrm{A}(\tau_{\mathrm{A}2}) e^{-\mathrm{i}\Omega_\mathrm{A}(\tau_{\mathrm{A}1} - \tau_{\mathrm{A}2})} W(\mathsf{x}_{\mathrm{A}1}, \mathsf{x}_{\mathrm{A}2}) \begin{bmatrix} 0 & 0 & 0 & 0 \\ 0 & 0 & 0 & 0 \\ 0 & 0 & 1 & 0 \\ 0 & 0 & 0 & 0 \end{bmatrix},
\end{aligned} \tag{A.4}
$$

$$
\begin{aligned}
&\bullet\ \mathrm{Tr}_\phi \left[\frac{\mathrm{d}\tau_\mathrm{A}}{\mathrm{d}t_2} \frac{\mathrm{d}\tau_\mathrm{B}}{\mathrm{d}t_1} \hat{H}_\mathrm{A}(\tau_{\mathrm{A}2}) \rho_0 \hat{H}_\mathrm{B}(\tau_{\mathrm{B}1}) \right] \\
&= \frac{\mathrm{d}\tau_\mathrm{A}}{\mathrm{d}t_2} \frac{\mathrm{d}\tau_\mathrm{B}}{\mathrm{d}t_1} \lambda_\mathrm{A} \lambda_\mathrm{B} \chi_\mathrm{A}(\tau_{\mathrm{A}2}) \chi_\mathrm{B}(\tau_{\mathrm{B}1}) \,\mathrm{Tr}_\phi \left[\hat{\phi}(\mathsf{x}_{\mathrm{A}2}) \left|0\right\rangle \left\langle 0\right| \hat{\phi}(\mathsf{x}_{\mathrm{B}1}) \right] \hat{m}_\mathrm{A}(\tau_{\mathrm{A}2}) \rho_{\mathrm{AB},0} \hat{m}_\mathrm{B}(\tau_{\mathrm{B}1}) \\
&= \frac{\mathrm{d}\tau_\mathrm{A}}{\mathrm{d}t_2} \frac{\mathrm{d}\tau_\mathrm{B}}{\mathrm{d}t_1} \lambda_\mathrm{A} \lambda_\mathrm{B} \chi_\mathrm{A}(\tau_{\mathrm{A}2}) \chi_\mathrm{B}(\tau_{\mathrm{B}1}) e^{-\mathrm{i}(\Omega_\mathrm{B}\tau_{\mathrm{B}1} - \Omega_\mathrm{A}\tau_{\mathrm{A}2})} W(\mathsf{x}_{\mathrm{B}1}, \mathsf{x}_{\mathrm{A}2}) \begin{bmatrix} 0 & 0 & 0 & 0 \\ 0 & 0 & 1 & 0 \\ 0 & 0 & 0 & 0 \\ 0 & 0 & 0 & 0 \end{bmatrix},
\end{aligned} \tag{A.5}
$$

$$
\begin{aligned}
&\bullet\ \mathrm{Tr}_\phi \left[\frac{\mathrm{d}\tau_\mathrm{B}}{\mathrm{d}t_2} \frac{\mathrm{d}\tau_\mathrm{A}}{\mathrm{d}t_1} \hat{H}_\mathrm{B}(\tau_{\mathrm{B}2}) \rho_0 \hat{H}_\mathrm{A}(\tau_{\mathrm{A}1}) \right] \\
&= \frac{\mathrm{d}\tau_\mathrm{B}}{\mathrm{d}t_2} \frac{\mathrm{d}\tau_\mathrm{A}}{\mathrm{d}t_1} \lambda_\mathrm{A} \lambda_\mathrm{B} \chi_\mathrm{A}(\tau_{\mathrm{A}1}) \chi_\mathrm{B}(\tau_{\mathrm{B}2}) \,\mathrm{Tr}_\phi \left[\hat{\phi}(\mathsf{x}_{\mathrm{B}2}) \left|0\right\rangle \left\langle 0\right| \hat{\phi}(\mathsf{x}_{\mathrm{A}1}) \right] \hat{m}_\mathrm{B}(\tau_{\mathrm{B}2}) \rho_{\mathrm{AB},0} \hat{m}_\mathrm{A}(\tau_{\mathrm{A}1}) \\
&= \frac{\mathrm{d}\tau_\mathrm{B}}{\mathrm{d}t_2} \frac{\mathrm{d}\tau_\mathrm{A}}{\mathrm{d}t_1} \lambda_\mathrm{A} \lambda_\mathrm{B} \chi_\mathrm{A}(\tau_{\mathrm{A}1}) \chi_\mathrm{B}(\tau_{\mathrm{B}2}) e^{-\mathrm{i}(\Omega_\mathrm{A}\tau_{\mathrm{A}1} - \Omega_\mathrm{B}\tau_{\mathrm{B}2})} W(\mathsf{x}_{\mathrm{A}1}, \mathsf{x}_{\mathrm{B}2}) \begin{bmatrix} 0 & 0 & 0 & 0 \\ 0 & 0 & 0 & 0 \\ 0 & 1 & 0 & 0 \\ 0 & 0 & 0 & 0 \end{bmatrix},
\end{aligned} \tag{A.6}
$$

$$
\begin{aligned}
&\bullet\ \mathrm{Tr}_\phi \left[\frac{\mathrm{d}\tau_\mathrm{B}}{\mathrm{d}t_1} \frac{\mathrm{d}\tau_\mathrm{B}}{\mathrm{d}t_2} \hat{H}_\mathrm{B}(\tau_{\mathrm{B}2}) \rho_0 \hat{H}_\mathrm{B}(\tau_{\mathrm{B}1}) \right] \\
&= \frac{\mathrm{d}\tau_\mathrm{B}}{\mathrm{d}t_1} \frac{\mathrm{d}\tau_\mathrm{B}}{\mathrm{d}t_2} \lambda_\mathrm{B}^2 \chi_\mathrm{B}(\tau_{\mathrm{B}1}) \chi_\mathrm{B}(\tau_{\mathrm{B}2}) \,\mathrm{Tr}_\phi \left[\hat{\phi}(\mathsf{x}_{\mathrm{B}2}) \left|0\right\rangle \left\langle 0\right| \hat{\phi}(\mathsf{x}_{\mathrm{B}1}) \right] \hat{m}_\mathrm{B}(\tau_{\mathrm{B}2}) \rho_{\mathrm{AB},0} \hat{m}_\mathrm{B}(\tau_{\mathrm{B}1}) \\
&= \frac{\mathrm{d}\tau_\mathrm{B}}{\mathrm{d}t_1} \frac{\mathrm{d}\tau_\mathrm{B}}{\mathrm{d}t_2} \lambda_\mathrm{B}^2 \chi_\mathrm{B}(\tau_{\mathrm{B}1}) \chi_\mathrm{B}(\tau_{\mathrm{B}2}) e^{-\mathrm{i}\Omega_\mathrm{B}(\tau_{\mathrm{B}1} - \tau_{\mathrm{B}2})} W(\mathsf{x}_{\mathrm{B}1}, \mathsf{x}_{\mathrm{B}2}) \begin{bmatrix} 0 & 0 & 0 & 0 \\ 0 & 1 & 0 & 0 \\ 0 & 0 & 0 & 0 \\ 0 & 0 & 0 & 0 \end{bmatrix}.
\end{aligned} \tag{A.7}
$$

Therefore,

$$\mathrm{Tr}_\phi[\rho^{(1,1)}] = \begin{bmatrix} 0 & 0 & 0 & 0 \\ 0 & P_\mathrm{B} & C^*_\mathrm{AB} & 0 \\ 0 & C_\mathrm{AB} & P_\mathrm{A} & 0 \\ 0 & 0 & 0 & 0 \end{bmatrix}, \tag{A.8}$$

where $P_\mathrm{A}, P_\mathrm{B}$, and C_AB are given by (2.44).

$\underline{\mathrm{Tr}_\phi[\rho^{(0,2)}] \text{ term:}}$

$$\begin{aligned}
\mathrm{Tr}_\phi[\rho^{(0,2)}] &= \mathrm{Tr}_\phi[\rho_0 \hat{U}^{(2)\dagger}] \\
&= \mathrm{Tr}_\phi \Bigg[-\rho_0 \int_\mathbb{R} \mathrm{d}t_1 \left(\frac{\mathrm{d}\tau_\mathrm{A}}{\mathrm{d}t_1} \hat{H}_\mathrm{A}(\tau_\mathrm{A}(t_1)) + \frac{\mathrm{d}\tau_\mathrm{B}}{\mathrm{d}t_1} \hat{H}_\mathrm{B}(\tau_\mathrm{B}(t_1)) \right) \\
&\qquad \times \int_{-\infty}^{t_1} \mathrm{d}t_2 \left(\frac{\mathrm{d}\tau_\mathrm{A}}{\mathrm{d}t_2} \hat{H}_\mathrm{A}(\tau_\mathrm{A}(t_2)) + \frac{\mathrm{d}\tau_\mathrm{B}}{\mathrm{d}t_2} \hat{H}_\mathrm{B}(\tau_\mathrm{B}(t_2)) \right) \Bigg] \\
&= -\int_\mathbb{R} \mathrm{d}t_1 \int_{-\infty}^{t_1} \mathrm{d}t_2 \, \mathrm{Tr}_\phi \Bigg[\frac{\mathrm{d}\tau_\mathrm{A}}{\mathrm{d}t_1} \frac{\mathrm{d}\tau_\mathrm{A}}{\mathrm{d}t_2} \rho_0 \hat{H}_\mathrm{A}(\tau_\mathrm{A}(t_1)) \hat{H}_\mathrm{A}(\tau_\mathrm{A}(t_2)) \\
&\qquad + \frac{\mathrm{d}\tau_\mathrm{A}}{\mathrm{d}t_1} \frac{\mathrm{d}\tau_\mathrm{B}}{\mathrm{d}t_2} \rho_0 \hat{H}_\mathrm{A}(\tau_\mathrm{A}(t_1)) \hat{H}_\mathrm{B}(\tau_\mathrm{B}(t_2)) \\
&\qquad + \frac{\mathrm{d}\tau_\mathrm{B}}{\mathrm{d}t_1} \frac{\mathrm{d}\tau_\mathrm{A}}{\mathrm{d}t_2} \rho_0 \hat{H}_\mathrm{B}(\tau_\mathrm{B}(t_1)) \hat{H}_\mathrm{A}(\tau_\mathrm{A}(t_2)) \\
&\qquad + \frac{\mathrm{d}\tau_\mathrm{B}}{\mathrm{d}t_1} \frac{\mathrm{d}\tau_\mathrm{B}}{\mathrm{d}t_2} \rho_0 \hat{H}_\mathrm{B}(\tau_\mathrm{B}(t_1)) \hat{H}_\mathrm{B}(\tau_\mathrm{B}(t_2)) \Bigg].
\end{aligned}$$

Each term can be calculated in the same way as before. Here, we provide two terms as an

example.

$$\bullet\ \mathrm{Tr}_\phi\left[\frac{\mathrm{d}\tau_\mathrm{A}}{\mathrm{d}t_1}\frac{\mathrm{d}\tau_\mathrm{B}}{\mathrm{d}t_2}\rho_0\hat{H}_\mathrm{A}(\tau_{\mathrm{A}1})\hat{H}_\mathrm{B}(\tau_{\mathrm{B}2})\right]$$

$$= \frac{\mathrm{d}\tau_\mathrm{A}}{\mathrm{d}t_1}\frac{\mathrm{d}\tau_\mathrm{B}}{\mathrm{d}t_2}\lambda_\mathrm{A}\lambda_\mathrm{B}\chi_\mathrm{A}(\tau_{\mathrm{A}1})\chi_\mathrm{B}(\tau_{\mathrm{B}2})\,\mathrm{Tr}_\phi\left[|0\rangle\langle 0|\,\hat{\phi}(\mathsf{x}_{\mathrm{A}1})\hat{\phi}(\mathsf{x}_{\mathrm{B}2})\right]\rho_{\mathrm{AB},0}\hat{m}_\mathrm{A}(\tau_{\mathrm{A}1})\hat{m}_\mathrm{B}(\tau_{\mathrm{B}2})$$

$$= \frac{\mathrm{d}\tau_\mathrm{A}}{\mathrm{d}t_1}\frac{\mathrm{d}\tau_\mathrm{B}}{\mathrm{d}t_2}\lambda_\mathrm{A}\lambda_\mathrm{B}\chi_\mathrm{A}(\tau_{\mathrm{A}1})\chi_\mathrm{B}(\tau_{\mathrm{B}2})e^{-\mathrm{i}(\Omega_\mathrm{A}\tau_{\mathrm{A}1}+\Omega_\mathrm{B}\tau_{\mathrm{B}2})}W(\mathsf{x}_{\mathrm{A}1},\mathsf{x}_{\mathrm{B}2})\begin{bmatrix}0&0&0&1\\0&0&0&0\\0&0&0&0\\0&0&0&0\end{bmatrix}, \tag{A.9}$$

$$\bullet\ \mathrm{Tr}_\phi\left[\frac{\mathrm{d}\tau_\mathrm{B}}{\mathrm{d}t_1}\frac{\mathrm{d}\tau_\mathrm{A}}{\mathrm{d}t_2}\rho_0\hat{H}_\mathrm{B}(\tau_{\mathrm{B}1})\hat{H}_\mathrm{A}(\tau_{\mathrm{A}2})\right] \tag{A.10}$$

$$= \frac{\mathrm{d}\tau_\mathrm{B}}{\mathrm{d}t_1}\frac{\mathrm{d}\tau_\mathrm{A}}{\mathrm{d}t_2}\lambda_\mathrm{A}\lambda_\mathrm{B}\chi_\mathrm{B}(\tau_{\mathrm{B}1})\chi_\mathrm{A}(\tau_{\mathrm{A}2})\,\mathrm{Tr}_\phi\left[|0\rangle\langle 0|\,\hat{\phi}(\mathsf{x}_{\mathrm{B}1})\hat{\phi}(\mathsf{x}_{\mathrm{A}2})\right]\rho_{\mathrm{AB},0}\hat{m}_\mathrm{B}(\tau_{\mathrm{B}1})\hat{m}_\mathrm{A}(\tau_{\mathrm{A}2})$$

$$= \frac{\mathrm{d}\tau_\mathrm{B}}{\mathrm{d}t_1}\frac{\mathrm{d}\tau_\mathrm{A}}{\mathrm{d}t_2}\lambda_\mathrm{A}\lambda_\mathrm{B}\chi_\mathrm{B}(\tau_{\mathrm{B}1})\chi_\mathrm{A}(\tau_{\mathrm{A}2})e^{-\mathrm{i}(\Omega_\mathrm{B}\tau_{\mathrm{B}1}+\Omega_\mathrm{A}\tau_{\mathrm{A}2})}W(\mathsf{x}_{\mathrm{B}1},\mathsf{x}_{\mathrm{A}2})\begin{bmatrix}0&0&0&1\\0&0&0&0\\0&0&0&0\\0&0&0&0\end{bmatrix}. \tag{A.11}$$

Hence,

$$\begin{aligned}
X^*_{\mathrm{AB}} &= -\int_\mathbb{R}\mathrm{d}t_1\int_{-\infty}^{t_1}\mathrm{d}t_2\frac{\mathrm{d}\tau_\mathrm{A}}{\mathrm{d}t_1}\frac{\mathrm{d}\tau_\mathrm{B}}{\mathrm{d}t_2}\lambda_\mathrm{A}\lambda_\mathrm{B}\chi_\mathrm{A}(\tau_{\mathrm{A}1})\chi_\mathrm{B}(\tau_{\mathrm{B}2})e^{-\mathrm{i}(\Omega_\mathrm{A}\tau_{\mathrm{A}1}+\Omega_\mathrm{B}\tau_{\mathrm{B}2})}W(\mathsf{x}_{\mathrm{A}1},\mathsf{x}_{\mathrm{B}2})\\
&\quad -\int_\mathbb{R}\mathrm{d}t_1\int_{-\infty}^{t_1}\mathrm{d}t_2\frac{\mathrm{d}\tau_\mathrm{B}}{\mathrm{d}t_1}\frac{\mathrm{d}\tau_\mathrm{A}}{\mathrm{d}t_2}\lambda_\mathrm{A}\lambda_\mathrm{B}\chi_\mathrm{B}(\tau_{\mathrm{B}1})\chi_\mathrm{A}(\tau_{\mathrm{A}2})e^{-\mathrm{i}(\Omega_\mathrm{B}\tau_{\mathrm{B}1}+\Omega_\mathrm{A}\tau_{\mathrm{A}2})}W(\mathsf{x}_{\mathrm{B}1},\mathsf{x}_{\mathrm{A}2})\\
&= -\int_\mathbb{R}\mathrm{d}t_1\int_{-\infty}^{t_1}\mathrm{d}t_2\frac{\mathrm{d}\tau_\mathrm{A}}{\mathrm{d}t_1}\frac{\mathrm{d}\tau_\mathrm{B}}{\mathrm{d}t_2}\lambda_\mathrm{A}\lambda_\mathrm{B}\chi_\mathrm{A}(\tau_{\mathrm{A}1})\chi_\mathrm{B}(\tau_{\mathrm{B}2})e^{-\mathrm{i}(\Omega_\mathrm{A}\tau_{\mathrm{A}1}+\Omega_\mathrm{B}\tau_{\mathrm{B}2})}W(\mathsf{x}_{\mathrm{A}1},\mathsf{x}_{\mathrm{B}2})\\
&\quad -\int_\mathbb{R}\mathrm{d}t_2\int_{-\infty}^{t_2}\mathrm{d}t_1\frac{\mathrm{d}\tau_\mathrm{B}}{\mathrm{d}t_2}\frac{\mathrm{d}\tau_\mathrm{A}}{\mathrm{d}t_1}\lambda_\mathrm{A}\lambda_\mathrm{B}\chi_\mathrm{B}(\tau_{\mathrm{B}2})\chi_\mathrm{A}(\tau_{\mathrm{A}1})e^{-\mathrm{i}(\Omega_\mathrm{B}\tau_{\mathrm{B}2}+\Omega_\mathrm{A}\tau_{\mathrm{A}1})}W(\mathsf{x}_{\mathrm{B}2},\mathsf{x}_{\mathrm{A}1})\quad(t_1\leftrightarrow t_2)\\
&= -\int_\mathbb{R}\mathrm{d}\tau_\mathrm{A}\int_{-\infty}^{t(\tau_\mathrm{A})}\mathrm{d}\tau_\mathrm{B}\,\lambda_\mathrm{A}\lambda_\mathrm{B}\chi_\mathrm{A}(\tau_\mathrm{A})\chi_\mathrm{B}(\tau_\mathrm{B})e^{-\mathrm{i}(\Omega_\mathrm{A}\tau_\mathrm{A}+\Omega_\mathrm{B}\tau_\mathrm{B})}W(\mathsf{x}_\mathrm{A}(\tau_\mathrm{A}),\mathsf{x}_\mathrm{B}(\tau_\mathrm{B}))\\
&\quad -\int_\mathbb{R}\mathrm{d}\tau_\mathrm{B}\int_{-\infty}^{t(\tau_\mathrm{B})}\mathrm{d}\tau_\mathrm{A}\,\lambda_\mathrm{A}\lambda_\mathrm{B}\chi_\mathrm{B}(\tau_\mathrm{B})\chi_\mathrm{A}(\tau_\mathrm{A})e^{-\mathrm{i}(\Omega_\mathrm{B}\tau_\mathrm{B}+\Omega_\mathrm{A}\tau_\mathrm{A})}W(\mathsf{x}_\mathrm{B}(\tau_\mathrm{B}),\mathsf{x}_\mathrm{A}(\tau_\mathrm{A}))
\end{aligned} \tag{A.12}$$

$$\begin{aligned}
&= -\lambda_\mathrm{A}\lambda_\mathrm{B}\int_\mathbb{R}\mathrm{d}\tau_\mathrm{A}\int_\mathbb{R}\mathrm{d}\tau_\mathrm{B}\,\chi_\mathrm{A}(\tau_\mathrm{A})\chi_\mathrm{B}(\tau_\mathrm{B})e^{-\mathrm{i}(\Omega_\mathrm{A}\tau_\mathrm{A}+\Omega_\mathrm{B}\tau_\mathrm{B})}\\
&\qquad\times\Big[W(\mathsf{x}_\mathrm{A}(\tau_\mathrm{A}),\mathsf{x}_\mathrm{B}(\tau_\mathrm{B}))\Theta(t(\tau_\mathrm{A})-t(\tau_\mathrm{B}))+W(\mathsf{x}_\mathrm{B}(\tau_\mathrm{B}),\mathsf{x}_\mathrm{A}(\tau_\mathrm{A}))\Theta(t(\tau_\mathrm{B})-t(\tau_\mathrm{A}))\Big].
\end{aligned} \tag{A.13}$$

Appendix B

Density matrix in BTZ spacetime

B.1 QFT in BTZ spacetime

B.1.1 AdS_3 and BTZ spacetimes

AdS_3 spacetime

BTZ spacetime can be constructed from AdS_3 spacetime. AdS_3 spacetime [i.e., $(2+1)$-dimensional anti-de Sitter spacetime] can be formulated as a maximally symmetric spacetime with negative curvature embedded in four-dimensional flat space with two timelike axes. We follow [133].

Let u, w be the timelike coordinates and x, y be the spacelike coordinates in such a flat space. Then the line-element of the flat space, $\mathrm{d}s_4^2$, reads

$$\mathrm{d}s_4^2 = -\mathrm{d}u^2 - \mathrm{d}w^2 + \mathrm{d}x^2 + \mathrm{d}y^2 \,. \tag{B.1}$$

AdS_3 is then expressed as a hypersurface in this flat space obeying

$$-u^2 - w^2 + x^2 + y^2 = -\ell^2 \,, \tag{B.2}$$

where $\ell = 1/\sqrt{-\Lambda}$ is the AdS length defined by using the cosmological constant Λ. The line-element of the embedded AdS_3 spacetime can be obtained from these two equations. One can change the coordinates to the so-called global static coordinate system (t, ρ, φ)

via

$$u = \ell \cosh\rho \sin(t/\ell)\,, \tag{B.3a}$$
$$w = \ell \cosh\rho \cos(t/\ell)\,, \tag{B.3b}$$
$$x = \ell \sinh\rho \sin\varphi\,, \tag{B.3c}$$
$$y = \ell \sinh\rho \cos\varphi\,. \tag{B.3d}$$

so that the line-element for AdS_3 reads

$$\mathrm{d}s^2 = \ell^2(-\cosh^2\rho \mathrm{d}t^2 + \mathrm{d}\rho^2 + \sinh^2\rho \mathrm{d}\varphi^2)\,, \tag{B.4}$$

where $t \in [0, 2\pi\ell]$, $\rho \in [0, \infty)$ and $\varphi \in [0, 2\pi)$. Although this is periodic in t and thereby the spacetime possesses closed timelike curves, we can introduce a universal covering space that allows $t \in \mathbb{R}$.

Let us rewrite the line-element of AdS_3 as

$$\mathrm{d}s^2 = \ell^2 \cosh^2\rho \left[-\mathrm{d}t^2 + \frac{1}{\cosh^2\rho}(\mathrm{d}\rho^2 + \sinh^2\rho \mathrm{d}\varphi^2)\right]\,, \tag{B.5}$$

and introduce

$$\mathrm{d}\chi \coloneqq \frac{\mathrm{d}\rho}{\cosh\rho}\,. \tag{B.6}$$

One can solve this equation to obtain

$$\cosh\rho = \frac{1}{\cos\chi}\,. \tag{B.7}$$

This relation and the fact $\rho \in [0, \infty)$ (and therefore $\cosh\rho \in [1, \infty)$) leads us to $\chi \in [0, \pi/2)$. Thus, we can perform a coordinate transformation from the global static coordinates (t, ρ, φ) to the *conformal coordinates* (t, χ, φ), which give the following line-element:

$$\mathrm{d}s^2 = \frac{\ell^2}{\cos^2\chi}(-\mathrm{d}t^2 + \mathrm{d}\Omega_2^2)\,, \tag{B.8}$$

where $\mathrm{d}\Omega_2^2 = \mathrm{d}\chi^2 + \sin^2\chi \mathrm{d}\varphi^2$ is the line-element of two-sphere.

We remark that the two-sphere $\mathrm{d}\Omega_2^2$ here is actually representing a half sphere since $\chi \in [0, \pi/2)$ rather than $[0, \pi]$. Namely, $\chi = 0$ and $\chi = \pi/2$ are the north pole and the equator of a unit sphere, respectively. The line-element given above is conformally equivalent to a spacetime described by $-\mathrm{d}t^2 + \mathrm{d}\Omega_2^2$ [see (2.21)]. If $\chi \in [0, \pi]$ then such a spacetime is known as the Einstein static universe. Therefore, AdS_3 is conformally equivalent to half of the Einstein static universe. The Penrose diagram for AdS is shown in Fig. B.1.

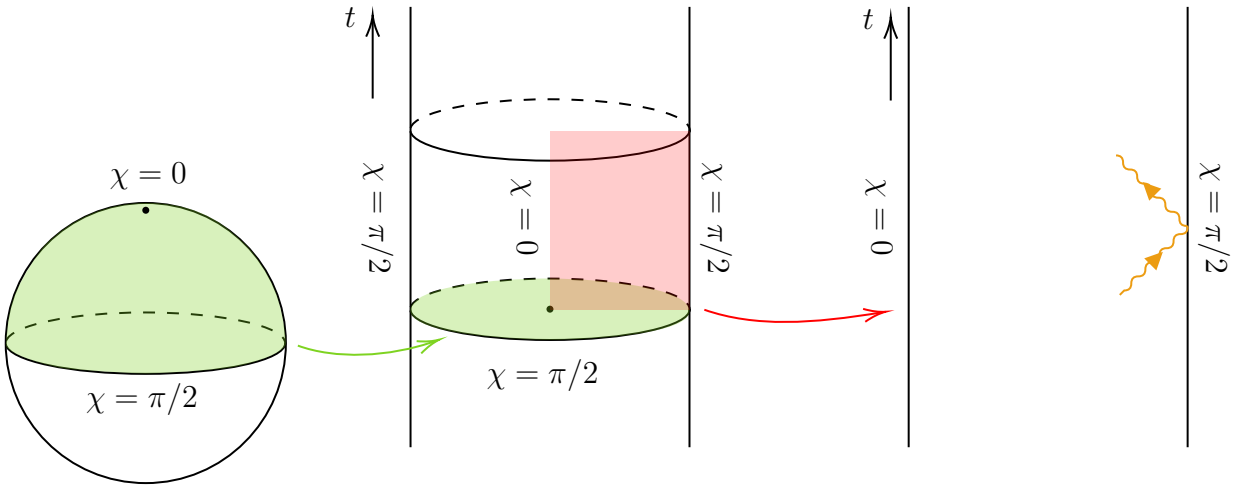

Figure B.1: The green region on the sphere represents a time slice of the half Einstein static universe. The Penrose diagram for anti-de Sitter spacetime is shown in the rightmost figure. The orange line represents a light ray bouncing off the boundary of AdS spacetime.

BTZ spacetime

While we now know that BTZ spacetime is a black hole spacetime in $(2+1)$-dimensions, historically, people had thought that black hole solutions do not exist in this dimension. This is because the Riemann tensor in $(2+1)$-dimension can be written in terms of the Einstein tensor $G_{\mu\nu} \equiv R_{\mu\nu} + \frac{1}{2} R g_{\mu\nu}$ and thereby, the Einstein field equation $G_{\mu\nu} = 8\pi G_{\mathrm{N}} T_{\mu\nu}$ allows us to express the Riemann tensor $R_{\mu\nu\rho\sigma}$ in terms of the stress-energy tensor $T_{\mu\nu}$. If we assume that there is no matter (i.e., $T_{\mu\nu} = 0$) then it leads to $R_{\mu\nu\rho\sigma} = 0$, which is $(2+1)$-dimensional flat spacetime. Even if we introduce the cosmological constant Λ, the vacuum solution to the Einstein field equations becomes (anti-)de Sitter spacetime, which is not a black hole solution. Let us call these flat, de Sitter, and anti-de Sitter solutions as trivial solutions.

However, one can think of spacetimes that are locally trivial but globally non-trivial. For example, the plane and cylinder are both locally trivial (flat), but they are topologically different; the cylinder is constructed by topologically identifying some points of the plane. BTZ black hole spacetime is locally trivial (AdS_3) but topologically different, and it can be constructed by a topological identification. In this sense, BTZ spacetime is a vacuum solution to the Einstein field equation with the negative cosmological constant, $G_{\mu\nu} + \Lambda g_{\mu\nu} = 0$, but topologically different from AdS_3 spacetime.

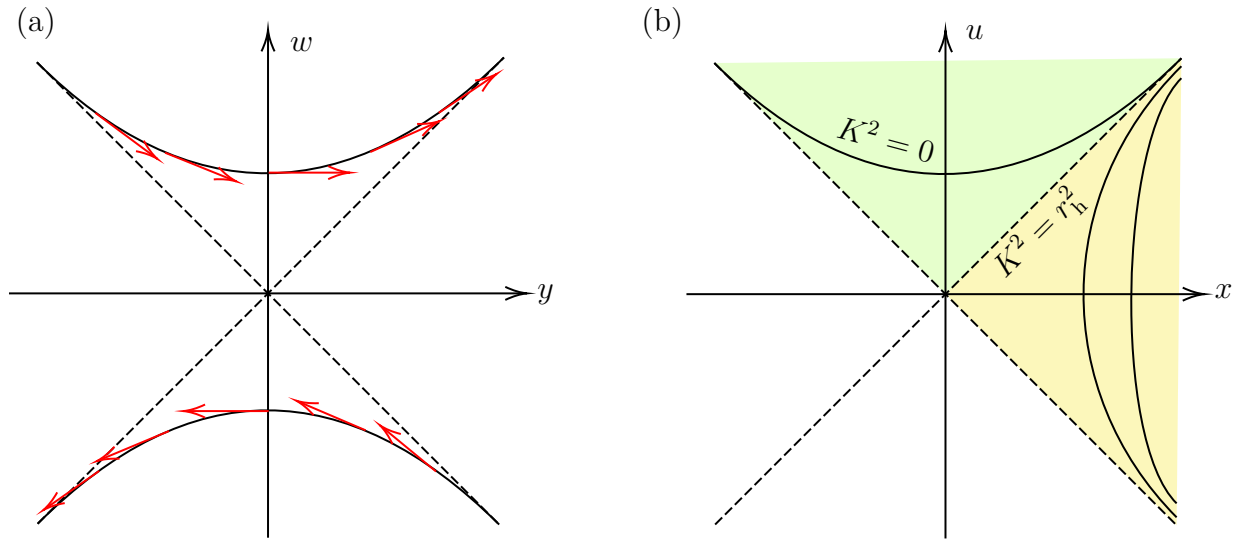

Figure B.2: (a) u, x-slice of the embedding space. The hyperbolas represent the surface of AdS_3 described by (B.2). The spacelike Killing vectors are depicted by red arrows. (b) The (u, x)-plane and the AdS_3 surfaces described by (B.11). The yellow and green regions are characterized by $u^2 - x^2 < 0$ and $u^2 - x^2 > 0$, respectively. Each hyperbola represents the surface of (B.11) with different K^2.

Let us begin with the embedding space (B.1) and the constraint (B.2) for AdS_3 spacetime. For fixed x, u, one can consider a two-dimensional (w, y)-plane. In this $x, u = const$ slice, the AdS_3 space is characterized by $-w^2 + y^2 = u^2 - x^2 - \ell^2$ from (B.2). By introducing a constant $r_{\rm h}$, one of the spacelike Killing vector field K on this hypersurface can be written as

$$K = \frac{r_{\rm h}}{\ell}(y\partial_w + w\partial_y)\,. \tag{B.9}$$

The norm of this Killing vector field is

$$K^2 \equiv K^\mu K_\mu = \frac{r_{\rm h}^2}{\ell^2}(w^2 - y^2)\,, \tag{B.10}$$

where $K^2 > 0$ since it is a spacelike vector. We can rewrite (B.2) by using K^2 as

$$u^2 - x^2 = \ell^2\left(1 - \frac{K^2}{r_{\rm h}^2}\right)\,. \tag{B.11}$$

We now allow u, x to vary and consider the (u, x)-plane in Fig. B.2(b). The AdS_3 spacetime is now described by the constraint (B.11) with $K^2 > 0$. The yellow and green regions are characterized by $x > |u|$ and $u > |x|$, respectively, and this means $u^2 - x^2 < 0$ for yellow and $u^2 - x^2 > 0$ for green. The surface of AdS_3 is described by (B.11), and each surface can be specified with the value of K^2. In the yellow region, $u^2 - x^2 < 0 \Rightarrow K^2 > r_\mathrm{h}^2$, thereby each surface can be specified by, for example, $K^2 = r_\mathrm{h}^2 + 1, r_\mathrm{h}^2 + 2, \cdots$. On the other hand, the surfaces in the green region have $K^2 < r_\mathrm{h}^2$, but the Killing vector field must be spacelike, $K^2 > 0$, so the surfaces stop at $K^2 = 0$, which will become the singularity of the black hole.

We now perform a coordinate transformation that respects (B.2) and the argument above:

$$u = \frac{\ell r}{r_\mathrm{h}} \cosh \frac{r_\mathrm{h} \varphi}{\ell} , \tag{B.12a}$$

$$x = \frac{\ell r}{r_\mathrm{h}} \sinh \frac{r_\mathrm{h} \varphi}{\ell} , \tag{B.12b}$$

$$w = \frac{\ell \sqrt{r^2 - r_\mathrm{h}^2}}{r_\mathrm{h}} \sinh \frac{r_\mathrm{h} t}{\ell^2} , \tag{B.12c}$$

$$y = \frac{\ell \sqrt{r^2 - r_\mathrm{h}^2}}{r_\mathrm{h}} \cosh \frac{r_\mathrm{h} t}{\ell^2} , \tag{B.12d}$$

where $t \in \mathbb{R}, r \in (0, \infty), \varphi \in \mathbb{R}$. This coordinate transformation leads us to the BTZ metric (4.1). However, the metric contains an infinitely long angle φ and the metric still describes AdS_3 in a different coordinate system. Since our spacelike Killing vector field in this coordinate system is just $K = \partial_\varphi$, we can perform a topological identification:

$$(t, r, \varphi) \sim (t, r, \varphi + 2\pi) , \tag{B.13}$$

and claim that φ and $\varphi + 2\pi$ represent the same point. The resulting metric describes BTZ black hole spacetime.

B.1.2 QFT

The Wightman function in BTZ black hole spacetime can be constructed from the Wightman function in AdS_3. Here, we first consider QFT in AdS_3 spacetime and then construct the BTZ Wightman function.

QFT in AdS_3

Recall that the formulation of QFT is well-defined in globally hyperbolic spacetimes. However, AdS_3 is not globally hyperbolic since its boundary is timelike (B.1). Therefore, we have to specify how a quantum field behaves at the boundary.

To properly define quantum fields in AdS_3 spacetime, we use the fact that it is conformally equivalent to the Einstein static universe (ESU) [134, 102]. Recall that the line-element of ESU is

$$\mathrm{d}s^2 = -\mathrm{d}t^2 + \mathrm{d}\chi^2 + \sin^2\chi \mathrm{d}\varphi^2 \,, \tag{B.14}$$

where $t \in \mathbb{R}, \chi \in [0, \pi]$, and $\varphi \in [0, 2\pi)$. We consider a massless, conformally coupled scalar field in ESU, satisfying the Klein-Gordon equation and proceed with quantization by defining a vacuum state $|0_{\mathrm{ESU}}\rangle$ with respect to a timelike Killing vector field ∂_t. The Wightman function, $W_{\mathrm{ESU}}(\mathsf{x}, \mathsf{x}')$, can be obtained by

$$W_{\mathrm{ESU}}(\mathsf{x}, \mathsf{x}') = \langle 0_{\mathrm{ESU}} | \hat{\phi}(\mathsf{x}) \hat{\phi}(\mathsf{x}') | 0_{\mathrm{ESU}} \rangle \ . \tag{B.15}$$

By using the fact that massless conformally coupled fields in conformally related spacetimes are related by (2.22), the Wightman function in AdS_3 (but admitting the leakage of the field from the northern to the southern hemispheres in Fig. B.1), $W_{\mathrm{A}}(\mathsf{x}, \mathsf{x}')$, can be constructed as

$$\begin{aligned} W_{\mathrm{A}}(\mathsf{x}, \mathsf{x}') &= \langle 0 | \hat{\phi}_{\mathrm{AdS}}(\mathsf{x}) \hat{\phi}_{\mathrm{AdS}}(\mathsf{x}') | 0 \rangle \\ &= \Omega^{-\frac{1}{2}}(\mathsf{x}) \Omega^{-\frac{1}{2}}(\mathsf{x}') \, \langle 0 | \hat{\phi}_{\mathrm{ESU}}(\mathsf{x}) \hat{\phi}_{\mathrm{ESU}}(\mathsf{x}') | 0 \rangle \qquad \text{(B.16)} \\ &= \frac{\sqrt{\cos\chi \cos\chi'}}{\ell} W_{\mathrm{ESU}}(\mathsf{x}, \mathsf{x}') \,, \qquad \text{(B.17)} \end{aligned}$$

where our conformal factor $\Omega(\mathsf{x})$ is $\Omega(\mathsf{x}) = \ell / \cos\chi$ from (B.8).

To implement the boundary condition at $\chi = \pi/2$, we employ the method of images. By defining $\tilde{\mathsf{x}} \coloneqq (t, \pi - \chi, \varphi)$, we can properly construct the Wightman function in AdS_3, $W_{\mathrm{AdS}_3}(\mathsf{x}, \mathsf{x}')$ as

$$W_{\mathrm{AdS}_3}(\mathsf{x}, \mathsf{x}') = W_{\mathrm{A}}(\mathsf{x}, \mathsf{x}') + \zeta W_{\mathrm{A}}(\tilde{\mathsf{x}}, \mathsf{x}') \,, \tag{B.18}$$

where $\zeta \in \mathbb{R}$ determines the property of the boundary. For example, $\zeta = 1$ and $\zeta = -1$ represent the Dirichlet and Neumann boundary conditions, respectively. One can also consider the transparent boundary condition, $\zeta = 0$.

QFT in BTZ

Since BTZ spacetime is constructed from AdS_3 by identifying $(t, r, \varphi) \sim (t, r, \varphi + 2n\pi)$ in the coordinate system (B.12d), we can utilize the field operator in AdS_3. In particular, let $\Gamma^n : (t, r, \varphi) \mapsto (t, r, \varphi + 2\pi n)$. Then the Wightman function in BTZ spacetime, $W_{\mathrm{BTZ}}(\mathsf{x}, \mathsf{x}')$, can be constructed from $W_{\mathrm{AdS}_3}(\mathsf{x}, \mathsf{x}')$ via the method of images [102]:

$$W_{\mathrm{BTZ}}(\mathsf{x}, \mathsf{x}') = \sum_{n=-\infty}^{\infty} W_{\mathrm{AdS}_3}(\mathsf{x}, \Gamma^n \mathsf{x}') \,. \tag{B.19}$$

One can show that this Wightman function satisfies the KMS condition with respect to time t and the vacuum state (which corresponds to $|0_{\mathrm{AdS}}\rangle$) is the Hartle-Hawking state [102]. One can also refer to [104, 135].

B.2 Derivation of matrix elements

Consider two static detectors on the same axis: $\Delta\varphi = 0$. We assume that the detectors switch at the same time so that

$$C_{\mathrm{AB}} = \lambda^2 \int_{\mathbb{R}} \mathrm{d}\tau_{\mathrm{A}} \int_{\mathbb{R}} \mathrm{d}\tau_{\mathrm{B}}\, e^{-\tau_{\mathrm{A}}^2/2\sigma^2} e^{-\tau_{\mathrm{B}}^2/2\sigma^2} e^{-\mathrm{i}\Omega(\tau_{\mathrm{A}} - \tau_{\mathrm{B}})} W_{\mathrm{BTZ}}(\mathsf{x}_{\mathrm{A}}(\tau_{\mathrm{A}}), \mathsf{x}_{\mathrm{B}}(\tau_{\mathrm{B}})), \tag{B.20}$$

where

$$W_{\mathrm{BTZ}}(\mathsf{x}_{\mathrm{A}}(\tau_{\mathrm{A}}), \mathsf{x}_{\mathrm{B}}(\tau_{\mathrm{B}})) = \frac{1}{4\pi\sqrt{2}\ell} \sum_{n=-\infty}^{\infty} \left[\frac{1}{\sqrt{\sigma_\epsilon(\mathsf{x}_{\mathrm{A}}, \Gamma^n \mathsf{x}_{\mathrm{B}})}} - \frac{\zeta}{\sqrt{\sigma_\epsilon(\mathsf{x}_{\mathrm{A}}, \Gamma^n \mathsf{x}_{\mathrm{B}}) + 2}} \right], \tag{B.21a}$$

$$\sigma_\epsilon(\mathsf{x}_{\mathrm{A}}, \Gamma^n \mathsf{x}_{\mathrm{B}}) = \frac{r_{\mathrm{A}} r_{\mathrm{B}}}{r_{\mathrm{h}}^2} \cosh\left(\frac{r_{\mathrm{h}}}{\ell} 2\pi n\right) - 1 - \frac{\sqrt{(r_{\mathrm{A}}^2 - r_{\mathrm{h}}^2)(r_{\mathrm{B}}^2 - r_{\mathrm{h}}^2)}}{r_{\mathrm{h}}^2} \cosh\left[\frac{r_{\mathrm{h}}}{\ell^2}\left(\frac{\tau_{\mathrm{A}}}{\gamma_{\mathrm{A}}} - \frac{\tau_{\mathrm{B}}}{\gamma_{\mathrm{B}}}\right) - \mathrm{i}\epsilon\right], \tag{B.21b}$$

where we used $t_j = \tau_j/\gamma_j$. Then C_{AB} becomes

$$C_{\mathrm{AB}} = \frac{\lambda^2}{4\pi\sqrt{2}\ell} \sum_{n=-\infty}^{\infty} \int_{\mathbb{R}} \mathrm{d}\tau_{\mathrm{A}} \int_{\mathbb{R}} \mathrm{d}\tau_{\mathrm{B}}\, e^{-\tau_{\mathrm{A}}^2/2\sigma^2} e^{-\tau_{\mathrm{B}}^2/2\sigma^2} e^{-\mathrm{i}\Omega(\tau_{\mathrm{A}} - \tau_{\mathrm{B}})} \left[\frac{1}{\rho^-(\mathsf{x}_{\mathrm{A}}, \Gamma^n \mathsf{x}_{\mathrm{B}})} - \frac{\zeta}{\rho^+(\mathsf{x}_{\mathrm{A}}, \Gamma^n \mathsf{x}_{\mathrm{B}})} \right], \tag{B.22}$$

where

$$\rho^{\pm}(\mathsf{x}_{\mathrm{A}},\Gamma^{n}\mathsf{x}_{\mathrm{B}}) \coloneqq \sqrt{\frac{r_{\mathrm{A}}r_{\mathrm{B}}}{r_{\mathrm{h}}^{2}}\cosh\left[\frac{r_{\mathrm{h}}}{\ell}2\pi n\right]\pm 1-\frac{\ell^{2}\gamma_{\mathrm{A}}\gamma_{\mathrm{B}}}{r_{\mathrm{h}}^{2}}\cosh\left[\frac{r_{\mathrm{h}}}{\ell^{2}}\left(\frac{\tau_{\mathrm{A}}}{\gamma_{\mathrm{A}}}-\frac{\tau_{\mathrm{B}}}{\gamma_{\mathrm{B}}}\right)-\mathsf{i}\epsilon\right]} \tag{B.23}$$

$$= \frac{\ell\sqrt{\gamma_{\mathrm{A}}\gamma_{\mathrm{B}}}}{r_{\mathrm{h}}}\sqrt{\cosh\alpha^{\pm}_{\mathrm{AB},\,n}-\cosh\left[\frac{r_{\mathrm{h}}}{\ell^{2}}\left(\frac{\tau_{\mathrm{A}}}{\gamma_{\mathrm{A}}}-\frac{\tau_{\mathrm{B}}}{\gamma_{\mathrm{B}}}\right)-\mathsf{i}\epsilon\right]}, \tag{B.24}$$

and

$$\alpha^{\pm}_{\mathrm{AB},\,n} \coloneqq \operatorname{arccosh}\left[\frac{r_{\mathrm{h}}^{2}}{\ell^{2}\gamma_{\mathrm{A}}\gamma_{\mathrm{B}}}\left(\frac{r_{\mathrm{A}}r_{\mathrm{B}}}{r_{\mathrm{h}}^{2}}\cosh\left[\frac{r_{\mathrm{h}}}{\ell}2\pi n\right]\pm 1\right)\right]. \tag{B.25}$$

We also used $\gamma_{j}=\sqrt{r_{j}^{2}-r_{\mathrm{h}}^{2}}/\ell$.

By changing the variables from τ_{A} and τ_{B} to t_{A} and t_{B}, respectively, via $t_{j}\coloneqq\tau_{j}/\gamma_{j}$,

$$C_{\mathrm{AB}}=\frac{\lambda^{2}\gamma_{\mathrm{A}}\gamma_{\mathrm{B}}}{4\pi\sqrt{2}\ell}\sum_{n=-\infty}^{\infty}\int_{\mathbb{R}}\mathrm{d}t_{\mathrm{A}}\mathrm{d}t_{\mathrm{B}}\,e^{-\gamma_{\mathrm{A}}^{2}t_{\mathrm{A}}^{2}/2\sigma^{2}}e^{-\gamma_{\mathrm{B}}^{2}t_{\mathrm{B}}^{2}/2\sigma^{2}}e^{-\mathsf{i}\Omega(\gamma_{\mathrm{A}}t_{\mathrm{A}}-\gamma_{\mathrm{B}}t_{\mathrm{B}})}\left[\frac{1}{\rho^{-}(t_{\mathrm{A}},t_{\mathrm{B}})}-\frac{\zeta}{\rho^{+}(t_{\mathrm{A}},t_{\mathrm{B}})}\right], \tag{B.26}$$

where

$$\rho^{\pm}(t_{\mathrm{A}},t_{\mathrm{B}}) \coloneqq \frac{\ell\sqrt{\gamma_{\mathrm{A}}\gamma_{\mathrm{B}}}}{r_{\mathrm{h}}}\sqrt{\cosh\alpha^{\pm}_{\mathrm{AB},\,n}-\cosh\left[\frac{r_{\mathrm{h}}}{\ell^{2}}\left(t_{\mathrm{A}}-t_{\mathrm{B}}\right)-\mathsf{i}\epsilon\right]}. \tag{B.27}$$

Further changing coordinates $u\coloneqq t_{\mathrm{A}}-t_{\mathrm{B}}$, $s\coloneqq t_{\mathrm{A}}+t_{\mathrm{B}}$, the corresponding Jacobian determinant is $J=1/2$, and so C_{AB} becomes

$$\begin{aligned}C_{\mathrm{AB}} = {}& \frac{\lambda^{2}\gamma_{\mathrm{A}}\gamma_{\mathrm{B}}}{8\pi\sqrt{2}\ell}\sum_{n=-\infty}^{\infty}\int_{\mathbb{R}}\mathrm{d}u\,e^{-(\gamma_{\mathrm{A}}^{2}+\gamma_{\mathrm{B}}^{2})u^{2}/8\sigma^{2}}e^{-\mathsf{i}\Omega(\gamma_{\mathrm{A}}+\gamma_{\mathrm{B}})u/2}\left[\frac{1}{\rho^{-}(u)}-\frac{\zeta}{\rho^{+}(u)}\right]\\ &\times\int_{\mathbb{R}}\mathrm{d}s\,e^{-(\gamma_{\mathrm{A}}^{2}+\gamma_{\mathrm{B}}^{2})s^{2}/8\sigma^{2}}e^{-(\gamma_{\mathrm{A}}^{2}-\gamma_{\mathrm{B}}^{2})us/4\sigma^{2}}e^{-\mathsf{i}\Omega(\gamma_{\mathrm{A}}-\gamma_{\mathrm{B}})s/2}\,.\end{aligned} \tag{B.28}$$

The s-integral can be analytically computed as

$$\begin{aligned}&\int_{\mathbb{R}}\mathrm{d}s\,e^{-(\gamma_{\mathrm{A}}^{2}+\gamma_{\mathrm{B}}^{2})s^{2}/8\sigma^{2}}e^{-(\gamma_{\mathrm{A}}^{2}-\gamma_{\mathrm{B}}^{2})us/4\sigma^{2}}e^{-\mathsf{i}\Omega(\gamma_{\mathrm{A}}-\gamma_{\mathrm{B}})s/2}\\ &=\frac{2\sigma\sqrt{2\pi}}{\sqrt{\gamma_{\mathrm{A}}^{2}+\gamma_{\mathrm{B}}^{2}}}\exp\left[-\frac{\Omega^{2}\sigma^{2}(\gamma_{\mathrm{A}}-\gamma_{\mathrm{B}})^{2}}{2(\gamma_{\mathrm{A}}^{2}+\gamma_{\mathrm{B}}^{2})}\right]\exp\left[\frac{(\gamma_{\mathrm{A}}^{2}-\gamma_{\mathrm{B}}^{2})^{2}}{8\sigma^{2}(\gamma_{\mathrm{A}}^{2}+\gamma_{\mathrm{B}}^{2})}u^{2}\right]\exp\left[\mathsf{i}\frac{(\gamma_{\mathrm{A}}-\gamma_{\mathrm{B}})^{2}(\gamma_{\mathrm{A}}+\gamma_{\mathrm{B}})\Omega}{2(\gamma_{\mathrm{A}}^{2}+\gamma_{\mathrm{B}}^{2})}u\right].\end{aligned} \tag{B.29}$$

By changing the variables $x \coloneqq r_{\mathrm{h}} u/\ell^2$, we find

$$C_{\mathrm{AB}} = \frac{\lambda^2 \gamma_{\mathrm{A}} \gamma_{\mathrm{B}}}{8\pi\sqrt{2}\ell} \frac{2\sigma\sqrt{2\pi}}{\sqrt{\gamma_{\mathrm{A}}^2 + \gamma_{\mathrm{B}}^2}} \exp\left[-\frac{\Omega^2\sigma^2(\gamma_{\mathrm{A}} - \gamma_{\mathrm{B}})^2}{2(\gamma_{\mathrm{A}}^2 + \gamma_{\mathrm{B}}^2)}\right]$$
$$\times \sum_{n=-\infty}^{\infty} \int_{\mathbb{R}} \mathrm{d}u \, \exp\left[-\frac{\gamma_{\mathrm{A}}^2 \gamma_{\mathrm{B}}^2}{2\sigma^2(\gamma_{\mathrm{A}}^2 + \gamma_{\mathrm{B}}^2)} u^2\right] \exp\left[-\mathrm{i}\frac{\gamma_{\mathrm{A}}\gamma_{\mathrm{B}}(\gamma_{\mathrm{A}} + \gamma_{\mathrm{B}})\Omega}{\gamma_{\mathrm{A}}^2 + \gamma_{\mathrm{B}}^2} u\right] \left[\frac{1}{\rho^-(u)} - \frac{\zeta}{\rho^+(u)}\right] \tag{B.30}$$
$$= 2K_C \sum_{n=-\infty}^{\infty} \mathrm{Re} \int_0^{\infty} \mathrm{d}x \, e^{-a_C x^2} e^{-\mathrm{i}\beta_C x} \left[\frac{1}{\sqrt{\cosh \alpha^-_{\mathrm{AB},n} - \cosh x}} - \frac{\zeta}{\sqrt{\cosh \alpha^+_{\mathrm{AB},n} - \cosh x}}\right], \tag{B.31}$$

where

$$a_C \coloneqq \frac{\gamma_{\mathrm{A}}^2 \gamma_{\mathrm{B}}^2}{2\sigma^2(\gamma_{\mathrm{A}}^2 + \gamma_{\mathrm{B}}^2)} \frac{\ell^4}{r_{\mathrm{h}}^2}, \tag{B.32a}$$
$$\beta_C \coloneqq \frac{\gamma_{\mathrm{A}}\gamma_{\mathrm{B}}(\gamma_{\mathrm{A}} + \gamma_{\mathrm{B}})}{\gamma_{\mathrm{A}}^2 + \gamma_{\mathrm{B}}^2} \frac{\ell^2}{r_{\mathrm{h}}} \Omega\,, \tag{B.32b}$$
$$K_C \coloneqq \frac{\lambda^2 \sigma \sqrt{\gamma_{\mathrm{A}}\gamma_{\mathrm{B}}}}{4\sqrt{\pi}\sqrt{\gamma_{\mathrm{A}}^2 + \gamma_{\mathrm{B}}^2}} \exp\left[-\frac{\Omega^2\sigma^2(\gamma_{\mathrm{A}} - \gamma_{\mathrm{B}})^2}{2(\gamma_{\mathrm{A}}^2 + \gamma_{\mathrm{B}}^2)}\right]. \tag{B.32c}$$

Although the integrand in Eq. (B.31) does not have a pole, one needs to be careful about the branch cuts as shown in Fig. B.3.[1] Equation (B.31) can be obtained by evaluating along L_1, C_ρ, and L_2 in the limit $R \to \infty$ and $\rho \to 0$, where ρ is the radius of the semicircle around the branch point.

Let us choose a contour in the complex plane and use the Cauchy integral theorem. To do so, consider a complex integral of Eq. (B.31):

$$\oint_C \mathrm{d}z \, e^{-az^2} e^{-\mathrm{i}\beta z} \left[\frac{1}{\sqrt{\cosh \alpha^-_{\mathrm{AB},n} - \cosh z}} - \frac{\zeta}{\sqrt{\cosh \alpha^+_{\mathrm{AB},n} - \cosh z}}\right]. \tag{B.33}$$

Assuming $\Omega > 0$, the integral (B.33) converges if $|e^{-az^2} e^{-\mathrm{i}\beta z}| = e^{-a(x^2 - y^2)} e^{\beta y} < 1$, where we used $z = x + \mathrm{i}y$, and so the contour C should be in $y < 0$ and $-x \le y \le x$. From this, we choose the contour $C = L_1 C_\rho L_2 L_3 L_4$ as shown in Fig. B.3 and by making use of

[1] For the general description of branch cuts, see [136].

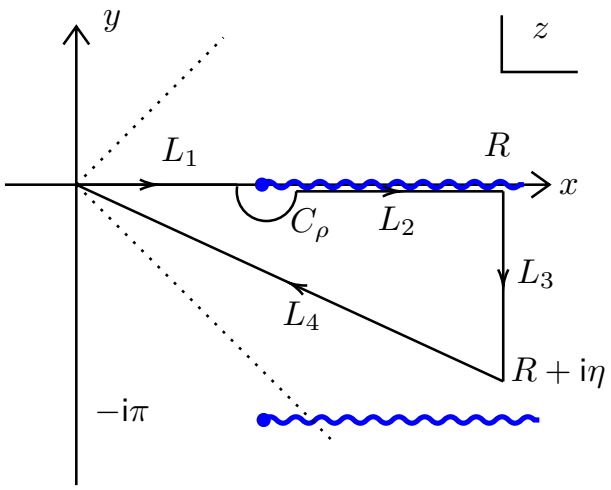

Figure B.3: Contour in a complex plane. Blue wiggly lines are the branch cuts and the contour is chosen so that the integral converges when $\Omega > 0$. The dotted lines represent $y = \pm x$, and the contour must be inside of this region.

the Cauchy integral theorem with the fact that $\lim_{R\to\infty} \int_{L_3} = 0$, Eq. (B.31) becomes an integral along L_4^{-1}:

$$C_{\mathrm{AB}} = 2K_C \sum_{n=-\infty}^{\infty} \lim_{R\to\infty} \mathrm{Re} \int_0^{R+\mathrm{i}\eta} \mathrm{d}z\, e^{-a_C z^2} e^{-\mathrm{i}\beta_C z} \left[\frac{1}{\sqrt{\cosh\alpha^-_{\mathrm{AB},\,n} - \cosh z}} - \frac{\zeta}{\sqrt{\cosh\alpha^+_{\mathrm{AB},\,n} - \cosh z}} \right], \tag{B.34}$$

where $\eta \in (-\pi, 0)$ and $\Omega > 0$; this is the expression we compute numerically.

Transition probability P

For the transition probabilities P_{A} and P_{B}, they are known to be [41]

$$\begin{aligned} P_{\mathrm{D}} = {} & \frac{\lambda^2\sigma^2}{2} \int_{\mathbb{R}} \mathrm{d}x\, \frac{e^{-\sigma^2(x-\Omega)^2}}{e^{x/T_{\mathrm{D}}} + 1} - \zeta \frac{\lambda^2\sigma}{2\sqrt{2\pi}} \mathrm{Re} \int_0^{\infty} \mathrm{d}x\, \frac{e^{-a_{\mathrm{D}}x^2} e^{-\mathrm{i}\beta_{\mathrm{D}}x}}{\sqrt{\cosh\alpha^+_{\mathrm{D},0} - \cosh x}} \\ & + \frac{\lambda^2\sigma}{\sqrt{2\pi}} \sum_{n=1}^{\infty} \mathrm{Re} \int_0^{\infty} \mathrm{d}x\, e^{-a_{\mathrm{D}}x^2} e^{-\mathrm{i}\beta_{\mathrm{D}}x} \left(\frac{1}{\sqrt{\cosh\alpha^-_{\mathrm{D},\,n} - \cosh x}} - \frac{\zeta}{\sqrt{\cosh\alpha^+_{\mathrm{D},\,n} - \cosh x}} \right), \end{aligned} \tag{B.35}$$

where $T_{\mathrm{D}} = r_{\mathrm{h}}/2\pi\ell^2\gamma_{\mathrm{D}}$ is the local temperature at $r = r_{\mathrm{D}}$ and

$$a_{\mathrm{D}} \coloneqq \frac{\ell^4\gamma_{\mathrm{D}}^2}{4\sigma^2 r_{\mathrm{h}}^2},\ \beta_{\mathrm{D}} \coloneqq \frac{\ell^2\gamma_{\mathrm{D}}\Omega}{r_{\mathrm{h}}}, \tag{B.36}$$

$$\alpha^{\pm}_{\mathrm{D},\,n} \coloneqq \operatorname{arccosh}\left[\frac{r_{\mathrm{h}}^2}{\gamma_{\mathrm{D}}^2\ell^2}\left(\frac{r^2}{r_{\mathrm{h}}^2}\cosh\left[\frac{r_{\mathrm{h}}}{\ell}2\pi n\right] \pm 1\right)\right]. \tag{B.37}$$

The first two terms, which correspond to $n = 0$, are the so-called AdS-Rindler terms and the last term ($n \neq 0$) is known as the BTZ term. The second and third integrals in (B.35) also have the same branch cut subtlety, but can be treated in the same manner as for C_{AB}.

Non-local correlation $X_{\mathbf{AB}}$

The derivation of X_{AB} is also very similar to that of C_{AB}. However, one has to be careful with the integration range.

$$\begin{aligned} X_{\mathrm{AB}} = &-\frac{\lambda^2\gamma_{\mathrm{A}}\gamma_{\mathrm{B}}}{4\pi\sqrt{2}\ell}\sum_{n=-\infty}^{\infty} \\ &\times \int_{\mathbb{R}} \mathrm{d}t_{\mathrm{A}} \int_{-\infty}^{t_{\mathrm{A}}} \mathrm{d}t_{\mathrm{B}}\, e^{-(\gamma_{\mathrm{A}}t_{\mathrm{A}})^2/2\sigma^2} e^{-(\gamma_{\mathrm{B}}t_{\mathrm{B}})^2/2\sigma^2} e^{\mathrm{i}\Omega(\gamma_{\mathrm{A}}t_{\mathrm{A}}+\gamma_{\mathrm{B}}t_{\mathrm{B}})} \left[\frac{1}{\rho^-(t_{\mathrm{A}},t_{\mathrm{B}})} - \frac{\zeta}{\rho^+(t_{\mathrm{A}},t_{\mathrm{B}})}\right] \\ &+ (\mathrm{A} \leftrightarrow \mathrm{B})\,, \end{aligned} \tag{B.38}$$

where $\rho^{\pm}(t_{\mathrm{A}}, t_{\mathrm{B}})$ is the same as (B.27). As before, one can change the coordinates as $u \coloneqq t_{\mathrm{A}} - t_{\mathrm{B}}$ and $s \coloneqq t_{\mathrm{A}} + t_{\mathrm{B}}$ with the Jacobian determinant $J = 1/2$, the double integral becomes

$$\int_{\mathbb{R}} \mathrm{d}t_{\mathrm{A}} \int_{-\infty}^{t_{\mathrm{A}}} \mathrm{d}t_{\mathrm{B}} \to \frac{1}{2}\int_{\mathbb{R}} \mathrm{d}s \int_{0}^{\infty} \mathrm{d}u\,. \tag{B.39}$$

It is then straightforward to have

$$\begin{aligned} X_{\mathrm{AB}} = &-\frac{\lambda^2\sigma}{4\sqrt{\pi}}\sqrt{\frac{\gamma_{\mathrm{A}}\gamma_{\mathrm{B}}}{\gamma_{\mathrm{A}}^2+\gamma_{\mathrm{B}}^2}}\exp\left[-\frac{\Omega^2\sigma^2}{2}\frac{(\gamma_{\mathrm{A}}+\gamma_{\mathrm{B}})^2}{\gamma_{\mathrm{A}}^2+\gamma_{\mathrm{B}}^2}\right] \\ &\times \sum_{n=-\infty}^{\infty}\int_0^{\infty} \mathrm{d}x\, e^{-a_X x^2} e^{-\mathrm{i}\beta_X x}\left(\frac{1}{\sqrt{\cosh(\alpha^-_{\mathrm{AB},n}) - \cosh(x-\mathrm{i}\epsilon)}} - \frac{\zeta}{\sqrt{\cosh(\alpha^+_{\mathrm{AB},n}) - \cosh(x-\mathrm{i}\epsilon)}}\right) \\ &+ (\mathrm{A} \leftrightarrow \mathrm{B})\,, \end{aligned} \tag{B.40}$$

where

$$a_X \coloneqq \frac{\ell^4}{2\sigma^2 r_{\rm h}^2}\frac{\gamma_{\rm A}^2\gamma_{\rm B}^2}{\gamma_{\rm A}^2+\gamma_{\rm B}^2}(=a_C)\,, \tag{B.41a}$$

$$\beta_X \coloneqq \frac{\Omega\ell^2}{r_{\rm h}}\frac{\gamma_{\rm A}\gamma_{\rm B}(\gamma_{\rm A}-\gamma_{\rm B})}{\gamma_{\rm A}^2+\gamma_{\rm B}^2}\,, \tag{B.41b}$$

Let $I_X(\mathrm{i}\epsilon)$ be

$$I_X(\mathrm{i}\epsilon) \coloneqq \int_0^\infty \mathrm{d}x\, e^{-a_X x^2} e^{-\mathrm{i}\beta_X x} f_n(x-\mathrm{i}\epsilon)\,, \tag{B.42}$$

where

$$f_n(x-\mathrm{i}\epsilon) \coloneqq \left(\frac{1}{\sqrt{\cosh(\alpha^-_{\mathrm{AB},n})-\cosh(x-\mathrm{i}\epsilon)}} - \frac{\zeta}{\sqrt{\cosh(\alpha^+_{\mathrm{AB},n})-\cosh(x-\mathrm{i}\epsilon)}}\right)\,. \tag{B.43}$$

Then, one will find that the second term (A↔B) is just $I_X(-\mathrm{i}\epsilon)$. Therefore, $X_{\rm AB}$ takes the following form.

$$X_{\rm AB} \sim I_X(\mathrm{i}\epsilon) + I_X(-\mathrm{i}\epsilon) \tag{B.44}$$

$$= I_X(\mathrm{i}\epsilon) + \int_0^{-\infty}(-\mathrm{d}x) e^{-\alpha_X^2(-x)^2} e^{-\mathrm{i}\beta_X(-x)} f_n(-x+\mathrm{i}\epsilon) \tag{B.45}$$

$$= \int_0^\infty \mathrm{d}x\, e^{-a_X x^2} e^{-\mathrm{i}\beta_X x} f_n(x-\mathrm{i}\epsilon) + \int_{-\infty}^0 \mathrm{d}x\, e^{-a_X x^2} e^{\mathrm{i}\beta_X x} f_n(x-\mathrm{i}\epsilon)\,, \tag{B.46}$$

where we have used $\cosh(-z)=\cosh(z)$. Thus, we finally obtain

$$X_{\rm AB} = -K_X \sum_{n=-\infty}^{\infty}\left[\int_0^\infty \mathrm{d}x\, e^{-a_X x^2} e^{-\mathrm{i}\beta_X x} f_n(x-\mathrm{i}\epsilon) + \int_{-\infty}^0 \mathrm{d}x\, e^{-a_X x^2} e^{\mathrm{i}\beta_X x} f_n(x-\mathrm{i}\epsilon)\right]\,, \tag{B.47}$$

where

$$K_X \coloneqq \frac{\lambda^2\sigma}{2\sqrt{\pi}}\sqrt{\frac{\gamma_{\rm A}\gamma_{\rm B}}{\gamma_{\rm A}^2+\gamma_{\rm B}^2}}\exp\left[-\frac{\Omega^2\sigma^2}{2}\frac{(\gamma_{\rm A}+\gamma_{\rm B})^2}{\gamma_{\rm A}^2+\gamma_{\rm B}^2}\right]\,. \tag{B.48}$$

This single integral has the same branch cuts as in $C_{\rm AB}$ and poles do not exist. However, since $\gamma_{\rm A}<\gamma_{\rm B}$, we have $\beta_X<0$ if $\Omega>0$, and so the first and second integrals have different contours. This is shown in Fig. B.4.

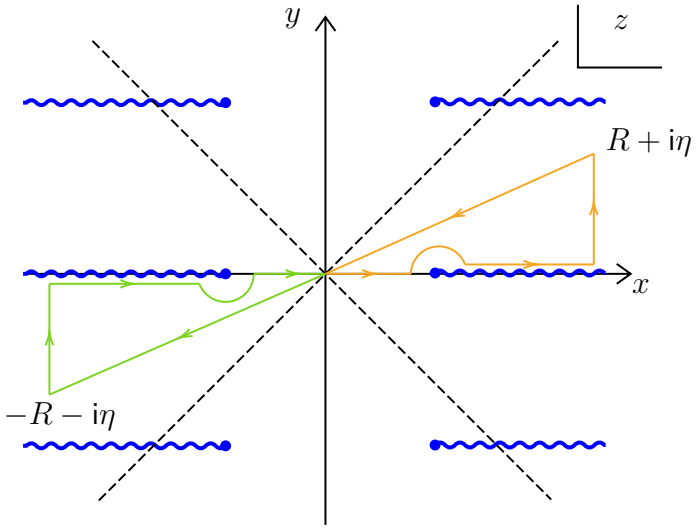

Figure B.4: Complex plane showing the branch cuts and contours for evaluating X_{AB}. The orange and green contours are used to evaluate the first and second integrals in (B.47), respectively. Note that there is no pole and the vertical contours does not contribute in the limit $R \to \infty$.

Appendix C

Free-faller's trajectory and kinematic relative velocity

C.1 Free-faller's trajectory

In this Appendix, we calculate the solution to the radial geodesic equation in Schwarzschild coordinates, with the goal of expressing the null coordinates u, v, U, V that appear in the definition of derivative coupling Wightman functions as functions of the free-falling detector's proper time.

Consider a freely falling observer who is initially at rest at $r_0 > r_\mathrm{h}$. The geodesic equations for a radially infalling observer are given by [133]

$$\ddot{t} = -\frac{2M}{r^2 f(r)} \dot{t}\dot{r}\,, \tag{C.1a}$$

$$\ddot{r} = -\frac{f(r)M}{r^2}\dot{t}^2 + \frac{M}{r^2 f(r)}\dot{r}^2\,, \tag{C.1b}$$

where the dotted derivative refers to the derivative with respect to proper time. The differential equation is also supplemented with a constraint for a massive test particle, namely that the geodesic is timelike:

$$-1 = g_{\mu\nu}\dot{x}^\mu \dot{x}^\nu = -f(r)\dot{t}^2 + \frac{1}{f(r)}\dot{r}^2, \tag{C.2}$$

where $\dot{x}^\mu = \mathrm{d}x^\mu/\mathrm{d}\tau$ is the four-velocity. By multiplying M/r^2 on both sides of (C.2) and substituting into (C.1b), we get

$$\ddot{r} = -\frac{M}{r^2}\,. \tag{C.3}$$

By integrating this with the initial conditions, $r(\tau_0) = r_0,\ \dot{r}(\tau_0) = 0$, where $\tau = \tau_0$ is the initial proper time, we obtain

$$\dot{r} = -\sqrt{\frac{r_\mathrm{h}}{r} - \frac{r_\mathrm{h}}{r_0}}\,. \tag{C.4}$$

Assuming that the observer starts from $r_0 = \infty$, the geodesic equations reduce to

$$\dot{t} = \frac{1}{1 - r_\mathrm{h}/r}\,, \tag{C.5a}$$

$$\dot{r} = -\sqrt{r_\mathrm{h}/r}\,, \tag{C.5b}$$

and so r can be obtained as [120]

$$r(\tau) = r_\mathrm{h}\left(\frac{\tau}{\tau_\mathrm{h}}\right)^{\frac{2}{3}}\,, \tag{C.6}$$

where $\tau_\mathrm{h} = -2r_\mathrm{h}/3$ is the horizon-crossing time. Note that $\tau \in (-\infty, 0)$, and the observer reaches the singularity as $\tau \to 0^-$.

Let us rewrite the geodesic equations in terms of the two null coordinates $v, u = t_\mathrm{s} \pm r_\star$ and the Kruskal-Szekeres null coordinates $V = 2r_\mathrm{h}e^{v/(2r_\mathrm{h})}$ and $U = -2r_\mathrm{h}e^{-u/(2r_\mathrm{h})}$. By using (C.5a) and (C.5b), we get

$$\dot{v} = \frac{1}{1 + \sqrt{r_\mathrm{h}/r}}\,, \tag{C.7a}$$

$$\dot{u} = \frac{1}{1 - \sqrt{r_\mathrm{h}/r}}\,, \tag{C.7b}$$

$$\dot{V} = \frac{V}{2r_\mathrm{h}}\frac{1}{1 + \sqrt{r_\mathrm{h}/r}}\,, \tag{C.7c}$$

$$\dot{U} = -\frac{U}{2r_\mathrm{h}}\frac{1}{1 - \sqrt{r_\mathrm{h}/r}}\,, \tag{C.7d}$$

for $r > 0$. Note that due to the local nature of the differential equations, the geodesic equations expressed in terms of these null coordinates extend into the black hole interior, in contrast to the Schwarzschild coordinate version which is only valid in the exterior region. Substituting (C.6) into these differential equations, we can obtain closed form expressions for u, v, U, V as functions of infalling τ,

$$v(\tau) = \tau - 2r_{\rm h} x^{\frac{1}{3}}(\tau) + r_{\rm h} x^{\frac{2}{3}}(\tau) + 2r_{\rm h} \ln\left[1 + x^{\frac{1}{3}}(\tau)\right] , \tag{C.8a}$$

$$u(\tau) = \tau - 2r_{\rm h} x^{\frac{1}{3}}(\tau) - r_{\rm h} x^{\frac{2}{3}}(\tau) - 2r_{\rm h} \ln\left[-1 + x^{\frac{1}{3}}(\tau)\right] , \tag{C.8b}$$

$$V(\tau) = 2r_{\rm h} e^{\frac{\tau}{2r_{\rm h}}} \exp\left[-x^{\frac{1}{3}}(\tau) + \frac{1}{2} x^{\frac{2}{3}}(\tau)\right] \left(1 + x^{\frac{1}{3}}(\tau)\right) , \tag{C.8c}$$

$$U(\tau) = 2r_{\rm h} e^{-\frac{\tau}{2r_{\rm h}}} \exp\left[x^{\frac{1}{3}}(\tau) + \frac{1}{2} x^{\frac{2}{3}}(\tau)\right] \left(1 - x^{\frac{1}{3}}(\tau)\right) , \tag{C.8d}$$

where $x(\tau) = \tau/\tau_{\rm h}$. One can check that at the singularity $r = 0$, we get $UV = 4r_{\rm h}^2$, as expected. Furthermore, these null coordinates take the extended values in the relevant regions; for instance, while the coordinate transformations for U, V are given for $U < 0, V > 0$, the solutions $U(\tau), V(\tau)$ can take all real values and hence include the black hole interior.

C.2 Kinematic relative velocity

Here, we review the notion of kinematic relative velocity (KRV) in [126].

Let us first define what relative velocity is. Let $u, u' \in T_p\mathcal{M}$ be two four-velocities defined on a single point $p \in \mathcal{M}$. Then u' can always be decomposed into the components parallel to u and its orthogonal space $u^\perp$ [see Fig. C.1(a)]:

$$\exists v \in u^\perp, \exists \gamma > 0, \text{ s.t. } u' = \gamma(u + v) , \tag{C.9}$$

where $\gamma := -g(u', u) = 1/\sqrt{1 - ||v||^2}$. The vector v represents how u' is deviated from u, and so we call this the relative velocity of u' observed by u.

KRV generalizes this definition to tangent vectors defined on two different points p and q on a spacelike simultaneity in a manifold by "bringing" them to one point. However, one has to "bring" a vector to another vector's tangent space in a mathematically consistent way. Such a procedure is parallel transport. Therefore, the basic idea of KRV is, first collect all spacelike simultaneous points $q \in \mathcal{M}$ of $p \in \mathcal{M}$, which is mathematically done by introducing the so-called Landau submanifold, and then parallel transport a vector

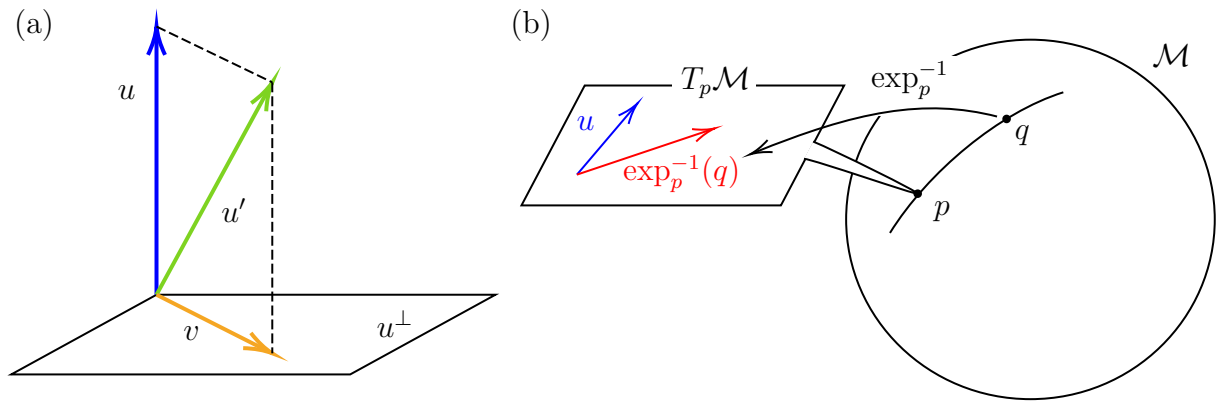

Figure C.1: (a) Defining the relative velocity v of u' with respect to u on a single point. (b) The process of construction of a spatial simultaneity. The curve connecting p and q is a geodesic.

$u' \in T_q\mathcal{M}$ to $T_p\mathcal{M}$ so that we can adopt the aforementioned definition of the relative velocity of u' observed by $u \in T_p\mathcal{M}$.

We assume that the event q is in the convex normal neighborhood of p, which means that there exists a unique geodesic connecting these two events. Let $u \in T_p\mathcal{M}$ be a four-velocity and $\exp_p : T_p\mathcal{M} \to \mathcal{M}$ an exponential map.[1] Then q becomes an event on a spacelike simultaneity of p in the following manner. The preimage of the exponential map, $\exp_p^{-1} : q \mapsto \exp_p^{-1}(q) \in T_p\mathcal{M}$, is an "initial vector" that determines the point q on the geodesic [Fig. C.1(b)]. Since we wish to have a spacelike simultaneity, this initial vector $\exp_p^{-1}(q)$ has to be spacelike. We can impose this by writing $g(\exp_p^{-1}(q), u) = 0$, where g is a metric and we used the fact that u is timelike. From this, let us construct a map

$$\begin{aligned} &\Phi_p : \mathcal{M} \to \mathbb{R}\,, \\ &\Phi_p : q \mapsto \Phi_p(q) \coloneqq g(\exp_p^{-1}(q), u)\,. \end{aligned} \tag{C.10}$$

Such a map turns out to be a submersion, which has a nice property where the preimage $\Phi_p^{-1} : \mathbb{R} \to \mathcal{M}$ is a submanifold of $\mathcal{M}$ [137]. Thus, $L_{p,u} \coloneqq \Phi_p^{-1}(0) \subset \mathcal{M}$ is a collection of events q that satisfies $g(\exp_p^{-1}(q), u) = 0$, meaning that they are on a surface of spacelike simultaneity of p, and this $L_{p,u}$ is called the Landau submanifold.

[1] The intuition of the exponential map is that one can determine the point on a geodesic once the initial position p and initial vector $\xi \in T_p\mathcal{M}$ is given since the geodesic equation is a second-order differential equation. The analogy for this is throwing a ball and predicting its landing point. The location and the velocity vector of the ball when you release determine the point where it will fall.

Since we now have the notion of spacelike simultaneity, the remaining task is to parallel transport a vector $u' \in T_q\mathcal{M}$, where $q \in L_{p,u}$, to $T_p\mathcal{M}$ and apply the notion of relative velocity. Let $\tau_{q,p} : T_q\mathcal{M} \to T_p\mathcal{M}$ be a parallel transport, then KRV (denoted by v) of u' with respect to u is found by $\tau_{q,p}u' = \gamma(u + v)$. Hence,

$$v = \frac{\tau_{q,p}u'}{-g(\tau_{q,p}u', u)} - u\,. \tag{C.11}$$